EUROPEAN COMMISSION
Community Research

ACSEPT
innovative solutions for sustainable nuclear energy

ACSEPT

(Contract Number: FP7-CP-2007-211 267)

DELIVERABLE D4.2.1

Proceedings Of The International Workshop

Lead Beneficiary: **CEA**

Due date of Deliverable: **31/05/2010** Actual submission date: **31/10/2010**

Authors:	S. BOURG

For the Lead Beneficiary	**Reviewed by Domain Coordinator**	**Approved by Coordinator**
Stéphane BOURG	**Christian EKBERG**	**S. BOURG**

Start date of project: **01/03/08** Duration: **48 Months**
Project Coordinator Organisation: CEA Revision: (0)
Project Coordinator: Stéphane Bourg

Project co-funded by the European Commission under the Euratom Research and Training Programme on Nuclear Energy within the Seventh Framework Programme		
Dissemination Level		
PU	Public	
RE	Restricted to a group specified by the partners of the ACSEPT project	
CO	Confidential, only for partners of the ACSEPT project	**X**

EXECUTIVE SUMMARY

From March 31st to April 2nd 2010, the First ACSEPT International Workshop organized in Hotel VIP Zurique in Lisbon, Portugal by ITN gathered more than 100 people from the ACSEPT Community - and specifically its young scientists - and more than 20 International Experts around Partitioning process development from basic data acquisition to process implementation (hydro and pyro), transmutation and waste management issues.

The Proceedings are available on the ACSEPT Website.

This deliverable contributes to the following work-packages:

DOMAIN 0
☐ WP0.1 ☐ WP0.2 ☐ WP0.3

DOMAIN 1
☐ WP1.1 ☐ WP1.2 ☐ WP1.3 ☐ WP1.4

DOMAIN 2
☐ WP2.1 ☐ WP2.2 ☐ WP2.3 ☐ WP2.4

DOMAIN 3
☐ WP3.1 ☐ WP3.2 ☐ WP3.3

DOMAIN 4
☐ WP4.1 ☒ WP4.2 ☐ WP4.3

OUTLINE

PART I

I INTRODUCTION

From March 31st to April 2nd 2010, the First ACSEPT International Workshop organized in Hotel VIP Zurique in Lisbon, Portugal by ITN gathered more than 100 people from the ACSEPT Community - and specifically its young scientists - and more than 20 International Experts around Partitioning process development from basic data acquisition to process implementation (hydro and pyro), transmutation and waste management issues.

The Proceedings are available on the ACSEPT Website.

II TABLE OF CONTENT

FIRST ACSEPT INTERNATIONAL WORKSHOP

31 March - 2 April 2010, HOTEL VIP ZURIQUE, LISBON PORTUGAL

Wed. 31st		
14:00	**OPENING**	**ACSEPT Coordinator**
14:05 - 14:45	**Welcome address**	**ITN representatives** Welcome & Presentation of ITN
14:45 - 15:15		**Dominique Warin** Minor Actinide Partitioning
15:15 - 15:45		**Janne Wallenius** Transmutation
15:45 - 16:15		**Gerald Ouzounian** Radioactive Waste Management, IGD-TP
16:15 - 16:45		*Coffee Break*
16:45 - 17:15	Fuel cycle and waste management strategies *co-chairs* *JP Glatz C. Ekberg*	**Peter Wikberg** Present status of the Swedish nuclear waste management programme
17:15 - 18:00		**Terry Todd** The U.S. Fuel Cycle Research and Development Program: Separations Research and Development
18:00 - 18:20		**Mikhael Kormilitsyn** Strategies and national programs of closed fuel cycles - Russian Expert Vision
18:20 - 18:40		**Uddharan Basak** IAEA Activities on Assessment of Partitioning Processes for Transmutation of Actinides
20:00	**Dinner (Social evening)**	
Thu. 1st		
8:10 - 8:30	Hydrometallurgy process developments *co-chairs* *E Aneheim and*	**Michal Sypula** Separation of An(III) from PUREX raffinate as an innovative-SANEX process based on a mixture of TODGA/TBP
8:30 - 8:50		**Julie Muller**

	G Vidick	Characterization of lanthanide and actinide complexes in the DIAMEX-SANEX process
8:50 - 9:10		**Andreas Wilden**
		1-cycle SANEX and GANEX process development studies performed at FZJ
9:10 - 9:30		**Fiona MacLachlan**
		Extraction Studies Of Potential Solvent Formulations For The GANEX Process
9:30 - 10:00		**Ken Nash**
		Investigations of The Fundamental Chemistry of the TALSPEAK Process
10:00 - 10:30		*Coffee Break*
10:30 - 11:00		**Kenji Takeshita**
		Extraction Separation of Trivalent Minor Actinides and Lanthanides by Hexadentate Nitrogen-donor Extractant, TPEN, and its Analogs
11:00 - 11:30	Hydrometallurgy process developments *co-chairs E Löfström-Engdahl and M Sypula*	**Vasiliy Babain**
		Fluorinated Diluents for HLW Processing –techological point of view
11:30 - 11:50		**Elin Löfström-Engdahl**
		The effects of diluents in solvent extraction - a literature study
11:50 - 12:10		**Irena Spendlikova**
		Extraction properties of some new pyridine molecules and search for better diluents
12:10 - 12:30		**Trong Hung Vu**
		Kinetics of extraction of Eu3+ ion by TODGA and CyMe4-BTBP studied using the RMC technique
12:45	*Lunch*	
14:00 - 14:20		**Alena Paulenova**
		Redox Chemistry of Neptunium in Solutions of Nitric Acid
14:20 - 14:40		**Frank Lewis**
		Studies on the Interaction of a Novel 6,6''-bis(1,2,4-triazin-3-yl)-2,2':6',2''-terpyridine Ligand with Ln(III) Ions and Am(III)
14:40 - 15:00	Hydrometallurgy actinide sciences and radiolysis *co-chairs I Spendlikova and A Wilden*	**Geoffrey Vidick**
		NMR applied to actinide ions and their complexes. In search of covalency effects
15:00 - 15:20		**Bruce Mincher**
		Irradiation Effects on Metal Oxidation States
15:20 - 15:40		**Ana Nunez**
		Towards “Stability Rules” for Radiolysis of bis-DGA compounds
15:40 - 16:00		**Steve Mezyk**
		Radiolytic stability of metal-complexed extraction ligands under aqueous acidic reprocessing conditions
16:00 - 16:30		*Coffee Break*

16:30 - 17:00	Pyrometallurgy actinide sciences and process developments *co-chairs* *J Svedkauskaite and M Gibilaro*	**K Nagarajan** Pyroprocess Research Activities at IGCAR, Kalpakkam, India
17:00 - 17:30		**Victor Ignatiev** Critical issues of nuclear energy systems employing molten salt fluorides: from ISTC #1606 to #3749 (1st year of project activity) and MARS/ EVOL co-operation.
17:30 - 17:50		**Jolanta Svedkauskaite** A high temperature heating device for the study of fission product release
17:50 - 18:10		**Tsuyoshi Murakami** Recent achievements and remaining challenges on pyrochemical reprocessing in CRIEPI
18:10 - 18:30		**Christophe Nourry** Pyro-reprocessing in molten salt media, from chlorides to fluorides
18:30 - 18:50		**Sebastien Jaskierowicz** Attempt to classify various molten fluoride mixtures according to their solvation powers regarding metal fluorides
18:50 - 19:10		**Rob Campbell-Kelly** Electrorefining of Cerium in LiCl-KCl Molten Salts
Fri. 2nd		
08:30 - 9:00	Material synthesis for fuel & targets *co-chairs* *C Tamain and H Daniels*	**Manuel Pouchon** Conversion processes: Internal Gelation and the Sphere-pac concept
9:00 - 9:20		**Marcin Brykala** Synthesis of uranium oxides by Complex Sol-Gel Processes (CSGP)
9:20 - 9:40		**Christelle Tamain** Synthesis and structural characterisation of mixed actinides An(IV)-An(III) oxalate compounds used as precursor for dedicated fuel or target
9:40 - 10:00		**Henrik Daniels** Synthesis of a ceramic Matrix for Actinide-Transmutation
10:00 - 10:30		*Coffee Break*
10:30 - 11:00	Training & Education	**Theodora Retegan & Jan John** A Combined Nuclear Technology and Nuclear Chemistry Master – A Unique Initiative at Chalmers University of Technology, Sweden the FP7 CA CINCH: Cooperation in education In Nuclear Chemistry
11:00 - 12:00	**Round table – panel**	**V. Babain, J.O. Liljenzin, K. Nash, R. Odoj, D. Warin - Chair: C. Ekberg**
12:00 - 12:30	Conclusive Remarks	**Jean-Paul Glatz**

12:45		*Lunch*
14:00 - 14:20		**Alexander Ossipenko** Partitioning of minor actinides and rare elements in system (Li, K, Cs)Cl/Ga.
14:20 - 14:40		**Alexander Maershin** Study of oxychloride compound formation in chloride melt by spectroscopic method
14:40 - 15:00		**Victor Ignatiev** ISTC 3749 progresses
15:00 - 15:20	**ISTC- ACSEPT Specific Meeting**	**Andrey Toropov** Verification of phase diagrams and study on lanthanides ions behavior in molten salt fluorides mixtures
15:20 - 15:40		**Valery Afonichkin** Salts purification and redox potential measurement for the molten LiF-ThF4-UF4 mixture
15:40 - 16:00		**Alexander Surenkov** Combined materials compatibility: Te corrosion of Ni-based alloys in molten salt fluorides. Characteristics and structure of alloys under study in conditions of delivery
16:00 - 16:20		**Olga Feinberg** Neutronic and fuel cycle consideration: from single stream to two fluid Th-U molten salt system
16:30	**End of the Meeting**	

IAEA Activities on Assessment of Partitioning Processes for Transmutation of Actinides

Uddharan Basak and Gary R Dyck
Nuclear Fuel Cycle and Materials Section
Nuclear Fuel Cycle and Waste Technology Division
Department of Nuclear Energy
International Atomic Energy Agency
P.O.Box 100, A-1400 , Vienna, Austria
Tel: +43 1 2600 22771, Fax: +43 1 26007, e-mail: u.basak@iaea.org

Abstract – *In these days of nuclear renaissance, appropriate management of radioactive materials arising from the nuclear fuel cycle back end is one of the most important issues related to the long term sustainability of nuclear energy. The present practice in the back end of the closed fuel cycle involves the recovery of uranium and plutonium from spent fuel by the aqueous based PUREX process for reuse in reactors and the conditioning of reprocessing waste into a form suitable for long term storage. The waste contains mainly fission products and transuranium elements immobilized in glass matrix. However, advanced fuel cycles incorporating partitioning of actinides along with minor actinides and their subsequent transmutation (P&T) in a fast neutron energy spectrum could be proliferation resistant and at the same time reduce the waste radiotoxicity by many orders of magnitude. Considering the importance of P&T on long term sustainability, the International Atomic Energy Agency has initiated many collaborative research programs in this area as part of our advanced fuel cycle activities. This paper presents the current and future activities on advanced partitioning methods, highlighting the challenges associated with these processes, fuel manufacturing techniques suitable for integration with reprocessing facility and the IAEA's minor actinide data base (MADB), as a part of integrated nuclear fuel cycle information system (iNFCIS).*

A. INTRODUCTION

The present generation of 439 reactors with installed capacity ~ 372 GWe derive energy mainly from the fission of ^{235}U and at the same time discharge spent nuclear fuel (SNF) almost at the rate of 10 500 t HM / annum. The spent fuel contains 95 – 96% uranium, 3 – 4% fission product, ~ 1% plutonium and ~ 0.1% minor actinides. Table 1 shows the composition of SNF from light water reactors (LWRs) and associated issues. Only 15% of the SNF is presently reprocessed by aqueous based PUREX (Plutonium URanium EXtraction) process for recycling of reprocessed uranium and plutonium in LWR and / or fast reactor and the reprocessing wastes consisting mainly of fission products & minor actinides are conditioned into a form suitable for long term storage. For first 100 years, fission products predominantly determine the radiotoxicity of the spent nuclear fuel and beyond that, it is plutonium and minor actinides. Once the plutonium is removed from SNF, the minor actinide determines the long term radiotoxicity. Figure 1 shows the relative radiotoxicity of different constituents in the spent nuclear fuel.

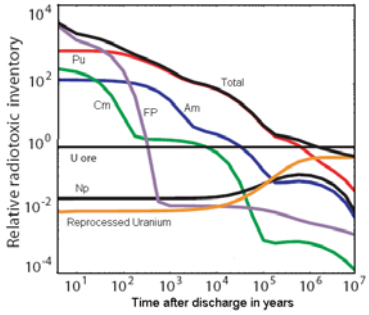

Figure 1: Relative radiotoxicity of the different components in spent nuclear fuel

Table 1: Composition of spent fuel from thermal reactors

Constituent	Composition (%)	Issue	Remarks
Uranium	~95 - 96	An energy resource.	Reprocessed uranium could be recycled as fuel in reactors
Plutonium	~ 1.0	An energy resource, but also the major contributor to long term radiotoxicity and heat load of waste. Separation Pu is of major proliferation concern.	Separated Pu could be recycled as fuel in reactors. However proliferation concerns could be reduced by not separating pure Pu.
Minor actinides, primarily Np, Am and Cm	~ 0.1	Important contributors to long term radiotoxity of waste. Proliferation concerns exist for separated Np.	Minor actinides can be burnt either alone or in combination with Pu in fast reactors.
Fission products	~ 3 - 4	FPs such as Cs and Sr are the primarily contributors to short term radiotoxicity and heat source in the waste. FPs namely Tc and I contribute to the long term radiotoxicity of the waste. Other FPs e.g noble metals could become valuable.	Storage of high level waste for a few hundred years or separation of Cs and Sr for separate disposal after a few hundred years of storage. Separated Cs has industrial applications.

To obtain public acceptance of future nuclear fuel cycle technology, new and innovative concepts must overcome the present concerns with respect to both environmental compliance and proliferation of fissile materials. Both these concerns can be effectively addressed through the multiple recycling of all transuranic elements (TRUs) in fast neutron reactor. This is only possible through a process known as partitioning and transmutation (P&T) as this scheme is expected to reduce the long-term radio-toxicity as well as the radiogenic heat production of the nuclear waste. After the removal of both plutonium and minor actinides through P&T processes, the radiotoxicity falls to a level of natural uranium ore within ~ 500years. In addition, P&T scheme is expected to extend the nuclear fuel resources on earth about 100 times because of the recycle and reuse of fissile actinides.

B. TRENDS IN P&T

Developmental efforts in recycling plutonium along with minor actinides in the future innovative nuclear energy systems are underway in several Member States of the International Atomic Energy Agency. R&D programs have also been launched in Member States to develop alternate reprocessing techniques and advanced partitioning processes that might help with nuclear waste management [1, 2]. Advanced processes aim for recovery of minor actinides and other long-lived fission products also for the purpose of transmuting them either in reactors or in accelerator driven systems (ADS). With ongoing time, the present generation of reprocessing plants has significantly improved the process technology in terms of flexibility for adopting high burn up and MOX fuel treatment, reduced waste generation, process simplification by reducing the number of cycles etc. However, the efforts are still in progress for further development of reprocessing technologies in order to address more challenging concerns, namely:

a) Proliferation issues associated with separated plutonium;
b) High level waste containing minor actinides and long lived fission products;
c) Economic and cost; and
d) Integration with facility for manufacturing of minor actinide bearing fuels that are being developed for use in future advanced nuclear reactors.

B.1. Developments in aqueous processes

The development of advanced separation methods is mainly based on improved PUREX process and directed towards the removal of minor actinides and long lived fission products from high level liquid waste so that the radiotoxicity and heat load of the final waste meant for either long term storage or disposal are reduced. The major steps involved are recovering minor actinides and lanthanides, purifying minor actinides from lanthanides, separating individual minor actinides and recovering Cs and Sr [3, 4].

The other process known as UREX (URanium EXtraction) is based on the changing the chemistry in the first separation step utilizing aceto-hydroxamic acid (AHA) so that only uranium is separated and plutonium along with minor actinides and fission products remain in the solution for further processing [5]. In fact, the development of a set of processes known as UREX+ is of interest as a part of US DOE's Avanced Fuel Cycle Initiative (AFCI).

B.2. Developments in pyro-chemical processing

Pyro-chemical processes exclude the use of both aqueous and organic media, and are based on liquid metals, molten salts or halides, usually at high temperature. Pyro-chemical process has the advantages over aqueous process for high chemical stability, radiation-resistance, high criticality-barrier, process simplicity, absence of high level liquid waste and inherent proliferation-resistance. As of now, Pyro-chemical separation of transuranium elements has only reached a stage of pilot-plant experiments. These processes were first investigated in the 1950´s as an alternative to PUREX because organic molecules used in PUREX had limited stability in the presence of strong ionizing radiation. In the initial stage, a pyro-chemical process was constructed at the Experimental Breeder Reactor II (EBR-II) in the USA. Later many concepts for pyro-chemical partitioning were developed and, in some cases, pilot plants were built and operated. Presently, three methods are receiving the major focus of attention in different countries [6].

- Molten salt electro-refining method for metallic fuels (developed by Argonne National Laboratory, USA)
- Electro-winning method for oxide fuels (developed by Russian Institute of Atomic Reactors, Russian federation)
- Fluoride volatility process of oxide and metallic fuels (developed by France, Russian Federation, Japan and USA),

However, compared to aqueous processes, the major challenges associated with pyro-processing are the requirement of oxygen and moisture free inert atmosphere for the plant and the need to develop materials that will withstand the high radiation and also should have excellent resistance to high temperature corrosion in molten salt and molten halides.The salient features of the aqueous and pyro-processes are shown in Table 2.

Table 2 Salient features of aqueous and pyro-processes

Process characteristics	**Aqueous process**	**Pyro process**	
		Metallic fuel	Oxide fuel
Nature of process	Continuous, high throughput	Batch, Limited throughput	Batch limited throughput
Solvent	Organic solvent, Nitric acid	LiCl-KCl, Cd, Bi	NaCl-KCl, CsCl
Operating temperature, K	< 373	~ 773	~ 973
Recovery of Pu, %	> 99.9	> 99.5	>99.3
Criticality	Needs severe control	Not severe	
Nuclear Material Accounting	Continuous accounting	Batch wise accounting	
Fuel manufacturing	Pelletisation, Vibro-packing	Injection casting	vibro-packing
High Level Waste	Nitrate solution	Chloride . -- Phosphate and chloride	
Technical maturity	Industrially demonstrated	Pilot scale facility	

B.3. Transmutation of MAs and LLFPs

Fast neutron reactors and Accelerator Driven Subcritical systems (ADS) play an important role by transmuting actinides as well as long lived fission products and contribute to environment protection and safe waste management. In addition, transmutation of MAs releases almost 5% of fission energy. Several studies have been performed for the application of ADS for minor actinide transmutation [7]. Minor actinide transmutation in ADS has been studied primarily in the context of a double strata scenario, where the bulk of plutonium is recycled in commercial reactors and only small amounts of minor actinides are transmuted in dedicated second stratum systems.

B.4. Integration with fuel manufacturing

The present generation of commercial nuclear reactors use either UO_2 (natural or enriched U) or $(U,Pu)O_2$ in the form of "pellets" manufactured by powder metallurgy (P/M) processes. The main process steps are: preparation of oxide powder from nitrate solutions; pre-compaction and granulation of oxide powder in most cases; cold–pelletisation; and high temperature sintering in hydrogen atmosphere
The major challenges in the P/M route are "radiotoxic dust hazard" associated with the generation and handling of large quantities of very fine powders of UO_2, highly radioactive PuO_2 and oxides of minor actinides and the poor flowability of powders. Hence, manufacturing processes, which avoid milling and grinding operations and deal with dust-free and free-flowing fuel materials are attractive as these processes would facilitate remote and automated fuel fabrication required for manufacturing of minor actinide bearing fuel in heavily shielded facility. Among these processes, sol-gel based "vibro-sol" or "gel pelletization" appears to be very promising as the sol-gel plant could be easily integrated with the spent fuel reprocessing plant and could be utilized for preparation of microspheres of MOX containing minor actinide oxides. Two or three size fractions of high density sintered microspheres are generally used for vibratory compaction for manufacturing fuel pins and for manufacturing fuel pellets, porous and easily crushable microspheres are used for cold pelletisation followed by high temperature sintering. Other advantages of sol-gel based processes are the absence of generation and handling of fine powders, amenability to automation and remotisation due to dust free and free flowability of sol gel derived microspheres, and high degree of micro-homogeneity of the constituent elements [8, 9].

C. IAEA ACTIVITIES

Many Member States and International Organizations are involved in the development of advanced nuclear fuel cycles that could effectively incorporate actinide recycling to reduce inventories of plutonium and minor actinides. In particular, several advanced partitioning methods are being developed and investigated in Member States. The review meeting of TWGNFCO (Technical working group on fuel cycle options and spent fuel management) in 2009 also indicated high priority for the activity concerning partitioning and transmutation of actinides. Considering the importance of partitioning and transmutation on long term sustainability, the agency has initiated many collaborative research programs in this area as a part of advanced fuel cycle activities.

The International Atomic Energy Agency (IAEA) has recently finalized a Coordinated Research Project (CRP) on "Study of process losses in separation process of partitioning and transmutation systems in view of minimizing long-term environmental impact" (2002-2008). One of the key-issues addressed in the CRP is the immense role of partitioning processes in actinide recycling that reduces long-term radio-toxicity considerably. The CRP involved experts from different organisations and institutes actively involved in developing P&T scheme. The scientific objectives of the CRP were:

- To minimize the environmental impact of actinides in the waste stream ;
- To develop element-specific, highly durable, materials for solidification and final disposal of residual actinides;
- To develop advanced characterisation methods for measurement of actinide hold-up in plants for the purpose of fissile material tracking as needed for nuclear material safeguards and criticality control;

- To establish element specific partitioning criteria to achieve a radiotoxicity reduction of about a factor of 100;
- To define proliferation resistance attributes for the processes and products;
- To compare advantages and disadvantages of aqueous and pyro- partitioning processes; and
- To assess the benefits of partitioning processes by reducing public radiation exposure, decreasing final repository capacity, reducing necessity of uranium mining and, consequently, diminishing the impact of uranium mill tailings.

A team of research scientists and experts had a several meetings between 2003 and 2008 and completed the document which is being published by the Agency [10]. The major findings and conclusions of the report are summarized as follows:

- Technological assessment
  - Compared to aqueous processes, pyro-processes are more compact, capable of processing of spent nuclear fuel with shorter cooling times as fused salts offer better radiation resistance;
  - Metal electro-refining has better potential for recovering minor actinides, while other pyro-processes require innovative technique to recover the same
  - The technical feasibility for a glass-bonded sodalite waste form using zeolite A as the waste matrix for chloride salt wastes from pyro-processes has only been demonstrated presently. However, the sodalite form has relatively low waste loading limit in comparison to borosilicate glass suitable for liquid high-level wastes from the aqueous processes;
  - While it is imperative to combine optimal options to make P&T efforts effective, the current assessment technologies for repository performance still remain at a scoping-study level;
  - Secondary wastes resulting from the various partitioning processes have also to be taken into account and due consideration should be given to their treatment and conditioning.
- Proliferation resistance
  - Implementation of any partitioning process supports non-proliferation of fissionable material. In planning and developing the process, special attention should be paid to minor actinides namely neptunium and americium;
  - The actinide mix with low U content exhibits properties that prohibit the use for a nuclear explosive because it will emit enough neutrons by spontaneous fission so hat a fission chain reaction occurs immediately when a critical mass is reached.
- Environmental compliance
  - The pyro-process has not yet been developed to minimize the process waste in order to achieve more than 99% of recovery efficiency on an engineering scale of deployment, as compared to more than 99.5% in the extraction process of the PUREX (Plutonium Uranium Extraction) process;
  - By P&T deployment, masses of major heat emitting radio-nuclides such as Sr-90, Cs-137, Pu-238, and Am-241, will be significantly reduced. This should be of potential benefits resulting from the simplification in the design of both containers and repository.

Very recently, the Agency organized a meeting on “Status and Trends in Advanced Partitioning Methods: Development in Pyro-chemical Processes” and the major objectives of the meeting were to review the recent developments in pyro-chemical processing and their impact in improving processing efficiency, reduction of radiotoxic losses, adoptability to remote fuel fabrication etc. In this meeting, significant progresses in pyro-chemical processes were reported in the following areas:

- Implementation plan in national nuclear fuel cycles,
- Process R&D and materials accounting,
- Engineering scale development and
- Shortening of the institutional control period (ICP) of the final waste.

Issues related to nuclear materials safeguards in pyroprocessing were also presented and discussed. Importance of nuclear materials accountancy including in-process nuclear materials measurement techniques for pyroprocessing was emphasized. Concept of "proliferation-resistance" for pyroprocessing was elaborated in various presentations. The Agency has plans to prepare a technical document on "Status and Trends in Advanced Partitioning Methods" during 2010 - 12 focusing the above areas.

There is an increased R&D effort among the Member States of the Agency to develop a technology that could be effectively utilized for reducing the amount of minor actinides and long lived fission products through transmutation in dedicated fast reactors or accelerators driven sub-critical system (ADS). As a part of information exchange, the Agency, in collaboration with the International Centre for Theoretical Physics (ICTP), Trieste organized the School on "Physics, Technology and Applications of Innovative Fast reactor Systems" in November, 2009. The Agency also organized two major international conferences related to utilization of ADS (AccApp '09) and Fast Reactors and Related Fuel Cycles (FR09) in 2009. As a part of collaborative R& D, the Agency has completed the Coordinated Research project on "Studies of Advanced Reactor Technology Options for Effective Incineration of Radioactive Waste "[11].

Integrated Nuclear Fuel Cycle Information System (iNFCIS)

The **iNFCIS** web site (http://www-nfcis.iaea.org) is designed as a "one stop" resource for technical and statistical information about nuclear fuel cycle activities worldwide, as reported to the IAEA. The system includes four databases and one computer simulation system published by the IAEA's Nuclear Fuel Cycle and Materials Section in the Division of Nuclear Fuel Cycle and Waste Technology. These are:

- Nuclear Fuel Cycle Information System (NFCIS);
- World Distribution of Uranium Deposits Database (UDEPO);
- Post Irradiation Examination Facilities Database (PIE) ;
- Nuclear Fuel Cycle Simulation System (NFCSS);
- Minor Actinide Property Database

Among these data bases, NFCSS and MADB are more relevant to researchers involved in P&T.
NFCSS is a scenario-based simulation system to estimate long-term nuclear fuel cycle material and service requirements as well as material raisings. The code uses simplified approaches to make estimation. NFCSS calculations can cover the period ranging from the beginning of nuclear energy production to 2050 or 2100. In order to support estimations for the future term, NFCSS stores historical data in its database (IAEA-TECDOC-1535).
Fresh fuel requirements and spent fuel isotopic composition are automatically calculated from a set of internal parameters that have been selected by experts and introduced in the program. The user may then choose to use spent fuel stockpiles to develop a recycling strategy. The estimation of accumulation of actinides including minor actinides is one of the capabilities of the simulation. Those accumulation estimations might be used to compare any future fuel cycle options for transmutation of minor actinides.
MADB is a bibliographic database on physico-chemical properties of selected Minor Actinide compounds and alloys. The materials and properties are selected based on their importance in the advanced nuclear fuel cycle options. Recently, the scope of R&D activities is increasing among Member States on several facets of Minor Actinide (MA) elements (namely Am, Np, and Cm) and their compounds owing to their accumulation in significant quantities due to enhanced use of nuclear energy. As these elements pose a very long-term radiological toxic burden to the environment, this has become a limiting factor for the growth of nuclear energy.

The issue of mitigation of radiological toxicity of actinides by advanced P&T methods has been addressed by the IAEA in its several meetings and TECDOCs. Since 1976, the IAEA has played a groundbreaking role in influencing the evolution of P&T technologies amongst all its Member States. In this context, the IAEA conducted a comprehensive review of thermodynamic data of all actinides elements and compounds and published a series of 14 reports (IAEA/STI/PUB/424) for a period between 1976 and 1992. These database series have become the de facto internal standard for chemical thermodynamic data of actinides and its compounds. Recent global R&D efforts on

advanced P&T methods in the last two decades have generated considerable information/data on MAs and its compounds encompassing various aspects of advanced nuclear fuel cycles.

The main idea behind the database initiative is to assemble information from the existing published literature on MAs especially thermo-physical as well as thermo-chemical properties pertinent and applicable to advanced partitioning methods as well as fuel/target fabrication subjects. The collection of bibliographic and technical information on MA data in selective areas and its review as well as assessment are divided into certain tasks. The present web-based database illustrates only bibliographic information together with technical data wherever available. The property database intends to cover thermodynamic, electro-chemical, phase-diagram and physical properties for the respective distinct unary and binary as well as multi-component oxide / nitride / halide / alloy MAs systems in molten as well as solid phases. In the first phase of this task, the scope of the database encompasses only the bibliographic information for pertinent properties to advanced pyro-chemical processing methods and fuel / target fabrication issues. In this context covering advanced aqueous partitioning methods was not considered in the present task.

D. CONCLUSION

Significant experience in the industrial plant scale reprocessing of spent fuels exists from thermal neutron reactors using the PUREX technology. While the PUREX process or its advanced versions may be used for aqueous reprocessing of fast reactor oxide fuels as well, a number of additional requirements come into picture due to the high Pu content of the fuel as well as the high levels of radioactivity associated with the irradiated fast reactor fuel. Considering the need for further reducing the cooling periods and increasing the burnup from economy and sustainability considerations, pyroprocessing technologies based on inorganic molten salts are being developed as alternatives for future fast reactors. Pyroprocessing technology is also ideally suited for metallic fuels besides being intrinsically more proliferation resistant. While waste management technologies for the fast reactor fuel based on aqueous reprocessing will be similar to those used for thermal reactor fuels, the treatment of pyroprocessed waste and its ultimate disposal would require further development. Thus, the development of fuel cycle technologies would continue to be a challenging area of activity. IAEA in collaboration with NEA / OECD organized several meetings and published technical reports in the recent years in this area of nuclear fuel cycle technology.

Aknowledgements
Authors wish to thank Mr. H. Tulsidas, Nuclear Fuel Cycle and Materials Section , IAEA for providing useful information on iNFCIS. Authors also thank Mr. Hans Forsstroem, Director, Division of Nuclear Fuel Cycle and Waste Technology, IAEA for his support on activities related to partitioning processes and Mr. Y. Sokolov, Deputy Director General, Department of Nuclear Energy, IAEA for his approval for publication of this paper.

References
1. NUCLEAR ENERGY AGENCY OF THE OECD, “Actnide and fission Product Partitioning and Transmutation”, Status and Assesment Report, OECD/NEA (1999).

2. INTERNATIONAL ATOMIC ENERGY AGENCY, “Implications of Partitioning and Transmutation in Radiocative Waste Mangement”, Technical Report Series 435, IAEA (2004).

3. ORGANIZATION FOR ECONOMIC CO-OPERATION AND DEVELOPMENT /NUCLEAR ENERGY AGENCY, Proc. of Tenth Information Exchange Meeting on Actinide and Fission Product Partitioningand Transmutation, Mito, Japan, 6-10 Oct 2008, OECD/NEA, Paris (2009).

4. AMERICAN NUCLEAR SOCIETY, Proc. Of GLOBAL 2007, Advanced Nuclear Fuel cycle Systems, September 9-13, 2007, Boise, USA, American Nuclear Society (2007)

5. JAMES J. LAIDER, “GNEP Spent Fuel Processing; Waste Streams and Disposition Options” Nuclear Technical Review, Washington, D.C., (2007).

6. ORGANIZATION FOR ECONOMIC CO-OPERATION AND DEVELOPMENT /NUCLEAR ENERGY AGENCY, “Pyrochemical Separation in Nuclear Applications- A status report”, OECD/NEA, NEA Report No. 5427(2004)

7. NUCLEAR ENERGY AGENCY / ORGANISATION FOR ECONOMIC CO-OPERATION AND DEVELOPMENT, “Accelerator-driven Systems (ADS) and Fast Reactors (FR) in Advanced Nuclear Fuel Cycles, A Comparative Study”, (2002).

8. INTERNATIONAL ATOMIC ENERGY AGENCY, “Sol-gel Processes for Fuel Fabrication”, IAEA-161(1974)

9. INTERNATIONAL ATOMIC ENERGY AGENCY, “Utilization of Particle Fuels in Different Reactor Concepts”, IAEA-TECDOC-286, IAEA, Vienna (1983).

10. INTERNATIONAL ATOMIC ENERGY AGENCY, “Assessment of Partitioning processes for Transmutation of Actinides” (To be published as IAEA-TECDOC).

11 INTERNATIONAL ATOMIC ENERGY AGENCY, “Advanced Reactor Technology Options for Utilization and Transmutation of Actinides in Spent Nuclear Fuel, IAEA-TECDOC-1626, 2009 (in print)

Separation of An(III) from PUREX raffinate as an innovative SANEX process based on a mixture of TODGA/TBP

Michal Sypula, Andreas Wilden, Christian Schreinemachers, Giuseppe Modolo
Institut für Energieforschung, Sicherheitsforschung und Reaktortechnik (IEF-6)
Forschungszentrum Jülich GmbH, 52425 Jülich, Germany
Tel: +49(0)2461 616282, Fax: +49(0)2461 612450
e-mail: m.sypula@fz-juelich.de

Abstract *– Within the ACSEPT project, an innovative SANEX process based on TODGA/TBP for selective An(III) separation from PUREX raffinate was studied. Oxalic acid usually used for Zr complexation is considered a weak point. An investigation to substitute oxalic acid with a different masking agent was carried out. A new masking agent already studied in FZJ was applied and showed good complexation properties towards Zr and Pd. Re-investigation of the formula of the actinide stripping solution was also performed. Good separation of Ln over Am was obtained by means of DTPA and malic acid. Glycine appeared to be the strongest within the tested buffers.*

A. INTRODUCTION

Several processes for recycling nuclear spent fuel have been designed and tested but only the PUREX process (U, Pu and Np recovery) has been employed on an industrial scale. After the partitioning step, Pu and U can be transferred back to the nuclear reactors as MOX fuel (mixed oxide). Recovered minor actinides can be converted into short-lived nuclides in advanced reactors (transmutation).
Within the ACSEPT project, a new innovative SANEX process (i-SANEX) combining two other separate processes, namely DIAMEX and SANEX, was investigated. This process consists of the co-extraction of Ln(III) and An(III) from the PUREX raffinate by a malonamide (e.g. DMDOHEMA) or diglycolamide (e.g TODGA), selective stripping of An(III) by polyaminocarboxylic acid (complexing agent) and carboxylic acid (buffer), and the stripping of Ln(III).

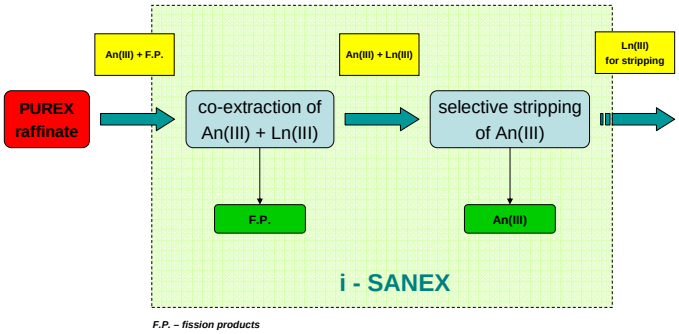

Figure 1. Innovative SANEX concept for separation of An(III) from PUREX raffinate

N,N,N',N'-tetraoctyl diglycolamide (TODGA) was considered a suitable extractant for co-extraction of An(III) + Ln(III). This ligand (Figure 2) possesses a very strong affinity towards An(III) and Ln(III) with distribution ratios over 300. Moreover, its high hydrolytic and radiolytic stability makes it an ideal extractant for nuclear purposes. Nevertheless, high loading of the organic solvent with metals causes formation of the third phase making it inapplicable in a continuous process. Modolo et al. studied the influence of tributylphosphate (TBP, Figure 2) on suppression of the third phase formation [1]. It has been found that 0.5 mol/L TBP added to the solvent acts as an organic phase modifier increasing the limiting organic concentration (LOC) up to 0.02 mol/L of Nd [1].

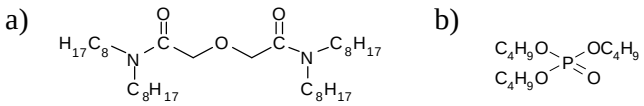

Figure 2. The chemical structures of the solvent components; a) TODGA, b) TBP

Due to the very high extraction strength of TODGA, some of the fission products were co-extracted together with An(III) + Ln(III). This problem was overcome by applying oxalic acid and N-(2-hydroxyethyl) ethylenediaminetriacetic acid (HEDTA) to suppress the extraction of Zr and Pd, respectively [1]. Two very successful counter-current tests (spiked and hot test) were carried out in FZJ and ITU [2,3]. This process was adopted by CEA for innovative SANEX by substituting the Ln+An stripping step with two new steps, namely An-stripping and Ln-stripping steps (Figure 3). During the co-extraction of Ln+An step, part of HNO_3 was extracted by TBP and further back-extracted, changing the pH of the An-stripping solution. Therefore, a buffer is needed. TODGA itself possesses a higher affinity towards Ln(III) than An(III). The separation between these two elements can be enhanced by means of a hydrophilic complexing agent i.e. HEDTA or DTPA (Figure 4).

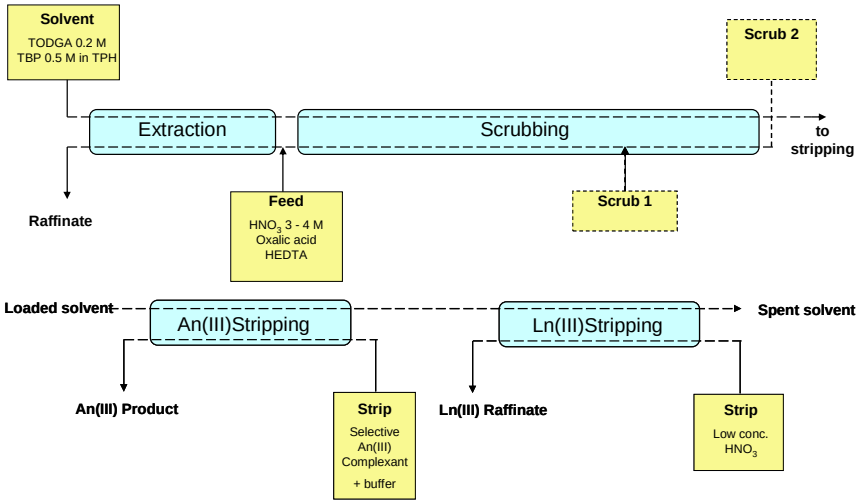

Figure 3. An exemplary flow-sheet of TODGA/TBP process for separation of An(III) from PUREX raffinate

Cold and spiked counter-current tests were performed by CEA [4] using DTPA as the An-complexing agent and malonic acid to buffer the solution for actinide stripping.
The weak point of this process is the use of oxalic acid in the extraction step. Oxalic acid is partly extracted by TBP in the extraction step and further back-extracted, changing the pH of the stripping solution (similar behaviour to nitric acid). Heres et al. already pointed out a very high sensitivity of the An(III) stripping step of the process towards pH. Furthermore, at a high oxalic acid concentration, a slow precipitation of lanthanide oxalates can appear.
Therefore, we proposed substituting oxalic acid with different Zr masking agen. Based on our previous studies, we decided to use a new hydrophilic masking agent which proved to efficiently complex Zr and Pd in the aqueous phase preventing their co-extraction with Ln+An.
We also re-investigated the formula of An-stripping solution to possibly increase the separation factor of lanthanides over actinides and improve stabilisation of the pH of the stripping solution.

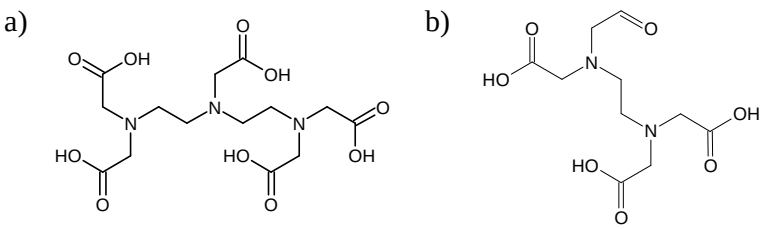

Figure 4. The chemical structures of a) DTPA, b) HEDTA

B. RESULTS AND DISCUSSION

B.1. Substitution of oxalic acid and HEDTA with the new masking agent

The extraction step was tested by contacting TODGA/TBP dissolved in TPH with a High Active Raffinate (HAR) simulate solution. Two parallel extractions were carried out: one with the new masking agent in the aqueous phase and one without. The results of this experiment (Table 1) show that the new masking agent efficiently suppresses the extraction of Zr and Pd. A slight increase in Sr extraction can be noticed when the masking agent is used. This is probably due to the lower loading of the organic phase with Zr (1071 mg/L in HAR solution). The same behaviour was observed in previous studies on complexation of Zr by oxalic acid [1].

Table 1: The content of the HAR solution and distribution ratios of its elements in the extraction step

		No masking agent	New masking agent
Element	Concentration [mg/L]	Distribution ratio D	
^{241}Am, ^{152}Eu	trace amounts	>100	>100
Y	90	>100	60
La	239	27	46
Ce	567	41	63
Pr	223	54	73
Nd	718	76	80
Sm	149	>100	71
Eu	34	>100	41
Gd	51	>100	43
Zr	1071	45	0.01
Pd	168	4.00	0.30
Sr	177	0.88	1.88
Ru	356	0.31	0.34
Mo	678	0.22	0.12
Cd	15	0.14	0.06
Rb	63	0.07	0.09
Ba	259	0.02	0.04
Sb	4.6	0.02	-
Cu	19	0.02	<0.01
Cr	93	0.01	0.01
Cs	542	<0.01	<0.01
Ni	40	<0.01	<0.01
Rh	73	<0.01	<0.01
Sn	11	<0.01	<0.01
Te	165	<0.01	<0.01
Ag	12	n.d.	n.d.
Al	2	n.d.	n.d.
Fe	1900	n.d.	n.d.
Na	1600	n.d.	n.d.
Se	10	n.d.	n.d.
HNO_3	3.1 mol/L		

* n.d. – not determinated

B.2. Re-investigation of the formula of the solution for actinides stripping

Five buffers were chosen for these studies, two already tested by CEA: glycolic acid and citric acid; and three new ones, namely malic acid, lactic acid and glycine (Figure 5).

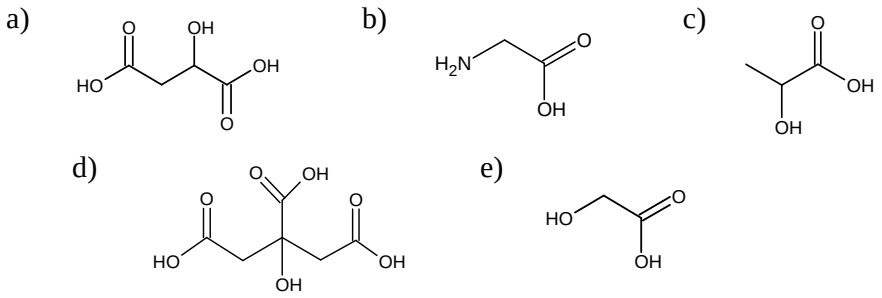

Figure 5. The chemical structures of a) malic acid, b) glycine, c) lactic acid, d) citric acid, e) glycolic acid

To improve the separation of Ln from An, two hydrophilic complexing agents were tested, namely HEDTA and DTPA (Figure 4). To keep the Ln(III) in the organic phase while An(III) were stripped to the aqueous phase, a salting-out agent was applied, namely $NaNO_3$. The results in Figure 5 show that malic acid and citric acid gave the highest separation factor of Eu/Am (>12) from all tested buffers when used with DTPA. Lactic acid also gave $SF_{Eu/Am}$ over 11 but this buffer is not strong enough to prevent pH changes. Citric acid appeared to be the best choice concerning separation of Eu/Am and buffering properties. Nevertheless, it was rejected from the beginning as CEA pointed out the difficulties with its destruction before the An co-conversion step. The strongest buffer at tested pH=2 was glycine, although the separation factor was slightly below 10 (when used with DTPA). A very interesting combination was glycine + HEDTA, giving a separation factor around 12 and the smallest pH change. In further studies, we focused only on a combination of DTPA with malic acid or glycine.

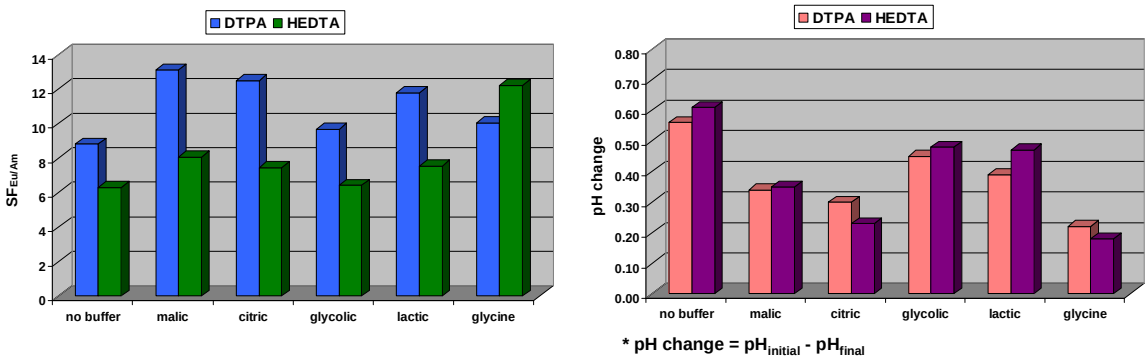

Figure 5. The influence of different buffers and complexing agents on separation factor of Eu/Am and pH change in the stripping solution

The influence of DTPA on the extraction of Am and Eu was also tested. The organic phase consisted of TODGA/TBP dissolved in TPH and loaded with An/Ln 2.5 solution of 0.5mol/L HNO_3. The aqueous phase of pH=2 contained DTPA, buffer (malic acid or glycine) and salting-out agent ($NaNO_3$). The results showed a decrease in the distribution ratios for both tested elements and an increase in the separation factor of Eu/Am while increasing the complexant concentration (Figure 6). This expected behaviour can be explained by DTPA forming stronger complexes with An(III) than with Ln(III). Therefore, the extraction of Ln(III) by TODGA is preferential as it causes the Ln/An separation factor to increase.

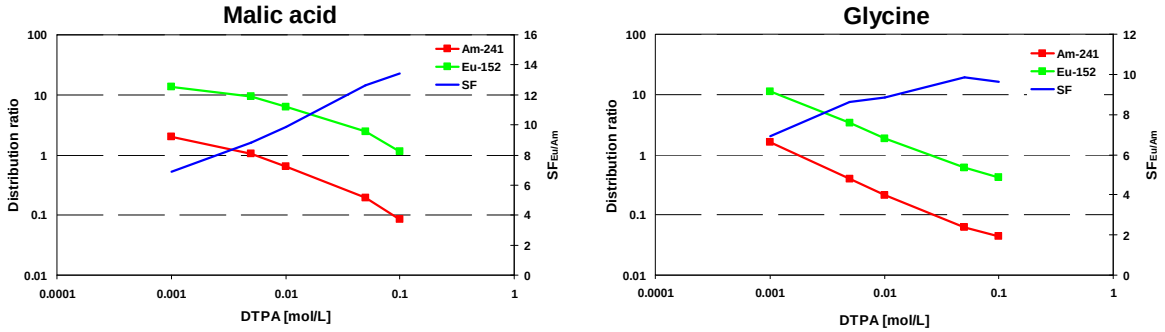

Figure 6. The influence of the complexant concentration on the extraction of ^{241}Am and ^{152}Eu

The back-extraction of Am from the loaded organic phase using a stripping solution of different pH was tested to obtain the best separation conditions. The stripping solution consisted of DTPA, malic acid and $NaNO_3$. Adjusted to pH=2 it gave the highest $SF_{Eu/Am}$ (Figure 7). The less extracted of all tested lanthanides at pH=2 was praseodymium, although its separation factor over Am was still high enough for efficient separation ($SF_{Pr/Am}$=6.7).

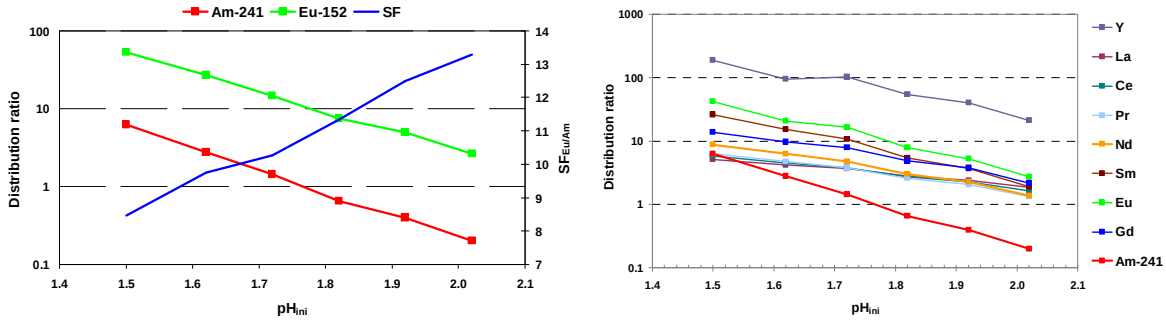

Figure 7. The influence of the pH of the stripping solution on the back-extraction of ^{241}Am and Ln (DTPA + malic acid)

The combination of DTPA, glycine and $NaNO_3$ at the optimal pH for An stripping (pH=1.9) gave lower $SF_{Eu/Am}$ than with malic acid. Nevertheless, the separation factor between samarium (the lowest distribution ratio within tested Ln) and Am reached 8.8 (Figure 8).

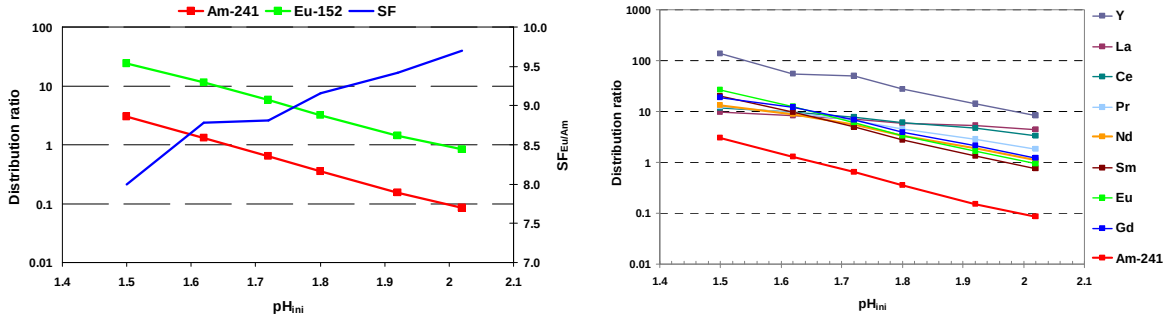

Figure 8. The influence of the pH of the stripping solution on the back-extraction of ^{241}Am and Ln (DTPA + glycine)

C. CONCLUSION

The TODGA/TBP process for An(III) separation from the PUREX raffinate studied within the ACSEPT project was successfully proven by two counter-current runs [4]. Nevertheless, the oxalic acid used in the extraction step was considered a weak point. Therefore, a new masking agent for Pd and Zr was

proposed. We also re-investigated the formula of the An-stripping solution. DTPA appeared to be a better complexing agent for An(III) separation than HEDTA. Nevertheless, the latter gave a reasonably high separation factor of Eu/Am (>12) when used with glycine. Within the tested buffers, the best buffering properties at pH=2 were shown by glycine, although with malic acid a higher $SF_{Eu/Am}$ was obtained. The optimal formula of the An-stripping solution appears to be the mixture of DTPA + malic acid + $NaNO_3$ at pH=2 or DTPA + glycine + $NaNO_3$ at pH=1.9.

Aknowledgements

Financial support for this research was provided by the European Commission (project ACSEPT – Contract No. FP7-CP-2007-211 267)

References

1. G. Modolo, H. Asp, C. Schreinemachers, H. Vijgen, “Development of a TODGA based Process for partitioning of actinides from a PUREX raffinate Part I: Batch extraction optimization studies and stability tests”, *Solvent Extr. Ion Exch.*, 25, *6*, 703–721 (2007).

2. G. Modolo, H. Asp, H. Vijgen, R. Malmbeck, D. Magnusson, C. Sorel, “Demonstration of a TODGA-Based Continuous Counter-Current Extraction Process for the Partitioning of Actinides from a Simulated PUREX Raffinate, Part II: Centrifugal Contactor Runs”, *Solvent Extr. Ion Exch.*, 26, *1*, 62–76 (2008).

3. D. Magnusson, B. Christiansen, J.P. Glatz, R. Malmbeck, G. Modolo, D. Serrano-Purroy, C. Sorel, “Demonstration of a TODGA-Based Continuous Counter-Current Extraction Process for the Partitioning of Actinides from a Simulated PUREX Raffinate, Part III: Centrifugal Contactor Run using Genuine Fuel Solution”, *Solvent Extr. Ion Exch.*, 27, *1*, 26–35 (2009).

4 X. Hérès, C. Sorel, M. Miguirditchian, B. Camès, C. Hill, I. Bisel, D. Espinoux, E. Catherine, B. Pascal, L. Brigitte, “Results of recent counter-current tests on An(III)/Ln(III) separation using TODGA extractant”, *Proc. of the Global 2009*, Paper 9384, Paris, France (2009).

Characterization of lanthanide and actinide complexes in the DIAMEX-SANEX process

Julie MULLER[1], Laurence BERTHON[1], Nicole ZORZ[1] and Jean-Pierre SIMONIN[2]
[1]*CEA, DEN, DRCP, SCPS, LILA, F-30207 Bagnols-sur-Cèze, France.*
[2]*Université Pierre et Marie Curie, PECSA, 4 place Jussieu, 75252 Paris Cedex 05.*
Tel: +33 (0) 4 66 33 94 26, Fax: +33 (0) 4 66 79 63 39, e-mail: julie.muller@cea.fr

Abstract *–In order to understand the mechanisms involved in the extraction processes developed to separate minor actinides, the organic phases have been characterized at macroscopic and molecular scale. The extraction of Eu(III), Am(III), nitric acid and water by the two extractants, DMDOHEMA and HDEHP, alone or in mixtures, has been investigated under a variety of experimental conditions and the ESI-MS technique has been then applied to characterize Eu(III) and Am(III) complexes in organic solutions.*

A. INTRODUCTION

In the framework of nuclear waste reprocessing, the DIAMEX (Diamide Extraction) - SANEX (Selective Actinide Extraction) process, developed by the CEA, is based on solvent extraction in order to separate the minor actinides from the high level liquid waste [1-2]. The separation of An(III) from the Ln(III) is accomplished by using a mixture of a malonamide and a dialkylphosphoric acid dissolved in an aliphatic diluent. The N,N'-dimethyl-N,N'-dioctylhexylethoxymalonamide (DMDOHEMA) and the di(2-ethylhexyl)phosphoric acid (HDEHP), Figure 1, are the reference extractants for this process. Under the highly acidic conditions of the aqueous phase, both An(III) and Ln(III) are extracted by the diamide. The separation and recovery of An(III) is then accomplished by contacting the loaded organic phase with a buffered solution (pH about 3) with presence of a complexing agent. With such conditions, the diamide is completely ineffective as an extractant for metal cations, while the organophosphoric acid exhibits efficient extraction and significant selectivity for Ln(III) over An(III).

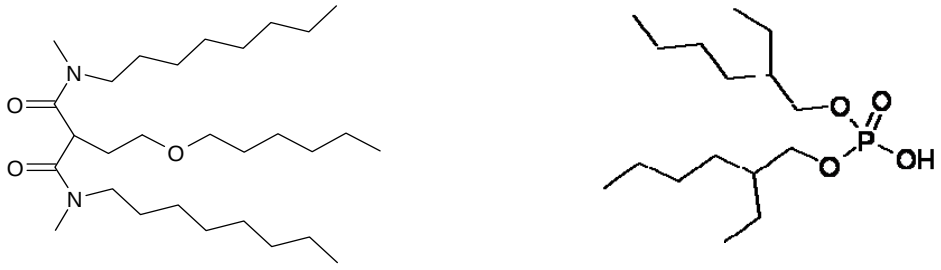

DMDOHEMA **HDEHP**

Figure 1: Structures of DMDOHEMA and HDEHP

In order to understand the mechanisms involved in the extraction process, the organic phases are first characterized at a macroscopic scale by the measurement of the extracting properties of water, nitric acid, europium and americium and then at a molecular scale by the electrospray ionization mass spectrometry (ESI-MS) technique.
A parametric study is performed when changing experimental conditions: the influence of the extractants concentration, the acidity of the aqueous phase, the nature of the metallic cation (europium and americium) and its concentration are investigated.
In this paper, the extracting behavior in acidic media and the analysis of the organic solution by ESI-MS are reported.

B. EXTRACTING BEHAVIOR IN ACIDIC MEDIUM

B.1. Water and nitric acid extraction

Water and nitric acid extraction has been investigated before extraction of metallic nitrates as a function of the acidity of the aqueous phase. As shown on Figure 2, HDEHP does not extract much water and nitric acid in the organic phase whereas DMDOHEMA extracts significant quantity of these solutes. The mixture of these two extractants does not extract more nitric acid than DMDOHEMA alone, but on the opposite, it extracts much more water than DMDOHEMA. As a consequence, the presence of HDEHP has an effect on water extraction.

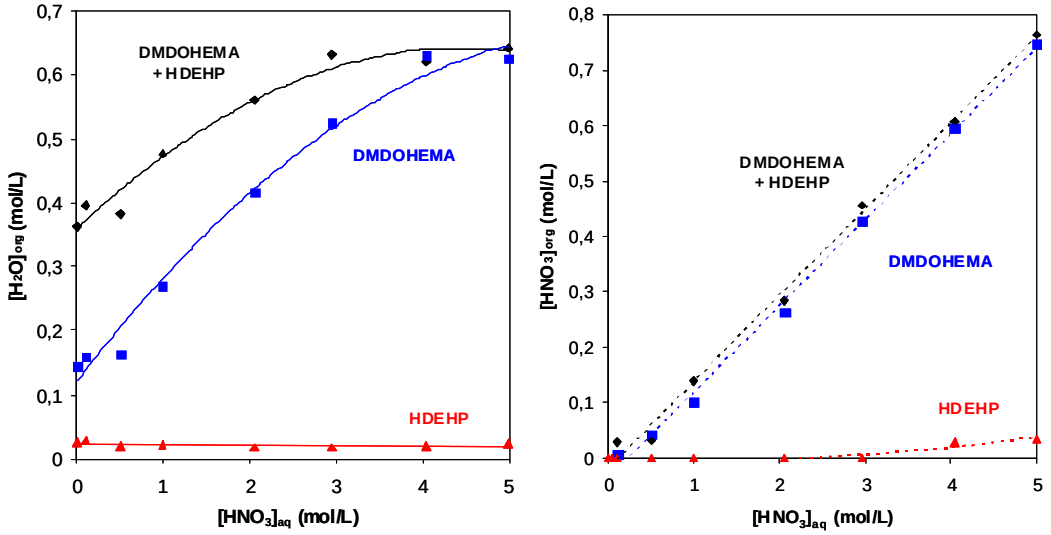

Figure 2: Water and nitric acid extraction by DMDOHEMA, HDEHP and DMDOHEMA-HDEHP mixture as a function of aqueous phase acidity. Aqueous phase: HNO_3. Organic phase: DMDOHEMA 0.6M in blue, HDEHP 0.3M in red and DMDOHEMA 0.6M-HDEHP 0.3M mixture in black, in HTP.

In order to understand the role of each extractant, the influence of their concentration on water and nitric acid extraction has been investigated in presence of acidic aqueous phase (HNO_3 1M and $LiNO_3$ 2M). The results (Figure 3) confirm that the addition of HDEHP has no effect on nitric acid extraction comparing to a DMDOHEMA solution, but a more complex effect is observed on water extraction. For malonamide concentration upper than 0.3M, the addition of HDEHP leads to an important increase of the water extraction. This effect is significant as soon as 0.01M of HDEHP is added to a malonamide solution.

In previous studies, Meridiano *et al.* [3] have shown that water extraction by DMDOHEMA in alkane is linked to the supramolecular organization of the malonamide solution. Thus, an explanation to interpret the water extraction behavior would be a modification of the supramolecular organization of the malonamide solution when adding HDEHP. This assumption is consistent with Gannaz studies [4,5] showing the formation of mixed micelles in the organic solution of DMDOHEMA 0.7M with another dialkylphosphoric acid: dihexylphosphoric acid, HDHP, at 0.3M concentration in alkane.

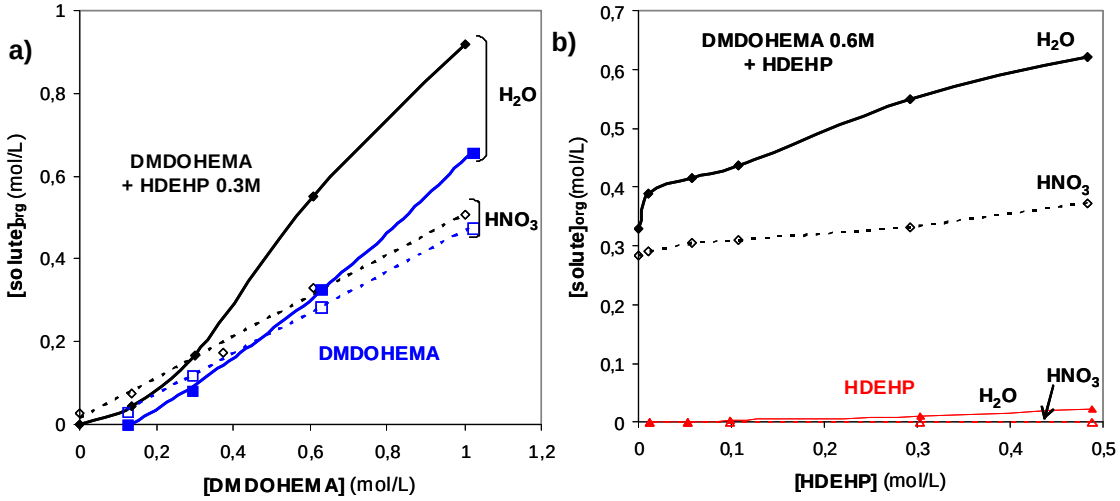

Figure 3: Water and nitric acid extraction by DMDOHEMA and DMDOHEMA-HDEHP mixture as a function of extractant concentration. a) Influence of DMDOHEMA concentration b) Influence of HDEHP concentration. Aqueous phase: HNO_3 1M and $LiNO_3$ 2M. Organic phase: DMDOHEMA in blue or HDEHP in red and DMDOHEMA + HDEHP in black, in HTP.

B.2.Am and Eu distribution ratios

The extraction of Eu(III) and Am(III) either by each extractant or by their mixture in HTP has been investigated under a variety of aqueous and organic phase conditions. When varying the acidity of the aqueous phase, the extraction by the mixture of the two extractants shows a behavior different from the two single extractants. Indeed, it indicates a synergistic effect around 1M nitric acid and an antagonistic effect at low acidity (Figure 4).

Moreover, at low acidities, the slope of the curve $D_M=f([HNO_3])$ indicates an exchange of 3 protons for the extraction of Eu or Am by HDEHP which is consistent with the previous data [6-8]. In presence of malonamide, the curves indicate an exchange of only 2 protons.

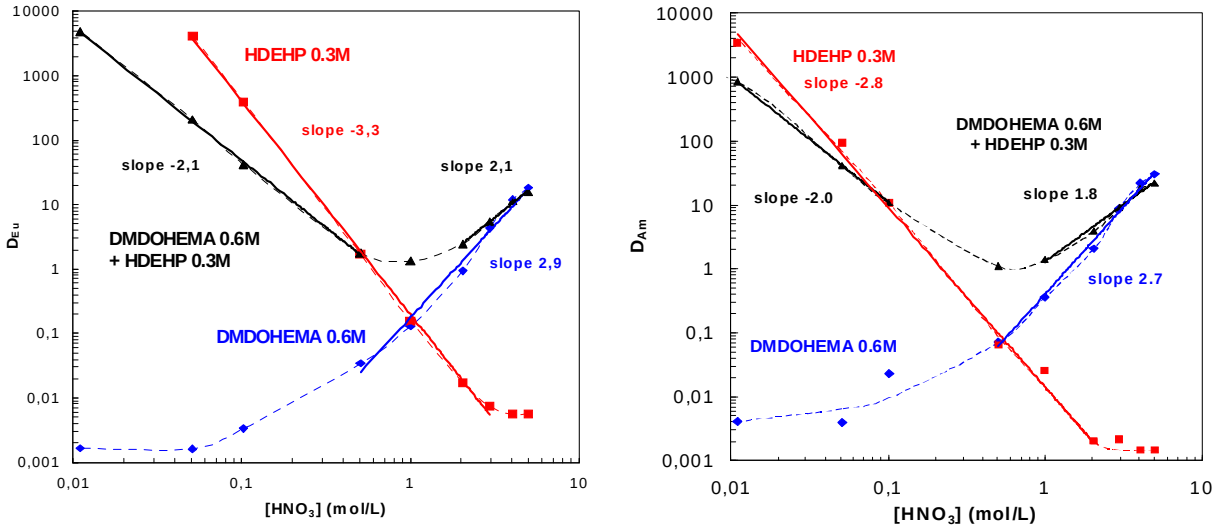

Figure 4: Eu and Am distribution ratio as a function of the aqueous nitric acid concentration. Aqueous phase: HNO_3. Organic phase: DMDOHEMA 0.6M in blue, HDEHP 0.3M in red and DMDOHEMA 0.6M + HDEHP 0.3M in black, in HTP.

In order to understand the origin of this behavior, the influence of extractants concentrations on Eu(III) and Am(III) extraction has also been investigated in acidic conditions. Figure 5 represents Eu and Am distribution ratio for DMDOHEMA and DMDOHEMA-HDEHP mixture in HTP as a function of the diamide concentration. The slopes of D_{Am} and D_{Eu} *vs.* malonamide concentration for the DMDOHEMA

alone are similar, indicating the same complexes stoichiometry. This is consistent with previous studies [3,5]. On the opposite, the slopes decrease in presence of HDEHP and are different for Am and Eu. It seems to indicate a change in the Am and Eu complexes stoichiometry in presence of DMDOHEMA and HDEHP.

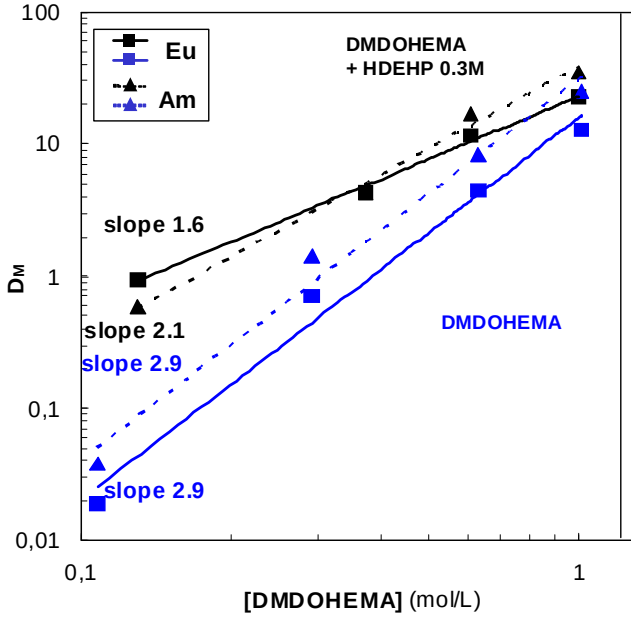

Figure 5: Am and Eu extraction as a function of DMDOHEMA concentration. Aqueous phase : HNO_3 1M and $LiNO_3$ 2M. Organic phase: DMDOHEMA in blue, DMDOHEMA + HDEHP 0.3M in black, in HTP

C. MOLECULAR SPECIATION BY ESI-MS

The electrospray ionization is a useful technique to get structural information about molecular complexes in solution. Indeed, ESI is a soft ionization mode allowing transfer of complexes from the solution to the gas phase with preservation of the metal-ligand interactions [9,10].

a) **b)**

Figure 6: Electrosptray ionization mass spectrometer Bruker Esquire LC a) before nuclearisation, b) after setting up in a glove box

C.1. Eu complexes

The first ESI-MS investigations in this field were obtained the mixture 0.6M DMDOHEMA - 0.3M HDEHP contacted with europium nitrate in 1M HNO_3 and 2M $LiNO_3$ aqueous phase (Figure 7). Diamide species identified were D_xEu^{3+} with $3 \leq x \leq 8$ and $D_xEu(NO_3)_z^{(3-z)+}$, and mixed species $D_xL_yEu(NO_3)_z^{a+}$ with $1 \leq x \leq 3$, $1 \leq y \leq 2$ and $0 \leq z \leq 2$. Assignment of these species is reported in Table 1. The presence of mixed ions Eu-DMDOHEMA-HDEHP was observed.

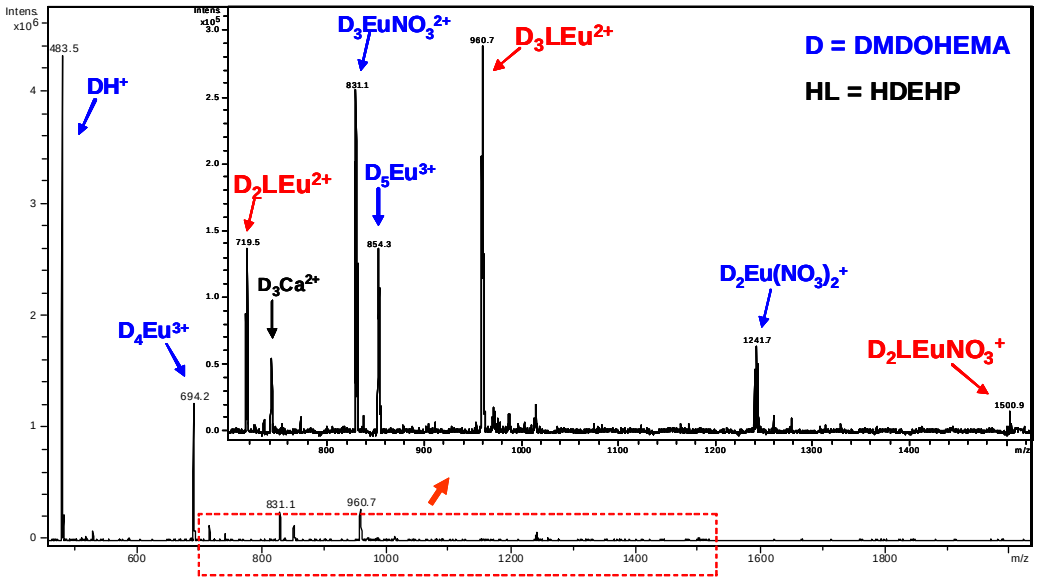

Figure 7 : Positive ESI mass spectrum of organic phase of DMDOHEMA-HDEHP mixture after Eu extraction. Aqueous phase: $Eu(NO_3)_3$ 0.1M, HNO_3 1M and $LiNO_3$ 2M. Organic phase: DMDOHEMA 0.6M + HDEHP 0.3M in HTP. Dilution 1/10th in ethanol and 1/100th in acetonitrile/water before analysis.

Spectra of the organic phase have also been recorded after contact with an aqueous phase of pH 3. Similar species are observed except ions containing nitrates. Therefore, mixed Eu-DMDOHEMA-HDEHP species are observed at both acidities.

Table 1: m/z ratio and species assignment in the positive ESI-MS data for the DMDOHEMA-HDEHP-M^{3+} system. (D stands for DMDOHEMA and HL for HDEHP)

Species	Base peak for Eu species m/z	Base peak for Am species m/z
$[D_3M]^{3+}$	533.4	563.3
$[D_4M]^{3+}$	694.2	724.1
$[D_5M]^{3+}$	854.2	884.2
$[D_6M]^{3+}$	1015.1	-
$[D_7M]^{3+}$	1175.8	-
$[D_8M]^{3+}$	1335.8	-
$[D_2M(NO_3)]^{2+}$	589.9	634.2
$[D_3M(NO_3)]^{2+}$	831.1	875.8
$[DM(NO_3)_2]^{+}$	759.3	
$[D_2M(NO_3)_2]^{+}$	1241.7	1330.2
$[D_2LM]^{2+}$	719.5	763.8
$[D_3LM]^{2+}$	960.7	1005.1
$[DL_2M]^{+}$	1277.8	1366.1
$[D_2L_2M]^{+}$	-	1847.9
$[DLM(NO_3)]^{+}$	1018.6	-
$[D_2LM(NO_3)]^{+}$	1500.9	1106.8
$[D_2(HL)L_2M]^{+}$	-	1588.4

In order to precise the domain of existence of these mixed species, the effect of the extractants concentration has been investigated in acidic medium. Mixed species are observed as soon as 0.01M HDEHP is added to the malonamide solution (Figure 8).

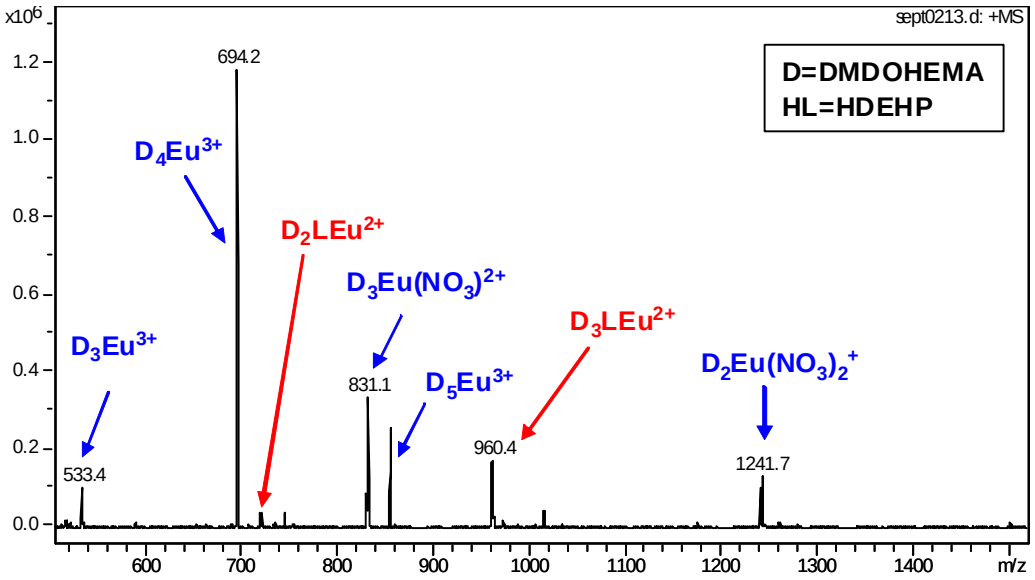

Figure 8: Positive ESI mass spectra of organic phase after Eu extraction. Aqueous phase: $Eu(NO_3)_3$ 0.1M, HNO_3 1M and $LiNO_3$ 2M. Organic phase: DMDOHEMA 0.6M + HDEHP 0.01M in HTP.

From the ESI-MS investigations with different experimental conditions, the complexes formed can be written as $D_xEu(NO_3)_3$ for the Eu extraction by the malonamide alone and D_xL_3Eu or $D_xL_2EuNO_3$ with $1 \leq x \leq 3$ for the mixed complexes. To explain the formation of these complexes, the following 3 possible equilibria are proposed:

$$x\overline{DMDOHEMA} + Eu^{3+} + 3NO_3^- \rightarrow \overline{DMDOHEMA_xEu(NO_3)_3} \quad \text{with } x \geq 3 \quad (1)$$

$$x\overline{DMDOHEMA} + 2\overline{HDEHP} + Eu^{3+} + NO_3^- \rightarrow \overline{DMDOHEMA_xDEHP_2EuNO_3} + 2H^+ \quad \text{with } 1 \leq x \leq 3 \quad (2)$$

$$x\overline{DMDOHEMA} + 3\overline{HDEHP} + Eu^{3+} \rightarrow \overline{DMDOHEMA_xDEHP_3Eu} + 3H^+ \quad \text{with } 1 \leq x \leq 3 \quad (3)$$

Equation 1 is consistent with the slope 3 obtained for the curve log D_{Eu} = f(log[DMDOHEMA]) and the stoichiometry of nitrates corresponds to the slope 3 in log D_{Eu} = f(log[HNO_3]). Equation 2 could explain the slope of -2 at low acidities and the presence of nitrates in mixed complexes observed by ESI-MS. Equation 3 suggests the stoichiometry for Eu extraction at low acidity, where nitrate concentration is very low.

C.2. Am complexes

Am(III) complexes formed with the DMDOHEMA-HDEHP mixture have been investigated by ESI-MS as well. However, in order to analyze metal-ligand complexes by ESI-MS, their relative concentrations in solution must be sufficient (i.e. > 1% of the total ligand concentration). Otherwise, the decrease of the ligand concentration leads to a decrease of the distribution ratio, and subsequently to a decrease of the complex proportion in the organic phase. To avoid the handling of concentrated americium solutions and to get information about Am complexes, experiments were performed in homogeneous phase (ethanol). Solutions containing DMDOHEMA, HDEHP, HNO_3 and ^{241}Am in ethanol were prepared and analyzed by ESI-MS. The mass spectrum shows the presence of Am-DMDOHEMA and mixed Am-DMDOHEMA-HDEHP species (Figure 9), similar with species identified with Eu(III).

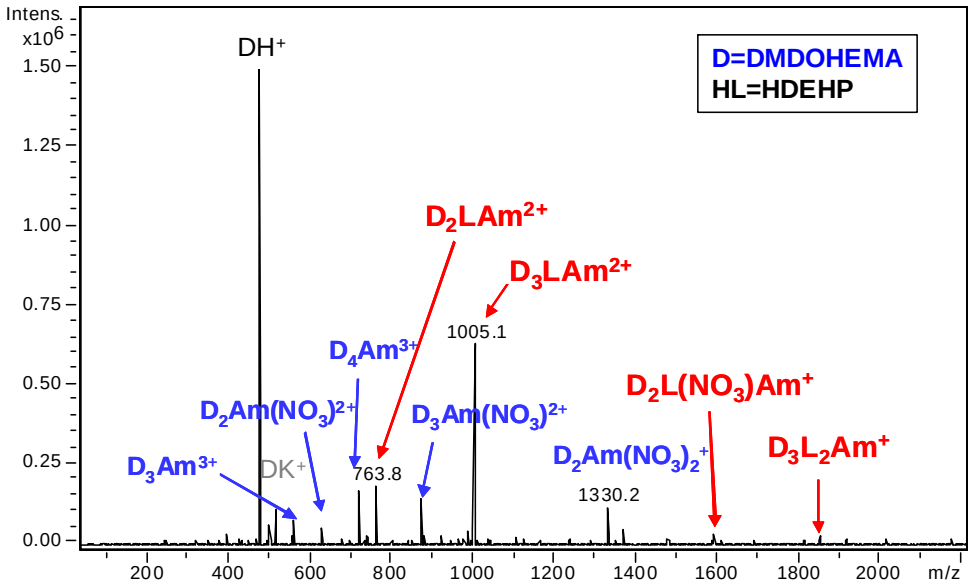

Figure 9 : Positive ESI mass spectrum of solution containing $5.3.10^{-4}$M DMDOHEMA, $2.7.10^{-4}$M HDEHP, 2.4 10^{-3}M HNO_3 and $2.7.10^{-4}$M of ^{241}Am in ethanol.

D. CONCLUSION

The extracting properties of the DMDOHEMA-HDEHP mixture have been studied with different conditions. The characterization of the organic phase without metal indicates an effect of HDEHP on the water extraction of the mixture but no effect on nitric acid extraction. It leads to a significant increase of the water extraction as soon as the amount of HDEHP is higher than 0.01M. This effect could be attributed to a possible modification of the supramolecular organization of the organic solution. Moreover, HDEHP induces a change of the value of the slope of D_M *vs*. malonamide concentration that could suggest a change in the cation environment.
The ESI-MS has been used to investigate Am and Eu complexes with the DMDOHEMA-HDEHP mixture. When the two extractants are present in the organic phase, mixed 'Metal-diamide-dialkylphosphoric acid' species are observed, whatever the acidity of the aqueous phase and even at low HDEHP concentrations.

In order to extend the study of the synergistic effect in acidic media and the antagonistic effect in low acidity, Eu and Am extractions will be performed. Further studies will then be focused on three different axes:

- coordination sphere of mixed Eu complexes with Time-Resolved Lazer-Induced Fluorescence Spectrometry and ^{17}O NMR;
- interaction between DMDOHEMA and HDEHP with low temperature NMR and calorimetry;
- supramolecular organization of the organic solutions.

References

1. P. Baron, X. Heres, M. Lecomte and M. Masson, *Proceedings of International Conference on Back-End of the Fuel Cycle : From Research to Solutions, Global 2001*, Paris, France (2001).

2. X. Hérès, C. Nicol, I. Bisel, P. Baron and L. Ramain, *Proceedings of the International Conference on Future Nuclear Systems, Global'99: Nuclear Technology - Bridging the Millennia*, 585-591, Jackson Hole, WY, USA (1999)

3. Y. Meridiano, L. Berthon, X. Crozes, C. Sorel, P. Dannus, M. R. Antonio, R. Chiarizia, and T. Zemb, "Aggregation in Organic Solutions of Malonamides: Consequences for Water Extraction", *Solvent Extraction and Ion Exchange*, 27, *5*, 607-637(2009).

4. M. R. Antonio, R. Chiarizia, B. Gannaz, L. Berthon, N. Zorz, C. Hill and G. Cote, "Aggregation in Solvent Extraction Systems Containing a Malonamide, a Dialkylphosphoric Acid and their Mixtures", *Separation Science and Technology*, 43, 2572-2605 (2008).

5. B. Gannaz, "Spéciations moléculaire et supramoléculaire de systèmes d'extraction liquide-liquide à base de malonamide et/ou d'acides dialkylphosphoriques pour la séparation An(III)/Ln(III)", *CEA Report R-6159* (2006).

6. M. P. Jensen, R. Chiarizia, V. Urban, "Investigation of the aggregation of the neodymium complexes of dialkylphosphoric, -oxothiophosphinic and –dithiophosphinic acids in toluene", *Solvent Extraction and Ion Exchange*, 19, *5*, 865-884 (2001).

7. B. Gannaz, R. Chiarizia, M. R. Antonio, C. Hill and G. Cote, "Extraction of Lanthanides(III) and Am(III) by Mixtures of Malonamide and Dialkylphosphoric Acid", *Solvent Extraction and Ion Exchange*, 25, 313 (2007).

8. E. Leclerc, D. Guillaumont, P. Guilbaud, L. Berthon, "Mass spectrometry and theoretical investigation of di-alkylphosphoric acid-lanthanide complexes", *Radiochimica Acta*, 96, 85-92 (2008).

9. J. M. Daniel, S. D. Friess, S. Rajagopalan, S. Wendt, R. Zenobi, "Quantitative determination of noncovalent binding interactions using soft ionization mass spectrometry", *Int. J. of Mass Spectr*., 216, 1-27 (2002).

10. V. B. Di Marco, G. G. Bombi, Electrospray mass spectrometry (ESI-MS) in the study of metal-extractant solution equilibria", *Mass Spectr. Rev*, 25, 347-379 (2006).

1-cycle SANEX process development studies performed at Forschungszentrum Jülich

Andreas Wilden, Michal Sypula, Christian Schreinemachers, Paul Kluxen, Giuseppe Modolo
Institut für Energieforschung, Sicherheitsforschung und Reaktortechnik (IEF-6)
Forschungszentrum Jülich GmbH, 52425 Jülich, Germany
Tel: +49(0)2461613965, Fax: +49(0)2461612450
e-mail: a.wilden@fz-juelich.de

Abstract *– In the framework of our research activities related to the partitioning of spent nuclear fuel solutions, the direct selective extraction of trivalent actinides from a simulated PUREX raffinate solution (1-cycle SANEX) was studied using a mixture of $CyMe_4BTBP$ and TODGA. The solvent showed a high selectivity for trivalent actinides with a high lanthanide separation factor. However the coextraction of some fission products, such as Cu, Ni, Zr, Mo, Pd, Ag and Cd was observed. The extraction of Zr and Mo could be suppressed using oxalic acid but the use of the well-known Pd complexant HEDTA was unsuccessful. During screening experiments with different amino acids, the sulphur-bearing amino acid L-Cysteine showed good complexation of Pd and prevented its extraction into the organic phase without influencing the extraction of trivalent actinides. A strategy for a single-cycle process is proposed within this paper.*

A. INTRODUCTION

The development of new and innovative processes for the processing of spent nuclear fuel solutions is a very intensively studied topic in nuclear research all over the world [1, 2]. As the liquid aqueous waste solution from reprocessing contains approx. 40 different elements in concentrations ranging from a few milligrams up to several grams per litre, the selective separation of trivalent actinides from this multi-element solution is one of the most challenging problems. The separation of the trivalent actinides from the lanthanides is a particularly difficult step, as the two groups of f-elements have very similar physical and chemical properties.
In Europe, the DIAMEX-SANEX (DIAmide EXtraction - Selective ActiNide EXtraction) partitioning process is one of the most promising strategies, which is foreseen to be converted from lab scale to industrial scale. The first step of this process (DIAMEX) uses a diamide extractant to coextract lanthanides and minor actinides from the highly acidic PUREX raffinate [3, 4]. In the subsequent step (SANEX), the trivalent actinides are separated from the lanthanides e.g. by the highly selective $CyMe_4BTBP$ extractant [5, 6]. A drawback of such a process design is the need for two separate processes using two different ligands. Within the current European project ACSEPT (Actinide reCycling by SEParation and Transmutation), a new process design is envisaged, the so-called "innovative SANEX" concept. In this strategy, the trivalent actinides and lanthanides are coextracted in a DIAMEX-type process. Then, the loaded solvent is subjected to several stripping steps. The first one concerns selectively stripping the trivalent actinides with selective water-soluble ligands followed by the subsequent stripping of trivalent lanthanides [7].
A more challenging route studied within this paper is the direct actinide (III) separation from the PUREX raffinate using a mixture of $CyMe_4BTBP$ and TODGA (structures shown in Figure 1) as extractants, the so-called 1-cycle SANEX process. A single process directly using the PUREX raffinate would reduce the number of cycles, thus saving the DIAMEX process, making the complete advanced reprocessing process more economical and easier.

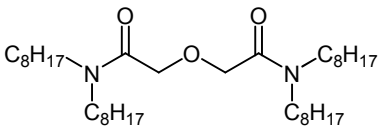

TODGA
N,N,N',N'-tetraoctyl-
diglycolamide

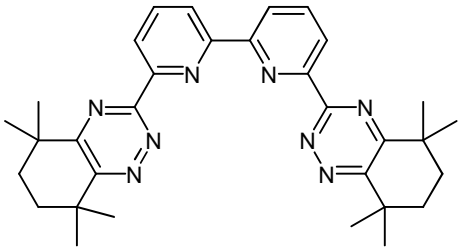

CyMe$_4$BTBP
6,6'-Bis(5,5,8,8-tetramethyl-
5,6,7,8-tetrahydrobenzo[1,2,4]-triazin-3-yl)-
[2,2']-bipyridine

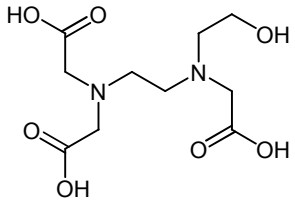

HEDTA
N-(2-Hydroxyethyl)-ethylendiamin-
N,N',N'-triacetic acid

Figure 1: Structures of TODGA, CyMe$_4$BTBP and HEDTA

Geist et al. have shown the CyMe$_4$BTBP molecule to be a very selective extractant for the separation of actinides from lanthanides [8]. Magnusson et al. demonstrated the performance of CyMe$_4$BTBP in a hot SANEX test using 0.25 mol/L of the malonamide DMDOHEMA as phase transfer catalyst [5]. The use of a phase transfer catalyst is necessary owing to the slow kinetics of the CyMe$_4$BTBP-molecule which can be significantly improved by the use of DMDOHEMA. Modolo et al. recently proposed that 0.25 mol/L DMDOHEMA can be substituted with 0.005 mol/L TODGA [9]. This system shows comparably good extraction properties and kinetic behaviour compared to DMDOHEMA, and the performance of the system was demonstrated in a spiked test. Both experiments used a DIAMEX raffinate solution containing actinides and lanthanides as a SANEX feed solution for the experiments. After a 20-stage counter-current process, an actinide product fraction containing >99.9% of the actinides with less than 0.1% lanthanides was obtained. Despite these very successful tests, the question arose as to whether it would be possible to directly and selectively extract the actinides from a PUREX raffinate solution leaving the lanthanides and the other fission products in the aqueous phase.

B. RESULTS AND DISCUSSION

B.1. Extraction from simulated HAR solution

Batch extraction studies were carried out with a synthetic PUREX raffinate. An organic phase consisting of 0.015 mol/L CyMe$_4$BTBP and 0.005 mol/L TODGA diluted in a mixture of TPH and 1-Octanol (40/60 v/v) was used as extractant. The composition of the synthetic PUREX raffinate solution and the corresponding distribution ratios of the elements for the extraction without adding any complexants are given in Table 1 (see column 3).

These preliminary results show that the direct extraction of Am and Cm from a synthetic PUREX raffinate solution is possible with good extraction of the actinides and a high separation factor of Am/Eu of 68. However, some non-lanthanide fission products were coextracted with the actinides, namely Zr, Ag, Cd, Mo, Ni, Cu and Pd. Zirconium and molybdenum play a major role, because their concentration in the PUREX raffinate solution is very high (1071 and 678 mg/L, respectively). Even a relatively low distribution ratio in this case leads to a considerable loading of the organic phase, thereby reducing the free extractant concentration available for the actinide extraction. Palladium (168 mg/L) must also be considered due to the higher concentration, whereas Ag (12 mg/L), Cd (15 mg/L), Ni (40 mg/L) and Cu (19 mg/L) are contained in smaller amounts.

The coextraction of Zr, Mo and Pd is a problem that was often overcome by the use of complexing agents, namely oxalic acid and HEDTA (Figure 1) in experiments concerning the DIAMEX process [10].

Table 1 shows the results for the addition of oxalic acid. It shows that the distribution ratios of Zr and Mo are reduced significantly by oxalic acid, as expected. The extraction behaviour of Ag, Cd, Ni, Cu and Pd is not affected very much by oxalic acid and the results furthermore show that Y is extracted much better due to the lower overall loading of the organic phase.

Table 1 also shows the results for experiments with the addition of HEDTA alone, and those with a mixture of oxalic acid and HEDTA. The experiment with HEDTA alone shows that the Zr distribution ratio is approximately halved compared to the experiment without the addition of complexants, but there is no influence on the extraction of Pd. This was not expected and experiments with Pd single-element solution showed no influence of the HEDTA concentration on the extraction of Pd. The experiment with a mixture of oxalic acid and HEDTA shows that the addition of HEDTA is not advantageous compared to the experiment with oxalic acid alone and that the use of HEDTA can be omitted.

Table 1: The extraction of actinides and fission products from a simulated PUREX raffinate with $CyMe_4BTBP$/TODGA

Element	Concentration [mg/L or as shown]	Without complexant	$C_2H_2O_4$	HEDTA	$C_2H_2O_4$ + HEDTA
		Distribution ratio			
^{241}Am	trace amounts	10.8	9.1	14.8	9.4
^{244}Cm	trace amounts	4.3	3.6	6.1	3.8
Y	90	0.04	0.85	0.15	0.73
La	239	<0.01	0.02	0.01	0.01
Ce	567	<0.01	0.03	0.01	0.02
Pr	223	0.01	0.04	0.02	0.03
Nd	718	0.02	0.06	0.04	0.05
Sm	149	0.07	0.14	0.10	0.13
Eu	34	0.16	0.24	0.14	0.25
^{152}Eu	trace amounts	0.06	0.22	0.10	0.20
Gd	51	0.08	0.17	0.08	0.15
Ni	40	30.0	18.4	32.1	37.3
Cu	19	4.88	15.7	19.1	5.60
Zr	1071	0.50	0.01	0.23	0.01
Mo	678	2.57	0.21	3.76	0.18
Pd	168	6.19	8.81	6.63	4.69
Ag	12	0.88	2.48	3.59	0.51
Cd	15	12.3	6.92	14.2	4.03
Cr	93	0.02	0.03	0.03	0.04
Sn	11	0.12	0.31	0.46	0.05
Sb	4.6	0.12	0.07	0.09	0.08
Rb	63	0.08	0.10	0.11	0.09
Ru	356	0.09	0.07	0.10	0.05
Rh	73	<0.01	<0.01	<0.01	<0.01
Te	165	0.03	<0.01	0.01	<0.01
Sr	177	<0.01	<0.01	0.01	<0.01
Ba	259	<0.01	<0.01	<0.01	<0.01
Cs	542	<0.01	<0.01	<0.01	<0.01
Al	2	n.d.	n.d.	n.d.	n.d.
Fe	1900	n.d.	n.d.	n.d.	n.d.
Se	10	n.d.	n.d.	n.d.	n.d.
Na	1600	n.d.	n.d.	n.d.	n.d.
HNO_3	3.2 mol/L				

n.d.: not determined

Organic Phase: 0.015 mol/L $CyMe_4BTBP$, 0.005 mol/L TODGA in TPH/1-Octanol = 40/60 (not pre-equilibrated with nitric acid)

Aqueous Phase: 3.2 mol/L HNO_3, solution with HAR elements, complexants as given in the table + tracers (^{241}Am, ^{244}Cm, ^{152}Eu), mixing time: 15 min.; T = 22°C ± 1°

B.2.Screening of different amino acids as masking agents for Pd

The aim of this work was to find a suitable masking agent for Pd. A number of amino acids and some amino acid derivatives were therefore tested for their influence on the Pd distribution ratio, together with ^{241}Am and ^{152}Eu. An overview of the tested complexants is shown in Figure 2. Amino acids were chosen because of their relatively complex coordination chemistry due to the presence of different donor atoms (O, N, S) in diverse structural constitutions thus allowing different chelate ring sizes, and because of their well solubility in aqueous solutions.
They were all tested in two concentrations, 0.1 and 0.2 mol/L. The results of the test with 0.1 mol/L amino acid are shown in Figure 3. The results of the test with 0.2 mol/L amino acid show a similar behaviour and therefore are not shown.

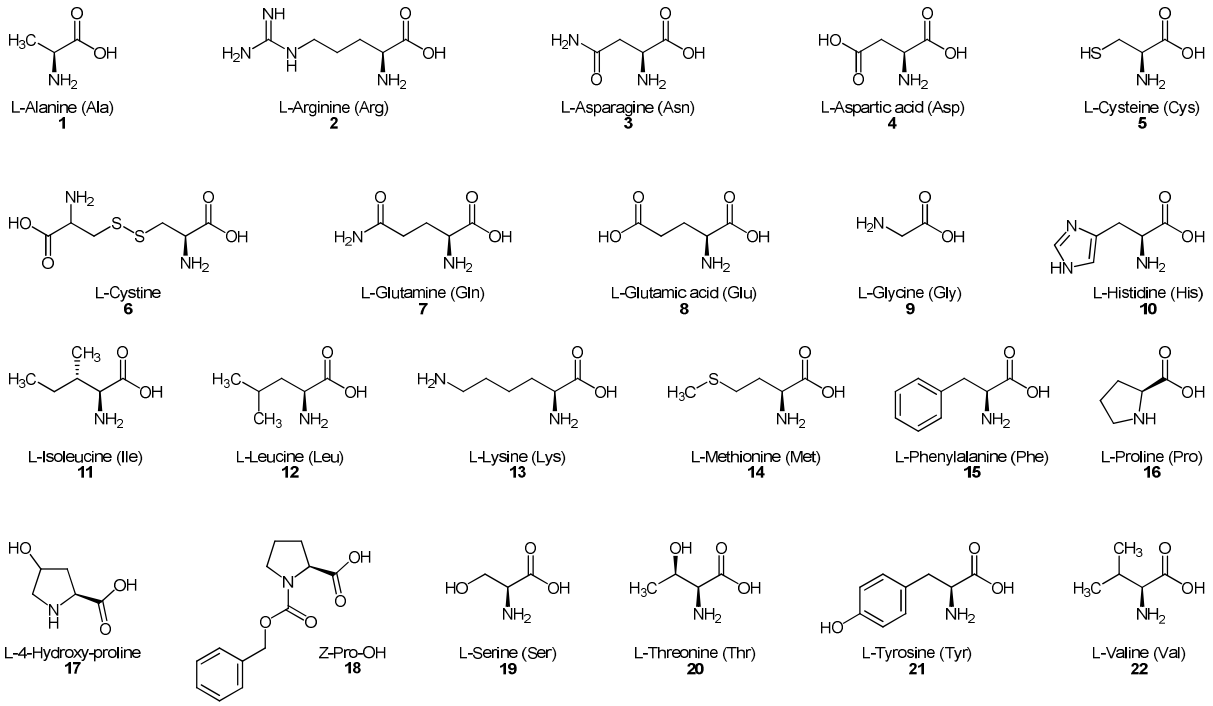

Figure 2: Overview of the tested amino acids and derivatives

Just two of the 22 tested amino acids showed a significant influence on the distribution ratio of Pd: L-Cysteine **5** and L-Cystine **6** (structures are shown in Figure 2). The Pd distribution ratios are reduced considerably and reach values below 1. Furthermore, they had no influence on the extraction of Am(III) and Eu(III). The distribution ratios of Am(III) and Eu(III), as well as the separation factor, remained unchanged. L-Cysteine was chosen for further studies, because of the structural similarity of the two molecules. L-Cystine is a dimer of two L-Cysteine molecules.

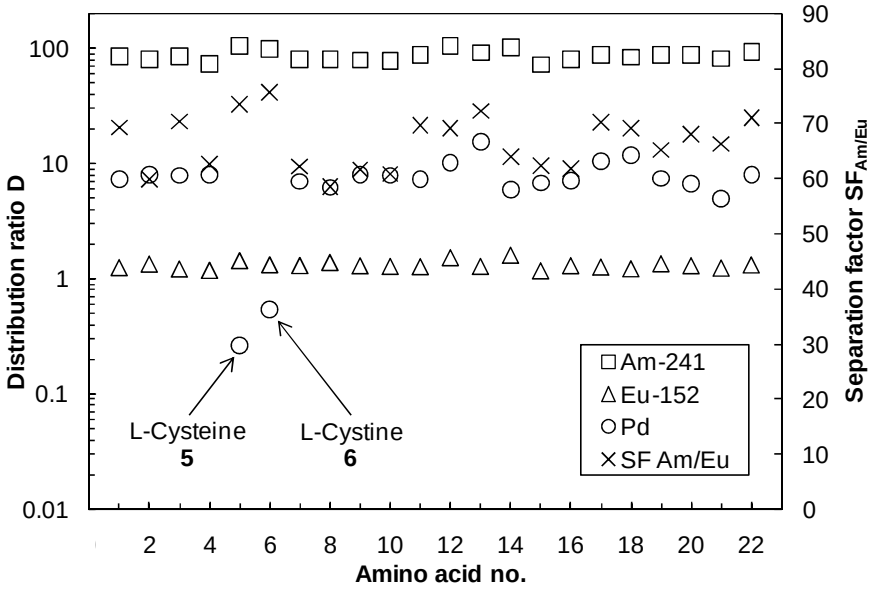

Organic Phase: 0.015 mol/L $CyMe_4BTBP$ + 0.005 mol/L TODGA in TPH/1-Octanol = 40/60 (not pre-equilibrated with nitric acid)

Aqueous Phase: 3 mol/L HNO_3, 150 mg/L Pd (0.0015 mol/L), 0.1 mol/L of different amino acids + tracers (^{241}Am, ^{152}Eu, ^{244}Cm, ^{252}Cf), mixing time: 15 min.; T = 22°C ± 1°C

Figure 3: Amino acid screening

B.3. Experiments with simulated HAR solution

The 1-cycle SANEX process is intended to be used to separate the minor actinides from a PUREX-raffinate solution. To test the new complexant under process relevant conditions a simulated PUREX-raffinate solution had been prepared with the composition shown in Table 1.
In the following batch experiments, a process-like extraction series was used. The composition of the aqueous phases is shown in Table 2. In the first step, the extraction step, 4 mL of the simulated PUREX-raffinate solution were contacted for 15 min. with 4 mL of a freshly prepared organic phase with the same composition as in the previous experiments (0.015 mol/L $CyMe_4BTBP$ + 0.005 mol/L TODGA in TPH/1-Octanol = 40/60). After phase separation, aliquots of each phase were taken for analysis and 3.0 mL of the remaining organic phase were contacted with 3.0 mL of a freshly prepared aqueous phase (Scrub I). Again after phase separation, aliquots of each phase were taken for analysis and 2.0 mL of the remaining organic phase were contacted with 2.0 mL of a freshly prepared aqueous phase (Scrub II). In the last step, called Strip, 1.0 mL of the separated organic phase was contacted with 1.0 mL of a freshly prepared aqueous phase.

Table 2: Composition of the aqueous phases used in the first experiment

	Step 1: Ex	Step 2: Scrub I	Step 3: Scrub II	Step 4: Strip
c(HNO_3) / mol/L	3.2	1.0	1.0	0.01
c(oxalic acid) / mol/L	0.3	0.2		
c(L-Cysteine) / mol/L	0.05	0.05		

During this first extraction experiment, L-Cysteine caused a voluminous precipitation, which is unwanted in a counter-current process. Therefore, the extraction series was altered as shown in Table 3. The experiment was conducted as described above.

Table 3: Composition of the aqueous phases used in the second experiment

	Step 1: Ex	Step 2: Scrub I	Step 3: Scrub II	Step 4: Strip
c(HNO_3) / mol/L	3.2	1.0	1.0	0.01
c(oxalic acid) / mol/L	0.3	0.2		
c(L-Cysteine) / mol/L			0.01	

During this experiment, no precipitate formed and no third phase formation was observed. Figure 4 shows that americium and curium are well extracted and that they stay in the organic phase during the washing steps. In the last step (Strip), they were back extracted into the aqueous phase. The trivalent lanthanides were not extracted well (with the highest distribution ratios for Europium) and therefore a high separation between the trivalent lanthanides and the actinides was achieved. The good back-extraction behaviour of the $CyMe_4BTBP$ system is advantageous for the development of a reversible process with recycling of the organic phase which could be reused after a possible solvent treatment.

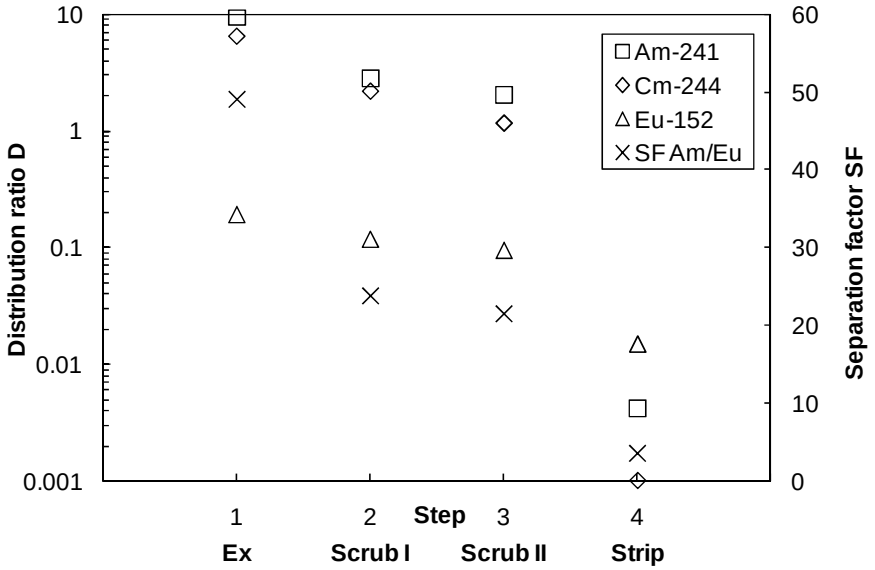

Organic Phase: Ex: 0.015 mol/L $CyMe_4BTBP$, 0.005 mol/L TODGA in TPH/1-Octanol = 40/60 (not pre-equilibrated with nitric acid; in the other steps, the loaded phase from the preceding step was used

Aqueous Phase: as shown in Table 3.

Figure 4: Distribution ratios and separation factor of ^{241}Am, ^{244}Cm and ^{152}Eu in a simulated four-step process using HAR simulate solution

Figure 5 shows the results from ICP-MS analysis for some selected inactive elements. In this figure, the concentration of the elements in the organic phase is depicted instead of the distribution ratio because the D-values of copper and nickel could not be determined due to their low concentration in the aqueous phase. The results show that copper and nickel are nearly completely extracted and that they stay in the organic phase during the whole experiment. They could possibly be scrubbed in an alkaline solvent treatment, but this topic was not investigated during this work. The extraction of zirconium and molybdenum was prevented by the use of oxalic acid and yttrium was scrubbed during the first two steps. Furthermore, the results show that palladium and silver were effectively scrubbed from the organic phase in the third step, the section with L-Cysteine addition.

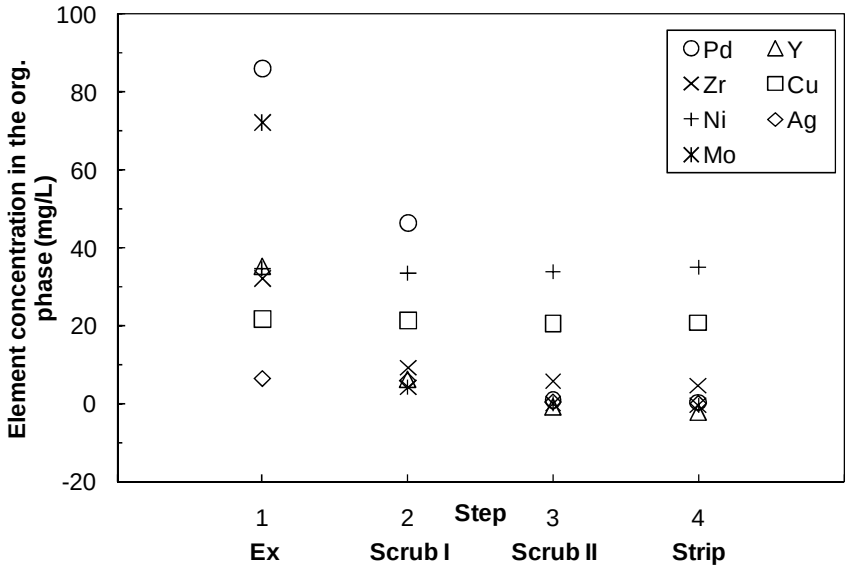

Organic Phase: Ex: 0.015 mol/L $CyMe_4BTBP$, 0.005 mol/L TODGA in TPH/1-Octanol = 40/60 (not pre-equilibrated with nitric acid; in the other steps, the loaded phase from the preceding step was used

Aqueous Phase: as shown in Table 3.

Figure 5: Organic phase concentration of some stable elements as determined by ICP-MS in a simulated four-step process using HAR simulate solution

C. CONCLUSION

In this work, it was shown that the direct and selective extraction of trivalent actinides from a synthetic PUREX raffinate solution as 1-cycle SANEX seems to be possible. Distribution ratios for trivalent actinides and the separation factor from the trivalent lanthanides were high. Nonetheless the reported system suffered from the coextraction of some of the non-lanthanide fission product elements. The extraction of the most abundant fission products Zr and Mo was suppressed satisfactorily by the use of oxalic acid. The extraction of the other elements was not influenced by the use of oxalic acid or HEDTA.

22 amino acids and derivatives were tested and L-Cysteine showed good complexation behaviour of Pd, without influencing the extraction of trivalent actinides. In a process-like extraction series, the practicability of the use of L-Cysteine as complexant for Pd and Ag was shown.

The high distribution ratios of Ni and Cu could be problematic for a continuous working industrial process. As the elements are not stripped back to the aqueous phase, they could possibly accumulate in the solvent and thereby disrupt the extraction process. More investigations have to be done to examine possible stripping conditions for the stripping of these elements. A possible solvent cleanup step has to be developed for the design of an industrial process.

Acknowledgements

Financial support for this research was provided by the European Commission (project ACSEPT – Contract No. FP7-CP-2007-211 267). M. R. S. Foreman, University of Reading, is greatly acknowledged for providing $CyMe_4BTBP$.

References

1. M. Nilsson and K. L. Nash, "Review Article: A Review of the Development and Operational Characteristics of the TALSPEAK Process," *Solvent Extr. Ion Exch.*, 25, *6,* 665-701 (2007).

2. C. Ekberg, A. Fermvik, T. Retegan, G. Skarnemark, M. R. S. Foreman, M. J. Hudson, S. Englund and M. Nilsson, "An overview and historical look back at the solvent extraction using nitrogen donor ligands to extract and separate An(III) from Ln(III)," *Radiochim. Acta*, 96, *4-5 EUROPART,* 225-233 (2008).

3. O. Courson, M. Lebrun, R. Malmbeck, G. Pagliosa, K. Romer, B. Satmark and J. P. Glatz, "Partitioning of minor actinides from HLLW using the DIAMEX process. Part 1 - Demonstration of extraction performances and hydraulic behaviour of the solvent in a continuous process," *Radiochim. Acta*, 88, *12,* 857-863 (2000).

4. R. Malmbeck, O. Courson, G. Pagliosa, K. Romer, B. Satmark, J. P. Glatz and P. Baron, "Partitioning of minor actinides from HLLW using the DIAMEX process. Part 2 - "Hot" continuous counter-current experiment," *Radiochim. Acta*, 88, *12,* 865-871 (2000).

5. D. Magnusson, B. Christiansen, M. R. S. Foreman, A. Geist, J. P. Glatz, R. Malmbeck, G. Modolo, D. Serrano-Purroy and C. Sorel, "Demonstration of a SANEX Process in Centrifugal Contactors using the CyMe4-BTBP Molecule on a Genuine Fuel Solution," *Solvent Extr. Ion Exch.*, 27, *2,* 97-106 (2009).

6. D. Magnusson, B. Christiansen, J.-P. Glatz, R. Malmbeck, G. Modolo, D. Serrano-Purroy and C. Sorel, "Towards an optimized flow-sheet for a SANEX demonstration process using centrifugal contactors," *Radiochim. Acta*, 97, *3,* 155-159 (2009).

7. X. Hérès, C. Sorel, M. Miguirditchian, B. Camès, C. Hill, I. Bisel, D. Espinoux, C. Eysseric, P. Baron and B. Lorrain, "Results of recent counter-current tests on An(III)/Ln(III) separation using TODGA extractant," Proc. of the GLOBAL 2009, 9384, Paris, France (2009).

8. A. Geist, C. Hill, G. Modolo, M. R. S. J. Foreman, M. Weigl, K. Gompper, M. J. Hudson and C. Madic, "6,6'-Bis(5,5,8,8-tetramethyl-5,6,7,8-tetrahydro-benzo[1,2,4]triazin-3-yl)[2,2']bipyridine, an effective extracting agent for the separation of americium(III) and curium(III) from the lanthanides," *Solvent Extr. Ion Exch.*, 24, *4,* 463-483 (2006).

9. G. Modolo, M. Sypula, A. Geist, C. Hill, C. Sorel, R. Malmbeck, D. Magnusson and M. R. S. J. Foreman, "Development and demonstration of a new SANEX-process for actininde(III)/Lanthanide(III) separation using a mixture of CyMe4BTBP and TODGA as selective extractant," Proc. of the Tenth Information Exchange Meeting on Actinide and Fission Product Partitioning and Transmutation, Mito, Japan (2008).

10. D. Serrano-Purroy, P. Baron, B. Christiansen, R. Malmbeck, C. Sorel and J. P. Glatz, "Recovery of minor actinides from HLLW using the DIAMEX process," *Radiochim. Acta*, 93, *6,* 351-355 (2005).

Diluent effects in solvent extraction

Elin Löfström-Engdahl[1,2], Emma Aneheim[1,2], Christian Ekberg[1,2], Mark Foreman[1,2], Gunnar Skarnemark[2]
Industrial Materials Recycling[1] and Nuclear Chemistry[2]
Department of Chemical and Biological engineering
Chalmers University of technology
SE-41296 Gothenburg, Sweden

Tel: +46(0)31-7722920, elinlo@chalmers.se

ABSTRACT

The fact that the choice of organic diluent is important for a solvent extraction process goes without saying. Several factors, such as e.g. price, flash point, viscosity, polarity etc. each have their place in the planning of a solvent extraction system.
This high number of variables makes the lack of compilations concerning diluent effects to an interesting topic. Often the interest for the research concerning a specific extraction system focuses on the extractant used and the complexes built up during an extraction. The diluents used are often classical ones, even if it has been shown that choice of diluent can affect extraction as well as separation in an extraction system. An attempt to point out important steps in the understanding of diluent effects in solvent extraction is here presented. This large field is, of course, not summarized in this article, but an attempt is made to present important steps in the understanding of diluents effects in solvent extraction. Trying to make the information concerning diluent effects and applications more easily accessible this review offers a selected summarizing of literature concerning diluents effects in solvent extraction.

1. INTRODUCTION

A solvent extraction process aims to extract solutes from one liquid phase to another. This can be done in order to separate two different solutes or to purify an aqueous phase from contamination. A solvent extraction system contains two immiscible liquid phases, one **aqueous phase** and one organic liquid, the **diluent**, and one or more **solute(s)**. In addition, in most extraction systems one or more **extractant(s)** is added to the diluent to increase extraction and separation. Sometimes a phase modifier is used to prevent disturbing third phase formation. The diluent, extractant(s) and phase modifiers together make up the **solvent**.
The solute often carries a charge in the aqueous phase and is surrounded by coordinated water molecules as well as **counter ions**. If there is a need for increased separation, a **suppressing agent** can be added to the aqueous phase. A suppressing agent keeps one specific solute in the aqueous phase while other metals can be extracted [1].

A solvent extraction denotes the transfer of a solute, for example a metal, from one liquid phase into another liquid phase. In the aqueous phase the solute is surrounded by water molecules, **hydrated**, while in the organic phase it is surrounded by diluent molecules, **solvated** [2]. Often in solvent extraction a solute forms extractable complexes with a chelating agent or a ligand. When trying to solvate or hydrate a complex two aspects play a rule. First a cavity -a hole- needs to be created in the liquid where the complex is placed. When the complex is placed in the cavity it will interact with surrounding molecules. The result of an extraction of a complex is therefore a function of the two steps; the transfer from the aqueous phase, including collapsing the cavity in the aqueous phase and breaking the bounds between the water molecules and the complex and the dissolving of the complex in the organic phase. To solvate the species in the organic phase a cavity needs to be created. When placing the complex in the cavity interactions between the complex and the diluent molecules are introduced. This implies that the characteristics of a extracted species play an important role in an extraction. To summarize: the **size** of the solute or complex influences the cavity size and therefore

the extraction as well as **possibilities for the complex to interact** with water molecules as well as diluent molecules [3][4].

The commonly most important factors during an extraction are the **partition** of the solute between the phases and the **separation** between two, or more, different solutes. The extent of the extraction is given by the **distribution ratio** (the D value). The distribution ratio is the ratio between the total analytical concentrations of the solute in the organic phase divided by the total concentration of the solute in the aqueous phase [1]. The separation factor (SF) is given by the ratio of the D values of the different metals, and is defined to be >1. According to IUPAC nomenclature the separation factor is denoted α [1]. However, since solvent extraction chemists often works using ionizing radiation for easy detection of D value and separation factor, α is not often used to avoid misinterpretation as alpha-radiation. To our knowledge the denotation SF followed by an index telling the elements is commonly used. For example $SF_{Am/Eu}$ equals $D_{Americium}/D_{Europium}$.

There are five types of extraction mechanisms [5]. The first type, Class A, is the **extraction of simple inorganic compounds.** This extraction mechanism takes place when a non charged solute itself or together with a non electrolytic extractant forms an adduct which distributes between the phases. Class B is **chelation extraction.** Chelation extraction occurs when a metal ion forms a neutral complex with one or more organic anions, chelation agents. A chelating agent is bidentate and occupies several coordinating sites of the metal creating a hydrophobic extractable complex. The hydrophobicity is increased since the chelation agent replaces coordinated water molecules as well as neutralises the charge of the metal. Class C is denoted **solvate extraction** and this extraction mechanism also includes the formation of an extractable complex. The metal charge is neutralized by an anion of a salt in the aqueous phase. Some or all of the remaining coordinating water molecules are replaced by coordination with an organic solvating agent. This agent may either be in the aqueous, organic or distributed between both phases. This replacement increases the hydrophobicity of the complex and increases the extraction. Class D denotes the **extraction of ion pairs**. A common example of ion pair extraction is when a metal, M^{v+} is exchanged towards v hydrogens from a hydrophobic complex soluble in the organic phase. The metal extracts as a part of the complex.
Class E includes **all other extraction mechanisms**, for example, crown ethers. Crown ethers have a ring structure that fits an atom with a certain ionic radius, forming a hydrophobic complex.
Notice that many extractants also combine several of the mechanisms mentioned above [5][6].

2. THEORY

2.1. History

Solvent extraction has a long tradition and references exist for example in the works by Raimundus Lullus in the 15th century. However, the more systematic investigations date back to the beginning of the 19th century. One of the first scientific references concerning solvent extraction was presented by Bucholz in 1805. Bucholz extracted uranium from a nitric acid solution into ether and back-extracted it into pure water [7]. The possibility to purify and separate chemical elements from each other made the solvent extraction an interesting field for curios researchers. Between the time from Bucholz first publication and the beginning of the twentieth century some basic scientific steps were taken. For example Jungfleisch and Berthelot described the distribution factor for several organic and inorganic compounds between ether or carbon disulphide and water [8]. In 1891 Nernst proposed that if a species has the same molecular formula in the organic phase as in the aqueous phase (for example $I_{2\ org}$ and $I_{2\ aq}$ but not $I_{2\ org}$ and $I^-_{2\ aq}$) the final distribution is independent of total solute concentration. This law is called the Nernst distribution law [9]. In 1902 Morse presented the extraction constants for extractable complexes (i.e. $HgCl_2$) [10]. The need for molecules which were able to increase extraction of specific ions and thereby increase separation factors made solvent extraction an expanding research field in the 20th century. Selective extractants for analytical purpose of several elements became available during the first decades of the century. Before the 1940´ties the solvent extraction technique was primary used for analytical purposes [6].

In the 1940s and 1950s the possibilities to produce pure uranium by reprocessing irradiated nuclear materials expanded the solvent extraction technique. The first large scale industrial solvent extraction plant for uranium recovery was built in 1942 by the Mallinckrodt Chemical Co in St Louis. It used the

same method as was presented by Bucholz more than 140 years earlier. High purities were achieved and ether was used and then ether was replaced by dibutyl methanol and methylisobutylketone [11]. At the same time increased understanding and rigorous research about extractant behavior made the extractants more effective. The development of selective extractants and solvation agents made it possible to use solvent extraction in a number of chemical and metalurgical processes in the 1950s and early 1960s [11]. One important milestone in the understanding of the solvent extraction process was the discovery of the synergistic effect in a solvent extraction system. A synergistic system is a system where two different extractants cooperate and the final D value is higher than the sum of the D value for the extractants. Notice that this definition only is valid for comparable conditions [1]. The synergistic effect is obtained when using solubilising organic ligands that replace coordinated water in an extractable complex [12]. By doing so, the hydrophobicity of the complex is increased and therefore the D value increases – as in the case of chelation extraction.

2.2. Demands on Diluents and Extractants

The choice of extractant(s) and diluent are two important aspects of a successful solvent extraction operation. In many cases the aqueous phase is acidic, basic or in other ways aggressive to the diluent and the extractant. This may affect both the long term behaviour of the extraction system as well as following chemical treatment such as scrubbing or striping. Also a radioactive or otherwise ionizing environment can destroy the diluent or the extractant. Preferably the diluent as well as the extractant(s) should be completely incinerable in order to reduce waste production. Following demands are summarised by Retegan [13]

- It should contain only carbon, hydrogen, nitrogen and oxygen to be totally incinerable This is important for nuclear systems where the waste shall be reduced [14].
- It should have a high flash point and preferably a high boiling point.
- It should have a low freezing point as well as low water solubility and a low chemical transformation rate with water, extractants and solute.
- The formation of a third phase should be avoided, thus diluents should not form third phases during loading conditions.
- A diluent used in ionizing environments should be resistant towards irradiation and, if not, be regenerable.

The properties of a usable extractant have been summarized by the following, similar, sentences by Andersson [15]

- It should contain only carbon, hydrogen, nitrogen and oxygen to be totally incinerable. This important for nuclear systems were the waste shall be reduced [14].
- An extractant used in ionizing environments should preferably be stable towards irradiation,
- It should not form third phases,
- It should not be soluble in the aqueous phase, but of course in the organic phase.
- It should form extractable complexes with the solute to be separated, preferably selectively, and this extracted complex should be possible to strip in reasonable manner.

These demands make screenings of every system used in a process an important evaluation step. If the solvent (remember: solvent=diluents+extractant+modifier...) is not resistant towards the aqueous phase it is of highly interest to improve this stability. If the solvent is not resistant towards irradiation it can be an alternative to use a scavenging molecule. Examples of such molecules are nitrobenzene [16] or sulphur hexaflouride [17].

2.3. Diluent categories

Since numerous of organic diluents are used in different liquid-liquid extraction systems, several attempts to categorize them have been made. One classification scheme of liquids, including hydrocarbons as well as highly polar molecules such as water, has been described by Marcus [2]. He uses the molecules capability of forming hydrogen bonding and from this creates five classes of liquids. Class one include liquids capable of forming three-dimensional networks of strong hydrogen bonds (Water, polyamino alcohols, hydroxi acids etc.). Class two includes other liquids that have both active hydrogen atoms and acceptor atoms, but rather than three dimensional networks they prefer forming chainlike oligomers (primary alcohols, carboxylic acids, primary and secondary amines etc.). Class three includes dipolar aprotic substances. They are solvents containing molecules with acceptor atoms but no active hydrogen atoms (ethers, ketones, aldehydes etc.). Class four covers liquids composed of molecules containing active hydrogen atoms but no acceptor atoms (e.g. chloroform). Finally, class five includes liquids without hydrogen bonding capability and without donor atoms, such as hydrocarbons, carbon disulfide and carbon tetrachloride. This classification results in different outcomes relevant to solvent extraction. For example; The diluents in class 1 are highly soluble in water and could not be used as organic phase, while diluents from class 3, ketones and aldehydes, react directly with inorganic compounds, forming extractable organic complexes. One example on such extraction in absence of extractant is given by Aneheim et al [18], where cyclohexanone by itself extracts metals. Ketones and aldehydes are aprotic dipolar molecules and since they only consist of donor atoms they tend not to dimerize or self associate.

Classes of diluents used for solvent extraction purposes are aliphatic molecules e.g. hexane, aromatic ones, e.g. benzene, ketones eg. cyclohexanone and alcohols e.g. octanol. During a screening, the aliphatic diluents are often considered in order to obtain high distribution ratios, easy handling and easy manufacturing. The type of molecules is typically included in class five according to the Marcus classification. They form no hydrogen bonds. Aliphatic diluents have a low polarizablity and a low dipole moment, which makes the cohesive forces in such solvents dependent on the dispersion interactions between the molecules. These interactions are weak, which means that separation of this kind of molecules is relatively easy. The energetic cost for cavity formation -formation of the hole in the liquid where a species can be placed- is proportional to the energy needed for separating the liquid molecules. This means that liquids exclusively interacting through dispersion interactions, weak attractive interactions, contain a low energy cost for cavity formation. On the other hand, there is no permanent dipole moment in aliphatic diluents which can increase attractive interactions between the complex and the diluent. Several authors have reported that aliphatic hydrocarbons are giving the most efficient extraction systems [19][20]. Healy et al. described high water solubility in the organic phase as a decreasing factor for extraction [21]. Water solubility is low in aliphatic molecules and higher in polar molecules and in diluents having a high dielectric constant. This theory therefore correlates with the one proposed where aliphatic ones, which have a low cavity cost, increase extraction. Among the aliphatic hydrocarbons the extraction seems to decrease with increasing number of carbon atoms in the chain. Siekierski et al. explained this with the solubility of the extractant in the diluents used [20].

The aromatic molecule benzene has no dipole moment. Therefore it is not supposed to extract charged species. On the other hand benzene has a slightly enhanced dielectric constant [2]. This implies the existence of some polarisable part of the molecule. This theory has been strengthened when benzene was described as a π-electron-donor that strongly interacts with polar complexes and thereby extracts them [22].

Long chained primary alcohols are included in class two and their interaction energy as well as their solubility in water decreases with longer aliphatic chains. Several diluent screenings have been performed using alcohols, for example by Nilsson et al [23]. Nilssons results showed surprisingly that shorter aliphatic chain in the alcohol increased extraction. Nilsson et al. explained this with the higher solubility of the extractant in the diluents containing a higher concentration of OH-groups. These diluents are the alcohols having a shorter aliphatic chain [16].

The consensus was for a long time that non polar diluents were the most effective for extraction efficiency explained by the small cost for cavity forming. However, when trying different combinations of extractants and diluents the opposite of this behaviour was observed. For example, Jaber et al. [24] tried surface active agents, such as polyethylene glycol (PEG), in combination with picrate acid for extraction. Surprisingly, this test indicated that diluents having a high dielectric constant, including high dipolarity and high water solubility [25][26], enhanced the extraction. This effect were explained by stabilizing of the helix formed complex by high dielectric medium as well as high solubility of the picrate anions in such diluent. Also the BTBP molecules show higher extraction into polar diluents [16]. The mentioned studies i.e. [24][16] are examples where the energetic cost for cavity formation is less important, since interactions with the diluent makes the extraction more favourable into medium having a higher dielectric constant. This shows that the nature of the diluent plays an important role in an extraction and that possibility to interact with the diluent is sometimes more important for enhanced extraction of a species than low energetic cost for cavity formation

2.4. Attempts to describe diluent interactions

The understanding of energy cost for cavity formation as an important aspect in the outcome of an extraction was early understood -as described by Taube et al and Marcus-. Therefore Hildebrandt and Scott developed a way of predicting the cohesive energies in a solution using the heat of vaporisation and summarized it in 1970 [27]. The cohesive energy density, c, is related to the heat of vaporisation of a liquid and valid for organic as well as aqueous phases in solvent extraction:

$$c = \frac{\Delta H_{vap} - RT}{V_m} \tag{2.1}$$

where ΔH_{vap} is the heat of vaporisation per mole, R is the gas constant, T is the temperature and V_m is the molar volume. The heat of vaporisation of a liquid is the energy required to separate the molecules in a liquid from each other, turning the liquid into a vapour. This energy can be translated as the amount of energy that holds the molecules together. Thus the Hildebrand solubility parameter is based on the assumption that the same intermolecular attractive forces have to be overcome to vaporise a liquid as to dissolve a solute in it:

$$\delta = \left[\frac{\Delta H_{vap} - RT}{V_m} \right]^{1/2} \tag{2.2}$$

the energy for cavity formation is given by

$$\Delta G_{Cav} = A_{Cav} V_B \delta_A^2 \tag{2.3}$$

where A_{cav} is the proportionality coefficient, V_B is the molar volume of the solute B and δ is the Hildebrandt solubility parameter for the diluent A. From this formula it is easily understood that the size of the complex influences the solvation.

With the basis in the theory concerning solubility parameters and by proposing the solubility parameters being a vector, composed of hydrogen bonding, polar interactions and dispersion interactions, Hansen et al. developed the Hansen solubility parameter. The result was successfully used for predicting the solubility of polymers and resins in solvents and plasticizers [28]. The Hansen parameter divides the Hildebrandt parameter in three parts, which corresponds to hydrogen interactions, dipole-induced dipole interactions and dispersion interactions.

$$\delta^2 = \delta_{Hydrogen}^2 + \delta_{Dipole}^2 + \delta_{Dispersion}^2 \tag{2.4}$$

The energy for a hydrogen interaction can be calculated from the typical energy value for a hydrogen bond. The dispersion interaction can be interpreted by using a homomorph of the molecule. A homomorph is a molecule as similar as possible to the interesting one, but in total absence of permanent dipole moments. By measuring the interactions for the homomorph solution the dispersion part of the Hansen parameter can be estimated. The value of a hydrogen bonding can be estimated from data given from IR spectroscopy

,

$$\delta^2_{Hydrogen} = \frac{20900N}{Vm} \tag{2.5}$$

where V_m is the molar volume and N is the number of hydrogen bonds. Böttcher et al. [29] have described a way of estimating dipole-dipole interactions. This estimation is given by

$$\delta^2_{Dipole} = \frac{12108}{V_m^2} \cdot \frac{\varepsilon_0\varepsilon - 1}{2\varepsilon_0\varepsilon + n_D^2} \cdot (n_D^2 + 2)\mu^2 \tag{2.6}$$

where ε is the dielectric constant of the medium, ε_0 is the dielectric constant for vacuum, n_D is the index of refraction for the sodium–D line, μ is the dipole moment of a single molecule and finally V_m is the molar volume.In order to increase the applicability of the Hansen parameter it has been further developed. One example is given by Wingefors et al [30].

The interactions between a species and a surrounding diluent are commonly coupled to the Gibbs free energy of solvation. In order to summarize the cavity cost and the gaining in interaction energy between the solute/complex and surrounding molecules, aqueous as well as diluent molecules, Kamlet and Taft developed the solvatochromic parameters for a number of elements. Such constants concerning numbers of diluents can be found in tables, diagrams etc. For example Kamlet and Taft, 1983 and Marcus, 2004 [31][2]. The free energy change for solvation of a solute is given by [2]

$$\Delta_{Solv}G^o_B = A_0 + A_\pi\pi^* + A_\alpha\alpha + A_\beta\beta + A_\delta\delta^2 \tag{2 .7}$$

where α is the hydrogen bonding donation parameter for the diluent, β is the hydrogen bonding acceptance parameter for the diluent and π is the polarity or polarizability parameter for the diluent. A is the characterized parameters for the solute. The first two terms shows the dispersion interactions, while the second two shows hydrogen interaction and the last term show the cavity cost.. By comparing the free energy for solvation in the organic phase with the free energy for solvation in the organic phase the extraction can be predicted. The common problem using this calculation is the lack of information concerning the nature of the complex and therefore the lack of parameters concerning the complex. Quantifying parameters for several complexes are highly time consuming, hence this equation is not commonly used for predicting extraction outcome. A regular diluent screening is often less time consuming and less expensive.

CONCLUSIONS

The summarized parameters affecting the outcome of an extraction can be summarized in the free energy for solvation in the aqueous and organic phases. In a solvation process the energy cost for cavity formation in the liquid and the energetic gain in interactions between the species and the surrounding molecules plays a role. The aqueous phase is often invariable during a solvent extraction process because of certain properties for dissolving metals or other solutes. Hence the interactions in the aqueous phase and the energy for cavity formation in the aqueous phase are not easily varied, while the diluent often can be adjusted. Therefore one important aspect to consider when designing a solvent extraction system is the nature of the diluent. The nature of the diluent influences the attractive energies between the extracted species and the organic phase as well as the energy needed for cavity formation.
Another important aspect is the nature of the extracted species which can enhance or decrease interactions with surrounding diluent. These parameters, the nature of diluent as well as nature of the extracted species, should preferably be taken into account when drawing conclusions concerning general extraction behaviour. By comparing the solvation in the aqueous phase and the organic phase the distribution of a complex can be predicted. The problem is the lack of information such as solvatochromic parameters concerning complexes and diluents.

The research today focuses on optimizing extraction system and in the absence of parameters concerning extracted complex the most reasonable thing to do so is to perform a diluent screening for novel extraction systems.

Acknowledgements

Grateful thanks to the Swedish Nuclear Fuel and Waste Management Company (SKB) and the European 7th Framework Program ACSEPT (project number: 211267) for financial support.

References

1. N. M. Rice and H. M. N. H. Irving and M. A. Leonard, Nomenclature for liquid-liquid distribution (solvent extraction*), Pure & Appl. Chem.*, 65, *11*, 2373-2396 (1993).

2. Y. Marcus: Rydberg J., Cox M., Musikas, Claude and Choppin R. Gregory, *Solvent extraction principles and practice*, chapter 2, Marcel Dekker, inc, New York (2004).

3. M. Taube, The influence of diluents polarity on the extraction of neptunium and uranium compounds to organic media, *Journal of Inorganic and Nuclear Chemistry*, Vol. 15, 171-176 (1959).

4. Y. Marcus, Solvent extraction and Ion exchange, chap. 11, Wiley-Interscience, London, (1969).

5. J. Rydberg: Rydberg J., Cox M., Musikas, Claude and Choppin R. Gregory, *Solvent extraction principles and practice*, chapter 4, Marcel Dekker, inc, New York (2004).

6. G. Skarnemark, to be published in Handbook on Nuclear Chemistry (2010).

7. Bucholz, C.F., Neues allgem*. J. der Chemie*, 4, 157 (1805).

8. Berthelot, M., Jungfleisch, *J. Ann. Chim. Phys.*, 26, 396 (1872).

9. Nernst, W., 1891*, Z. phys. Chem*., 8, 110

10. Morse, H., *Z.* Uber die dissociation der Merkurhaloide*, Phys. Chemie*, 41, 709, (1902).

11. Cox: Rydberg J., Cox M., Musikas, Claude and Choppin R. Gregory, *Solvent extraction principles and practice*, chapter 1, Marcel Dekker, inc, New York (2004).

12. W. R. Walker and N. C. LI, Metal complexes involved in solvent extraction and their role in the synergistic effect, *J. lnorg. Nucl. Chem*., 27, 411- 417 (1965).

13. T. Retegan, The Influence of Diluents and Side Groups of the Ligands on Liquid-Liquid Extraction of Actinides and Lanthanides, Thesis for the degree of licentiate, Chalmers University of Technology, Gothenburg, Sweden (2007).

14. Madic, C.; Hudson, M. J. High Level Waste Partition by means of Completely Incinerable Extractants, Final Report, European Commission Contract No. FI2W-CT91-0112, EUR 18038 (1998).

15. S. E. C. Andersson, Extraction properties of some nitrogen-containing extractants and determination of nitrate complex formation for lanthanides and selected actinide using solvent extraction, thesis for the degree of doctor, Chalmers University of Technology, Gothenburg, Sweden (2005).

16. M. Nilsson, S. Andersson, C. Ekberg, M. R. S. Foreman, M. J. Hudson, G. Skarnemark, Inhibiting radiolysis of BTP molecules by addition of nitrobenzene, *Radiochimica acta.* 94, 103-106 (2006).

17. K-D Asmus and J. H. Fendler, The reaction of sulphur hexafluoride with hydrated electrons, *The journal of physical chemistry*, 72, 12, 4285- 4289 (1968).

18. E. Aneheim, C. Ekberg, A. Fermvik, M. R. Foreman, T. Retegan, G. Skarnemark, A TBP/BTBP-based GANEX Separation Process – Part 1: Feasibility, *Accepted in Solvent extraction and Ion exchange* (2010).

19. F. Islam and H. Rahman and M. Ali, Solvent extraction separation study of Ti(IV) Fe(III) and Fe (II) from aqueous solutions with di-2-ethyl hexyl phosphoric acid in benzene, *Journal of inorganic nuclear chemistry*, 41, 217-221 (1978).

20. S. Siekierski, The influence of diluents on extraction of europium and thorium nitrates by tri-n-butylphosphate, *Journal of inorganic nuclear chemistry*, 24, 205-214 (1961).

21. T. V. Healy, synergism in the extraction of di-tri- and tetravalent metal ions-II, *J. Inorg. Nucl. Chem*, 19, 328-339 (1961).

22. Tatsuya Sekine and Teruhiko Ishii, Studies of the liquid-liquid partition systems 7. The solvent extraction of mercury chloride, bromide, iodide and thiocyanate with some organic solvents, *Bulletin of the chemical society of Japan*, Vol. 43, 2422-2429 (1970)

23. M. Nilsson, S. Andersson, C. Ekberg, M.R.S Foreman, M. J Hudson,J. Liljenzin, D. Magnusson, and G. Skarnemark, Extraction properties of 6,6´-bis-(5,6-dipentyl-[1,2,4]triazin-3-yl)-[2,2]bipyridinyl (C5-BTBP). *Solvent extraction and Ion exchange*, 24, 3, 299-318, (2005).

24. A. M. Y. Jaber, A-E Al-Naser, Liquid-Liquid extraction of some lanthanide metal ions by polyoxyalkylene systems, *Talanta*, 44, 1719-1728 (1997).

25. Organic solvents, physical properties and methods of purification 3rd edition, Riddick and Bunger, p. 356, John Wiley & Sons, Inc, New York (1970)

26. Organic solvents, physical properties and methods of purification 3rd edition, Riddick and Bunger, p. 398, John Wiley & Sons, Inc, New York (1970)

27. J. H. Hildebrand, Prausnitz, Scott, R. L. Regular and related solutions, appendix 5, Van Nostrand Reinhold Ltd, New York (1970).

28. Hansen C.M., The Three Dimensional Solubility Parameter – Key to Paint Component Affinities: I. Solvents, Plasticizers, Polymers and Resins, *Journal of Paint Technology*, vol 39, 505,104-117, (1967).

29. Böttcher C.J.F. *Theory of electric polarization*, Chapter five, Elsevier, New York (1925)

30. S. Wingefors, J-O- Liljenzin and E. Saalman, Three dimensional solubility parameters for the correlation and prediction of liquid-liquid partition constants of metal chelate complexes, *Proc. Of ISEC,* Liege, Belgium, paper 3-15A 80-116 (1980)

31. R.W Taft, J-L M. Abboud, M. J. Kamlet and M. H Abraham, Linear energy relationships 23. A comprehensive collection of the solvatochromic parameter and some methods for simplifying the generalized solvatochromic equation, *Journal of Organic chemistry*, 48, 2877-2887 (1983)

Studies on the Interaction of a Novel 6,6''-bis(1,2,4-triazin-3-yl)-2,2':6',2''-terpyridine Ligand with Lanthanide(III) Ions and Americium(III)

Frank W. Lewis,*[a] Laurence M. Harwood,*[a] Michael J. Hudson,[a] Michael G. B. Drew,[a] Giuseppe Modolo,[b] Michal Sypula,[b] Jean F. Desreux,[c] Nouri Bouslimani[c] and Geoffrey Vidick[c]

[a] *Department of Chemistry, The University of Reading, Whiteknights, Reading RG6 6AD, UK. Fax: +44 (0) 1183786121; Tel: +44 (0) 1183787417; E-mail: f.lewis@reading.ac.uk, l.m.harwood@reading.ac.uk*
[b] *Forschungszentrum Jülich GmbH, Sicherheitsforschung und Reaktortechnik, D-52425 Jülich, Germany. Tel: + 492461614896; E-mail: g.modolo@fz-juelich.de*
[c] *Coordination and Radiochemistry, University of Liège, Sart Tilman B16, B-4000 Liège, Belgium. Fax: + 3243664739; Tel: + 3243663501; E-mail: jf.desreux@ulg.ac.be*

Abstract *– The new solvent extraction reagent 6,6''-bis(5,5,8,8-tetramethyl-5,6,7,8-tetrahydro-1,2,4-benzotriazin-3-yl)-2,2':6',2''-terpyridine ($CyMe_4$-BTTP) has been synthesized in 4 steps from 2,2':6',2''-terpyridine. Detailed NMR and mass spectrometry studies indicate that the ligand forms 1:2 complexes with lanthanide(III) perchlorates where the aliphatic rings are conformationally constrained whereas 1:1 complexes are formed with lanthanide(III) nitrates where the aliphatic rings are conformationally mobile. An optimized structure of the 1:2 solution complex with Yb(III) was obtained from the relative magnitude of the induced paramagnetic shifts. X-ray crystallographic structures of the ligand and of its 1:1 complex with Y(III) were also obtained. In the absence of a phase-modifier, $CyMe_4$-BTTP in 1-octanol showed a maximum distribution coefficient of Am(III) of 0.039 (±20%) and a maximum separation factor of Am(III) over Eu(III) of 12.0 from nitric acid solution. The metal(III) cations are extracted as the 1:1 complex from nitric acid solutions. The generally low distribution coefficients observed compared with the BTBPs arise because the 1:1 complex of $CyMe_4$-BTTP is considerably less hydrophobic than the 1:2 complexes formed by the BTBPs. In $M(BTTP)^{3+}$ complexes, there is a competition between the nitrate ions and the ligand for the complexation of the metal.*

A. INTRODUCTION

Over the last three decades, research in Europe has resulted in the development of the combination of the DIAMEX and SANEX processes for the reprocessing of spent nuclear fuel produced in the PUREX process. These processes consist of the co-separation of trivalent actinides and lanthanides (DIAMEX process),[1] followed by the subsequent separation of actinide(III) from lanthanide(III) in the SANEX process.[2] If these trivalent actinides (particularly americium and curium) are removed from the waste (partitioning) and converted by neutron fission (transmutation) into shorter-lived or stable elements, the remaining waste loses most of its long-term radiotoxicity. Partitioning and transmutation are therefore considered attractive options for reducing the burden on geological waste disposal.[3]

The development of *N*-heterocyclic ligands which are capable of separating actinides from lanthanides has thus been the subject of intensive research.[4] Two classes of ligand have emerged that show both high affinities and high selectivities towards the trivalent actinides; the tridentate 2,6-bistriazinylpyridines (BTPs)[5] **1** and the quatridentate 6,6'-bistriazinyl-2,2'-bipyridines (BTBPs)[6] **2** (Figure 1). One member of the BTBP ligands ($CyMe_4$-BTBP **3**)[7] in particular has shown many of the desirable qualities (stability towards hydrolysis and relative stability towards radiolysis, reversible metal binding which allows stripping, etc) for use in an industrial separation process. Its suitability for a SANEX process has been demonstrated recently in a 'hot-partitioning demonstration test' on genuine spent fuel solution.[8] However, the stripping of the metal cation from the $CyMe_4$-BTBP complexes was rather slow.

The coordination chemistry and solvent extraction properties of the related bistriazinyl-2,2':6',2''-terpyridine (BTTP) ligands **4** with trivalent cations have not been previously studied. The

introduction of an additional pyridine ring into the BTBP framework could lead to a moderate reduction in the affinity of the ligand towards americium and therefore enhanced stripping. Herein we describe the synthesis, selective extraction and coordination chemistry of the novel ligand 6,6''-bis(5,5,8,8-tetramethyl-5,6,7,8-tetrahydro-1,2,4-benzotriazin-3-yl)-2,2':6',2''-terpyridine (CyMe$_4$-BTTP) **5**.

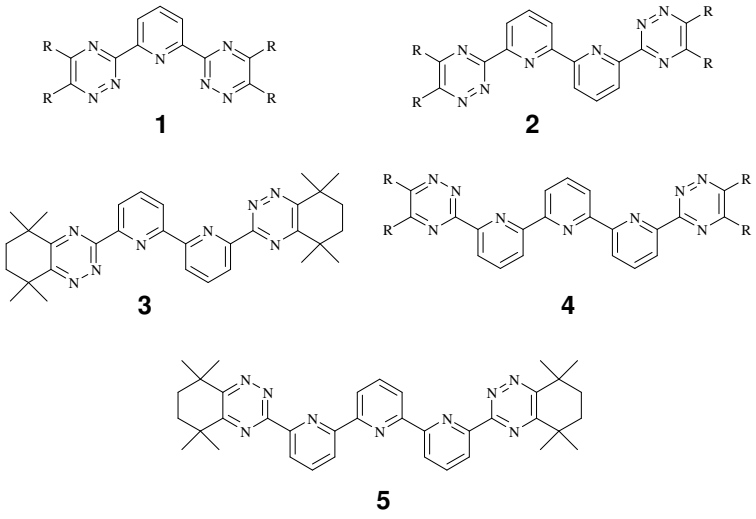

Figure 1: The structures of the BTP, BTBP and BTTP molecules.

B. RESULTS AND DISCUSSION

As an extension of our work on actinide(III)-selective organic ligands, our aim was to synthesize CyMe$_4$-BTTP **5**, which is a symmetrical molecule similar to CyMe$_4$-BTBP **3**[7] (Figure 1). The molecule **5** has two outer 1,2,4-triazinyl moieties bound to a central terpyridine core meaning that there is one additional pyridine ring compared with **3**. It was expected that the comparison between **5** and **3** would prove useful in the future design of selective actinide extractants. Moreover, the coordination chemistry of **5** has not been previously reported. Accordingly, 2,2':6',2''-terpyridine was converted in two steps to the dinitrile **6**[9] in 17% overall yield by formation of the bis-*N*-oxide [10] using *m*-CPBA, followed by a modified Reissert-Henze reaction (Scheme 1).[11] The reaction of **6** with hydrazine hydrate[12] afforded the novel dicarbohydrazonamide **7** which on treatment with 3,3,6,6-tetramethylcyclohexane-1,2-dione[13] in refluxing THF in the presence of triethylamine gave the novel bistriazinylterpyridine **5** as a yellow solid. To our knowledge, this is the first reported example of this class of ligand. Ligand **5** showed low solubility in dodecane but showed good solubility in n-octanol (up to 0.01 mol/L). The solvent extraction studies reported herein were subsequently carried out in n-octanol.

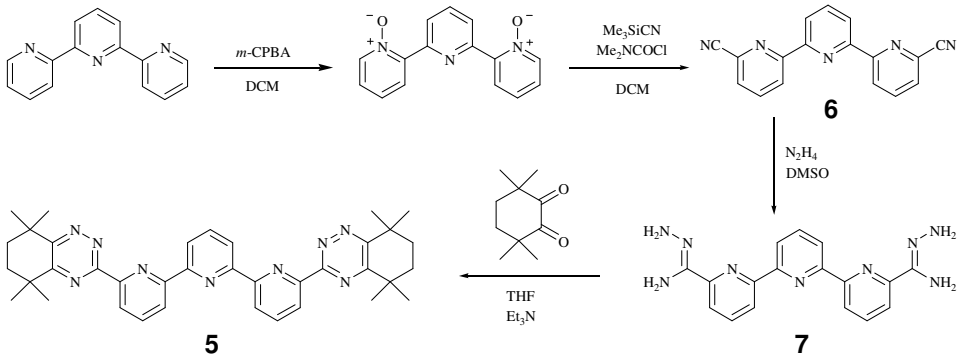

Scheme 1: Synthesis of CyMe$_4$-BTTP 5.

B.1.Solvent Extraction Studies

The distribution coefficients and the separation factors for $CyMe_4$-BTTP **5** in 1-octanol as a function of nitric acid concentration are shown in Figure 2. In the absence of a phase-modifier, the distribution coefficients for Am(III) are greater than those for Eu(III) at nitric acid concentrations of 1.0-4.0 mol dm^{-3} and reach a maximum value of 0.039 at 2.0 mol dm^{-3}. In comparison, $CyMe_4$-BTBP **3** gives a distribution coefficient of approximately 4.5 at a nitric acid concentration of 0.5 mol dm^{-3}.[7] The resulting separation factors were largely uniform over this range of nitric acid concentration increasing to a maximum of 12.0 before decreasing to 6.6 in 4.0 molar nitric acid. However, some emulsion formation was observed at all nitric acid concentrations except 4.0 molar. These results show that ligand **5** will not extract Am(III) to any significant extent regardless of nitric acid concentration (DAm < 1).

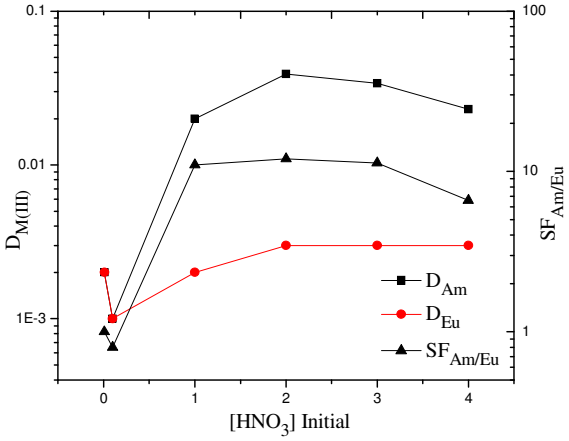

Figure 2: Extraction of Am(III) and Eu(III) by $CyMe_4$-BTTP 5 in n-octanol as a function of nitric acid concentration.

This led us to carry out the extractions in the presence of certain additives that confer a greater hydrophobicity on the extracted species. In the presence of 2-bromohexanoic acid,[14] higher distribution coefficients were obtained for both Am(III) and Eu(III) at low nitric acid concentrations but these values decreased rapidly at higher acidities. The distribution coefficients for Am(III) were greater than those for Eu(III), while the separation factors increased to a maximum value of 20.5 before decreasing sharply at higher nitric acid concentrations (Figure 3, left). This decrease at higher nitric acid concentrations is probably due to the inability of 2-bromohexanoic acid to dissociate and form a more lipophilic complex with the Am($CyMe_4$-BTTP)$^{3+}$ cation. These results indicate that an effective extraction of Am(III) is only possible at low nitric acid concentrations. Employing *N,N*-dimethyl-*N,N*-dioctyl-2-(2-hexoxyethyl) malondiamide (DMDOHEMA)[7-8,15] as a phase-modifier did not lead to any significant improvement. The maximum distribution coefficient for Am(III) observed in this case was 0.213 at 3.0 molar nitric acid while the highest separation factor observed was 10.8 in 1.0 molar nitric acid (Figure 3, right). The decrease in selectivity at higher nitric acid concentrations is presumably due to the non-selective extraction of both Am(III) and Eu(III) by DMDOHEMA itself, rather than by **5**. This reduction in selectivity in the presence of DMDOHEMA is also observed with the BTBP ligands.[6]

Whilst $CyMe_4$-BTTP **5** clearly shows some selectivity for Am(III) over Eu(III), the distribution coefficients for Am(III) were uniformly low in nitric acid concentrations of 0.01 molar and above and generally decreased with decreasing pH. The distribution coefficients for Am(III) are significantly lower than those for the BTPs and the BTBPs. $CyMe_4$-BTTP **5** is thus less effective as a selective An(III) extractant compared to the bistriazinylpyridines (BTPs) **1**[5] and the bistriazinylbipyridines (BTBPs) **2**.[6] It is likely that the lower extraction efficiency exibited by **5** is due to its inability to completely enclose the coordination sphere of the metal, leaving vacant coordination sites to which other ligands (eg: nitrate, water) can bind.

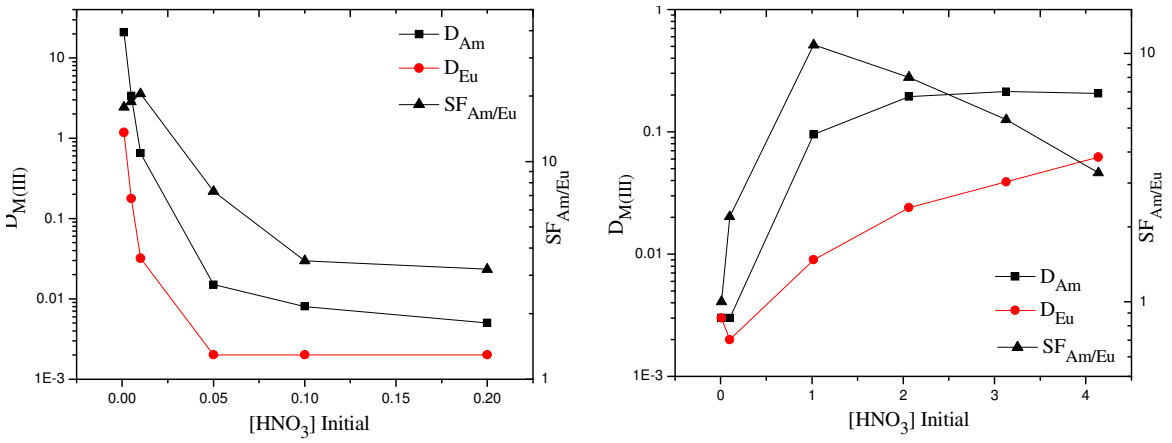

Figure 3: Left: Extraction of Am(III) and Eu(III) by $CyMe_4$-BTTP 5 + 2-bromohexanoic acid (1 mol/L) in n-octanol as a function of nitric acid concentration. Right: Extraction of Am(III) and Eu(III) by $CyMe_4$-BTTP 5 + DMDOHEMA (0.25 mol/L) in n-octanol as a function of nitric acid concentration.

B.2.Crystallography

The X-ray crystal structure of $CyMe_4$-BTTP **5** was determined and is shown in Figure 4 (left) together with the atomic numbering scheme. The five aromatic rings in $CyMe_4$-BTTP **5** are approximately planar with successive torsion angles (from left to right in Figure 5) between the aromatic rings of 19.6(1), -9.1(1), 1.5(1) and -24.7(1)°. As expected the conformation of the central pyridine ring is *trans*, *trans* from the relative positions of the pyridine nitrogen atoms. When bound to a metal, terpyridine will have the *cis*, *cis* conformation. The *trans*, *trans* conformation however is usually found when terpyridine is not chelating as the *ortho* hydrogens in adjacent rings do not clash. The conformations of the outer triazine rings show that N(11) is *trans* to N(21) and N(51) is *trans* to N(41). This is somewhat unexpected as in previous work on the BTPs **1**[5] and BTBPs **2**[6] the relative positions of adjacent triazine and pyridine rings were *cis*. However, this *cis* conformation is found when chelating to a metal, as it is N(15) and N(55) that binds rather than N(11) and N(51).

We next attempted to prepare complexes of **5** with various lanthanides by ad-mixture of DCM solutions of **5** with solutions of ln(III) nitrates in acetonitrile in both 1:1 and 2:1 ratios of ligand:metal, followed by slow evaporation over several days. However, in the case of europium, cerium and lanthanum(III) nitrate, suitable crystals were not obtained despite repeated attempts and any crystals that were obtained turned out to be of the free ligand **5** rather than the desired complexes. We then used the corresponding perchlorate salts but again suitable crystals of the complexes could not be obtained with europium, lanthanum or ytterbium(III). One notable exception however was yttrium(III) perchlorate. Its complex with **5** is shown in Figure 4 (right).

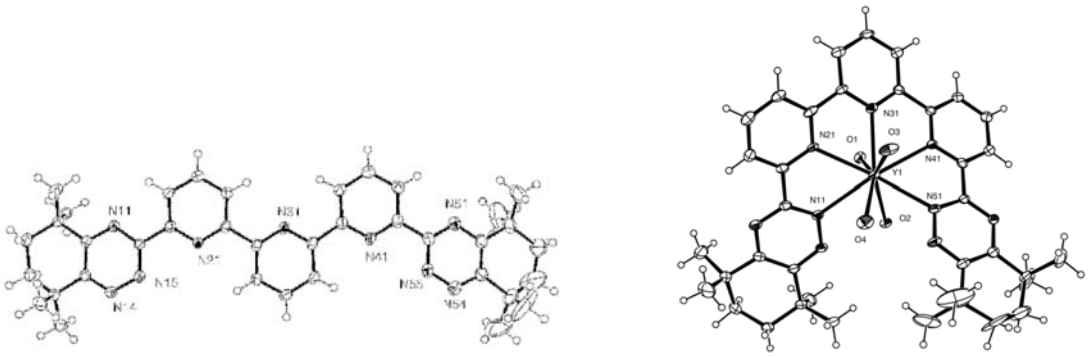

Figure 4: Left: The molecular structure in the crystal of $CyMe_4$-BTTP 5 with ellipsoids at 50% probability. Right: Y(III) complex of $CyMe_4$-BTTP 5 with ellipsoids at 50% probability. Counterions have been omitted for clarity. Hydrogen atoms on water molecules were not located and are not included.

The complex was synthesized by admixture of a DCM solution of **5** (2 equivalents) with an aqueous solution of yttrium(III) perchlorate (1 equivalent) in CH_3CN, followed by slow evaporation over several days. This afforded crystals of the complex suitable for X-ray analysis. A 1:1 complex was obtained despite two equivalents of the ligand **5** being used during the crystal growing. This may be

because the 1:1 complex packs better in the solid state than the 1:2 complex. The complex is a mononuclear helicate with all five ligand coordination sites bound to the metal in addition to four aqua ligands. The five donor nitrogen atoms form a distorted equatorial plane with deviations of 0.498(3), -0.480(4), -0.009(4), 0.503(4) and -0.512(3) respectively. The metal is -0.026(3)Å from the plane with two water molecules above and two below this plane. The helicity of the complex is indicated by sucessive N-C-C-N torsion angles (from left to right in Figure 4, right) of 8.1(9), -15.6(9), -10.5 (9) and 1.7(1)°. The five bond lengths from the metal are Y-O 2.331(5), 2.356(5), 2.378(5), 2.381(5)Å and Y-N(11) 2.614(6), Y-N(21) 2.518(6), Y-N(31) 2.504(6), Y-N(41) 2.535(6), Y-N(51) 2.584(6)Å.

B.3.Nuclear Magnetic Resonance and Theoretical Studies

Solution-phase NMR studies were undertaken in order to establish the nature of the complexed species in solution. The stoichiometry of the lanthanide complexes of $CyMe_4$-BTTP **5** was deduced form nuclear magnetic relaxation dispersion titrations with Gd(III) as shown in Figure 5.[16,17] The decrease in relaxation rate (or relaxivity) upon formation of a paramagnetic complex was used to establish its stoichiometry.[16] As solvent molecules are removed from the paramagnetic centres, their protons relax more slowly in the bulk of the solution. Relaxivity is thus decreasing and a plateau is finally reached once a complex is fully formed. This procedure has been successfully used for the BTPs **1**[16] but in the present case, the perchlorate complex precipitated once a 2:1 **5**:Gd(III) ratio was reached. The exact value of the relaxation plateau is thus uncertain but it seems clear that a 2:1 ligand:metal complex is essentially formed as we obtained a linear relaxivity decrease until this concentration ratio was reached. Similarly, a precipitate was observed once the ligand:metal ratio was between 0.8 and 1.5 in the presence of nitrate ions. This could mean that a 1:1 complex is the major species in anhydrous acetonitrile.

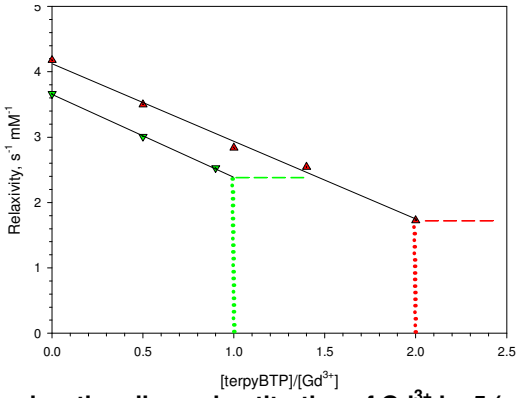

Figure 5: Nuclear magnetic relaxation dispersion titration of Gd^{3+} by 5 (anhydrous CD_3CN, 25°C); ▲: perchlorate salt, ▼: nitrate salt. Solubility limits are indicated by vertical dotted lines and relaxivity plateaux are tentatively presented as horizontal dash lines.

In view of the uncertainty of the stoichiometries of the complexes, we initiated an electrospray mass spectrometry study of the perchlorate solutions. The ES-MS spectrum of a solution of $Gd(ClO_4)_3$ with 2.5 equivalents of $CyMe_4$-BTTP **5** was recorded. Intense mass peaks were observed for the protonated free ligand and for its sodium complex together with a peak assigned to the bis-complex at m/z = 460.19. In contrast, the electrospray mass spectrum of a 1:1 mixture of **5** and $Yb(NO_3)_3$ displayed a peak at m/z = 909.27 corresponding to the 1:1 complex $[Yb(\mathbf{5})(NO_3)_2]^+$ in addition to mass peaks due to the protonated free ligand and its sodium complex. No peak corresponding to the bis-complex was observed even for 1:3 mixtures of $Yb(NO_3)_3$ and **5**.

We next recorded the ^{1}H NMR spectrum of the Eu(III) bis-complex in perchlorate medium. The Eu(III) ion is not suitable for a conformational analysis because the dipolar contribution to the paramagnetic shifts is comparable to the contact contribution, but this ion causes minimal broadening of the NMR peaks and well-resolved spectra are usually obtained.[18] A qualitative analysis of the NMR spectra is thus greatly facilitated. As shown in Figure 6, this was indeed the case for the bis-complex of **5**. As expected, the spectrum of the Eu(III) complex exhibited five resonances due to the terpyridine moiety. Surprisingly, four resonances due to the methyl groups and four resonances due to four different types of methylene protons were also observed. In contrast, the free ligand **5** and its Lu(III) complex exhibited a pair of singlets for the methyl groups and an 8-proton multiplet for the methylene protons as expected for rapidly inverting tetramethylcyclohexenyl groups. It thus seems

that the aliphatic tetramethylcyclohexenyl rings of the metal complexes are conformationally constrained on the NMR time scale used in the present work. Rapid inversion of the cyclohexenyl groups appears to be prevented by steric hindrance, a phenomenon that is readily observed for the Eu(III) complex because of the large induced paramagnetic shifts. An expanded view of the methylene resonances clearly shows the complex coupling patterns of the methylene protons. Two resonances only would be expected if the tetramethylcyclohexenyl groups were conformationally mobile. We also recorded a H-H COSY spectrum of the bis-complex with Eu(III) in order to confirm that there are indeed four types of methylene protons that are all coupled together. Crosspeaks are found for the four types of methylene protons as well as for the two groups of terpyridine protons.

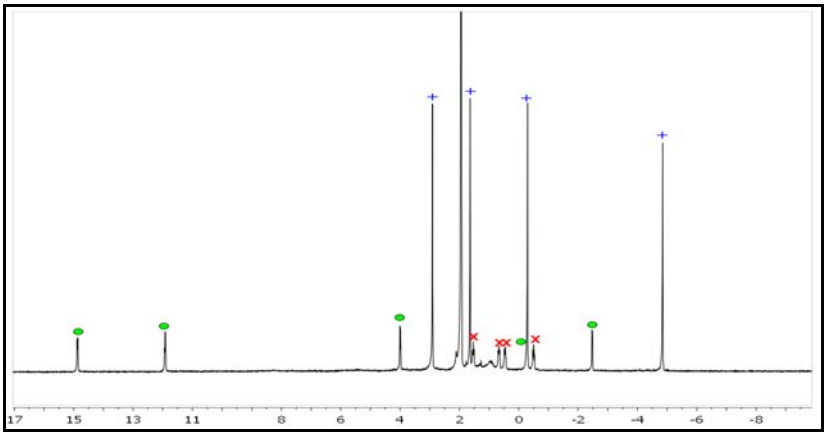

Figure 6: ^{1}H NMR spectrum of a 2:1 5:Eu(ClO$_4$)$_3$ mixture in anhydrous CD$_3$CN at 25°C. Peak assignments: *meta* and *para* protons in the central pyridine ring (●): -2.45 and -0.25 ppm; *meta* and *para* protons in the outer pyridine rings (●): 14.85, 11.90 and 4.0 ppm; methyl protons (+): 2.90, 1.53, -0.29 and -4.83 ppm; methylene protons (x): 1.53, 0.62, 0.45 and -0.50 ppm.

Figure 7 presents the ^{1}H NMR spectrum of the Yb(III) perchlorate bis-complex of **5**. There are again resonances for four different methylene protons and four different methyl groups. Coupling patterns are again observed for the four methylene peaks, an unusual feature because the NMR resonances of Yb(III) complexes are usually so broad that *J* couplings cannot be observed. The COSY spectrum clearly shows all the expected cross peaks and a ^{13}C-^{1}H HSQC correlation confirms the peak assignments and clearly shows which of the methylene peaks are due to two protons on the same carbon atom. The latter spectrum displays two ^{13}C peaks each connected with two methylene protons as expected for rigid tetramethylcyclohexenyl rings. The methylene proton coupling patterns are also in keeping with a rigid structure. No spectral changes were observed in the limited temperature range available with acetonitrile and we were thus unable to estimate the energy barrier for conformational inversion.

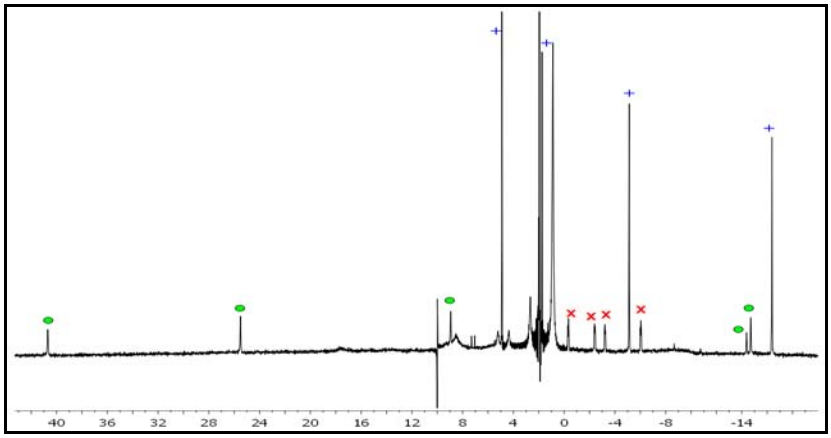

Figure 7: ^{1}H NMR spectrum of a 2:1 5:Yb(ClO$_4$)$_3$ mixture in anhydrous CD$_3$CN at 25°C. Peak assignments: *meta* and *para* protons in the central pyridine ring (●): -14.38 and -14.69 ppm; *meta* and *para* protons in the outer pyridine rings (●): 40.69, 25.51 and 8.52 ppm; methyl protons (+): 4.84, 1.83, -5.12 and -16.38 ppm; methylene protons (x): -0.32, -2.40, -3.22 and -6.04 ppm.

Yb(III) is the ideal ion for a conformational analysis as it induces essentially pure dipolar shifts.[17,19] The solution structures of its complexes can be inferred from these shifts provided the complexes under study display some form of symmetry and are conformationally rigid.[18] We thus decided to deduce the solution structure of the bis-complex of **5** from the relative magnitude of the paramagnetic shifts induced by Yb(III). A molecular model of the bis-complex was obtained starting with structures built with the Chem3D program (CambridgeSoft, MA, USA) with either two planar ligands perpendicular to each other or at an angle or with the aromatic rings in a twisted conformation so as to obtain metal-nitrogen distances close to 3 Å. All structures were optimized by a force field approach using parameters published by Cundari et al. for Gd(III) complexes.[20] Finally, full optimizations were performed using the SPARKLE Yb(III) parameter set that was proposed by Simas et al.[21] and that is included in MOPAC 2009. The minimum energy geometry with expected Yb(III)-N distances (2.41-2.43 Å) was obtained starting from the twisted arrangement.

Different views of the optimized structure are presented below in Figure 8. The structure is a mononuclear double-helicate with the metal ion at the centre of a bicapped square antiprismatic arrangement of donor atoms. Each central pyridine ring is located above the centre of a square face formed by the nitrogen atoms of the two adjacent pyridine rings and by the nitrogen atoms of two triazine units belonging to the other ligand in the bis-complex. A bicapped square-antiprismatic arrangement is the most favoured geometry when one sphere is surrounded by 10 spheres[22] and the optimized geometry of Yb(**5**)$_2^{3+}$ is in keeping with the stereochemical arrangement predicted by theory. It should also be noted that some of the aromatic rings in the ligands are slightly bowed, a feature that is often found in complexes with high coordination numbers even in phenanthroline rings.[23] A bowed arrangement of **5** is also observed in the crystal structure of [Y(**5**)$(H_2O)_4$]$(ClO_4)_3$ (Figure 4). A ligand deformation is of course detrimental to the thermodynamic stability of complexes but is probably imposed by the necessity to rearrange one or more ligands so as to completely encapsulate the metal ion. The optimised geometry of the [Yb(**5**)$_2$]$^{3+}$ complex is similar to the coil structure found for a Eu(III) homoleptic bis-complex with the terpytz ligand that was published by Giraud et al. (EFAXUF in the Cambridge Structural Database).[24] In this crystallographic structure, the metal ion occupies the centre of an irregular bicapped trigonal prismatic assembly of nitrogen atoms that is close to a square antiprismatic arrangement.

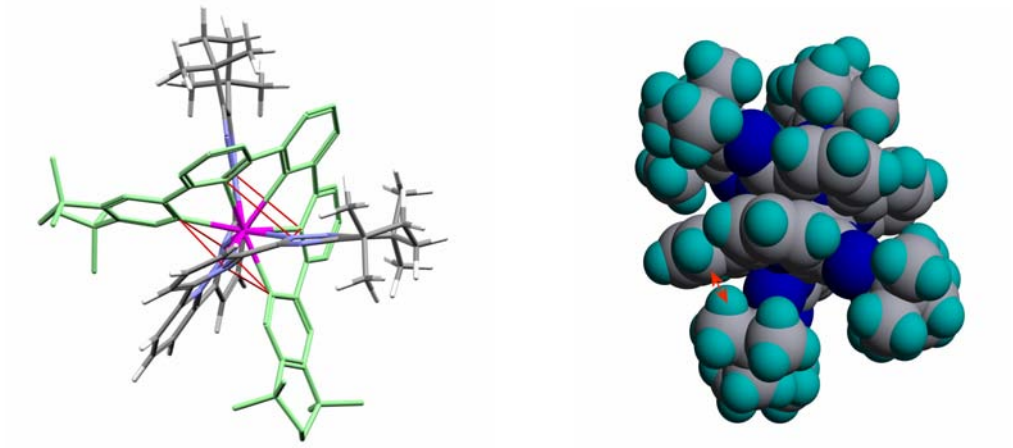

Figure 8: Optimized structure of the bis-complex Yb(5)$_2^{3+}$ complex. Left: The carbon skeleton of one ligand is coloured in green and the protons are removed for clarity. The two square faces of the square antiprism are shown in red. Right: Space-filling model of the Yb(5)$_2^{3+}$ complex. The red arrow shows one of the interatomic distances that is smaller than the sum of the van der Waals radii (2.75 instead of 3.05 Å).

The induced paramagnetic shifts δ_i were computed from the spectra of Yb(**5**)$_2^{3+}$ and of diamagnetic Lu(**5**)$_2^{3+}$ that was used as a reference. The geometric factors in Equation 1 that relate these shifts with magnetic susceptibility terms were deduced from the structure shown in Figure 11.

$$\delta_i = \frac{1}{12\pi r^3}\left[\left(\chi_{zz} - \frac{1}{2}\left(\chi_{xx} + \chi_{yy}\right)\right)\left\langle 3\cos^2\theta_i - 1\right\rangle + \left(\chi_{xx} - \chi_{yy}\right)\left\langle \sin^2\theta_i \cos 2\psi_i\right\rangle\right]$$

Equation 1.

where χ_{xx} χ_{yy} and χ_{zz} are magnetic susceptibility terms characteristic of the investigated complex and thus identical for all nuclei. The factors r_i, θ_i and φ_i are the polar coordinates of proton i giving rise to chemical shift δ_i in the set of axes of the magnetic susceptibility tensor with the metal ion at the centre. The full dipolar equation has to be used because Yb(**5**)$_2^{3+}$ is not an axially symmetric complex.[17,18] However, the orientation of the magnetic susceptibility axes is well-defined as one of them must coincide with the C_2 axis joining the two central pyridine nitrogen atoms and the metal ion. The two other magnetic susceptibility axes must be located in the plane perpendicular to the C_2 axis and must be oriented so as to obtain identical geometric factors for protons giving rise to the same NMR resonance in the two ligands. The x (or y) axis thus bisects one of the square faces of the antiprism. The magnetic susceptibility terms in Equation 1 were computed by solving a set of 13 linear equations established for the 13 resonances displayed by [Yb(**5**)$_2$]$^{3+}$ for which the geometric factors were deduced from the geometric model shown in Figure 8. An excellent correlation was obtained between the calculated and the experimental shifts as shown in Figure 10 (left) with:

$$\chi_{zz} - \frac{1}{2}\left(\chi_{xx} + \chi_{yy}\right) = (-2883 \pm 187)\ \text{A}^3 \qquad \chi_{xx} - \chi_{yy} = (2490 \pm 301)\ \text{A}^3$$

The NMR analysis fully supports the structure obtained by the force field calculations and the geometry of the bis-complex Yb(**5**)$_2^{3+}$ is thus very close to or identical to the structure shown in Figure 8 above. The ring-inversion barrier of cyclohexene is rather low (23 kJ/mol) and the aliphatic substituents on the triazine moieties of **5** were not expected to be conformationally rigid. Several inter-ligand distances involving the cyclohexenyl units are smaller than the sum of the van der Waals distances as shown in Figure 8. Altough it is partially stabilized by π-π interactions between aromatic rings, the Yb(III) bis-complex is sterically crowded and is unable to withstand the competition with other coordinating ligands as shown below in the case of the nitrate ion.

The partitioning of actinides from lanthanides is performed in nitric acid solutions and information is thus also needed on the structure of the lanthanide nitrate complex of **5**. The NMR titration data (see Figure 5) suggest that a 1:1 complex is formed in the presence of nitrate ions and the crystallographic structure of the 1:1 complex with $Y(ClO_4)_3$ has been obtained (Figure 4). One may wonder whether this structure is maintained in solution. The spectrum of a 1:1 mixture of **5**:$Yb(NO_3)_3$ in acetonitrile is presented in Figure 9. This spectrum displays resonances for the Yb(III) complex in addition to peaks due to the free ligand. In our experimental conditions, there is a competition between the nitrate ions and the ligand **5** for the complexation of the metal ion. Adding an excess of Yb(III) displaces the equilibrium towards the 1:1 complex and the free ligand resonances completely disappear. The Yb(**5**)$^{3+}$ peaks remain broad in all conditions and their assignment is difficult except from the relative areas. Moreover, none of the 2D NMR techniques applied to the perchlorate complex could be used because of the broadness of the peaks. Only the protons due to the methyl groups and the para proton in the central pyridine group can be assigned with certainty. Moreover, the number of resonances clearly indicates that the tetramethylcyclohexenyl groups are inverting rapidly on the NMR timescale we used in contrast with what we observed for the Yb(III) perchlorate complex. As expected for a mono-complex, the structure is thus much less crowded and the tetramethylcyclohexenyl rings are free to invert rapidly (it should however be noted that the shift range is 25 ppm instead of 60 ppm for the perchlorate complex. Peak coalescences are thus more easily reached).

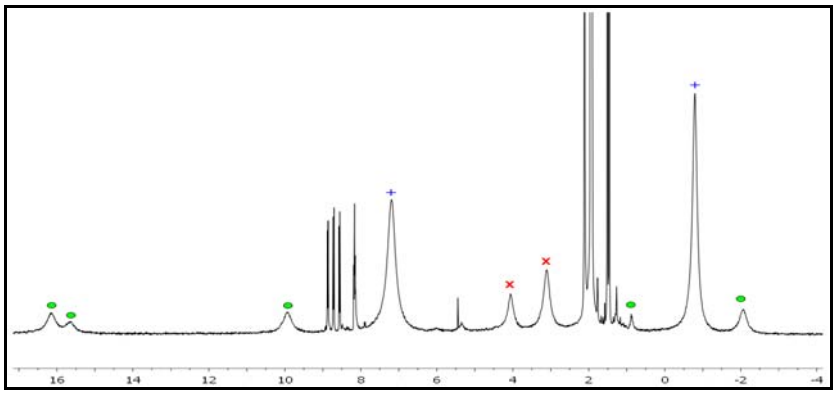

Figure 9: ^{1}H NMR spectrum of a 1:1 mixture of 5:$Yb(NO_3)_3$ in anhydrous CD_3CN at 25°C. Tentative peak assignments: *meta* and *para* protons of the pyridine rings (●): 16.18, 15.96, 9.96, 0.91 and -2.08 ppm; methyl protons (+):7.20 and -0.79 ppm; methylene protons (x); 4.06 and 3.11 ppm. Narrow resonances between 8 and 9 ppm and between 1 and 2 ppm are due to the free ligand, acetonitrile and trace water.

Despite these uncertainties, we deduced the dipolar geometric factors in Equation 1 above from the crystallographic structure of the Y(**5**)$^{3+}$ mono-complex (Figure 4) and we made a fit between these factors and the induced paramagnetic shifts of the Yb(III) nitrate complex. A reasonably good agreement was obtained (Figure 10, right) and the solution and solid state structures are therefore probably similar. The magnetic susceptibility axes were oriented as follows: the z axis joins the metal ion with the nitrogen atom and the *para* carbon atom of the central pyridine unit, the x (or y) axis is perpendicular to the plane formed by the central pyridine ring and the metal ion. This analysis may explain the relatively low distribution coefficients observed in nitrate media (Figure 2) as the 1:1 complex of **5** with Am(III) would be expected to be considerably less hydrophobic than the corresponding 1:2 complex. Better agreement between the experimental and the calculated paramagnetic shifts could probably be obtained by orienting the magnetic susceptibility axes differently. However, the uncertainties in the assignment of the NMR resonances and on the exact orientation of the magnetic susceptibility tensor in a low symmetry structure would remain and efforts in that direction would not be very fruitful. At this stage, one can only say that the solution and solid state structures of Yb(**5**)$^{3+}$ are probably close.

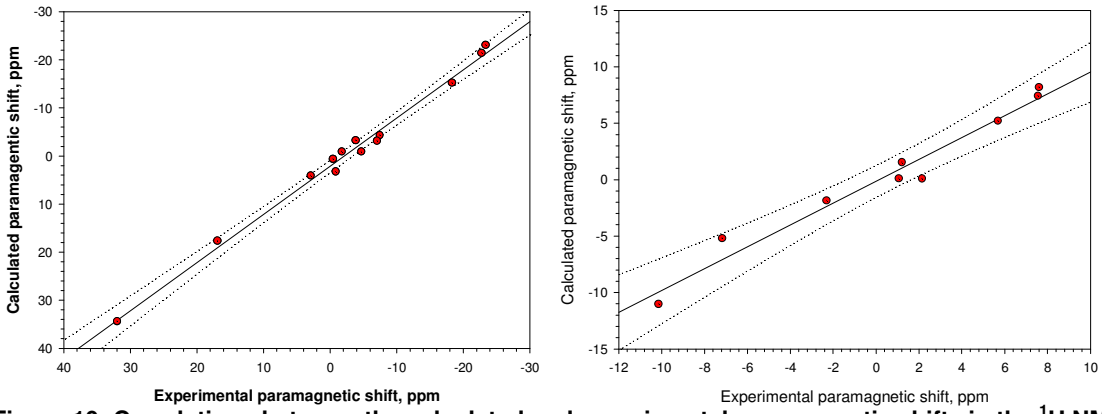

Figure 10: Correlations between the calculated and experimental paramagnetic shifts in the ^{1}H NMR spectra of (a) Left: $[Yb(5)_2](ClO_4)_3$; slope = 1.00, intercept = 2.13. (b) Right: $[Yb(5)](NO_3)_3$; slope = 0.97, intercept = -0.15. 99% intervals are shown with dotted lines in each case.

C. CONCLUSION

We have synthesized the first example of a (1,2,4-triazin-3-yl)-2,2':6',2''-terpyridine ligand and its ability to separate An(III) from Ln(III) has been examined. Low binding affinities for Am(III) but good selectivities for Am(III) over Eu(III) are observed in 1-octanol in the absence of a phase-modifier. The addition of 2-bromohexanoic acid increases the distribution coefficient at low acidities. The separation factor decreases at higher acidities when DMDOHEMA is used as a phase-modifier. The stoichiometries and solution structures of the complexes with Gd(III), Eu(III) and Yb(III) have been determined by nuclear magnetic relaxation dispersion titrations, 1D and 2D NMR techniques and mass spectrometry. In the presence of perchlorate ions the ligand forms highly crowded 1:2 bis-complexes where the aliphatic substituents are conformationally immobile on the NMR timescale (250-400 MHz). The solution structure of the 1:2 complex of **5** with $Yb(ClO_4)_3$ has been deduced from the relative magnitude of the induced paramagnetic shifts. The complex is a mononuclear double helicate where the metal adopts a bicapped square antiprism coordination geometry. In contrast, in the presence of nitrate ions the ligand forms less-crowded 1:1 complexes where the aliphatic substituents are conformationally mobile on the NMR time scale. The nitrate ions compete effectively with the ligand for coordination sites on the metal leading to poorly-extracted complexes of low hydrophobicity. A mononuclear helical 1:1 complex is formed between **5** and $Y(ClO_4)_3$ and its X-ray structure was determined.

Aknowledgements

We thank the Nuclear Fission Safety Program of the European Union for support under the ACSEPT (FP7-CP-2007-211 267) contract and under FP7. We also thank the EPSRC and the University of Reading for funds for the X-Calibur system. The Belgian team also acknowledge the financial support of the Fonds de la Recherche Scientifique (FNRS) of Belgium.

References

1. (a) A. Facchini, L. Amato, G. Modolo, R. Nannicini, C. Madic, P. Baron, *Sep. Sci. Technol.*, 2000, **35**, 1055-1068. (b) D. Serrano-Purroy, P. Baron, B. Christiansen, R. Malmbeck, C. Sorel, J.-P. Glatz, *Radiochim. Acta*, 2005, **93**, 351-355. (c) D. Serrano-Purroy, B. Christiansen, J.-P. Glatz, R. Malmbeck, G. Modolo, *Radiochim. Acta*, 2005, **93**, 357-361. (d) G. Modolo, H. Vijgen, D. Serrano-Purroy, B. Christiansen, R. Malmbeck, C. Sorel, P. Baron, *Sep. Sci. Technol.*, 2007, **42**, 439-452.

2. (a) C. Madic, M. J. Hudson, J.-O. Liljenzin, J.-P. Glatz, R. Nannicini, A. Facchini, Z. Kolarik, R. Odoj, *Progr. Nucl. Energ.*, 2002, **40**, 523-526. (b) C. Hill, D. Guillaneux, L. Berthon, C. Madic, *J. Nucl. Sci. Technol.*, 2002, (Sup. 3), 309-312.

3 (a) J. Magill, V. Berthou, D. Haas, J. Galy, R. Schenkel, H.-W. Wiese, G. Heusener, J. Tommasi, G. Youinou, *Nuclear Energy*, 2003, **42**, 263-277. (b) International Atomic Energy Agency, Technical Reports Series, ISSN 0074–1914 no. 435, Vienna, Austria, 2004.

4. (a) C. Madic, B. Boullis, P. Baron, F. Testard, M. J. Hudson, J-O. Liljenzin, B. Christiansen, M. Ferrando, A. Facchini, A. Geist, G. Modolo, A. G. Espartero, J. De Mendoza, *J. Alloys Compounds*, 2007, **444-445**, 23-27. (b) C. Ekberg, A. Fermvik, T. Retegan, G. Skarnemark, M. R. S. Foreman, M. J. Hudson, S. Englund, M. Nilsson, *Radiochim. Acta*, 2008, **96**, 225-233. (c) Z. Kolarik, *Chem. Rev.*, 2008, **108**, 4208-4252.

5. (a) M. G. B. Drew, D. Guillaneux, M. J. Hudson, P. B. Iveson, M. L. Russell, C. Madic, *Inorg. Chem. Commun.*, 2001, **4**, 12-15. (b) M. G. B. Drew, D. Guillaneux, M. J. Hudson, P. B. Iveson, C. Madic, *Inorg. Chem. Commun.*, 2001, **4**, 462-466. (c) C. Boucher, M. G. B. Drew, P. Giddings, L. M. Harwood, M. J. Hudson, P. B. Iveson, C. Madic, *Inorg. Chem. Commun.*, 2002, **5**, 596-599. (d) M. G. B. Drew, C. Hill, M. J. Hudson, P. B. Iveson, C. Madic, T. G. A. Youngs, *Dalton Trans.*, 2004, 244-251. (e) M. Nilsson, S. Andersson, C. Ekberg, M. R. S. Foreman, M. J. Hudson, G. Skarnemark, *Radiochim. Acta*, 2006, **94**, 1-4. (f) M. G. B. Drew, M. R. St J. Foreman, A. Geist, M. J. Hudson, F. Marken, V. Norman, M. Weigl, *Polyhedron*, 2006, **25**, 888-900. (g) M. J. Hudson, C. E. Boucher, D. Braekers, J. F. Desreux, M. G. B. Drew, M. R. St J. Foreman, L. M. Harwood, C. Hill, C. Madic, F. Marken, T. G. A. Youngs, *New. J. Chem.*, 2006, **30**, 1171-1183.

6. (a) M. G. B. Drew, M. R. S. J. Foreman, C. Hill, M. J. Hudson, C. Madic, *Inorg. Chem. Commun.*, 2005, **8**, 239-241. (b) M. R. St J. Foreman, M. J. Hudson, A. Geist, C. Madic, M. Weigl, *Solvent Extr. Ion Exch.*, 2005, **23**, 645-662. (c) M. Nilsson, S. Andersson, F. Drouet, C. Ekberg, M. Foreman, M. Hudson, J-O. Liljenzin, D. Magnusson, G. Skarnemark, *Solvent Extr. Ion Exch.*, 2006, **24**, 299-318. (d) M. Nilsson, C. Ekberg, M. Foreman, M. Hudson, J-O. Liljenzin, G. Modolo, G. Skarnemark, *Solvent Extr. Ion Exch.*, 2006, **24**, 823-843. (e) M. R. S. Foreman, M. J. Hudson, M. G. B. Drew, C. Hill, C. Madic, *Dalton Trans.*, 2006, 1645-1653. (f) T. Retegan, C. Ekberg, I. Dubois, A. Fermvik, G. Skarnemark, T. Johnsson Wass, *Solvent Extr. Ion Exch.*, 2007, **25**, 417-431. (g) C. Ekberg, I. Dubois, A. Fermvik, T. Retegan, G. Skarnemark, M. G. B. Drew, M. R. S. Foreman, M. J. Hudson, *Solvent Extr. Ion Exch.*, 2007, **25**, 603-617. (h) T. Retegan, C. Ekberg, S. Englund, A. Fermvik, M. R. S. Foreman, G. Skarnemark, *Radiochim. Acta*, 2007, **95**, 637-642. (i) J.-C. Berthet, P. Thuéry, M. R. S. Foreman, M. Ephritikhine, *Radiochim. Acta*, 2008, **96**, 189-197.

7. A. Geist, C. Hill. G. Modolo, M. R. St J. Foreman, M. Weigl, K. Gompper, M. J. Hudson, *Solvent Extr. Ion Exch.*, 2006, **24**, 463-483.

8. D. Magnusson, B. Christiansen, M. R. S. Foreman, A. Geist, J.-P. Glatz, R. Malmbeck, G. Modolo, D. Serrano-Purroy, C. Sorel, *Solvent Extr. Ion Exch.*, 2009, **27**, 97-106.

9. (a) V-M. Mukkala, C. Sund, M. Kwiatkowski, P. Pasanen, M. Högberg, J. Kankare, H. Takalo, *Helv. Chim. Acta.*, 1992, **75**, 1621-1632. (b) C. Galaup, J-M. Couchet, S. Bedel, P. Tisnès, C. Picard, *J. Org. Chem.*, 2005, **70**, 2274-2284. (c) J. M. Veauthier, C. N. Carlson, G. E. Collis, J. L. Kiplinger, K. D. John, *Synthesis*, 2005, 2683-2686.

10. R. P. Thummel, Y. Jahng, *J. Org. Chem.*, 1985, **50**, 3635-3636.

11. W. K. Fife, *J. Org. Chem.*, 1983, **48**, 1375-1377.

12. F. H. Case, *J. Org. Chem.*, 1965, **30**, 931-933.

13. (a) P. Jones, G. B. Villeneuve, C. Fei, J. DeMarte, A. J. Haggarty, K. T. Nwe, D. A. Martin, A-M. Lebuis, J. M. Finkelstein, B. J. Gour-Salin, T. H. Chan, B. R. Leyland-Jones, *J. Med. Chem.*, 1998, **41**, 3062-3077. (b) K. Kikuchi, S. Hibi, H. Yoshimura, N. Tokuhara, K. Tai, T. Hida, T. Yamauchi, M. Nagai, *J. Med. Chem.*, 2000, **43**, 409-419.

14. Z. Kolarik, U. Mullich, F. Gassner, *Solvent Extr. Ion Exch.*, 1999, **17**, 23-32.

15. D. Serrano-Purroy, P. Baron, B. Christiansen, R. Malmbeck, C. Sorel, J.-P. Glatz, *Radiochim. Acta*, 2005, **93**, 351-355.

16. M. J. Hudson, C. E. Boucher, D. Braekers, J. F. Desreux, M. G. B. Drew, M. R. St J. Foreman, L. M. Harwood, C. Hill, C. Madic, F. Marken, T. G. A. Youngs, *New. J. Chem.*, 2006, **30**, 1171-1183.

17. I. Bertini, C. Luchinat, G. Parigi, *Solution NMR of Paramagnetic Molecules*, Elsevier, Amsterdam, 2001.

18. (a) J. F. Desreux, C. N. Reilley, *J. Am. Chem. Soc.*, 1976, **98**, 2105-2109. (b) R. S. Ranganathan, N. Raju, H. Fan, X. Zhang, M. F. Tweedle, J. F. Desreux, V. Jacques, *Inorg. Chem.*, 2002, **41**, 6856-6866.

19. J. A. Peters, J. Huskens, D. J. Raber, *Prog. Nucl. Magn. Reson. Spectrosc.*, 1996, **28**, 283-350.

20. T. R. Cundari, E. W. Moody, S. O. Sommerer, *Inorg. Chem.*, 1995, **34**, 5989-5999.

21. G. B. Rocha, R. O. Freire, N. B. da Costa Jr., G. F. de Sá, A. M. Simas, *Inorg. Chem.*, 2004, **43**, 2346-2354.

22. D. L. Kepert, *Inorganic Stereochemistry*, Springer-Verlag, Berlin, 1982.

23. N. E. Dean, R. D. Hancock, C. L. Cahill, M. Frisch, *Inorg. Chem.*, 2008, **47**, 2000-2010.

24. M. Giraud, E. S. Andreiadis, A. S. Fisyuk, R. Demadrille, J. Pecaut, D. Imbert, M. Mazzanti, *Inorg. Chem.*, 2008, **47**, 3952-3954.

Irradiation effects on neptunium oxidation states

Bruce J. Mincher
Aqueous Separations and Radiochemistry Department
Idaho National Laboratory
PO Box 1625
Idaho Falls, ID 83415-6180 USA
Tel: 1-208-533-7499, Fax: 1-208-533-7471, e-mail: bruce.mincher@inl.gov

Abstract *– Preliminary results describing the spectroscopic observation of neptunium valence state changes in irradiated aqueous nitric acid are presented. The reduction of Np(VI) to Np(V) is attributed to radiolytically-produced nitrous acid. No evidence was found for the catalyzed oxidation of Np(V) at nitric acid concentrations of 0.09 – 4.0 M.*

A. INTRODUCTION

The successful implementation of hydrometallurgical separations requires the preparation and maintenance of metal ions in known oxidation states. Trivalent metals such as the lanthanides or americium, for example, are not extracted in the PUREX process, while hexavalent uranium and tetravalent plutonium are complexed. In some cases, such as the separation of uranium in the PUREX process, the TBP complexation of U(VI) does not require heroic efforts to maintain the necessary oxidation state. Other elements have multiple oxidation states that occur within the range of acidities and redox potentials found in the process and the relative abundance of these may be an artefact of process conditions, including irradiation. Neptunium is especially problematic in this regard.

The co-extraction of neptunium in solvent extraction processes is complicated because it can exist as extractable Np(IV) and Np(VI), or inextractable Np(V) within the range of conditions encountered in the process. Often, all three oxidation states are simultaneously present with the standard potentials (E^o) between these states in aqueous acidic solution each being ~ 1 V. [1] Regardless of the initial preparation of a favored oxidation state using appropriate reagents, a complicated series of redox and disproportionation reactions follows to create a solution of mixed oxidation states.

Although neptunium has been recovered in various PUREX processes [2] its complicated redox reactions under PUREX conditions are still being studied worldwide to improve process efficiency. A number of studies have attempted to define the parameters under which neptunium extraction is adversely affected and to create models which can be used to predict neptunium valence states under various process conditions. [3] In this paper, the initial results for an experimental program investigating the change in neptunium redox speciation in nitric acid solution as a function of absorbed γ-ray dose are presented.

B. EXPERIMENTAL METHODS

Samples of 237-neptunium in nitric acid solution from on-hand stock at the Idaho National Lab were irradiated in sealable cuvettes (Helma USA, Plainville, NY). These cuvettes contain supracil optical windows that do not darken upon γ-irradiation. Once the cuvettes were loaded they were irradiated in sealed fashion, at a location in the irradiator with a well-characterized dose rate. This dose rate was determined using standard Fricke dosimetry, and the absorbed doses to the samples were then calculated based on the duration of the irradiation. The irradiator was a Nordion Gammacell 220E (Nordion Corporation, Ottawa, Canada) containing a 20,000 Ci 60-cobalt source. The sample cell base-line dose rate was 0.151 kGy min^{-1}, and the temperature during irradiation was 48^{o}C, due to γ-heating of the irradiator shielding.

Immediately following irradiation the sample absorbance was measured using a Cary 50 UV/Vis absorption spectrophotometer (Varian Inc., Palo Alto, CA, USA), over the range 400-1100 nm. The absorbance of Np(V) was measured using the sharp absorbance peak at 981 nm. The absorbance of Np(VI) was observed as a broad absorbance at < 450 nm. Neptunium(VI) also has a sharp absorbance feature at ~ 1200 nm. However, this wavelength is not observable with the Cary 50.

C. RESULTS AND DISCUSSION

Samples of 5.5 x 10^{-3} M neptunium were prepared by repetitive metathesis with nitric acid, and finally dissolved in varying concentrations of HNO_3. The resulting solutions were observed spectroscopically and contained a mixture of Np(V) and Np(VI). No Np(IV) was found in these experiments.

These samples were then irradiated with γ-rays in a series of absorbed doses over the range 0—50 kGy, with spectroscopic measurements made at selected intervals. A steady decrease in Np(VI) occurred, as measured by the reduction in the absorbance below 450 nm. The decrease in Np(VI) was accompanied by an increase in Np(V), as measured at 980 nm. This is shown in Figure 1 using the 0.9 M HNO_3 solution as an example. The increase in peak height at 980 nm versus absorbed dose is shown in Figure 2, for 0.09 M, 0.9 M and 4 M HNO_3 solutions. The increase in Np(V) absorbance occurred in all irradiated acid concentrations, and is clearly faster at the lower acid concentrations. The maximum absorbance at 980 nm for an unirradiated 100% Np(V) solution in 0.9 M HNO_3 was 1.60 ± 0.06, corresponding to ε = 291 L mol^{-1} cm^{-1}. Assuming this ε holds for all acid concentrations, approximate G_o values for the reduction of Np(VI) may be calculated as 0.84, 0.35, and 0.11 μmol Gy^{-1}, in 0.09, 0.9, and 4 M HNO_3, respectively.

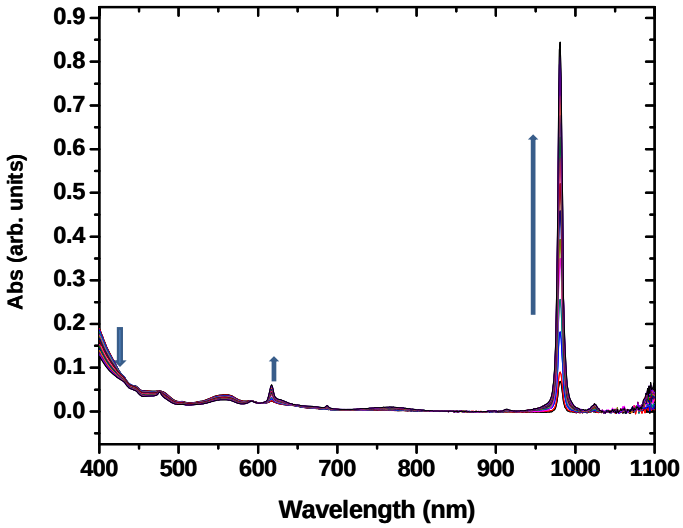

Figure 1: The production of Np(V) in an irradiated solution of 1.3 mg mL^{-1} neptunium in 0.9 M HNO_3. The sharp peaks at 981 and 617 nm show the increase in Np(V) concentration, while the decrease in broad absorbance below 450 nm shows the decrease in Np(VI) concentration.

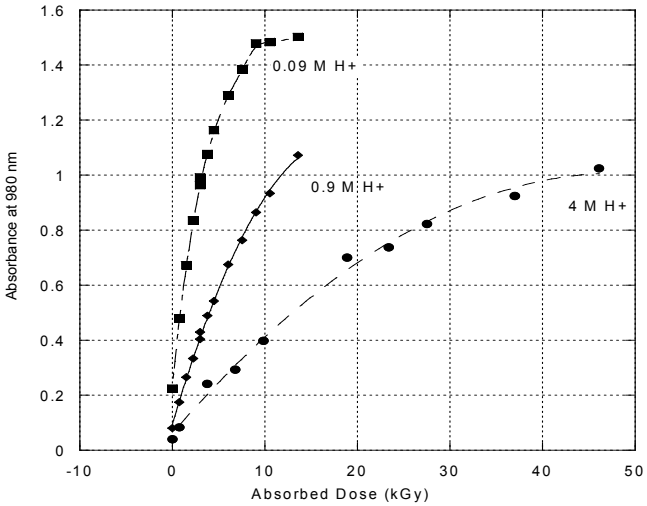

Figure 2: Neptunium (V) absorbance versus absorbed dose in different irradiated nitric acid concentrations. Note the more rapid increase in Np(V) absorbance at lower acid concentrations.

The valence state of neptunium in aqueous nitric acid is generally considered to depend on the concentration of nitrate, acidity and nitrous acid according to Equation 1: [5]

$$NpO_2^+ + 3/2H^+ + 1/2NO_3^- \leftrightarrow NpO_2^{2+} + 1/2HNO_2 + H_2O \quad (1)$$

For our unirradiated samples, preparation at higher concentrations of nitric acid favored higher initial concentrations of Np(VI), in agreement with Equation 1. It can also be seen that nitrous acid favors the reduction of Np(VI) to Np(V). Nitrous acid is a product of direct nitric acid radiolysis: [6]

$$HNO_3 \text{ -}\backslash\!/\backslash\!/\backslash\!\rightarrow {}^{\bullet}O + HNO_2 \quad (2)$$

We irradiated various concentrations of nitric acid and measured the production of nitrous acid by HPLC. These results are shown in Figure 3. It can be seen that nitrous acid production is greater for higher concentrations of nitric acid. As much as 3 mM HNO_2 was produced in 4 M HNO_3 at 40 kGy absorbed dose. The initial fast production of nitrous acid begins to level off with increasing dose, with a maximum of < 4 mM for 4 M HNO_3. Similarly, the reduction of Np(VI) in 4 M HNO_3 appears to level off at absorbed doses > 50 kGy. This plateau in nitrous acid production has been attributed to the reaction of nitrous acid with radiolytically-produced hydrogen peroxide, which oxidizes nitrous acid back to nitric acid via a peroxynitrous acid intermediate as shown in Equation 3: [7, 8]

$$H_2O_2 + HNO_2 \rightarrow HOONO \rightarrow H^+ + NO_3^- + H_2O \quad (3)$$

Further evidence that Np(VI) reduction is due to reaction with nitrous acid is provided by the fact that reduction continues for a short time (~ 1 h) when sample irradiation is terminated. This implicates a relatively long-lived radiolytically-produced reducing agent. Thus, we conclude that the generation of nitrous acid in irradiated nitric acid promotes Np(VI) reduction. In contrast to this expectation it is frequently reported that small amounts of nitrous acid promote catalytic oxidation of Np(V) to Np(VI). [2, 5, 9] However, we found no evidence of neptunium oxidation in these preliminary experiments. Excess amounts of nitrite are reported to reduce neptunium to Np(V), as expected from Equation 1. [10]

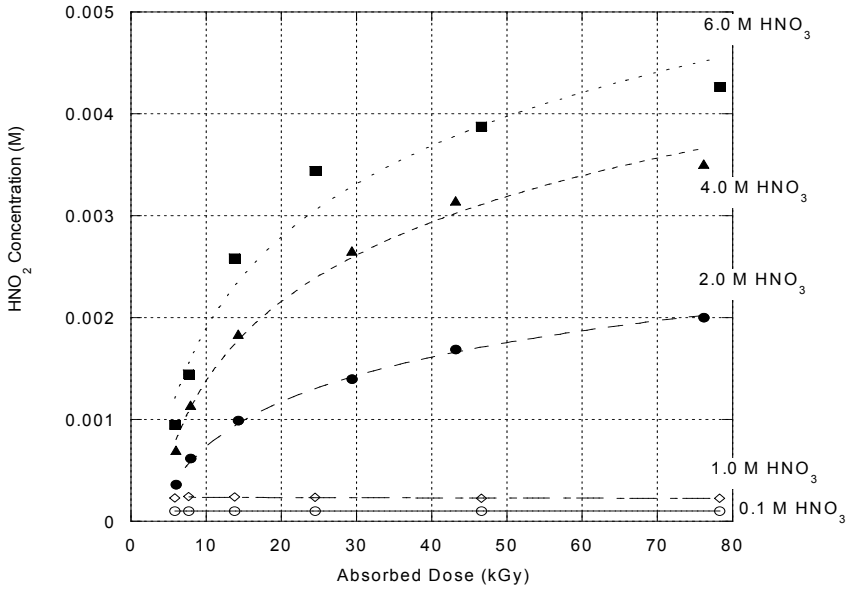

Figure 3: The radiolytic generation of nitrous acid in varying concentrations of nitric acid.

D. CONCLUSION

Experiments were designed to monitor the valence state of neptunium in irradiated nitric acid solution using UV/Vis spectroscopy. In preliminary results we have shown that Np(VI) is reduced to Np(V) by irradiation, at a rate that depends on the nitric acid concentration. This coupled with the finding that reduction continues for a short time after the completion of the irradiation suggests that the long-lived radiolysis product nitrous acid is responsible for this reduction. We have also reported yields for the generation of nitrous acid in varying concentrations of irradiated nitric acid. No evidence for the catalytic oxidation of Np(V) to Np(VI) was found. In future experiments we will investigate the effect of nitrous acid scavengers, added nitrite salts, and the valence state changes in these irradiated solutions.

Acknowledgements

The author thanks G. Elias of INL for the measurement of the nitrous acid concentrations and L. Martin of INL for help with UV/Vis spectroscopic measurements. This work was funded by the INL-LDRD program, sponsored by the U.S. Department of Energy, under DOE Idaho Operations Office contract DE-AC07-99ID13727.

References

1. S. KIHARA, Z. YOSHIDA, H. AOYAGI, K. MAEDA, O. SHIRAI, Y. KITATSUJI, and Y. YOSHIDA, "A Critical Evaluation of the Redox Properties of Uranium, Neptunium and Plutonium Ions in Acidic Aqueous Solutions. *Pure and Applied Chemistry 71*, 1771, (1999).

2. R. E. ISAACSON and B. F. JUDSON, "Neptunium Recovery and Purification at Hanford." *I&EC Process Design and Development*, 3, *4*, 296, (1964).

3. M.V. VLADIMIROVA, "Mathematical Modeling of the Radiation-chemical Behavior of Neptunium in Nitric acid. Equilibrium States." *Radiokhimiya*, *37*, 446, (1995).

4. C. KELLER, *The Chemistry of the Transuranium Elements*, pp. 194-295, Verlag Chemie GmbH, Weinheim (1971).

5. T.H. SIDDALL III and E.K. DUKES, "Kinetics of HNO_2 Catalyzed Oxidation of Neptunium (V) by Aqueous Solutions of Nitric Acid." Journal of the American Chemical Society, *81*, 790, (1959).

6. P.-Y. JIANG, R. NAGAISHI, T. YOTSUYANAGI, Y. KATSUMURA, and K. ISHIGURE, "γ-radiolysis Study of Concentrated Nitric Acid Solutions." Journal of the Chemical Society, Faraday Transactions, *90*, 93, (1994).

7. D. VIONE, V. MAURINO, C. MINERO, D. BORGHESI, M. LUCCHIARI, and E. PELIZZETTI, "New Processes in the Environmental Chemistry of Nitrite: 2. The Role of Hydrogen Peroxide." Environmental Science and Technology, *37*, 4635, (2003).

8. P.K. BHATTACHARYYA and R. VEERARAGHAVAN, "Reaction Between Nitrous Acid and Hydrogen Peroxide in Perchloric Acid Medium." International Journal of Chemical Kinetics, *9*, 629, (1977).

9. Z.KOLARIK and E.P. HORWITZ, "Extraction of Neptunium and Plutonium Nitrates with n-octyl(phenyl)-N,N-diisobutyl-carbamoylmethylphosphine oxide." Solvent Extraction and Ion Exchange, *6*, 247, (1988).

10. W.L. POE, A.W. JOYCE and R.I. MARTENS, "Np^{237} and Pu^{238} Separation at the Savannah River Plant." I&EC Process Design and Development, 3, *4*, 314, (1964).

Radiolytic stability of metal-complexed extraction ligands under aqueous acidic reprocessing conditions

Stephen P. Mezyk*, Delora K. Gaskins, Thomas D. Cullen
Department of Chemistry and Biochemistry
California State University at Long Beach
Long Beach, CA, 90840, USA

Leigh R. Martin, Bruce J. Mincher
Idaho National Laboratory, Aqueous Separations and Radiochemistry Department, P.O. Box 1625, Idaho Falls, ID, 83415-6180 USA

Tel: 562-985-4649, Fax: 562-985-855, e-mail:smezyk@csulb.edu

ABSTRACT

The oxidative stability of the Eu3+ metal-complexed extraction ligand diethylenetriaminepentaacetic acid (DTPA) has been investigated through its reaction rate constant with the hydroxyl radical under TALSPEAK acidic pH conditions. In aqueous solution at pH 3.00 and 2.00 these reaction rate constants were determined using thiocyanate competition kinetics, with values of (5.75 ± 0.38) x 109 and (3.68 ± 0.06) x 109 M-1 s-1, respectively. These values are slightly higher than the corresponding rate constants determined for only the DTPA protonated ligands at these pH's, determined by the same methodology. Based on literature pKa values and composite rate constant measurements at multiple pH values, individual rate constants for the species DTPA-H5, DTPA-H4- and DTPA-H32- of 2.69 x 109, 3.40 x 109 and 3.26 x 109 M-1 s-1 have been determined.

A. INTRODUCTION

The partitioning of the long-lived α-emitters and the high-yield fission products from dissolved nuclear fuel is key for the safe recycling of nuclear fuel and disposition of high-level waste. The future reprocessing of light water reactor fuel is likely to be based on aqueous solvent extraction technologies, and consist of the sequential separation of uranium, fission products, and trivalent actinides from lanthanides. Since these solvent extraction systems will operate under highly radioactive conditions, both the solvents and ligands used must be robust toward radiolytically-induced degradation in an irradiated mixed organic, aqueous acidic environment. Therefore, an understanding of their radiation stability is important to the design of a practical system.

The separation of the minor actinides in the last step of the reprocessing system is one of the more formidable challenges associated with the design of an advanced fuel cycle.[1] The partitioning of americium and curium could reduce high-level-waste long-term storage requirements by as much as two orders of magnitude. However, the selective extraction of these trivalent actinides is complicated by the high concentration of the trivalent lanthanide fission products. The lanthanides represent about a third of the total fission product inventory and have very similar chemical properties.

Current concepts for this final separation rely on the use of soft-donor nitrogen or sulfur-containing ligands that favor complexation with the 5f orbitals of the actinides.[2] In the USA, the most developed process is the TALSPEAK (Trivalent Actinide Lanthanide Separation by Phosphorous reagent Extraction from Aqueous Komplexes) process,[3,4] based upon the competition between bis(2-ethylhexyl)phosphoric acid (HDEHP) in the organic phase and lactate-buffered diethylenetriamine pentaacetic acid (DTPA) in the aqueous phase.

The presence of radiation throughout both phases will result in a mixture of radical and ionic species that will react with, and degrade, the extraction ligands. While some recent work[5] has been reported on the kinetics and reaction mechanisms for the lactic acid additive used in TALSPEAK, kinetic data have only been reported for the basic pH, deprotonated, forms of DTPA.[6,7] There have been no reports on the radical-based degradation of these ligands when they are complexed with lanthanides or actinides, which is the predominant state of the aqueous phase in the TALSPEAK process. This is an important parameter to determine, as it has previously been shown[8,9] that radical rate constants for metal-complexed crown ethers can change by over a factor of two (see Table 1) by complexation with

a simple metal cation. Although it appeared that the •OH oxidation reactions were less affected than the e_{aq}^- and H• reductions, a quantitative knowledge of these data

Table 1. Summary of reaction rate constants for hydroxyl radical (•OH), hydrated electron (e_{aq}^-) and hydrogen atom (H•) with crown ethers in aqueous solution.[8,9]

Species	$k_{•OH}$ $M^{-1} s^{-1}$	k_{eaq^-} $M^{-1} s^{-1}$	k_H $M^{-1} s^{-1}$
18C6	6.0×10^9	4×10^6	1.9×10^8
18C6-K+	1.0×10^{10}	$< 10^6$	5.5×10^7
CH18C6	1×10^{10}	5×10^6	9×10^7

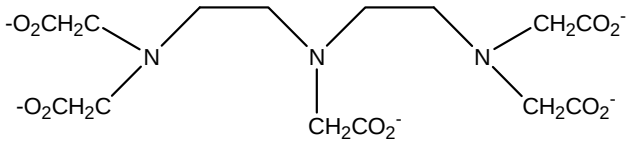

Figure 1. Structure of fully deprotonated DTPA (diethylenetriamine pentaacetic acid) ligand.

under real-world conditions is necessary for an understanding and optimization of the large-scale reprocessing chemistry. Therefore, in this study we have undertaken the first investigation into the hydroxyl radical reaction kinetics with DTPA (see Figure 1) under TALSPEAK pH conditions, as well as its Eu^{3+} metal-loaded form.

B. EXPERIMENTAL

The DTPA and $Eu(NO_3)_3$ used in this study were supplied by Idaho National Laboratory and thiocyanate was from Aldrich (99.9+%). All were used as received. Kinetic studies were performed on solutions made using Milli-Q water (>18.1 MΩ) illuminated by a UV lamp to maintain total organic carbon concentrations (TOC) <13 µg/L, as measured by an on-line TOC analyzer.

The radical kinetics were obtained using the linear accelerator/transient UV-visible absorption spectroscopy system at the University of Notre Dame Radiation Laboratory.[10,] This accelerator produces an 8 MeV electron beam with 2-3 ns pulses each of 2-10 Gy which generated about 1-5 µM total radicals. Room temperature solutions were passed through a continuous flow quartz irradiation cell at a flow rate sufficient to ensure that each electron pulse occurred on a fresh sample, thus minimizing any interference from formed products. Typically 5-20 pulses were averaged to obtain a single kinetic trace. The temperature of irradiation was measured by a calibrated thermocouple placed in the solution flow directly above the irradiation cell.

For solutions with solute concentrations less than 0.1 M, the pulsed electron irradiation degrades the solvent water by the stoichiometry:[11]

$$H_2O \xrightarrow{radiolysis} [0.28]\,^{\bullet}OH + [0.06]H^{\bullet} + [0.27]e^-_{aq} + [0.05]H_2 + [0.07]H_2O_2 + [0.27]H_3O^+ \qquad (1)$$

where the coefficients in brackets are the species individual G-values (yields) in µmol Gy^{-1} of absorbed dose. The kinetic study of only hydroxyl radicals above pH 2.0 was achieved by pre-saturating solutions with N_2O gas ([N_2O] = 24.5 mM), which both removes dissolved oxygen from the system and converts the reducing hydrated electrons and some hydrogen atoms to •OH:[11]

$$e^-_{aq} + N_2O + H_2O \rightarrow {}^{\bullet}OH + OH^- + N_2 \qquad k_2 = 9.1 \times 10^9\ M^{-1} s^{-1} \qquad (2)$$

$$H^{\bullet} + N_2O \rightarrow {}^{\bullet}OH + N_2 \qquad k_3 = 2.1 \times 10^6\ M^{-1} s^{-1} \qquad (3)$$

This was done to effectively double the initial •OH radical concentration, which improved the signal quality. For pH =1 solutions, pre-saturation of the solutions by pure oxygen ([O_2] = 1.25 mM) quantitatively removed both reducing radicals through the reactions:[11]

$$e^-_{aq} + O_2 \rightarrow O_2^{-\bullet} + H^+ \leftrightarrow HO_2^{\bullet} \qquad k_4 = 1.9 \times 10^{10}\ M^{-1} s^{-1},\ pK_4 = 4.8 \qquad (4)$$

$$H^{\bullet} + O_2 \rightarrow HO_2^{\bullet} \qquad k_5 = 1.2 \times 10^{10}\ M^{-1} s^{-1} \qquad (5)$$

Table 1: Summary of literature hydroxyl radical reaction rate constants for DTPA at various pH's.[6,7]

pH	k_{OH} $M^{-1} s^{-1}$
7.0	5.2×10^9
9.5	6.5×10^9
11.0	2.2×10^9
12.2	2.9×10^9
7.0	5.3×10^9

Standard thiocyanate dosimetry [11] for absolute $^{\bullet}OH$ concentrations generated by each electron pulse was conducted daily at 475 nm using N_2O saturated, 10^{-2} M thiocyanate solutions ($G\varepsilon = 5.2 \times 10^{-4}$ m^2 Gy^{-1}).[12]

The rate constant error limits reported here are the combination of experimental precision and estimated compound purity.

C. RESULTS AND DISCUSSION

A literature survey showed that hydroxyl radical reaction rate constants with only DTPA had been measured under basic pH conditions[6,7] (see Table 2). A consistently decreasing value trend is noted for increasing pH. However, as TALSPEAK is designed to operate at the lactic acid buffer pH of 3.6, we first required this rate constant to be determined.

The electron pulse radiolysis of a 500 μM DTPA solution at pH 3.0 did not give any significant transient absorption in the UV-visible range (260 – 750 nm). Therefore, the rate constant for the reaction

$$^{\bullet}OH + DTPA \rightarrow \text{products} \qquad (6)$$

was determined using thiocyanate (SCN^-) competition kinetics. Upon oxidation by the hydroxyl radical thiocyanate produces a strong $(SCN)_2^{\bullet-}$ transient absorption at 475 nm:[11]

$$^{\bullet}OH + SCN^- (+ SCN^-) \rightarrow OH^- + (SCN)_2^{-\bullet} \qquad k_7 = 1.05 \times 10^{10}\ M^{-1} s^{-1} \qquad (7)$$

This competition for hydroxyl radicals by SCN^- and DTPA can be analytically solved to give the expression

$$\frac{Abs^o(SCN)_2^{\bullet-}}{Abs(SCN)_2^{\bullet-}} = 1 + \frac{k_6[DTPA]}{k_7[SCN^-]} \qquad (8)$$

where $Abs^o(SCN)_2^{-\bullet}$ is the maximum absorbance measured for the thiocyanate solution without any DTPA present and $Abs(SCN)_2^{-\bullet}$ is the reduced absorbance in the presence of this competitor. Typical data for DTPA are shown in Figure 2a, where decreasing absorptions of $(SCN)_2^{-\bullet}$ are observed for increasing amounts of DTPA added. From the transformed plot of ratio of the absorbance intensities against the ratio of concentrations (Figure 2b) the k_6 rate constant can be readily determined, and for this pH of 3.13, a value of $k_6 = (3.13 \pm 0.08) \times 10^9\ M^{-1} s^{-1}$ is obtained.

These measurements were repeated for more acidic pHs, with all rate constant data summarized in Table 3. However, these values are composite rate constant values, with contributions from three separate DTPA protonation states:

$$k_{meas} = k_{DTPA\text{-}H5}\,[DTPA\text{-}H5] + k_{DTPA\text{-}H4}\,[DTPA\text{-}H4] + k_{DTPA\text{-}H3}\,[DTPA\text{-}H3] \qquad (9)$$

From known DPTA pK values[13] we can readily calculate the fractions present under each pH kinetics measurement (see Figure 3), and thus deduce the individual rate constants for each species. These individual values are summarized in Table 4, and while slower than observed at neutral pH, they are reasonably consistent over the range pH = 1 – 3.

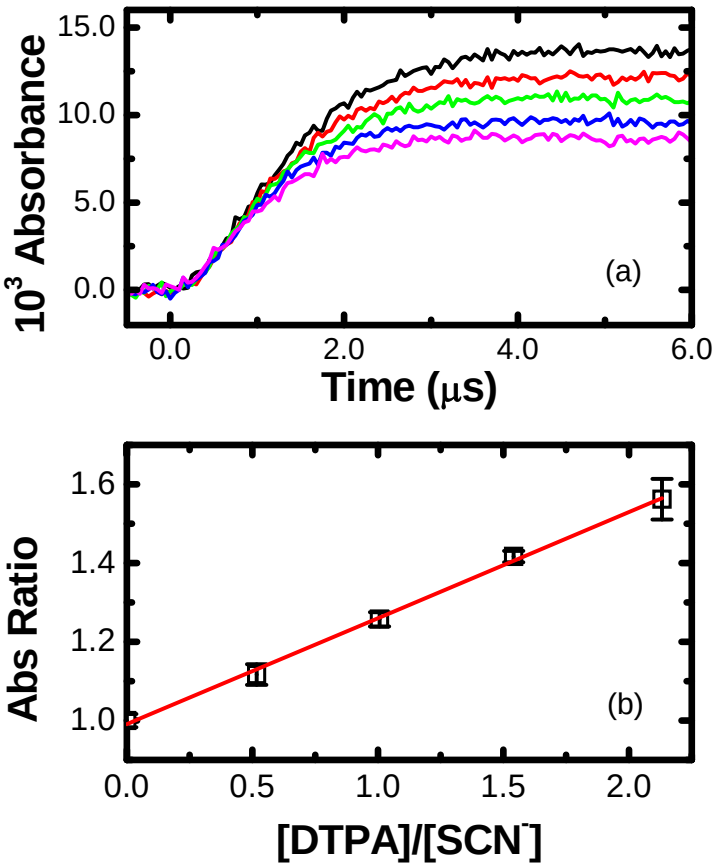

Figure 2. a) Transient absorbance of $(SCN)_2^-$ from N_2O-saturated 118.6 μM KSCN solution containing zero (black), 61.4 (red), 119.3 (green), 182.8 (blue) and 252.7 (magenta) μM DTPA at pH 3.13. b) Transformed competition kinetics plot from data of a). Solid red line corresponds to weighted linear fit, with intercept of 0.99072 ± 0.00885 and slope of 0.2694 ± 0.0069, corresponding to a rate constant for $^{\bullet}OH$ reaction with DTPA of k = (3.13 ± 0.08) x 10^9 M^{-1} s^{-1} at this pH (R^2 = 0.998).

Table 3. Speciation values and measured rate constants for OH + DTPA at 22.1°C.[13]

pH	$f_{DTPA-H3^{2-}}$	$f_{DTPA-H4^{-}}$	$f_{DTPA-H5}$	$^{\bullet}OH$ + DTPA rate constant M^{-1} s^{-1}
3.12	0.6765	0.2572	0.01951	(3.13 ± 0.08) x 10^9
2.00	0.09067	0.4544	0.4544	(3.06 ± 0.06) x 10^9
1.22	0.004651	0.1411	0.8542	(2.79 ± 0.11) x 10^9

For the measurement of metal-loaded DTPA in acidic solution, solutions containing a fixed concentration of thiocyanate (~100 μM), DTPA (~200 μM) and varying amounts of Eu^{3+} salt (0 – 200 μM) were dissolved in N_2O-saturated solution. Although no ligand-metal binding constants under these acidic conditions were found in the literature, the strong binding constants for Eu-DTPA under more basic conditions (typically $\beta > 10^{22}$, see Table 4) meant that we could reasonably assume that all the Eu^{3+} was complexed. This allowed a simple extension of the above competition kinetics equation to be derived, to include the additional reaction

$$^{\bullet}OH + \text{Eu-DTPA} \rightarrow \text{product} \qquad (10)$$

of

$$\frac{Abs^{o}(SCN)_2^{\bullet-}}{Abs(SCN)_2^{\bullet-}} = 1 + \frac{k_6[DTPA]}{k_7[SCN^-]} + \frac{k_{10}[Eu-DPTPA]}{k_7[SCN^-]} \qquad (11)$$

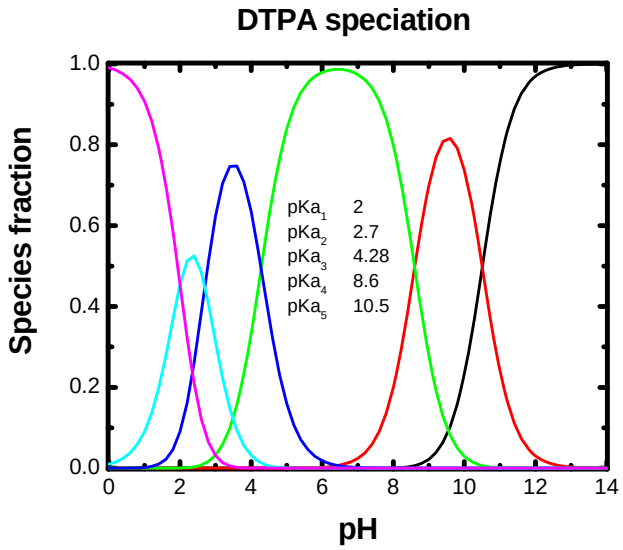

Figure 3. Calculated speciation of DTPA based on literature pK_a values.[13]

Table 4. Calculated individual rate constants for acidic DTPA species.

Species	•OH + DTPA k values M^{-1} s^{-1}
$k_{DTPA-H3}2-$	**3.26×10^9**
$k_{DTPA-H4}-$	**3.40×10^9**
$k_{DTPA-H5}$	**2.69×10^9**

Table 5. log β complexation constants for Eu-DTPA[13]

	10°C	25°C	40°C	55°C
$DTPA^{5-} + Eu^{3+} \rightarrow EuDTPA^{2-}$	21.31	21.00	20.80	20.88
$DTPA^{5-} + H^{+} + Eu^{3+} \rightarrow EuDTPA^{-}$	23.69	23.27	23.07	22.86

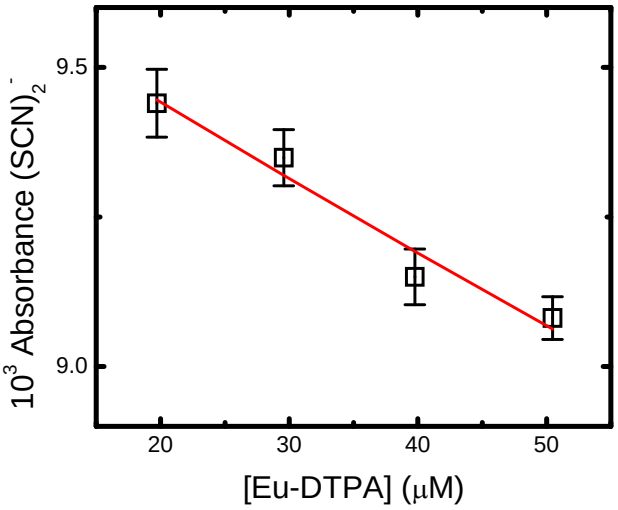

Figure 4. Decrease in $(SCN)_2^{-\bullet}$ absorption from electron pulse irradiated 95.6 μM SCN^- with added 200 μM DPTA and varying $Eu(NO_3)_3$ at pH 3.00 and 21.7°C. Solid line is fit to data according to Equation (11) with $k_{10} = (5.75 \pm 0.38) \times 10^9$ M^{-1} s^{-1}.

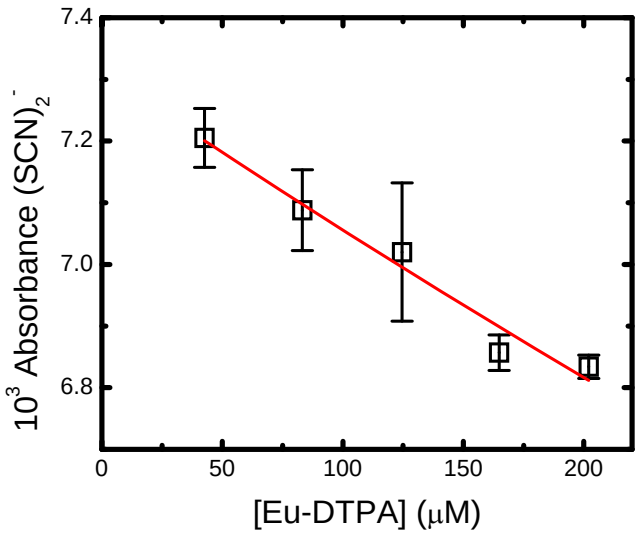

Figure 5. Decrease in $(SCN)_2^{-\bullet}$ absorption from electron pulse irradiated 106.5 μM SCN^- with added 200 μM DPTA and varying $Eu(NO_3)_3$ at pH 2.00 and 22.2°C. Solid line is fit to data according to Equation (11) with $k_{10} = (3.68 \pm 0.06) \times 10^9$ M^{-1} s^{-1}.

Knowing the individual k6 and k7 rate constants, the concentrations of added thiocyanate and DTPA, and assuming that all the Eu3+ is complexed by the DTPA, this equation can be fitted to the decrease in the (SCN)2-• absorbance with increasing Eu concentration to obtain the desired k10 rate constant. This is shown in Figures 4 and 5 for pH 2.00 and 3.00, respectively with corresponding rate constants calculated as k10 = (5.75 ± 0.38) x 109 M-1 s-1 and (3.68 ± 0.06) x 109 M-1 s-1. It is seen that the hydroxyl radical reaction rate constant for Eu-loaded DTPA is generally faster (up to a factor of two) than for the free ligand under these conditions.

It is clear that additional work is required to fully elucidate the importance of these metal-loaded ligand systems. We are presently trying to determine the -values for the Eu-DTPA complexes under TALSPEAK conditions, which will be key in correctly determining their individual hydroxyl radical reactivity. Moreover, we plan to extend these measurements to other lanthanide/actinides, as well as perform mass spectrometric measurements on the stable products formed in these oxidations.

D. ACKNOWLEDGEMENTS

This work was funded by the INL-LDRD program, U.S. DOE Office of Nuclear Energy, Science and Technology under DOE Idaho Operations Office contract DE-AC07-99ID13727. Work was performed at the Radiation Laboratory, University of Notre Dame which is supported by the U.S. Department of Energy Office of Basic Energy Sciences.

REFERENCES

1. B.J. Mincher, G. Modolo, S.P. Mezyk, *Solvent Extr. Ion Exch*., accepted for publication 2010.
2. K.L. Nash, C. Madic, J. Mathur, J. Lacquement, Chapter 24: Actinide Separation Science and Technology. *The Chemistry of the Actinide and Transactinide Elements*, 3rd Edition, 2622-2798, Springer New York (2006).
3. M. Nilsson, K.L. Nash, K.L, *Solvent Extr. Ion Exch*. 25, 665-701 (2007).
4. B. Weaver, F.A. Kappelmann, *J. Inorg. Nucl. Chem*. 30, 263-272 (1968).
5. L.R. Martin, S.P. Mezyk, B.J. Mincher, *J. Phys. Chem. A*, 113, 141-145 (2009).
6. D.E. Cabelli, J.D. Rush, M.J. Thomas, B.H.J. Bielski, *J. Phys. Chem.* 93, 3579-3586 (1989)
7. V.G. Thomas, S.B. Srivastava, P.N. Moorthy, *J. Radioanal. Nucl. Chem*., 136, 443-447 (1989)
8. B.G. Ershov, A.F. Seliverstov, N.L. Sukhov, A.V. Gordeev, *Khim. Vys. Energij*, 21,119-122, (1987).
9. A.F. Seliverstov, B.G. Ershov, *Khim. Vys. Energij,* 22, 203-206, (1988).

10. K. Whitman, S. Lyons, R. Miller, D. Nett, P. Treas, A. Zante, R.W. Fessenden, M.D. Thomas, Y. Wang, Linear accelerator for radiation chemistry research at Notre Dame 1995. *Proceedings of the '95 Particle Accelerator Conference and International Conference on High Energy Accelerators,* Dallas, TX (1996).
11. G.V Buxton, C.L. Greenstock, W.P. Helman, A.B. Ross, *J. Phys. Chem. Ref. Data* 17, 513-886, (1988).
12. G.V Buxton, C.R. Stuart, *J. Chem. Soc., Faraday Trans.* 91, 279-282 (1995).
13. L Rao, *Understanding Actinide/Lanthanide Speciation under TALSPEAK Conditions,* AFCI Research and Development Campaign – Separations Annual Report 2009.

A high temperature heating device for the study of fission product release from nuclear fuel

Jolanta Švedkauskaitė-Le Gore, Niko Kivel and Ines Günther-Leopold
Paul Scherrer Institute
5232 Villigen PSI, Switzerland
Tel: +41 56 310 5564, Fax: +41 56 310 2203, e-mail: jolanta.svedkauskaite@psi.ch

Abstract – *At the Paul Scherrer Institute a high temperature inductive heating furnace, which can heat fuel samples up to 2300°C, has been developed in order to study the release of fission products. The furnace can be directly connected to an inductively coupled plasma mass spectrometer for online monitoring of the released elements and does not require their trapping before measurement. This paper describes the design of the inductive heating furnace, discusses its operating parameters, limitations and illustrates foreseen applications.*

A. INTRODUCTION

Removal of volatile and semi-volatile fission products from spent nuclear fuel by thermal and thermochemical treatment has been a subject of research for several decades. This topic focuses on the release of volatile elements induced by high temperatures, trapping the released products and finally their determination by inductively coupled plasma mass spectrometry (ICP-MS) or gamma analysis [1, 2, 3, 4].
The process of heating samples in air is known as voloxidation. The processing step employs high temperature and oxidizing gas to promote the oxidation of UO_2 to U_3O_8. This technique has been studied extensively in early 70's and has led to the development of several processes such as OREOX – oxidation and reduction of oxide, AIROX – Atomics International reduction oxidation and DEOX – decladding via oxidation. All these process applications can be used to prepare the fuel for hydrochemical, pyrochemical or DUPIC (direct reuse of PWR fuel in CANDU reactors) processes [5, 6, 7] However, none of these processes have been operated on a commercial scale so far. In the past decade these processes have returned to favor, due to concern about the effective management of spent nuclear fuel. To address this issue various development concepts of head-end reprocessing are under investigation by national research laboratories and by international cooperation.
The Paul Scherer Institute (PSI) in Switzerland started recently a research project called HERACLES (head-end reprocessing studies by thermal and thermochemical treatment of fuels). Objectives of the project are to study the release of the fission products during the high temperature treatment of spent oxide fuel, to perform real time measurements of fission products and to carry out the thermodynamic modeling to support these actions. This paper focuses on the design and implementation of a high temperature heating device for the study of fission product release and presents first experimental results.

B. EXPERIMENTS AND RESULTS

B.1. InVap design

The inductive heating device (InVap) was designed as successor of the heated laser ablation cell (HeLAC), which had a temperature limitation of about 700°C and is described elsewhere [8]. The design of the InVap was carried out in a computer aided engineering (CAE) approach. This approach is based on the definition of boundary conditions followed by the selection of the best candidate technique for the given purpose. After the technique is selected, a 3D model is created and optimized by modeling of gas flows in the apparatus and maximum feasible temperature.
The following boundary conditions were predefined for the device:

- maximum sample temperature greater 2000°C
- ramping of the temperature with heating rates as low as 10 K/min

- capability to handle irradiated fuel
- oxidative (for pre-oxidation) and reductive gas atmosphere
- direct connection to an ICP-MS

In order to meet these criteria laser heating, electrothermal vaporization and inductive heating were assessed. Since emission of infrared light is the dominating effect at temperatures >2000°C the power loss due to radiation has to be considered. This led to exclusion of a heating by laser, because the power loss would demand a very powerful and costly laser or make an infrared reflector in the close vicinity of the sample mandatory. For electrothermal vaporization a graphite tube, holding the sample, is heated by the Joule effect. Very high electrical currents are necessary to heat the graphite tube and the commercially available devices are designed for pulse operation rather than slowly increasing the power over a long time. Further the sample handling is hampered by the fact that the sample has to be placed on the L'Vov platform in the graphite tube. For this procedure the tube has to be removed from the furnace and later carefully be realigned.

The technique selected as most promising candidate is inductive heating of a graphite crucible. Inductive heaters are available in nearly any power range and the shape of the load coil can be freely selected. Further, the load coil can be covered with silver to act as a reflector for the infrared radiation. The devices are designed for continuous operation at full power and can ramp the power at almost any rate.

The materials for the device were carefully selected since they have to stand high temperatures but must not interact with the inductive heating, except the crucible. A schematic and picture of the InVap are given in

Figure 1. A quartz tube (30 mm ID) was selected as outer wall in the heated region. Quartz can stand temperatures of >1000°C at almost full mechanical strength and is not prone to thermal shock. To support the crucible a MgO ceramic pillar is used. The material has a maximum working temperature of 2400°C and is not affected by the inductive heater. Even though first experiments revealed that the high temperature gradient in the pillar caused cracking due to high thermal tension, this issue could be circumvented by stacking two crucibles on each other to reduce the temperature gradient in the insulating pillar. The base and the lid of the device are made from aluminum and serve as connection units for gas and cooling water. A quartz window in the lid is used as observation port for temperature measurement by a pyrometer. The void of the device is flushed with argon at different flow rates. The first stream at a low flow rate of 0.5 L/min enters at the base and flows as carrier gas around the crucible. The carrier gas can be mixed with pure oxygen or a hydrogen/argon mixture to adjust for oxidative or reductive atmosphere. A second argon stream at a flow rate of 0.8 – 1.0 L/min is used to quench the hot carrier gas and is introduced beneath the quartz window. The ICP-MS (Element 2, ThermoFisher, Bremen, Germany) is connected via a 2 mm ID PTFE tubing from the lid of the InVap. The load coil of the inductive heater is made from silver plated copper with a rectangular cross section and has 35 mm ID. The coil is positioned at the same level as the sample crucible and is directly connected to the high frequency matching network. The matching network itself is connected to the generator (TNX5 compact, Plustherm Point GmbH, Wettingen, Switzerland) which provides the 105 kHz high frequency. The heater is operated in an open control circuit, meaning no feed back from the pyrometer is used for the control. This was necessary because the pyrometer has only a measurement range of 750 – 2500°C. To cover the lower temperature range the output power was calibrated to the temperature of the crucible during the installation and qualification of the device as shown in Figure 2.

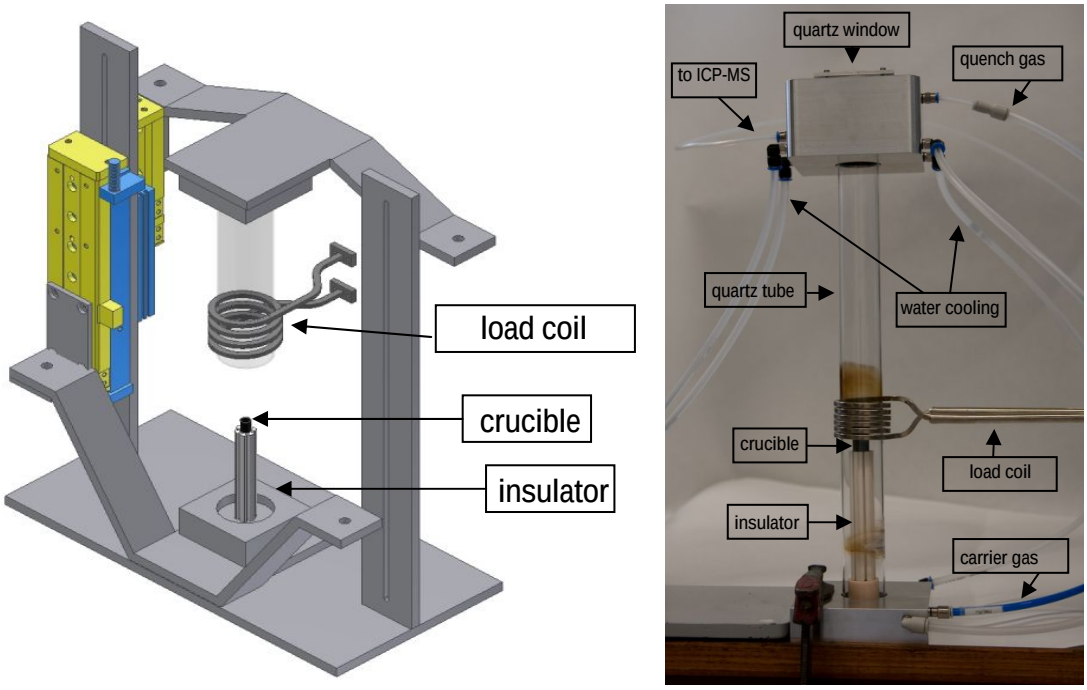

Figure 1: Schematic and picture of the InVap device

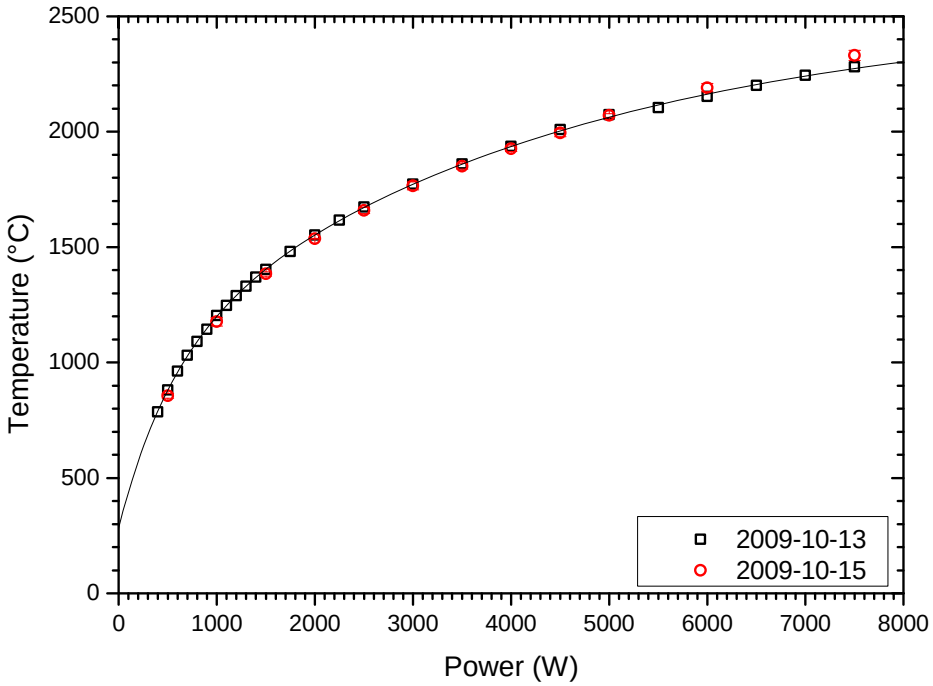

Figure 2: Calibration of the temperature with the forward power of the inductive heater

B.2. Samples used for experiments

The simulated fuel (SIMFUEL) used in this study was prepared at Chalk River Laboratories, Canada, as described elsewhere [9, 10]. The UO_2 based SIMFUEL composition, additives and impurities with concentrations greater than 10 µg/g, are listed in Table 1.

Table 1: Composition of the SIMFUEL from Chalk River Laboratories

Element	Concentration (µg/g)
Mg	10 ± 3
Al	36 ± 7
Cr	11 ± 2
Ni	10 ± 2
Ga	29 ± 6
Sr	1600 ± 200
Zr	2200 ± 200
Mo	180 ± 40
Ru	50 ± 10
Rh	13 ± 6
Pd	260 ± 50
Ba	1000 ± 100
La	900 ± 200
Ce	2700 ± 300
Nd	4500 ± 500
Th	18 ± 4

B.3. Temperature measurements

Figure 3 shows the sample temperature as a function of the applied generator power. At maximum power a temperature of about 2300°C can be achieved. The heater temperature profile, a ramp-up and hold function, is easily programmable and fully controlled using a LabVIEW program. The InVap can heat a sample to the maximum temperature within a couple of minutes. Therefore, the temperature and time parameters can be changed depending on the needs of a particular experiment.

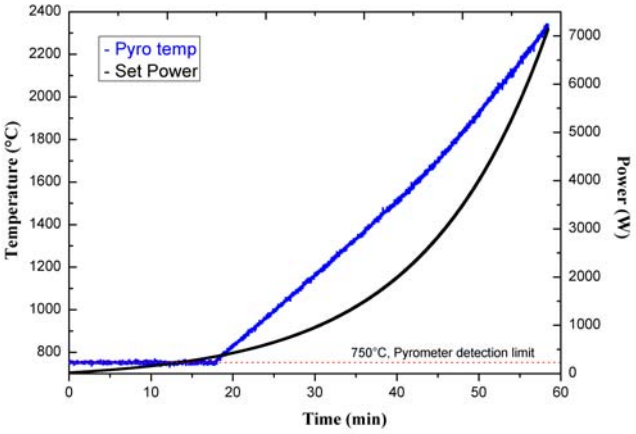

Figure 3: Power and temperature vs. time

B.4. Release measurements by ICP-MS

Samples are put into the graphite crucible which is then placed on the insulator in the InVap (Fig. 2). Once the InVap is closed and flushed with the carrier gas to remove air the optimization of the ICP-MS parameters has to be performed. ICP-MS optimization is critical as instrument signals are a function of a variety of parameters. Therefore, ICP-MS was optimized to ensure best instrument stability instead of the maximum signal intensity. Instrumental parameters are listed in Table 2. Due to current experimental set-up, the impurity of Xe in Ar gas was used for optimization. The modification

of experimental set-up, which will allow to introduce an internal standard, is currently in progress. After the ICP-MS optimization the samples were heated for the first test measurements with a ramp-up of 50 K/min to the maximum temperature, then the maximum temperature was hold for 30 min.

Table 2: ICP-MS operating parameters

Instrument type	Element 2
Coolant gas flow	16 L/min
Auxiliary gas flow	1 L/min
Sample gas	1 L/min
Additional gas	0.25 L/min
Extraction voltage	1800 V
SEM voltage	2200 V
Sampling cone	Aluminum

During the heating the ICP-MS measures the elemental release from SIMFUEL. The release of various elements versus temperature and time is shown in Figure 4. The plotted data were smoothed to capture release pattern as the ICP-MS had signal stability problems. The signal noise might be related to the dry plasma conditions. From laser ablation ICP-MS experiments it is known that the moisturizing of carrier gas improves the overall signal stability [11]. This effect will need to be verified for the present experimental set-up by repeating the experiments with a moisturized carrier gas. The addition of an internal standard must also be implemented via the addition of a standard solution to the gas stream.

Reproducibility of the results was checked by repeating the experiments under the same conditions several times. The outcome obtained showed that the intensities were reproducible; however the release curves were shifted to lower temperatures. This indicates that some material may condense on the walls of the InVap and in the transfer lines.

Additional experiments were done with ^{134}Cs and ^{99m}Tc in order to identify these possible memory effects due to condensation. These elements were chosen since they have different evaporation temperatures and are gamma emitters, which make identification of condensation on different parts of equipment much easier. Solutions of ^{134}Cs or ^{99m}Tc were placed in a graphite crucible and dried on a hot plate. After the sample was dried a gamma measurement was performed to obtain the starting activity of the sample. The samples were then placed in the InVap and heated using the same heating profile used for the release experiments. Once heating of the sample was done, gamma measurements on the graphite crucible were performed again. The results showed that the Cs is completely evaporated whereas 50% of the Tc remains in the crucible for the applied temperature regime. That is expected since the evaporation temperature of Tc is much lower than for Cs. Severe ^{134}Cs condensation of around 55% was found on the quartz tube and around 10% on the transfer line. For ^{99m}Tc condensation on the quartz tube is around 10% and around 1% on the transfer line.

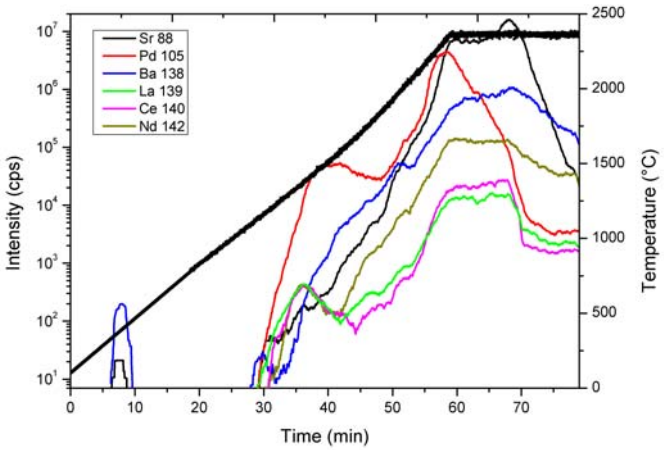

Figure 4: Elemental release from SIMFUEL

C. CONCLUSION AND OUTLOOK

This paper presents the design and first applications of the InVap. It has been demonstrated that this device is capable of heating samples up to 2300°C and can be successfully used for the release of elements, as well as it can be dedicated to heat treatment on other kind of samples. The experimental setup can be used for online measurement of released elements. However, condensation of the elements on the quartz tube and transfer line needs to be reduced.
Modifications of the set-up, such as moisturizing of the carrier gas and addition of an internal standard, will be implemented as soon as necessary equipment will be delivered. Afterwards experiments of fission products release from SIMFUEL will be repeated. Results obtained from those tests will demonstrate if the signal stability can be improved by moisturizing the carrier gas. As soon as problems concerning condensation and signal stability are under control experiments with active materials will be performed.

Acknowledgements

The authors are grateful to Chalk River Laboratories, Canada for supplying the SIMFUEL samples and to Hp. Linder for gamma analysis. This work is supported by the ACSEPT project within the European 7th Framework Program (FP7).

References

1. B. R. Westphal, J. J. Park, J. M. Shin, G. I. Park, K. J. Bateman and D. L. Wahlquist, ”Selective Trapping of Volatile Fission Products with an Off-Gas Treatment System”, *Separation Science and Technology*, 43, 2695 (2008)
2. B. R. Westphal, K. J. Bateman, R. P. Lind, K. L. Howden and G. D. Del Cul, “Fission Products Removal from Spent Oxide Fuel by Head-End Processing”, *Proc. GLOBAL 2005*, p. 345, Atomic Energy Society of Japan, Tsukuba, Japan (2005)
3. L. D. Trowbridge, G. D. Del Cul and D. Collins, “Application of Advanced Head End Reprocessing Concepts to a Fluoride Volatility Flowsheet”, *Proc. GLOBAL 2005*, p. 011, Atomic Energy Society of Japan, Tsukuba, Japan (2005)
4. J. H. Goode, “Voloxidation: removal of volatile fission products from spent LMFBR fuels“, Technical Report, Oak Ridge National Lab, United States (1973)
5. M. S. Yang, H. Choi, C. J. Jeong, K. C. Song, J. W. Lee, G. I. Park, D. D. Kim, W. I. Ko, J. J. Park, K. H. Kim, H. H. Lee and J. H. Park, “The Status and Prospect of DUPIC Fuel Technology“, *Nuclear Engineering and Technology*, 38, 3, 359 (2006)
6. T. R. Thomas, “AIROX nuclear fuel recycling and waste management“, *Proc. GLOBAL 1993*, US DOE, Seattle, United States (1993)
7. K. K. Bae, B. G. Kim, Y. W. Lee, M. S. Yang and H. S. Park, “Oxidation behavior of unirradiated UO_2 pellets“, *Journal of Nuclear Materials*, 209, *3*, 274 (1994)
8. J. Švedkauskaitė-Le Gore, N. Kivel, I. Günther-Leopold, “Real Time Measurement of Fission Products Released from Spent Nuclear Oxide Fuel by Thermal Treatment“, *Proc. GLOBAL 2009,* p. 1337, French Nuclear Energy Society, Paris, France (2009)
9. P. G. Lucuta, R. A. Verrall, Hj. Matzke and B. J. Palmer, “Microstructural Features of SIMFUEL – Simulated High-Burnup UO_2 – based Nuclear Fuel“, *Journal of Nuclear Materials*, 178, 48 (1991)
10. P. G. Lucuta, R. A. Verrall, Hj. Matzke and I. L. Hastings, “Characterization and thermal properties of hyperstoichiometric SIMFUEL”, *Proc. 3rd Int. Conf. on CANDU Fuel*, p. 261, Canadian Nuclear Society, Toronto, Canada (1992)
11. C. O’Connor, B. L. Sharp, P. Evans, “On-line additions of aqueous standards for calibration of laser ablation inductively coupled plasma mass spectrometry: theory and comparison of wet and dry plasma conditions”, *Journal of Analytical Atomic Spectrometry*, 21, 556 (2006)

Recent achievements and remaining challenges on pyrochemical reprocessing in CRIEPI

Tsuyoshi Murakami, Koichi Uozumi, Yoshiharu Sakamura, Masatoshi Iizuka
Hirokazu Ohta, Takanari Ogata and Tadafumi Koyama
Central Research Institute of Electric Power Industry
2-11-1 Iwadokita, Komae-shi, Tokyo 201-8511 Japan
Tel:+81-3-3480-2111, Fax:+81-3-3480-7956, e-mail:m-tsuyo@criepi.denken.or.jp

Abstract *– Central Research Institute of Electric Power Industry (CRIEPI) has proposed an integrated fuel cycle concept for light water reactor and metal fuel fast breeder reactor for closing actinide cycle with Partitioning and Transmutation scenario. This paper reviews a state of the art pyrochemical reprocessing (electrorefining, electroreduction and pyropartitioning) and metal fuels containing minor actinides (MAs) which are the key challenges to establish the proposed fuel cycle. CRIEPI continues to develop pyrochemical reprocessing of which reliability is high enough to evaluate its industrial applicability. Recently, engineering-scale electrodes for electrorefining process were developed; the anode and solid cathode pair so called high-throughput electrorefiner, and the novel liquid Cd cathode equipped with a system to transport liquid Cd to the following cathode process. The feasibility of these electrodes was demonstrated. The novel oxide fuel reduction process was proposed to increase the reduction rate, where porous oxide fuel pellets were served to the electroreduction process. ~100g UO_2 pellet was successfully reduced to metallic state within 10 hours. Almost all of MAs was recovered from genuine high-level liquid waste (HLLW) through the pyropartitioning process (denitration, chlorination, and reductive-extraction). This demonstrated that MAs contained in HLLW from PUREX were introduced into the metal fuel cycle. Postirradiation tests of fast reactor metal fuels containing MAs and rare earths are being carried out.*

A. INTRODUCTION

The aim of Partitioning and Transmutation of actinides and fission products is to reduce the burden of managing the high-level radioactive wastes. CRIEPI has proposed an integrated fuel cycle of light water reactor (LWR) and metal fuel fast breeder reactor (FBR) cycles with realizing Partitioning and Transmutation scenario.[1-2] Figure 1 represents how the metal fuel FBR cycle is combined with the LWR cycle. U, Pu and minor actinides (MAs) contained in the spent metallic fuels are recovered electrochemically in a molten chlorides bath (electrorefining process). The recovered actinides are casted into the metallic fuels and MAs in the fuels are transmuted efficiently in the metal fuel FBR. MAs contained in the high-level liquid waste (HLLW) from the PUREX process are introduced into the metal fuel FBR cycle by applying the pyropartitioning process where their chemical states are converted to be applicable to the metal fuel FBR cycle. Oxide fuels (UO_2 or MOX from PUREX and spent LWR fuels) are reduced electrochemically to the metallic state in a molten chlorides bath

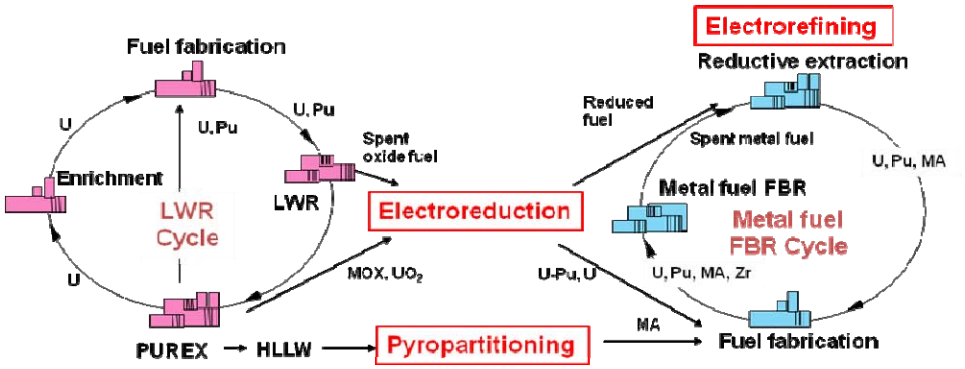

Figure 1 Integrated system of LWR and metal fuel FBR cycles.

(electroreduction) to be supplied to the metal fuel FBR cycle. As described above, the pyrochemical reprocessing technology is applied in the proposed fuel cycle. This is because the pyrochemical reprocessing has the following advantages. Since Pu is principally recovered with other actinides in the electrorefining process, the high proliferation resistance is expected to be achieved. Since the reaction media used in the pyrochemical reprocessing is molten salts which has a higher stability against the radiation compared with the solvents for aqueous processing, the pyrochemical reprocessing technology is suitable for treating the short-cooled and high MA content fuels. Parts of the proposed fuel cycle was reviewed in the framework of Japanese OMEGA (Options Making Extra Gains from Actinide and fission products) Project at 2009, and will be reviewed in the framework of FaCT (Fast Reactor Cycle System Technology Development) Project.

This paper describes an overview of the recent R&D achievements on the pyrochemical reprocessing in CRIEPI, especially on electrorefining, electroreduction and pyropartitioning. Furthermore, CRIEPI has developed MA-containing metal fuels in cooperation with the Institute for Transuranium Elements (ITU). In the previous study, it was confirmed that U-Pu-Zr fuels containing 5wt% or less MAs and rare earths (REs) can be fabricated homogeneously with no significant change in the mechanical or thermal properties compared with the usual U-Pu-Zr ternary alloy fuel.[3] The irradiation experiments of the metal fuel containing MAs and REs are briefly reviewed in this paper.

B. Concept of Pyrochemical Reprocessing of Metal and Oxide Fuels

The major step in pyrochemical reprocessing is the electrorefining process. Eutectic LiCl-KCl melts are used as the electrolyte at 773 K. Cut and chopped spent metallic fuels (U-Zr or U-Pu-Zr) are placed in metallic anode baskets and immersed in the eutectic LiCl-KCl melts containing actinide ions. Actinides in the fuel dissolve anodically in the melts. Noble metal fission products remain in the anode basket, while the other fission products also dissolve. Two kinds of cathode are employed; the solid cathode made of iron and the liquid Cd cathode. According to the reduction potentials on the solid cathode and on the liquid Cd cathode, U is selectively recovered on the solid cathode, and U, Pu and MAs (Np, Am and Cm) are recovered into the liquid Cd cathode simultaneously. Fission products of alkaline metals and alkaline earth metals accumulate in the melt, while small amounts of rare earth fission products are contained in the liquid Cd cathode.[4]

Oxide fuels are reduced to the metallic state through the electroreduction process to be introduced into the metal fuel FBR cycle. In the electrolytic reduction process, oxide fuels are loaded at the cathode in a molten chloride bath that dissolves oxide ions (O^{2-}). At the cathode, oxide is electrochemically reduced into metallic state to form O^{2-} in the melts. The O^{2-} is transported through the melts and discharges at the anode to evolve O_2 gas.[5]

For the recovery of MAs from HLLW generated by PUREX process, we have been developing pyropartitioning process.[1,6] The pyropartitioning process consists of a denitration step which converts elements in HLLW into oxides by calcination in air, followed by a chlorination step where the denitrated material is converted to chlorides by using chlorine gas and carbon, and a reductive-extraction step which separates actinide elements from fission products in molten salt/liquid metal system.

C. Developments in Electrorefining Process

In order to develop the process flowsheet of which reliability is high enough to evaluate the industrial applicability, several experiments have been performed to measure the material balances in detail. Sequential electrorefining tests of unirradiated Pu fuels were demonstrated successfully as the joint study with JAEA. Material balance of Pu was confirmed to be mostly maintained at 100% with respect to the initial amount at each step of the sequence.[7] Electrorefining tests using the irradiated U-Pu-Zr fuel which is a part of the METAPHIX fuel are being carried out under the collaboration with JRC-ITU (Fig. 2).

Figure 2 Laboratory-scale test facility for irradiated fuels installed in JRC-ITU.

CRIEPI has continued to develop the electrorefiner which is applicable for industrialization. The engineering-scale anode and solid cathode pair, called the high-throughput electrorefiner module, was developed as shown in Fig. 3.[8] The module consists of a cylindrical cathode and anode baskets rotating inside the cathode. After a certain amount of uranium is anodically dissolved and deposited on the inner surface of the cathode, the anode baskets are replaced with a dedicated mechanism equipped with scraper blades. By rotating the scraper blades, the uranium deposits on the surface of the cathode are removed and collected in the cathode product container placed at the bottom of the module. By using the high-throughput electrorefiner module, the throughput of 32.9 g-U/h/litter-electrode volume was achieved with a high current efficiency. This value should be sufficiently high for the practical use.

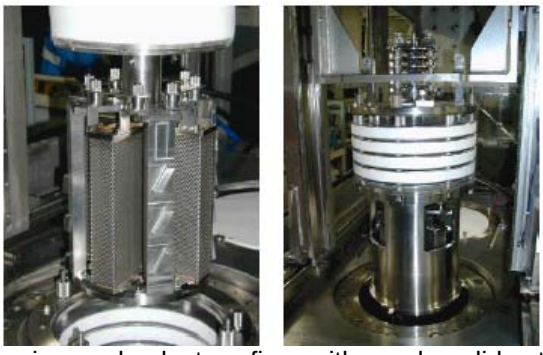

Figure 3 Engineering-scale electrorefiner with anode-solid cathode assembly.

In the conventional concept of liquid Cd cathode processing, the ceramic crucible containing Cd-An alloy is moved to the following Cd distillation process to separate An from Cd after electrorefining process. Then, distilled Cd is moved back to the ceramic crucible being the liquid Cd cathode. In order to avoid a thermal shock, however, it is necessary to take much time for preheating and cooling of the ceramic crucible before and after each process. Therefore, the novel concept was proposed for the practical use of the liquid Cd cathode.[9] The proposed liquid Cd cathode module has the system to transport the liquid Cd containing An to the following Cd distillation process. Advantages of this novel concept are not only that neither preheating nor cooling of the ceramic crucible is required but that life span of the ceramic crucible would be extended. The integrated tests of electrorefining, liquid Cd alloy transportation and Cd distillation were performed using the engineering-scale liquid Cd cathode module, where Gd was used as the simulated material of Pu. The engineering-scale liquid Cd cathode was installed in 780 mm dia. electrorefiner which was placed in the large-scale Ar glove box (Fig. 4). The obtained recovery ratio and the throughput were high enough to demonstrate the feasibility of the novel concept of the liquid Cd cathode.

Figure 4 Large-scale Ar glove box (left) and engineering-scale electrorefiner with liquid Cd cathode and liquid transport system (right).

D. DEVELOPMENTS IN ELECTROREDUCTION PROCESS

CRIEPI has been developing the electrolytic reduction process since 2001. Conversion of UO_2 and MOX to metallic form was firstly demonstrated.[5] Then, reduction mechanism was investigated in various molten salt baths such as $CaCl_2$, LiCl and LiCl-KCl eutectic.[10-13] These tests indicated that the LiCl salt bath was the most suitable for UO_2 and MOX reduction and the oxide reduction rate was practically determined by the transport of oxide ions from the oxide in the cathode basket to the bulk

salt. The obtained results allowed us to propose a unique pretreatment process to improve the reduction rate.[14-15] In the proposed pretreatment process, spent oxide fuel is separated from cladding by voloxidation when UO_2 is oxidized to U_3O_8. The resulting oxide fuel powder is reduced to UO_2 again in H_2 gas stream, compacted into green pellets and sintered at a high temperature. As a result, porous oxide fuel pellets are obtained. In the subsequent electrolytic reduction process, the pellets are loaded in a cathode basket made from a large-mesh net. The expected advantages of applying the proposed pretreatment process are as follows. Since the pellets are porous and the cathode basket is made from a large-mesh net, molten salts easily permeates inside the pellets and oxide ions are smoothly discharged from the cathode basket. Since we need not handle a fine powder in the subsequent process, the loss of oxide fuels as well as contamination with fine oxide dust can be prevented.

The porous UO_2 pellets were fabricated from U_3O_8 powder as shown in Fig. 5(left). 103.6g of porous UO_2 pellets were loaded in the cylindrical cathode basket made from a large-mesh net. Current-controlled electrolysis was performed to reduce the UO_2 at 650˚C in a LiCl melt containing Li_2O. The applied current was initially 15 A and decreased stepwise as the reduction progressed. The electrolysis was terminated at 9.2 h, where 66.1 A-h had passed in total. Figure 5(right) shows the inside of the cathode basket after electrolysis, indicating the pellets maintained the cylindrical shape. The polished cross section of the pellet exhibited a metallic sheen. Therefore, it was verified that all the UO_2 pellets were reduced to metallic uranium. The current efficiency was calculated to be 62%. After the electrolysis, the reduction products were easily taken out from the cathode basket, which is another practical advantage.

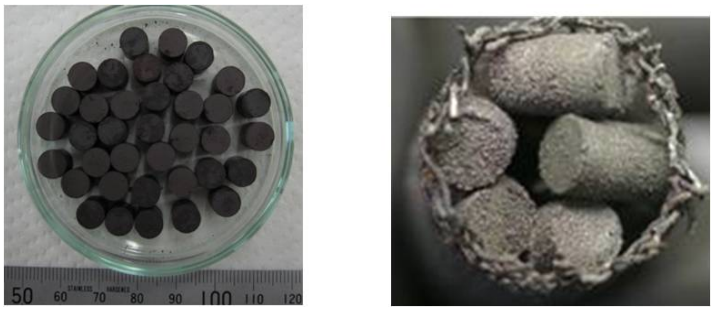

Figure 5 Over view of UO_2 pellets fabricated from U_3O_8 powder (left) and the pellets after the electroreduction.

E. DEVELOPMENTS IN PYROPARTITIONING OF MA FROM HLLW

A hot cell experiment to recover MAs from 520g of genuine HLLW was performed.[16] At the denitration step, the HLLW was dried at around 100°C and calcined at around 500°C under air flow (Fig. 6(left)). Almost all of the actinides and fission products (FPs) were expected to remain in the denitrated material. Then, the denitrated material melted together with LiCl-KCl eutectic salt was chlorinated by pure chlorine gas at around 650 °C (Fig. 6(right)). Analysis of chlorination product samples indicated that almost all of the actinides, rare-earth FPs, alkaline-earth FPs, and alkaline FPs remained in the chlorination product salt, probably as their chloride forms. On the contrary, some FPs such as Zr and Mo evaporated during the chlorination as expected from previous experiments using a simulating HLLW.[17]

A part of the chlorinated product was served for the demonstration test of reductive-extraction. After the addition of Cd-Li reductant, almost 100% of TRUs in the initial HLLW were recovered into liquid Cd phase, which suggested the complete reaction and negligible mass loss of TRUs in denitration, chlorination and reductive-extraction steps. The separation behaviors of actinide elements

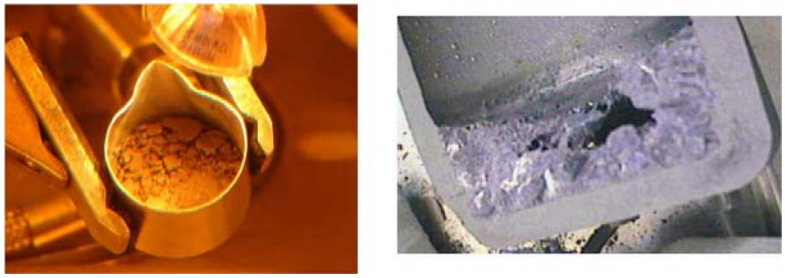

Figure 6 Recovered material after denitration (left) and section of chlorinated product salt (right).

from FPs in molten salt/liquid Cd system were quite similar to that of previous experiments using un-irradiated materials.

F. POSTIRRADIATION EXAMINATIONS OF FAST REACTOR METAL FUEL CONTAINING MA

Metal fuels containing MAs and REs have been irradiated in the fast reactor PHÉNIX from December 2003 to May 2008 with the support of Commissariat à l'Energie Atomique (CEA).[18] In this experiment, two types of MA-containing fuel pins including U-19Pu-10Zr-2MA-2RE and U-19Pu-10Zr-5MA / U-19Pu-10Zr-5MA-5RE, together with the reference fuel pin of U-19Pu-10Zr were irradiated. It was evaluated from the actual reactor power history that the discharged burnup goal of ~2.5at.%, ~7.0at.% or ~10.0at.% was almost attained. Destructive postirradiation examinations such as plenum gas analysis and observation by optical microscopy for low-burnup fuel pins were started.[19] Figure 7 shows an example of optical metallography results for U-19Pu-10Zr-5MA-5RE. The distribution of fuel matrix phases and the characteristic appearance of MA (and RE) inclusions were observed. Quantitative examinations on the redistribution behavior of the fuel constituents and MA transmutation performance will be conducted hereafter.

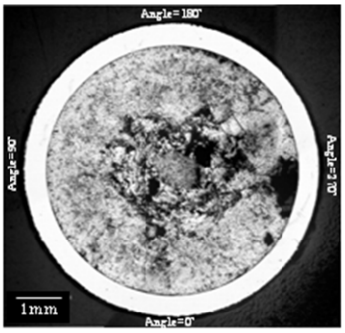

Figure 7 Cross-sectional view of U-19Pu-10Zr-5MA fuel irradiated at 320mm from the bottom of the fuel stack.

G. CONCLUSION

CRIEPI has demonstrated the feasibility of the pyrochemical reprocessing from laboratory-scale experiments and recently, progressed to the next stage for developing engineering-scale process equipments.

The electrorefining process was demonstrated by using the engineering-scale electrorefiner. Anode and solid cathode pair, called the high-throughput electrorefiner module, was developed and the throughput of 32.9 g-U/h/litter-electrode volume was achieved with a high current efficiency. This value should be sufficiently high for the practical use. The novel concept was proposed for the practical use of the liquid Cd cathode which equipped the system to transport the liquid Cd to the following cathode processing. The feasibility of the novel liquid Cd cathode was demonstrated using Gd as the simulated material. In near future, electrorefining tests using irradiated metal fuels will be carried out.

The novel oxide reduction process was proposed, where porous oxide pellets fabricated from the spent oxide fuels were served to the electroreduction process. It was confirmed that ~100g of UO_2 pellets were completely reduced to metal within 10 hours. The remaining challenge is to develop an anode material which is practically suitable for the electroreduction process of spent oxide fuels.

A hot cell experiment to recover MAs from genuine high-level liquid waste (HLLW) through the pyropartitioning process (denitration, chlorination, and reductive-extraction) was performed. Almost 100% of the TRUs contained in the initial HLLW were recovered. This suggested the complete reaction and negligible mass loss of TRUs in the all steps in the pyropartitioning process. The separation behaviors of actinide elements from rare-earth FPs were quite similar to that of previous experiments using un-irradiated material. Therefore, the pyropartitioning process was successfully demonstrated.

Metal fuels containing MAs and REs were irradiated in the fast reactor PHÉNIX. The discharged burnup goal of ~2.5at.%, ~7.0at.% or ~10.0at.% was almost attained. The postirradiation experiments such as plenum gas analysis and optical microscope observation for the low burnup fuel (~2.5at.%) was started. Quantitative examinations on the redistribution behavior of the fuel constituents and MA transmutation performance will be conducted.

Since the pyrochemical reprocessing is expected to be a key technology in the fuel cycles scenario, CRIEPI will continue to develop the pyro-reprocessing process keeping up with the times.

Aknowledgements

We would like to acknowledge these activities have been successfully achieved through strong collaboration with JAEA and with JRC-ITU. Parts of this work are the results of “Development and improvement of electrorefining process” and “Development of engineering technology basis for electrometallurgical pyroprocess equipment”, “Application of electrochemical reduction to pyrochemical reprocessing for oxide nuclear fuel”, entrusted to CRIEPI by Ministry of Education, Culture, Sports, Science and Technology of Japan (MEXT).

References

1. T. Koyama, Y. Sakamura, T. Ogata and H. Kobayashi, “Pyroprocess and Metal Fuel Development for Closing Actinide Fuel Cycle with Reduced Waste Burden”, Proc. of GLOBAL2009, September 6-11, 2009, France, Paris, pp.1261-1267 (2009).

2. T. Inoue, T. Yokoo and T. Nishimura, “Assessment of Advanced Technologies for the Future Nuclear Fuel Cycle”, Proc. Int. Conf. on Future Nuclear Systems, GLOBAL'99, CD-ROM, American Nuclear Society, Jackson Hole, USA (1999).

3. M. Kurata, T. Inoue, L. Koch, J.-C. Spirlet, C. Sari, and J.-F. Babelet, “Development of Transmutation Technology of Long-Lived Nuclides -Properties of the Alloy Including MA and RE-”, Report No. T92005, Central Research Institute of Electric Power Industry (1992) (in Japanese).

4. T. Kato, T. Inoue, T. Iwai and Y. Arai, “Separation behaviors of actinides from rare-earths in moltensalt electrorefining using saturated liquid cadmium cathode”, J. Nucl. Mater., 357, 105 (2006).

5. M. Kurata, T. Inoue, J. Serp, M. Ougier, J.-P. Glatz, “Electro-chemical Reduction of MOX in LiCl”, J. Nucl. Mater., 328, 97 (2004).

6. T. Inoue, M. Sakata, H. Miyashiro, T. Matsumura, A. Sasahara, and N. Yoshiki, “Development of partitioning and transmutation technology for long-lived nuclides”, Nucl. Technol., 93, 206-220 (1991).

7. M. Kurata, N. Yahagi, S. Kitawaki, A. Nakayoshi and M. Fukushima, "Sequential Electrolysis of U-Pu Alloy Containing a Small Amount of Am to Recover U- and U-Pu-Am Products", J. Nucl. Sci. Technol., 46 (2009) 175.

8. M. Iizuka, K. Uozumi, T. Ogata, T. Omori and T. Tsukada, "Development of an Innovative Electrorefiner for High Uranium Recovery Rate from Metal Fast Reactor Fuels", J. Nucl. Sci. Technol., 46, (2009) 699.

9. T. Koyama, T. Hijikata and T. Inoue, "Development of engineering technology basis for industrialization of pyrometallurgical reprocessing", Global 2007, 1038-1043, Boise, Idaho(2007).

10. Y. Sakamura, M. Kurata and T. Inoue, "Electrochemical Reduction of UO_2 in Molten LiCl or LiCl-KCl eutectic", Proc. 7th International Symposium on Molten Salts Chemistry & Technology (MS7), p. 597, Toulouse, France (2005).

11. Y. Sakamura, M. Kurata and T. Inoue, “Electrochemical Reduction of UO_2 in Molten $CaCl_2$ or LiCl”, J. Electrochem. Soc., 153, D31 (2006).

12. M. Iizuka, Y. Sakamura and T. Inoue, “Electrochemical Reduction of (U-40Pu-5Np)O_2 in Molten LiCl Electrolyte”, J. Nucl. Mater., 359, 102 (2006).

13. M. Iizuka, T. Inoue, M. Ougier, J. P. Glatz, “Electrochemical Reduction of $(U,Pu)O_2$ in Molten LiCl and $CaCl_2$ Electrolytes”, J. Nucl. Sci. Technol., 44, 801 (2007).

14. Y. Sakamura, M. Iizuka and T. Inoue, “Development of Oxide Reduction Process to Bridge Oxide Fuel Cycle and Metal Fuel Cycle”, Proc. Global 2009, pp.9176, Paris, France (2009).

15. Y. Sakamura and T. Omori, “Electrolytic Reduction and Electrorefining of Uranium to Develop Pyrochemical Reprocessing of Oxide Fuels”, Nucl. Technol., to be published.

16. K. Uozumi, M. Iizuka, M. Kurata, T. Inoue, T. Koyama, M. Ougier, R. Malmbeck, and J.-P. Glatz, “Demonstration of pyropartitioning process to recover TRUs from genuine high-level liquid waste”, Proc. Global 2009, pp.9086, Paris, France (2009).

17. M. Kurata, K. Kinoshita, T. Hijikata, and T. Inoue, “Conversion of simulated high-level liquid waste to chloride for the pretreatment of pyrometallurgical partitioning process”, J. Nucl. Sci. Technol., 37, 8, 682-690 (2000).

18. H. Ohta, T. Yokoo, T. Ogata, T. Inoue, M. Ougier, J-P. Glatz, B. Fontaine and L. Breton, ‘Irradiation Experiment on Fast Reactor Metal Fuels containing Minor Actinides to 7 at.% Burnup’, Proc. Global 2007, USA, Boise (2007).

19. H. Ohta, D. Papaioannou, T. Ogata, T. Yokoo, T. Koyama, V. V. Rondinella and J.-P. Glatz, “Postirradiation Examinations of Fast Reactor Metal Fuels Containing Minor Actinides –Fission Gas Release and Metallography of ~2.5at% Burnup Fuels-”, Proc. Global 2009, pp.9241, Paris, France (2009).

Electrochemistry of uranium in molten fluorides

C. Nourry[a], P. Souček[a], L. Massot[b], R. Malmbeck[a], P. Chamelot[b] and J.-P. Glatz[a]
[a]*European Commission, JRC, Institute for Transuranium Elements, Postfach 2340, 76125 Karlsruhe, Germany*
[b]*Laboratoire de Génie Chimique (LGC), Département Procédés Electrochimiques, CNRS-UMR 5503, Université de Toulouse III - Paul Sabatier, 31062 Toulouse cedex 9, France*
Tel: +49-7247-951863 , Fax: +49-7247-95199124 , e-mail: Christophe.Nourry@ec.europa.eu

Abstract: *This article is focused on the electrochemical behaviour of U ions in the LiF-CaF_2 (79-21 wt.%). On W electrode, U(III) is reduced in one step into U metal. U(III) can also be oxidised into U(IV). Both systems have been studied; obtained results are in a good agreement with previous studies. On Ni electrode, depolarisation effect due to intermetallic compounds formation has been observed.*

A. Introduction

Nowadays, solutions used for the nuclear fuel waste management are disposal or single recycling of U and Pu. For the future, a closed fuel cycle concept is considered for the Generation IV reactor types [1]. This scenario has advantages to decrease the volume and radiotoxicity of the final waste, to be more proliferation resistant and to save large amount of uranium for new fuel fabrication.

Pyrochemical reprocessing is one of the promising routes explored for a complete actinide management. It has been proven that molten chloride media are suitable to perform dissolution and pyrochemical reprocessing of metallic or oxide fuel [2-5]. In the case of Molten Salt Reactor, the molten salts are used as fuel and primary coolant. In this case, high neutron capture of chloride ions excludes the use of molten chlorides and molten fluorides will be more appropriated. Due to very demanding working conditions (higher melting point, corrosion, oxide dissolution…), molten fluorides and properties of actinides in those media are unfamiliar. To our knowledge, only few electrochemical studies have been published concerning actinides electrochemistry in molten fluorides [6,7].

This article is focused on the electrochemical behaviour of U ions in the LiF-CaF_2 eutectic mixture (79-21 Wt %) on W (inert) and Ni (reactive) electrodes.

B. Experimental

B.1. Electrochemical experiments

All the electrochemical experiments and melt preparation were done in a glove box under pure argon atmosphere (< 5ppm of oxygen and moisture). Electrochemical experiments and electrodeposition runs were carried out with a three-electrode set-up connected to a PAR 273 potentiostat using CorrWare2 electrochemical software. A Pt wire immerged in the salt is used as comparison electrode [8]. Working electrodes were made of 1 mm diameter W or Ni wire and the counter electrode was a Mo wire bent into the shape of a spiral.

B.2. Preparation of the melt

Boron nitride was selected as material for the crucible. Pure LiF and CaF_2 (Alfa Aesar, 99.99% ultra dry, packed under argon) were used for the solvent preparation. The eutectic LiF-CaF_2 (79-21 wt.%) was prepared in the glove box by mixing of the pure chemicals with no additional treatment. U ions were produced by chemical oxidation of metallic uranium by bismuth ions. A first melt was prepared with an excess of Bi, leading to the formation of U(IV) a second with an excess of U leading to U(III) :

$$4Bi^{3+} + U = 3U^{4+} + Bi \qquad \text{eq.(1)}$$

$$Bi^{3+} + U = U^{3+} + Bi \qquad \text{eq.(2)}$$

Theses two melts are respectively prepared for the analysis of the U(IV)/U(III) and U(III)/U(IV) systems.

Bi^{3+} was introduced into the melt in form of BiF_3 (Alfa Aesar 99.999%) and a Bi pool was placed at the bottom of the crucible to recover the formed metallic Bi, as shown in Fig. 1.

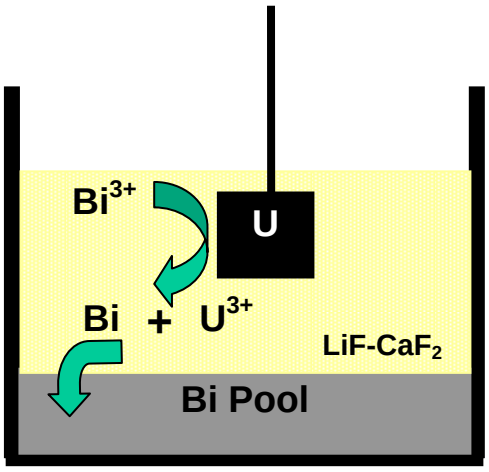

Figure 1: scheme of the set-up used for the melt preparation

The conditions used for the melts preparation are summarized in table 1:

Table 1: preparatory conditions for the two melts

$m_{LiFCaF2}$ (g)	m_{BiF3} (g)	m_{Uplate} (g)	reaction time	colour of the salt
30.00	1.532	1.045	~16h	Green (U(IV))
29.83	0.905	0.904	~9h	violet (U(III))

B.3. Analytical techniques

To obtain the precise solute concentration in the melt, a sample of salt (~30mg) was dissolved in 4ml of HCl (8M) heated at 80°C. The amount of uranium was determined by inductively coupled plasma-mass spectrometry analysis (ICP-MS). The U(IV) concentration in the preparation was 1.7 wt% and U(III) concentration was 1.6 wt%.

C. Electrochemical analysis of the U system

A comparison of cyclic voltammograms plotted in the pure solvent (black curve) and in the melt containing U ions (red curve) is shown in Fig. 2.

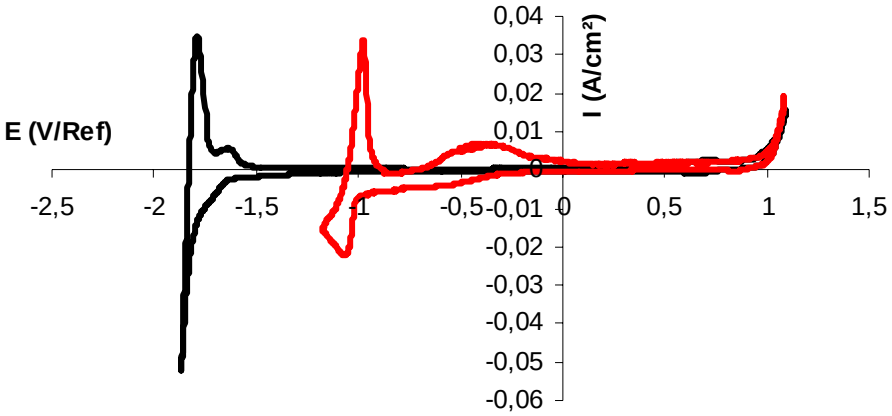

Figure 2: comparison of cyclic voltammograms plotted in $LiF-CaF_2$ (black curve) and in $LiF-CaF_2$- UF_4 (1.7wt%) (red curve) at 1083K; WE: W, CE: Mo, RE: Pt; v =100mV/s.

Addition of U ions in the melt drives to the apparition of two systems observed on the voltammogram:

- a soluble-soluble system at -0.5 V/ref
- a system leading to a solid phase formation at -1.1 V/ref.

C.1. Reversibility of the system

Cyclic voltammetry and square wave voltammetry were used in this work and the reversibility of both systems was checked for those two techniques at different scan rate and frequency.

1. Cyclic Voltammetry

Criteria for reversibility are the linearity of the peak intensity with the square root of the frequency (Fig. 3) and the invariance of the peak potential with the scan rate (Fig. 4) [9]. Generally, a system is considered irreversible if the peak potential is linear with the logarithm of the scan rate.

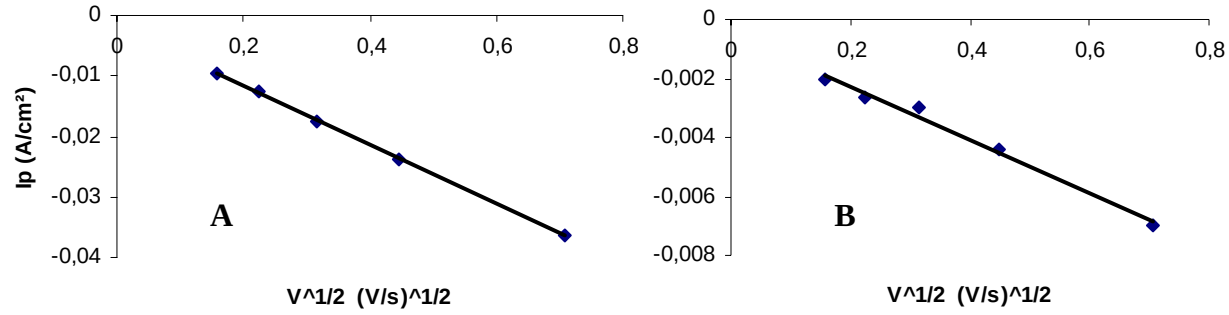

Figure 3: Variation of the peak intensity of U systems vs. the square root intensity of the sweep rate, A corresponds to the more cathodic and B to the more anodic one.

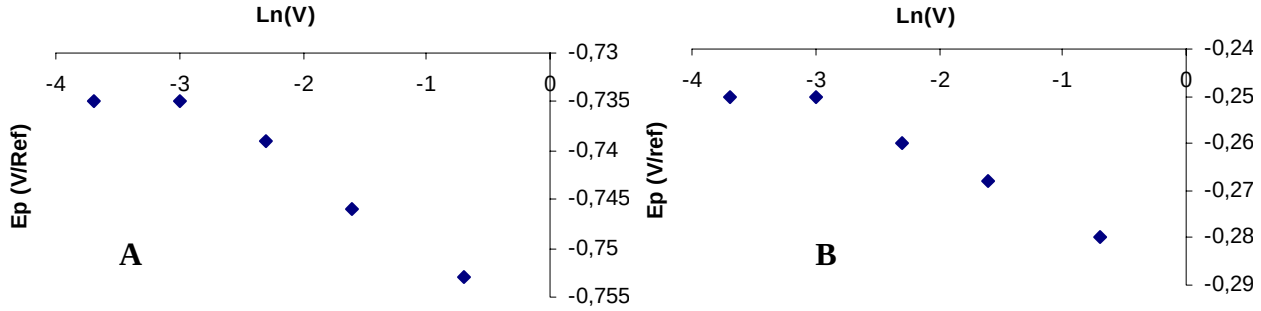

Figure 4: Variation of the U systems peak potential vs. the logarithm of the sweep rate, A corresponds to the more cathodic and B to the more anodic one.

Figures 3 and 4 show that the systems can be considered as reversible, limited by mass transport, for scan rate below 50 mV/s and irreversible, limited by charge transfer, for higher scan rates.

2. Square-wave Voltammetry

A typical square wave voltammogram of the system is show in figure 5.

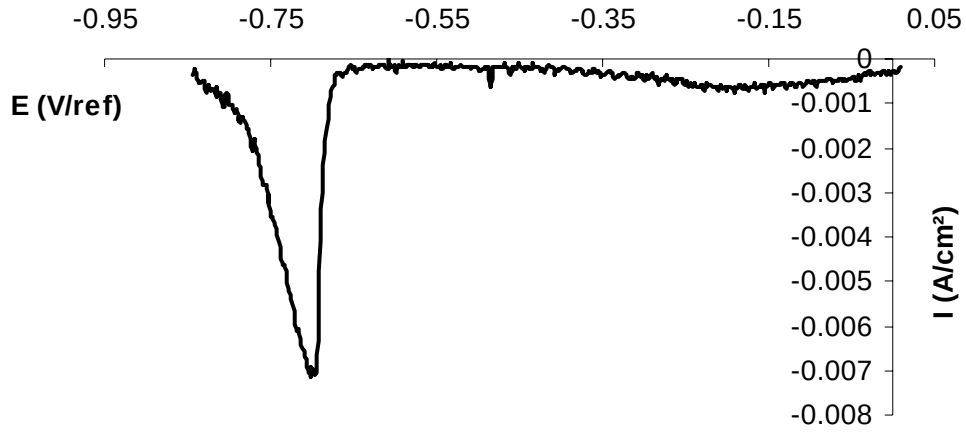

Figure 5: Square wave voltammogram of the LiF-CaF_2-UF_4 (1.7 wt%) system at 1083K; WE: W, CE: Mo, RE: Pt; f = 9Hz.

The two systems observed with cyclic voltammetry are on the square-wave voltammogram. The difference in terms of potential is due to the shift of the Pt comparison electrode potential. The evolution of both peaks intensity versus the square root of the frequency is reported in Fig. 6.

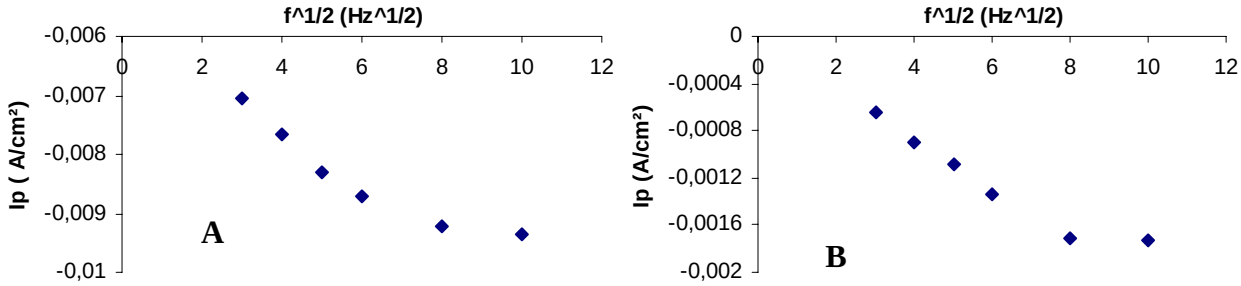

Figure 6: Variation of the U systems peak intensity, A corresponds to the more cathodic and B to the more anodic one.

The variation of the peaks intensity with the square root of the frequency was linear in the 9-36Hz range and proves that for this frequencies, both systems are reversible [10,11]. For higher frequency, the system is irreversible.

C.2. Number of exchanged electrons

The number of exchanged electrons was calculated from square wave voltammetry technique, applying equation (3), which is valid for reversible systems [10-12].

$$W_{1/2} = 3.52\frac{RT}{nF} \qquad \text{eq.(3)}$$

$W_{1/2}$ is the half width of the peak (V), R is the ideal gas constant (J mol^{-1} K^{-1}), T is the absolute temperature (K), *n* is the number of exchanged electrons and *F* is the Faraday constant (C mol^{-1}). Calculations were done with square waves voltammograms plotted at 9Hz. For the soluble-soluble system, it was possible to directly apply the equation 2. However, in case of the second system, the signal was modified due to the formation of a solid deposit. The peak was decomposed in two half Gaussian curves. The more negative one, non-influenced by nucleation, was extrapolated to from the complete Gaussian curve. Fig. 7 shows a comparison between the experimental curve and the deconvoluted signal.

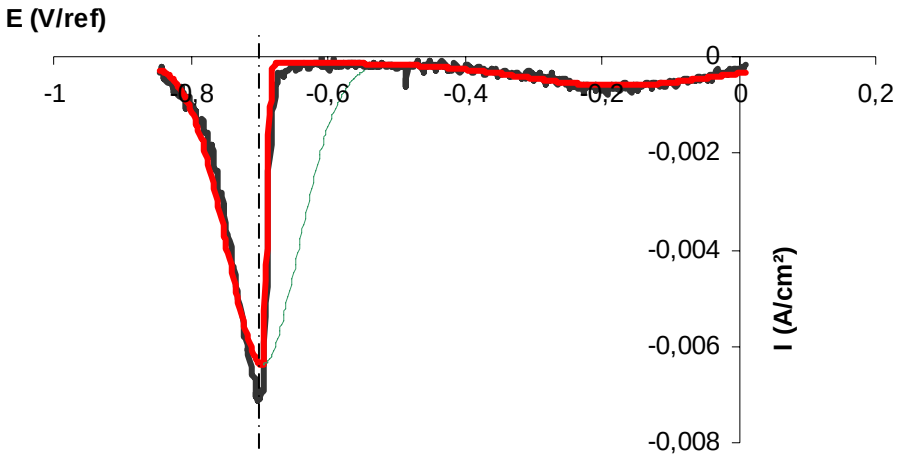

Figure 7: Comparison of the experimental square wave voltammogram plotted at 9Hz (black curve) with the deconvoluted signal (red curve); in green, the extrapolated part

According to equation 2, the number of exchanged electrons for the first system is 1.03 ± 0.1 electron and 2.9 ± 0.2 for the second system. Other technique used to determine the number of exchanged electrons consists in subtracting the potential of the peaks observed in cyclic voltammetry for the initial scan Epc (cathodic part) and the for the reverse scan Epa (anodic part). This difference ΔEp is linked to the number of exchanged electrons for reversible systems according to equation 4 [12]:

$$\Delta E_p = 2.23\frac{RT}{nF} \qquad \text{eg.(4)}$$

The number of exchanged electrons obtained by this method for the first system is 1.02 ± 0.1 electron and 2.52 ± 0.2 for the second system.

According to those results, the reduction of U(IV) into U metal in LiF-CaF_2 medium occurs in two steps, the first involve one electron and lead to the formation of U(III) and the second involves three electrons and lead to the formation of U metal:

$$U(IV) + e^- \rightarrow U(III) \qquad \text{eq.(5)}$$
$$U(III) + 3\ e^- \rightarrow U(0) \qquad \text{eq.(6)}$$

C.3. Determination of the diffusion coefficient

Diffusion coefficients were calculated using cyclic voltammetry, applying the Randles-Sevcik equation (eq 7) for the U(IV)-U(III) system and the Berzins-Delahaye [13,14] equation (eq 8) for the U(III)-U(0) system. For a soluble reaction product, the equation 7 is used to describe the evolution of the cyclic voltammogram peak intensity with the scan rate:

$$I_p = 0.446(nF)^{3/2}(RT)^{-1/2} C\ D^{1/2} v \qquad \text{eq.(7)}$$

And for an insoluble product, equation 8 is applied:

$$I_p = 0.61(nF)^{3/2}(RT)^{-1/2} C\ D^{1/2} v \qquad \text{eq.(8)}$$

Ip is the peak intensity (A cm^{-2}), *C* is the electroactive substance concentration at the electrode surface (mol cm^{-3}), *D* is electroactive substance diffusion coefficient (cm^2 s^{-1}) and *v* is the potential sweep rate (V s^{-1}).

At 1090 K, U(IV) diffusion coefficient is equal to 3.7 ± 0.1 10^{-5} cm²/s and U(III) diffusion coefficient is equal to 2.4 ± 0.1 10^{-5} cm²/s. In the same media, at 1083 K, Hamel et al [7] have found $D_{U(III)}$ = 2.2 10^{-5} cm²/s and in LiF-NaF at 993 K $D_{U(IV)}$ = 1.5 10^{-5} cm²/s. Those results are in good agreement with the values evaluated by this work.

C.4. Electrochemical study on a Ni reactive electrode

Fig. 8 shows a comparison between two cyclic voltammograms plotted on W (blue curve) and on Ni (red curve).

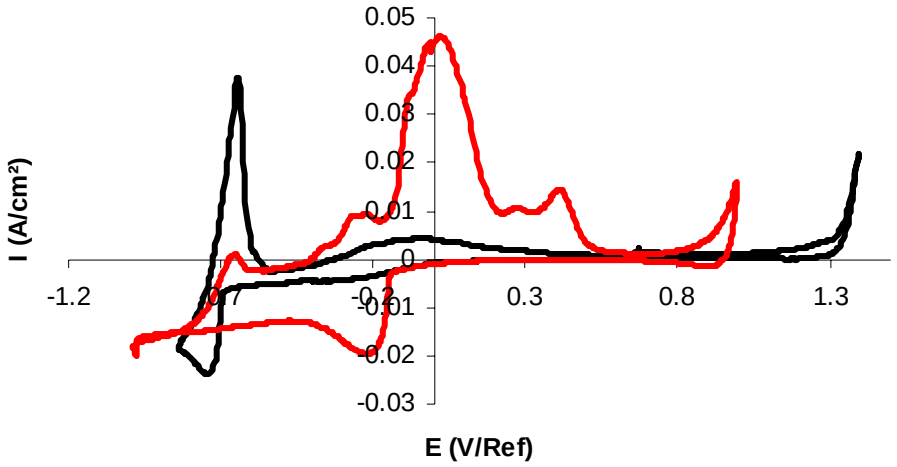

Figure 8: Comparison of cyclic voltammograms plotted in LiF-CaF_2- UF_4 (1.7wt%) at 1083K; WE: W (black curve) Ni (red curve), CE: Mo, RE: Pt; v =100mV/s.

The red curve exhibits a peak at -0.2 V not observed on the black curve. This peak corresponds to the reduction of uranium ions into metal to form intermetallic compounds with the electrode substrate. This phenomenon is called Under Potential Depostion. The depolarisation is roughly 0.5 V. The presence of many oxidation waves corresponds to the reoxidation of the different compounds formed during the reduction step.

D. Conclusion

The electrochemical behaviour of U(III) has been studied in molten LiF-CaF_2. The obtained results are in agreement with the literature and shows that U(III) is reduced into U metal in one step controlled by diffusion in solution. The phenomenon known as Under Potential Depostion has been observed on Ni electrode. These first results are encouraging for the development of a spent fuel reprocessing in molten fluorides, recovering actinides on reactive electrodes. The next step that consists of separation of actinides from a solvent containing fission products is under investigation in ITU.

Aknowledgements

The authors wish to thank M. Cardinale for ICP-MS analysis as well as M. Ougier and A. Rodrigues for experimental support. This work was carried out with European Commission financial support in the 7th Framework programme, under the contract 211267 "ACSEPT".

References

1. A Technology Roadmap for Generation IV Nuclear Energy Systems. 2002, U.S. DOE Nuclear Energy Research Advisory Committee at the Generation IV International Forum, GIF-002-00, available online: http://gif.inel.gov/roadmap/.

2. Cassayre, L., et al., Investigation of Electrorefining of Metallic Alloy Fuel onto Solid Al Cathodes. *Journal of Nuclear Materials*, 2007. 360: p. 49-57.

3. Souček, P., et al., Electrorefining of U-Pu-Zr-alloy fuel onto solid aluminium cathodes in molten LiCl-KCl *Radiochimica Acta*, 2008. 96: p. 315-322.

4. Iizuka, M. et al, Electrochemical reduction of (U–40Pu–5Np)O2 in molten LiCl electrolyte *Journal of Nuclear Materials*, 359, Issues 1-2, 2006, p 102-113.

5. Iizuka, M et al, Electrochemical Reduction of $(U,Pu)O_2$ in Molten LiCl and $CaCl_2$ Electrolytes, *Journal of nuclear science and technology*, Vol 44, 5 2007, p 801-813.

6. Lacquement, J. et al, Potentialities of fluoride-based salts for specific nuclear reprocessing: Overview of the R&D program at CEA, Journal of Fluorine Chemistry 130, 2009, 18–21

7. Hamel C. et al, Reduction process of uranium(IV) and uranium(III) in molten fluorides *Electrochimica Acta* 52, 2007, 3995–4003

8. Berghoute Y., et al, *Journal of Electroanalytical*. Chemistry. 365, 1994, 171.

9. Southhampton Electrochemistry Group, *Instrumental Methods in Electrochemistry*, Chap 6, Ellis Horwood Series in Physical Chemistry 1985.

10. Chamelot P. et al, *Electrochimica Acta* 39, 1994, 2571.

11. Chamelot P. et al, *Electrochimica Acta* 47, 2002, 3423.

12. Trémillon B. *Electrochimie analytique et réactions en solution*, tome 2, Chap 9, Masson, 1993.

13. Berzins T. et al, *Journal of the American Chemical Society*, 75, 1953, 555.

14. Store T. et al, *Journal of the Applied Electrochemistry* 30, 2000, 1351.

Attempt to classify various molten fluoride mixtures according to their solvation powers regarding metal fluorides

S. Jaskierowicz[*#], S. Delpech[*#], C. Slim[#], G. Picard[#]
* Institut de Physique Nucléaire d'Orsay
[#]*Laboratoire d'Electrochimie, de Chimie des Interfaces et de Modélisation pour l'Energie*
Ecole Nationale Supérieure de Chimie de Paris – Chimie Paristech
11 rue Pierre et Marie Curie – 75231 Paris Cedex 05
Tel: (33) 1.55.42.12.34 , Fax: (33)1.44.27.67.50, e-mail: sebastien-jaskierowicz@chimie-paristech.fr

Abstract *– The choice of a molten reaction media to perform a chemical process can be only based on the knowledge of its intrinsic properties. Often unknown, it becomes necessary to determine or to estimate it. In this work, we describe the possibility to use under certain conditions a redox couple as an indicator of the acidity power of melts. The accuracy of measurements and the possibility of their improvements are discussed.*

A. INTRODUCTION

The molten salt fast reactor is one of the six concepts which were selected as a possible concept for the IVth generation of nuclear energy system. The particularity of molten salt reactor is to use a liquid fuel constituted of fluoride salt mixture: LiF, ThF_4, UF_4 (or PuF_3). The chemical issues addressed for this concept are the chemical properties of the salt (on which depend the solubilities and the properties of fission products), the pyrochemical methods required for the spent fuel reprocessing and the control of the redox potential of the fuel salt which insures the structural material resistance.
.
In this work we were specially interested by the fluoro-acidity of fluoride mixtures and the impact on the solvation of metal fluorides which depends mainly on the activity of fluoride ions. Solvation of oxide compounds is also a function of fluoro-acidity but the nature of the heavy cation fluoride constituting the mixture is also implicated.

In this way, a concept of pF indicator electrode was developed providing, through potentiometric measurements, a relative fluoro-acidity scale leading to classify and quantify the acidity of various fluoride mixtures.

B. ANALYTICAL CORRELATION BETWEEN POTENTIAL AND FLUORO-ACIDITY

B.1. Recall of the fluoro-acidity and solvoacidity concepts

Fluoro-acidity is defined from the following anion exchange:

$$MF_x^{3-x} \Leftrightarrow MF_{x-y}^{3-x-y} + F^- \qquad (1)$$

MF_x^{3-x} is a donor of F^- and called a fluorobase, and $MF_{x-y}^{3-x-y^-}$ is an acceptor and called a fluoroacid.
If we consider now a molten mixture constituted of one light and one heavy metal fluorides, the latter being more acidic interacts strongly with fluoride anions and gives rise to the formation of one or several complexes such as described above. In that case, melt is totally dissociated into ions and the heavy metal complex can undergoes a self dissociation such as eq. (1). This process is called solvoacidity.
.
Three kinds of fluoride F^- are known:

- F^- is not part of a coordination, it is a free fluoride,
- F^- is part of a coordination,
- F^- is part of a coordination and form a bridge between two complexes.

The more a salt contain free fluoride, the more its basicity is pronounced. The eutectic LiF-NaF-KF (46,5:11,5:42 mol%), also called FLiNaK, contains only the free form of fluoride. It is the most basic molten fluoride salt. Free fluoride quantities, consequently acidity or basicity of a salt is directly connected to its ability to solubilize other species such as LnF_3.

The equilibrium constant of equation (1):

$$k = \frac{a_{MF_x^{3-x}}}{a_{MF_{x-y}^{3-x-y}} . a_{F^-}} \quad (2)$$

where a_i stands for the activity of i in the fluoride melt, shows that notions of acidity or basicity are directly link with the activity of F^- in these melt.

B.2. Towards a potentiometric indicator of the acidity power of a melt

Our approach is based on the behaviour of the reversible redox system in melts. In our case, the system Ni(II)/Ni was chosen [2]. Dissolution of solid NiF_2 leads to a "solvation" reaction due to the interaction of this fluoride with melt. Hence Ni(II) can exist under the form of Ni^{2+}, NiF^+ (if NiF_2 acts as a fluoride anion donor), NiF^{3-}, NiF_4^{2-} (if NiF_2 is acidic). So the stable solvated species of NiF_2 reflects the fluoroacidity power of melt. Besides the potential of the Ni(II)/Ni electrochemical system which depends on the activity of Ni(II) i.e. the nature of the solvated species of NiF_2, becomes a real indicator of the acidity power of melt.

Differences of potential (ΔE) were measured between two electrodes (described in experiment). In order to compare the potentials, one of the electrodes remained the same while in the others the fluoride mixture which serves as solvent were changed. Due to its specificity (most basic fluoride melt) FLiNaK were chosen as the solvent of the unchanged electrode, which then plays the role of comparison electrode.

The electrochemical indicator is the couple NiF_2/Ni whose system is supposed to obey to the following equation (3).

$$NiF_2 + 2e^- \Leftrightarrow Ni + 2F^- \quad (3)$$

The potential of the system (FLiNaK + NiF_2/Ni) is defined by Nernst's law and is described by equation (4).

$$E_{FLiNaK} = (E^0_{NiF_2/Ni})_{FLiNaK} + \frac{2.3RT}{2F}(\log \frac{a(NiF_2)_{FLiNaK}}{a(F^-)^2_{FLiNaK}}) \quad (4)$$

Where:

$E^0_{NiF2/Ni}$ = standard redox potential of the system NiF_2/Ni
R = ideal gas constant
T = temperature in Kelvin
F = Faraday constant
$a(NiF_2)_{FLiNaK}$ = activity of NiF_2 in molten FLiNaK
$a(F^-)_{FLiNaK}$ = activity of F^- in molten FLiNaK

The general expression for activity is:

$$a(NiF_2) = x(NiF_2) \times Y(NiF_2)$$

Where x(NiF_2) is the mole fraction and Y(NiF_2) is the activity coefficient of NiF_2

Various fluoride mixtures, called investigated salt (IS), were used as solvents in the second electrode, these systems potentials (salt + NiF_2/Ni) are described by the general equation (5).

$$E_{IS} = (E^0_{NiF_2/Ni})_{IS} + \frac{2.3RT}{2F}(\log \frac{a(NiF_2)_{IS}}{a(F^-)^2_{IS}}) \quad (5)$$

Nernst equation (4) & (5) leads to an expression of ΔE as a function of NiF_2 and F^- activity, equation (6).

$$\Delta E = ((E^0_{NiF_2/Ni})_{IS} - (E^0_{NiF_2/Ni})_{FLiNaK}) + \frac{2.3RT}{2F}(\log \frac{a(F^-)_{FLiNaK}.a(NiF_2)_{IS}}{a(NiF_2)_{FLiNaK}.a(F^-)^2_{IS}}) \quad (6)$$

Being chosen as the reference salt, the F^- activity in FLiNaK was considered to be 1. The standard potential of NiF_2/Ni is based on thermodynamical data and is independent of the composition of the melt. Consequently equation (6) turns into equation (7).

$$\Delta E = \frac{2.3RT}{2F}(\log \frac{a(NiF_2)_{IS}}{a(NiF_2)_{FLiNaK}.a(F^-)^2_{IS}}) \quad (7)$$

In equation (7) ΔE is an experimental data as well as T, $x(NiF_2)_{salt}$, $x(NiF_2)_{FLiNaK}$ but $Y(NiF_2/Ni)_{FLiNaK}$, $Y(NiF_2/Ni)_{salt}$ and $a(F^-)_{salt}$ are unknown. By isolating these unknown variables, we can have access to a value depending on $a(F^-)_{salt}$ as shows in equation (8).

$$\varphi = \log \frac{\gamma(NiF_2)_{IS}}{\gamma(NiF_2)_{FLiNaK}.a(F^-)^2_{IS}} = \frac{2F}{2.3RT}\Delta E - \log(\frac{(x_{NiF_2})_{IS}}{(x_{NiF_2})_{FLiNaK}}) \quad (8)$$

This value reflects the relative fluoro-acidity of a melt, based on a comparison with FLiNaK. A scale can be created taking the FLiNaK fluoro-acidity as the origin.

C. EXPERIMENT

C.1. Technical

LiF, NaF, KF, AlF_3 and ZrF_4 salt were purchased from Sigma-Aldrich, while ThF_4 was provided by Rhodia and UF_4 by IPNO.
Six salts related to nuclear applications were prepared:

- LiF-NaF-KF (46.5:11.5:42 mol%),
- LiF-ThF_4 (77:23 mol%),
- KF-AlF_3 (50:50 mol%),
- LiF-UF_4 (70:30 mol%),
- LiF-ZrF_4. (50:50 mol%),
- LiF-ZrF_4 (70:30 mol%).

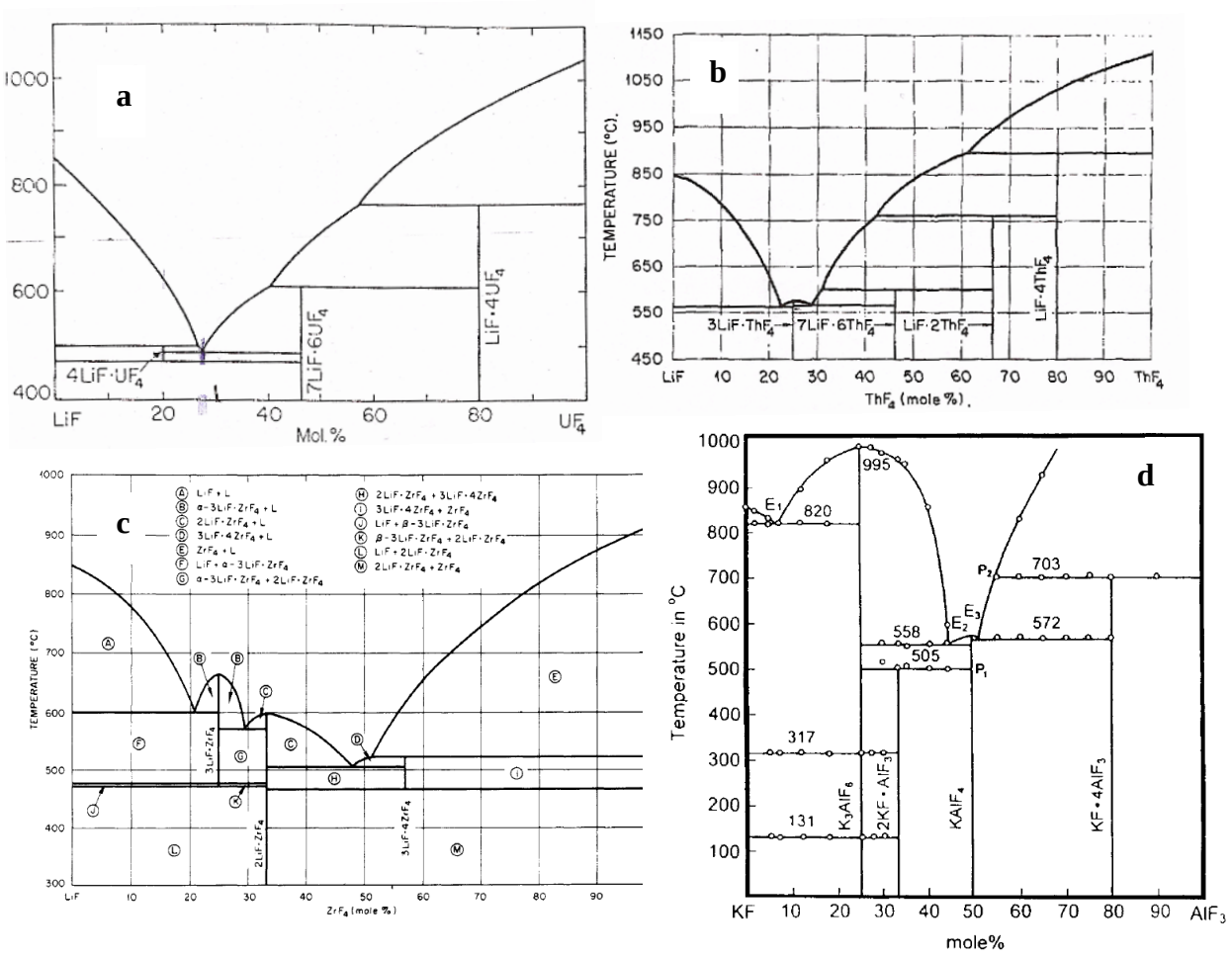

Figure 1: Phase diagrams of: (a) LiF-UF_4 after [3], (b) LiF-ThF_4 after [4], (c) LiF-ZrF_4 after [5], (d) KF-AlF_3 after [6].

Fig.1 shows that salt composition were chosen close to their eutectics.

Working electrodes were made of quartz tubes filled with one of the above salts. Each salts component were weighted and mixed with about 0.1g NiF_2 (Sigma-Aldrich, 99.99% purity) in a dry glove box under argon. The electrical contact was realized with a Ni wire (1 mm diameter). The indicator redox system is NiF_2/Ni. The indicator electrode taken as reference for the measure of the relative fluoroacidity was made on the same principle with a mixture of LiF, NaF and KF.

A 50 g eutectic mixture of 46.5 mol% LiF, 11.5 mol% NaF and 42 mol% KF with no further purification was prepared and melted in order to assure ionic conduction between the two electrodes. The salt was put into a 150 mL quartz crucible and introduced into an electrochemical reactor (Fig. 2). The reactor was then heated in a tubular furnace (80 cm), connected to a regulation monitor provided by TANER/France, until the working temperature was reached, constantly under argon atmosphere. Electrodes are then immerged in melt.

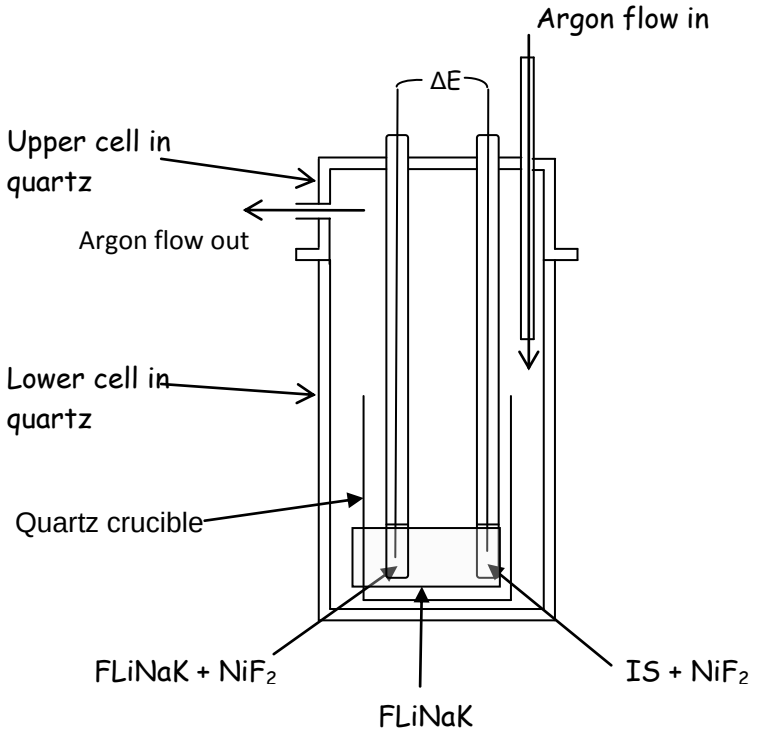

Figure 2: Experimental set up

The electrochemical measurements were performed with an EG&G potentiostat-galvanostat mod. 273 coupled with a PC computer.

C.2. Salts preparation validation

We wanted to ensure that the junction potentials were zero or negligible. For this, measurements of ΔE were made between two identical electrodes. Each one was prepared independently using the same method. ΔE is recorded versus time (Fig.2). If the method for preparing the salts is correct, these two salts should be identical in composition and ΔE should be measured at 0 V/Ref.
ΔE was recorder during 30 minutes. The value measured was 0V (Fig.3), and thus junction potentials are then negligible.

D. ELECTROCHEMICAL EVALUATION OF FLUORO-ACIDITY

*D.1. **Potentiometric** measurements*

Measurements were made at 605°C with a FLiNaK-filled electrode taken as the reference.
Fig.2 shows potential versus time of six various mixtures.

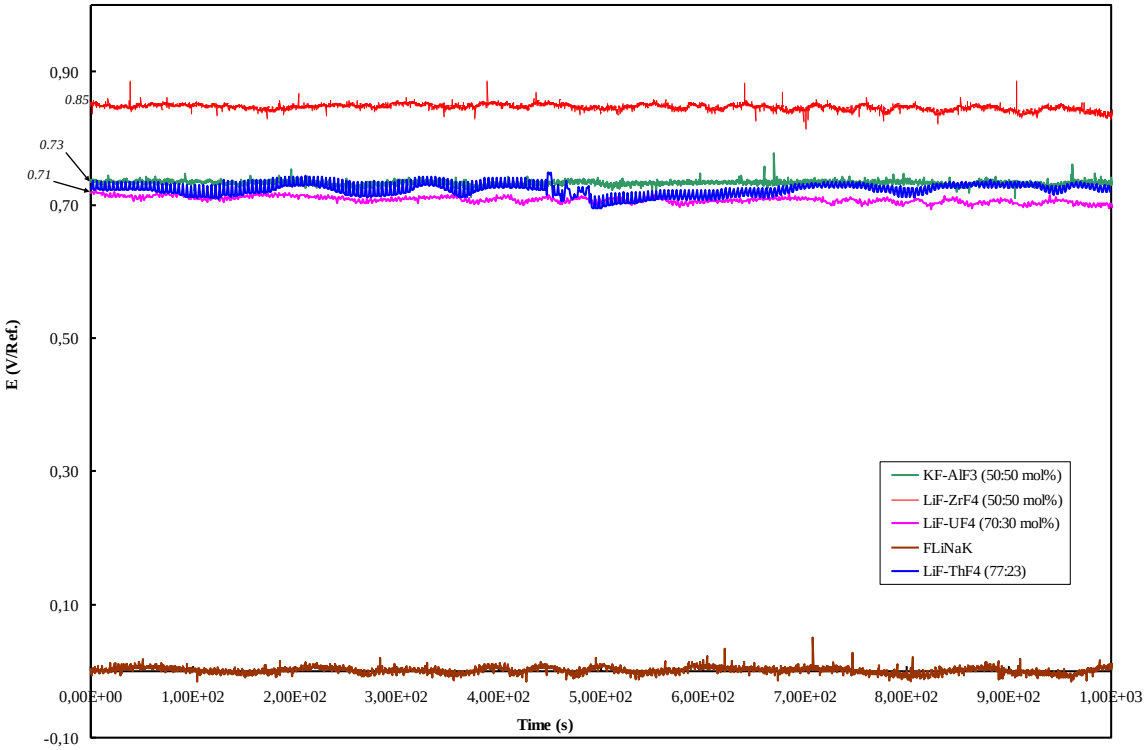

Figure 3: Differences of potential versus time between FLiNaK-filled electrode and various fluorides based electrodes (FLiNaK in brown, LiF-ThF_4 in blue, LiF-UF_4 in black, KF-AlF_3 in green, LiF-ZrF_4 in red)

Table 1: Melts compositions uses as solvent in various electrodes

Melts	Components	Molar fraction	x(NiF_2)	ΔE (V/Ref.)
FLiNaK (reference)	LiF	0.459	0.0103	0
	NaF	0.114		
	KF	0.415		
LiF-ZrF_4	LiF	0.44	0.021	0.85
	ZrF_4	0.54		
LiF-ZrF_4	LiF	0.69	0.0205	0.76
	ZrF_4	0.29		
KF-AlF_3	KF	0.490	0.0199	0.73
	AlF_3	0.491		
LiF-UF_4	LiF	0.7	0.0334	0.71
	UF_4	0.3		
LiF-ThF_4	LiF	0.75	0.0276	0.73
	ThF_4	0.23		

Differences in potential between salts at 50:50 mol% (LiF-ZrF_4 and KF-AlF_3) and salts at about 70:30 mol% (LiF-UF_4 and LiF-ThF_4) can be explained by different activity coefficients for NiF_2 and F^- in each melt (equation (3)). The nature and coordination of the heavy nuclei are mainly concerned by the activities coefficients variation. Coordinations of Th^{+IV}, U^{+IV} and Zr^{+IV} were studied by L. M. Toth *et al.* [7-10]Th^{+IV} were also studied by Bessada *et al* [11]. These studies shows, in our range of composition, that for LiF-UF_4 the coordination of U was either 7 or 8 without further precision on U molar fraction, while for LiF-ThF_4 for a 77:23mol% melt the coordination of Th^{+IV} were shown to be 7.

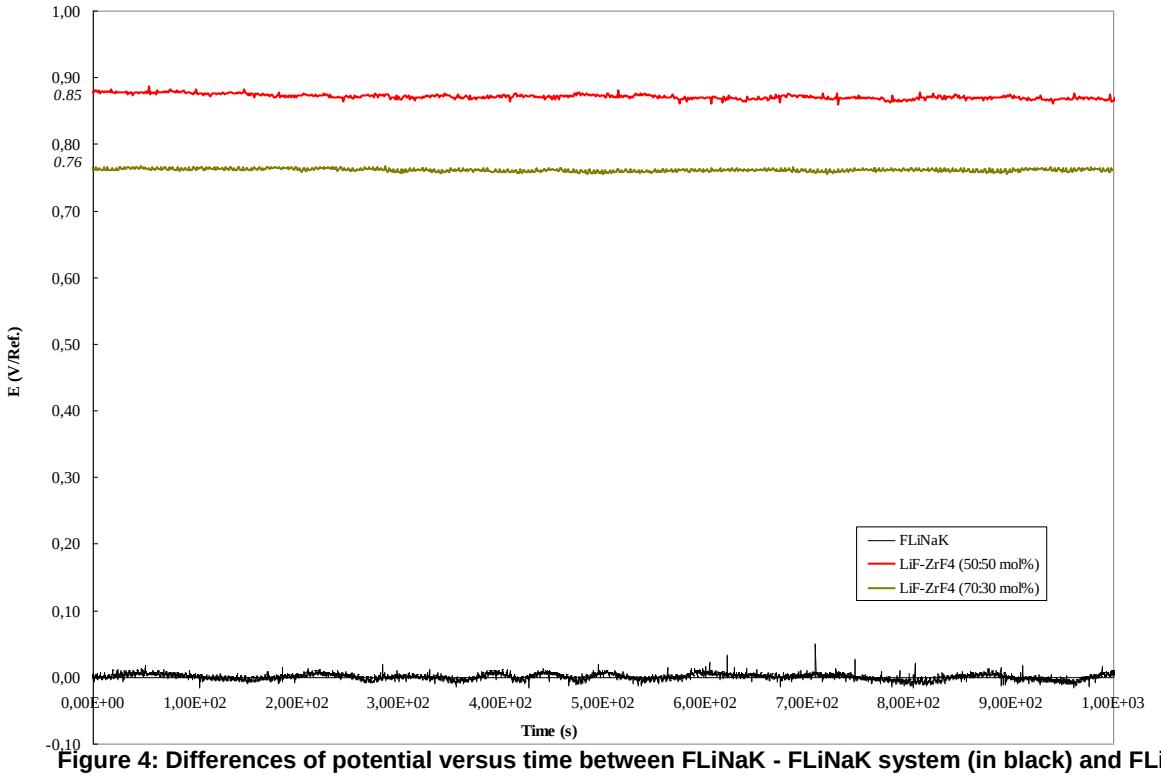

Figure 4: Differences of potential versus time between FLiNaK - FLiNaK system (in black) and FLiNaK – LiF-ZrF_4 system with various ZrF_4 compositions (ZrF_4: 50 mol% in red, 30 mol% in yellow)

Fig.4 shows two LiF-ZrF_4 compositions which were studied:

- LiF-ZrF_4 (50:50 mol%) with 0.85 V/Ref.,
- LiF-ZrF_4 (70:30 mol%) with 0.76 V/Ref.

As showed by L. M. Toth *et al.* [6] Zr coordination is related to its proportion in these melt. They showed that in LiF-NaF-ZrF_4 melt with 40 mol% ZrF_4, the coordination of zirconium was 5 or 4 while for a 25-33 mol% of ZrF_4, Zr coordination was 7. This means there is less free fluoride in the 50:50 mol% melt than in the 70:30 mol% melt, in consequence the 50:50 mol% salt is more acid than the 70:30.
Regarding ΔE measurements, a difference is seen between the two melts. The most acid is also the one with the higher ΔE: 0.85 V/Ref against 0.75 V/ref. for the most basic.
These elements showed that a link exists between potentials and acidity of a fluoride melt.

D.2. Fluoroacidity relative scale

Based on these results and on Nernst's laws, see equation (3-8), we try to build a scale reflecting the relative acidity compared to FLiNaK. This leads to a scale representing melts acidity. It is a very indirect measure of fluoro-acidity because our value depends not only on F^- activity, but also on activity coefficient of NiF_2 in each melt.
The mathematical expression of what we call "fluoro-acidity" in order to simplify the speech, is shown by equation (9).

$$\varphi = \frac{2F}{2.3RT}\Delta E - \log\left(\frac{(x_{NiF_2})_{IS}}{(x_{NiF_2})_{FLiNaK}}\right) \quad (9)$$

This equation gives a numerical value, based on experimental data which permit to classify various mixtures.

Table 2: Melts "fluoro-acidity" (φ) value and coordination of heavy nucleus

Melts	ΔE (V/Ref.)	φ	HN coordination
LiF-ZrF_4 (50:50 mol%)	0.85	10.08	ZrF_5^- [10] ZrF_6^{2-}
LiF-ZrF_4 (70:30 mol%)	0.76	9.02	ZrF_7^{3-} [10]
KF-AlF_3	0.73	8.68	KF_5^{2-} [12] KF_6^{3-}
LiF-UF_4	0.71	8.68	UF_7^{3-} [7,8] UF_8^{4-}
LiF-ThF_4	0.73	8.8	ThF_7^{3-} [9,11]

Concerning the correlation between coordination and acidity, L. M. Toth *et al.* showed the existence of equilibrium between coordination similar as the acidity-basicity equilibrium, see equation 1:

$$ZrF_8^{4-} \Leftrightarrow ZrF_7^{3-} + F^-$$
$$UF_8^{4-} \Leftrightarrow UF_7^{3-} + F^-$$
$$ThF_8^{4-} \Leftrightarrow ThF_7^{3-} + F^-$$

In our composition range for these three salts, the acidic species are the most important species. Meanwhile salts with higher content of heavy nuclei are known to possess a coordination of 6 or less and to be more acid than salts with lower heavy nuclei content. Which mean that our scale seems to follow the same evolution as the acidity of the salts: the more the salts are acid, the more the heavy nuclei content is high, the higher our value is.

This leads to create the scale presented in fig.5. Heavy nucleus coordination is also shown on this scale.

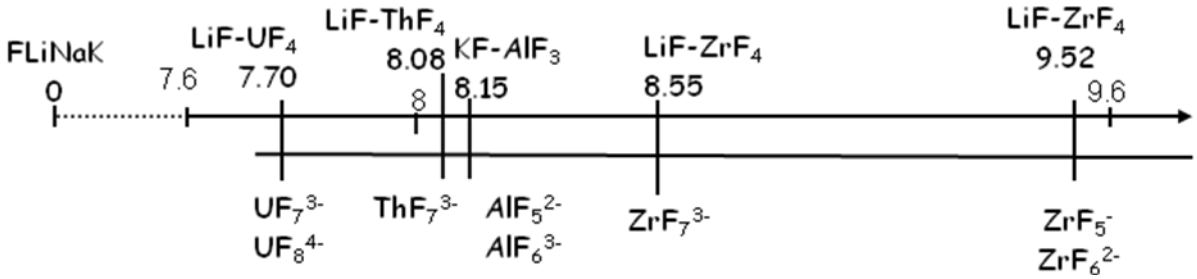

Figure 5: "Fluoro-acidity" scale. Known coordinations are also reported.

This scale allows us to see the relative acidity between melts and give us indication on which salt can be solubilized in LiF-ThF_4 (for example).
Studies are in progress concerning LiF-LnF_3 salts.

E. CONCLUSION

This work was conducted with the aims to develop an electrochemical protocol to compare the relative acidity power of fluoride melts by considering the fact that with a properly chosen electrochemical system, informations about the activity of fluoride anion can be derived.
We have so been able to classify the five fluoride melts selected for use in the nuclear domain, FLiNaK being the common denominator.

This scale is currently being improved in particular by making precise measurements of the activity coefficients of nickel fluoride in melts as well as their solubilities.
Further work will be carried out with two investigation lines: firstly to determine the fluoro-acidity power of selected ternary mixtures: (LiF-ThF_4-UF_4 and/or LiF-ThF_4-LnF_3), and secondly to deduce the relative redox power of melts taking as the thermodynamic reference the fluoride/fluorine electrochemical system.

Aknowledgements

The authors wish to thank PCR-ANSF of PACEN (Programme sur l'Aval du Cycle et l'Energie Nucleaire) of the Centre National de la Recherche Scientifique (CNRS) and Rhodia for financial supports of these studies. One of the authors (S. J.) thanks Rhodia for a grant.

References

1. S. DELPECH, E. Merle-Lucotte, D. Heuer, M. Allibert, V. Ghetta, C. Le-Brun, X. Doligez and G. Picard, *J. Fluoro. Chem.,* 130, 11 (2009).

2. D. L. MANNING, *J. Electroanal. Chem.,* 7, 302 (1964).

3. C. J. BARTON, H. A. Friedman, W. R. Grimes, H. Insley, R. E. Moore and R. E. Thoma, *J. Am. Ceram. Soc.,* 41, 67 (1958).

4. R. E. THOMA, H. Insley, B. S. Landau, H. A. Friedman and W. R. Grimes, *J. Phys.. Chem.,* 63, 1266 (1959).

5. R. E. THOMA, H. Insley, H. A. Friedman and G. M. Hebert, *J. Chem. Eng. Data,* 10, 219 (1965).

6. R. CHEN, G. Wu and Q. Zhang, *J. Am. Ceram. Soc.,* 83, *12*, 3196 (2000).

7. J. P. YOUNG, *Inorg. Chem.,* 6, 1486 (1966).

8. L. M. TOTH, *J. Phys. Chem.,* 75, *5,* 631 (1971).

9. L. M. TOTH and G. E. Boyd, *J. Phys. Chem.,* 77, *22,* 2654 (1973).

10. L. M. TOTH and G. E. Boyd, *J. Phys. Chem.,* 77, *11,* 1384 (1973).

11. C. BESSADA, A. Rakhmatullin, A. L. Rollet and D. Zanghi, *J. Nucl. Mat.,* 360, 43 (2007).

12. B. GILBERT and T. Materne, *Appl. Spectrosc.,*44, *2,* 299 (1990).

Electrorefining of Cerium in LiCl-KCl Molten Salts

R.P. Campbell-Kelly, T.J. Paget
AWE Plc
Aldermaston, UK, RG7 4PR
e-mail: rob.p.campbell@awe.co.uk

Electrorefining of cerium from cerium-gallium alloys has been demonstrated in lithium chloride-potassium chloride salts at temperatures below 500°C, with excellent current efficiencies and high product yields. These experiments are being carried out as non-active trials for a process for the purification of impure actinide metals.

The results reported show anodic current efficiencies consistently close to 100%, and in several experiments complete oxidation of the cerium in the feed occured. The cathodic product is hard and metallic, and incorporates a significant amount of salt into its structure. The product can be consolidated into a dense, pure metal by melting under calcium chloride at 850°C. The yield of this consolidation step varies between 16 and 75%, seeming to depend on the total mass of metal being consolidated and the quality of inert atmosphere.

A small-scale electrochemical cell has been demonstrated which will be used in initial active experiments.

A. INTRODUCTION

Actinides can be purified by electrolysis in a molten salt. Depending on the melting points of the actinide and the salt system used, the metal may be in either a solid or molten state. In a review of the literature, Willit et al [1] reported that for Uranium, electrorefining normally takes place below the melting point of the pure metal. This can be either via a solid anode/solid cathode process, or by the use of liquid alloys, such as uranium-cadmium anodes or uranium-nickel cathodes.

In contrast, plutonium is typically purified with both the feed and product in the liquid state, e.g. in sodium chloride-potassium chloride (NaCl-KCl) salt [1]. The efficiency of the process is limited because a build-up of impurities causes the anode freezes towards the end of the process, leaving a Pu residue which cannot be processed further. Work at Argonne reported by Blumenthal and Brodsky [2] has demonstrated that electrorefining of Pu is possible in the solid state; high purities are possible, and the process is not limited by the build-up of impurities. Further work by Miller et al [3] suggests that impurities would collect as a liquid at the surface of the feed and drip down, revealing fresh plutonium surface. Ideally, a reference electrode is required to ensure that impurities are not oxidised from the anode.

In recent years our group has worked to develop a “solid anode” process for the purification of impure actinides. This focussed on demonstrating the feasibility of the process using cerium as a non-active simulant [4]. The generation of cerium oxychloride has also been investigated; cyclic voltammetry in some runs suggested that concentrations would increase throughout the experiment [5]. However, this effect was not consistently reproducible.

This paper reports further investigations into solid anode electrorefining of cerium, including the effect of operating temperature and the development of a small-scale electrochemical cell for active trials.

B. EXPERIMENTAL AND PROCEDURE

Lithium chloride (LiCl, Fisher Scientific, 98%), potassium chloride (KCl, Fisher Scientific, 99%) and calcium chloride dihydrate ($CaCl_2.2H_2O$, Fisher Scientific, Analytical reagent grade) were dried by heating under vacuum to at least 150°C (LiCl) or 200°C (KCl, $CaCl_2$), and stored in an inert

atmosphere glovebox prior to use. Cerium chloride ($CeCl_3$, Alfa Aesar, 99.5%) and silver chloride (AgCl, Alfa Aesar, 99.9%) were used as-procured. LiCl-KCl eutectic salt (44.7wt% LiCl) with 1wt% $CeCl_3$ was mixed, fused in a 750°C furnace (element temperature) under argon, and the cast block broken into smaller pieces for use in experiments.

The cathode was made from silver steel (high carbon steel, 0.95-1.25wt% carbon). In Experiments 1-4, this was a 2mm diameter rod, whilst in Experiments 5-6 this was a 1mm diameter rod with a 15mm x 15mm paddle welded onto the end. In Experiments 1-4 a 2mm tungsten rod was also present to use as the working electrode for cyclic voltammetry. The anode was a steel basket which could hold the feed. Cerium-gallium alloy (Ce-Ga, 10wt% Ga) was procured from Johnson Matthey (REacton grade) in glass ampoules. This was cut to the required size within an inert atmosphere glovebox, and polished with a metal file and glass paper prior to use.

The reference electrode consisted of a Pythagoras ion-conductive tube procured from Multi-Lab. This contained approximately 1g of a finely ground LiCl-KCl-2wt% AgCl, previously fused under argon at 750°C, and a 0.5mm silver wire (Alfa Aesar, 99.9%). When the top of the reference electrode would be exposed to the air, the top was sealed using epoxy resin.

An alumina stirrer was present in all experiments; in Experiments 1-4 this was a “cricket bat” stirrer 25mm wide, whilst in Experiments 5 and 6 a smaller, 12mm wide stirrer was used. The use of a smaller stirrer would be expected to slow the mass transport of Ce^{3+} ions through the salt.

Experiments were prepared in an inert atmosphere glovebox to limit the exposure to moisture. Chunks of fused LiCl-KCl-1wt%$CeCl_3$ salt were added to a ceramic, (alumina or zirconia-coated alumina) crucible. This was then heated in a top-loading furnace within either an inert atmosphere glovebox or an argon-purged vessel within a fume cupboard. The cell design for Experiments 5 and 6 is shown in Figure 1.

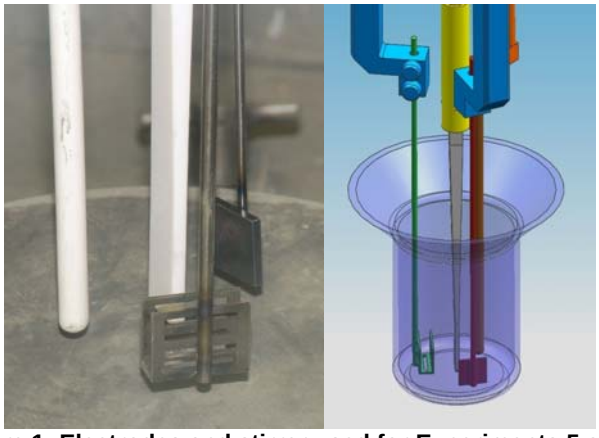

Figure 1: Electrodes and stirrer used for Experiments 5 and 6

Electrochemistry was conducted using an Autolab™ PGSTAT30 potentiostat with a current booster capable of delivering up to 20A. This was controlled by a desktop PC running the General Purpose Electrochemistry Software (GPES) application. Electrorefining was typically conducted using the Chronoamperometry (CA; constant potential) setting, although in a few instances the Chronopotentiometry (CP; constant current) setting was used. Cyclic Voltammograms (CVs) were conducted using the “staircase” setting. CVs require a working electrode of a small surface area, and preferably of an inert material (e.g. tungsten). It was not therefore possible to perform CVs in Experiments 5 and 6 where only larger, steel electrodes were present.

Experiments 1-4, which took place in an argon-purged vessel within a fume cupboard, were conducted in a systematic manner to investigate oxychloride production. Electrorefining was interrupted at regular intervals and cyclic voltammetry used to investigate the presence of oxychloride. Between experiments, the temperature and electrode potential were varied, whilst other variables were kept as consistent as possible; experimental parameters are shown in Table 1. In Experiment 3, the temperature was increased after 24 hours to investigate the effect on current.

Experiments 5 and 6, which took place under argon in a glovebox furnace, tested the small-scale electrochemical cell developed for active use, allowing as little as 150g of salt to be used. However, in this set-up there is no electrode present which can be used as a working electrode for cyclic voltammetry. The temperature in both experiments was approximately 475°C (530°C element temperature).

Table 1: Parameters for experiments conducted

Exp #	Salt (g)	Temp (°C)	Cathode	Stirrer diameter (mm)	Electrode Potential (V, vs Ag/AgCl)	Feed mass (g)
1	306	395	2mm rod	25	0.2	11.5
2	300	490	2mm rod	25	0.2	10.7
3	302	395*	2mm rod	25	0.4	12.6
4	354	490	2mm rod	25	0.4	11.4
5	220	475	15mm paddle	12	0.2-0.3	4.6
6	315	475	15mm paddle	12	0.2-1.0	6.4
*Temperature increased to 490°C after 24 hours						

On breaking out the experiment, the used feed was removed from the anode basket, and rinsed with hot water to remove adhered salt; the length of wash was brief (typically less than one minute) to limit the chemical oxidation of cerium. The feed was then weighed to allow a mass loss to be calculated. The cathode was sealed in a bag as soon as possible to limit any reaction with the atmosphere. The salt was removed from the crucible, which in most cases required breaking. The salt was carefully broken open to see whether any product fell from the cathode, with any product-rich areas saved for consolidation.

To consolidate the metallic product, the product-rich salt or cathode (as applicable) were placed at the bottom of a small, round-bottomed crucible, and covered by a layer of $CaCl_2$ salt to limit reaction with any traces of oxygen or moisture present in the argon atmosphere. This was then heated to above 800°C (950°C element temperature), and gentle stirring used to help the beads of metallic cerium to coalesce. The consolidation data reported includes the consolidation of products from electrochemistry runs other than those described above.

C. RESULTS AND DISCUSSION

Results of all experiments are summarised in Table 2.

Table 2: Results of all experiments reported

Exp #	Charge passed (C)	Mass loss from anode (g)	Anode current efficiency* (%)	Product on cathode	Product in salt
1	6856	3.7	111	Light granular deposits	Yes
2	11989	5.9	102	Light granular deposits	Yes
3a	3370	NA	NA	NA	NA
3b†	10919	5.4	102	Dense, bulky deposits	Yes
4	21009	10.3	101	Electrode frozen into salt; similar to Experiment 3b	
5	8530	4.4	106	Dense, bulky deposits	No
6	5000	2.5	103	Dense, bulky deposits	No
* Based on theoretical mass oxidised, as calculated from Formula 1 from Formula 1 † Includes charge passed after temperature increased to 490°C					

C.1. Experiments 1-4

Each experiment varied according to the temperature and applied potential as follows; Experiment 1, 395°C and 0.2V vs Ag/AgCl; Experiment 2, 490°C and 0.2V; Experiment 3, 395°C and 0.4V; Experiment 4, 490°C and 0.4V. All other parameters were kept as similar as possible.

C.1.1. Cyclic Voltammograms

The intent for these experiments was to establish the conditions in which cerium oxychloride would be generated. However, only traces of oxychloride were seen throughout the experiments, and unlike previous experiments there was no consistent growth of peak height with time. Figure 2 shows a CV taken from Experiment 2. The $Ce^{0/3+}$ couple can be clearly seen, with a reduction peak at -2.20V vs

Ag/AgCl and an oxidation peak at -1.98V. The suggested $CeO^{0/+}$ couple can be seen with a reduction peak at -2.0V and oxidation peak at -1.55V or -1.39V.

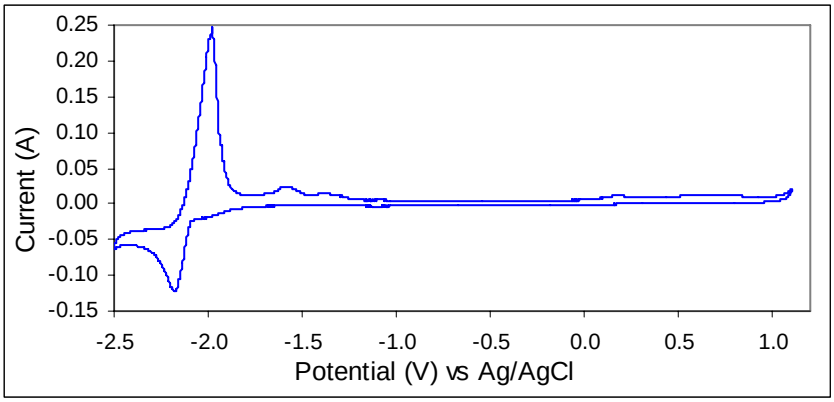

Figure 2: Cyclic Voltammogram from Experiment 2

Although the peaks attributed to oxychloride were seen only sporadically, the peak positions show a reasonable fit with those seen in previous work, and with those reported by Smolenski et al [6], see Table 3. It should be noted that the Smolenskii work took place in NaCl-KCl, and therefore differences in potentials would be expected; however separations between Ce^{3+} and CeO^{+} should be similar. There is no clear correlation of experimental parameters when significant generation of oxychloride has occurred. One suggested cause which has not been investigated is the presence of loose oxide powder left in the crucible during manufacture.

Table 3: Comparison of electrode potentials assigned to cerium and cerium oxychloride

	Reduction Potential			Oxidation Potential		
	Ce^{3+}	CeO^{+}	Difference	Ce^{3+}	CeO^{+}	Difference
Previous Work	-2.19	-2.01	0.18	-1.96	-1.24	0.73
This work	-2.18	-2.00	0.18	-1.98	-1.39	0.59
Smolenskii et al [6]	-1.82	-1.55	0.27	-1.72	-0.92	0.80

C.1.2. Electrorefining (chronoamperometry)

The chronoamperometry data (Figure 3) for the four experiments shows an effect from temperature that had not previously been observed. Experiments 2 and 4, which took place at higher temperatures, showed a high initial current which gradually decayed through the course of the experiment. In contrast, Experiments 1 and 3, which took place at lower temperatures, showed consistently low currents except during the first two hours, where the temperature was slightly higher (420°C in exp 1 and 410°C in exp 3) due to the heating profile used. This temperature dependence was tested further in Experiment 3; after 14 hours at 390°C and very low currents, the temperature was increased by 100°C over one hour. The response of the current was prompt and linearly proportional to the temperature increase (Figure 4).

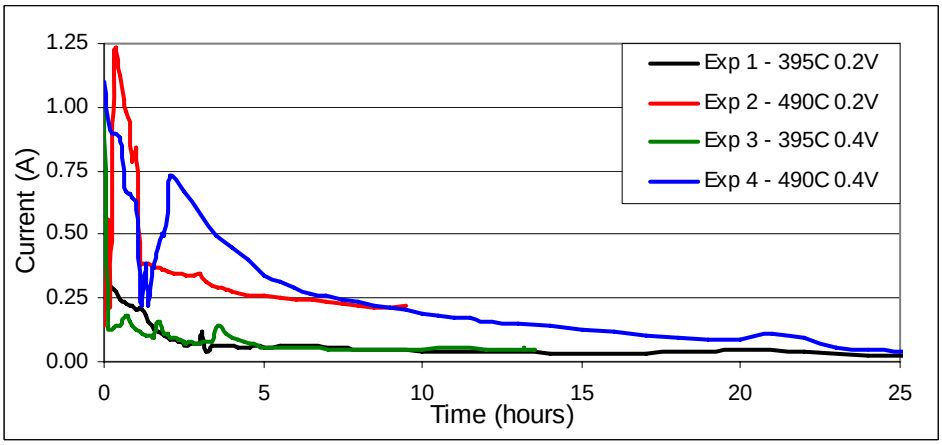

Figure 3: Chronoamperometry data from Experiments 1-4

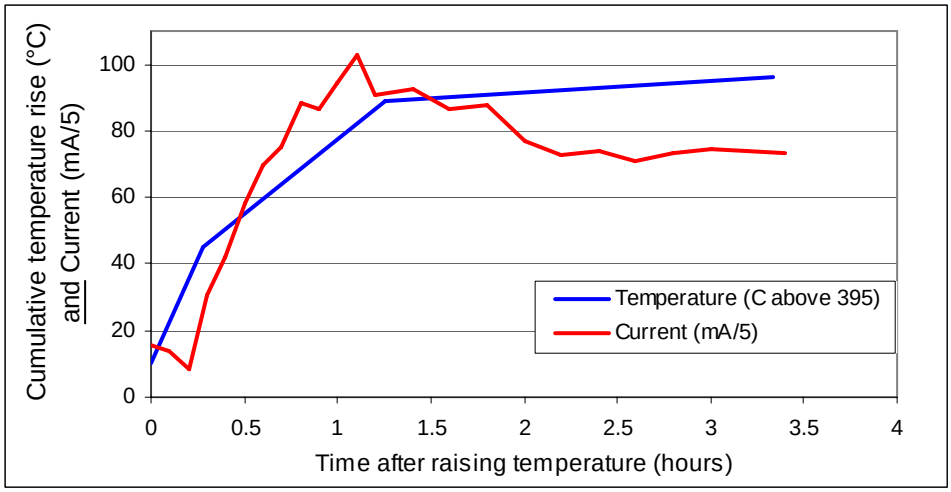

Figure 4: Comparison of current and temperature from Experiment 3

The reason for the very low currents at temperatures below 400°C is not clear. It is unlikely to be only due to increased diffusion through the salt at higher temperatures, as other alloys, e.g. zinc-tin, have been successfully electrorefined at temperatures below 400°C [4]. However, it may be related to the fact that at the higher temperatures the cerium-gallium alloy is close to its melting point of around 500°C. As suggested above in Experiment 3, there may be a direct relationship between the maximum current and the temperature.

Differences in the electrode potential did not prove significant in these experiments. Experiments 1 and 3 (both at 395°C, but at 0.2V and 0.4V vs Ag/AgCl respectively) showed similar chronoamperometry behaviour, as did Experiments 2 and 4 (both at 490°C, but at 0.2V and 0.4V respectively). Experience has suggested that the current is dependent on a range of factors, including mass transport (stirring), applied potential, temperature, and the amount (weight or surface area) of feed available for oxidation. This suggests that in this experiment, the current was limited by a factor other than potential, but does not mean that the potential does not have an effect on the currents obtained.

Current efficiencies were calculated based on the charge passed, and the mass loss from the anode, by Formula 1, which for cerium electrorefining reduces to Formula 2. Experiments 1-4 all gave current efficiencies at slightly more than 100%. However, small amounts of cerium may have been removed from the feed during the process of washing salt from the used feed; if this is the case then the calculated value of current efficiency would be slightly too high.

$$Current\ Efficiency\,(\%) = 100 \times \frac{mass\ loss \times n \times F}{M \times Q} \qquad (1)$$

$$Current\ Efficiency\,(\%) = 206600 \times \frac{mass\ loss}{Q} \qquad (2)$$

(n = electrons, F = Faraday constant, M = elemental mass, Q = charge)

C.1.3. Products

In Experiments 1 and 2, only small quantities of dull grey metal were on the electrode when withdrawn from the salt. After washing, these appeared granular (Figure 5a) and turned white rapidly on exposure to air. However, larger quantities of metal were found in the salt directly below the cathode, presumably having fallen off the cathode when withdrawn from the salt.

In Experiment 3, a dense deposit of metal approximately 20mm in diameter remained on the electrode after being withdrawn from the salt (Figure 5b), with a further quantity in the salt below. The cathode from Experiment 4 was frozen into the salt because of a failure of the argon gas; this appeared similar to the product of Experiment 3, with a dense product around the cathode, and some areas of a less dense product slightly further away (Figure 5c).

In all of the experiments at least some of the metal product fell from the cathode, suggesting that a cathode with a larger surface area is required to enable the product to cling to it, and for this reason the small "paddle" stirrer was acquired for the next set of experiments.

Figure 5a (left): Light granules from Experiment 2
Figure 5b (centre): Dense product from Experiment 3
Figure 5c (right): Product in salt from Experiment 4

C.2. Experiments 5 and 6

Two experiments were undertaken using the scaled down equipment designed for initial active experiments. Results for the Experiments are shown in Table 2.

C.2.1. Chronoamperometry

Experiment 5 ran to completion, with the current-time trace (Figure 6) showing a gradual decline with time; from an initial value of 0.4A, to 0.2A after 4 hours, to 0.1A after 8 hours, to zero after 19 hours. Each time electrochemistry was restarted there was a significant drop in current in the first few minutes, e.g. from ~1.5A to ~0.3A; a much greater drop than seen in Experiments 1-4. This type of behaviour has previously been associated to conditions with relatively poor mass transport, and may be attributable to the smaller stirrer used.

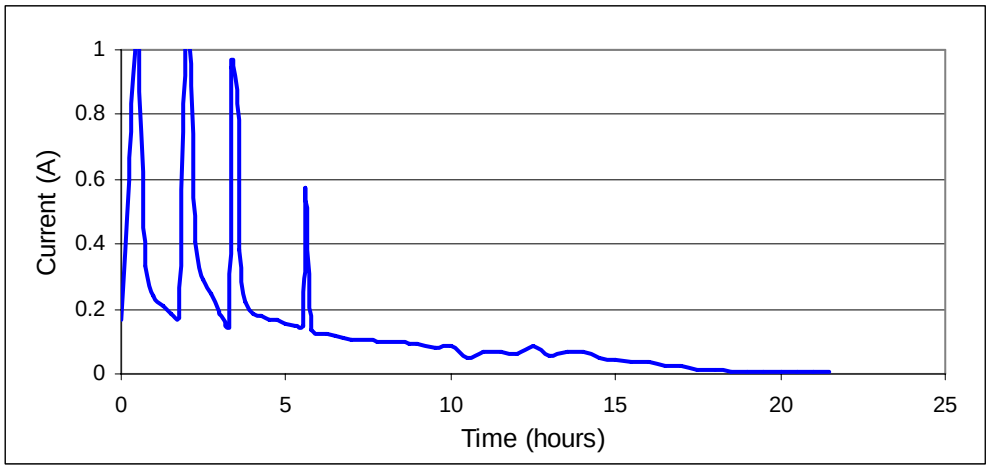

Figure 6: Chronoamperometry data from Experiment 5

In Experiment 6, currents were stable at around 0.3A for 2 hours before becoming erratic, with sudden jumps to large positive or negative currents. This type of behaviour has previously been attributed to a problem with the reference electrode; in this case, it began clashing with the stirrer at the same time as currents became erratic.

After this it was run under constant current conditions for a further two hours, with the applied potential gradually rising from -1.3V (vs Ag/AgCl) to -1.0V, at which point the experiment was terminated. The total charge passed, approximately 5000C, corresponds to oxidation of approximately one-third of the feed.

C.2.2. Products

The cathode product of Experiments 5 and 6 were similar, with hard, thick deposits of metallic product approximately 25mm across. Both cathodes gained substantially more weight than the total feed going into the experiment, suggesting that the deposits incorporated 50-75wt% of salt. When first removed from the furnace the deposits lost their metallic lustre over the course of several hours, and developed a white surface layer of oxide when stored in a glovebox over a period of weeks.

Experiment 5 appeared to run to completion; the feed remaining at the anode was small and dark, and fell apart with no obvious reaction when immersed in hot water. This was filtered to give 0.2g of a fine, black powder. In contrast, in Experiment 6, a distinct piece of feed was left behind which visibly reacted with hot water, producing 0.4g of a flocculent grey-white deposit in addition to 3.5g of used feed which remained intact. The observation of Experiment 6 suggest cerium reacting to form cerium oxide, with the differing observations in Experiment 5 suggest little or no cerium remained at the anode.

If it is assumed that all the Ce in Experiment 5 was oxidised (90% of a 4.6g feed, or 4.15g), the total charge passed corresponds to 100% current efficiency at the anode. In Experiment 6, the recorded mass loss suggests an anode current efficiency of 103%.

In both experiments no metal was seen in the salt, suggesting that the entire product remained on the cathode. The alumina crucible used in Experiment 5 had reacted strongly with the salt and had to be broken to remove the salt. Experiment 6 used a zirconia-coated alumina crucible with tapered side. The frozen salt block could be removed from this by inverting and tapping firmly on the glovebox floor, with the crucible appearing to be suitable for reuse. The zirconia coating gives a much smoother surface than the untreated alumina, which seems to limit the amount of sticking which occurs when reactive species such as $CeCl_3$ are present.

C.3. Consolidation

Five consolidation processes have been undertaken, including the products from Experiments 2, 4 and 5. Recoveries and process parameters are included in Table 4.

Table 4: Data obtained from consolidation experiments to date

Consolidation Run	Experiment ID in this paper	Mass loss from anode (g)	Consolidated metal (g)	Consolidation recovery (%)*
1	NA	9.2	3.2	35
2	2	3.7	1	17
3	4	10.3	6.6	64
4	NA	4	3.1	78
5	5	4.4	1.3	31
* Actually combined yield of cathodic efficiency and consolidation yield				

After successful consolidations, the bulk of the salt is a clean white with no deposits present. The product is found at the bottom of the crucible as spherical, or slightly flattened, metal pieces of 1-10mm diameter. These are shiny and have a slightly yellowy surface finish (see Figure 7). The salt immediately surrounding the metal product is often light –medium grey, possibly suggesting slight oxidation of the metal.

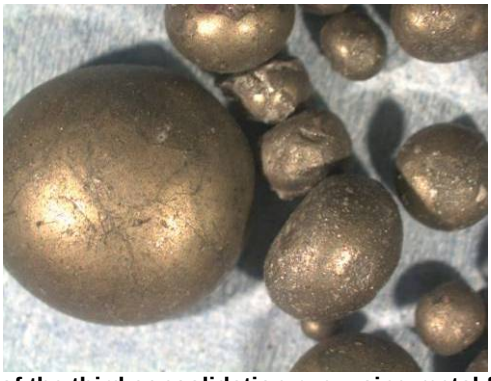

Figure 7: Product of the third consolidation run, using metal from Experiment 4

The casting efficiency from consolidation is variable, ranging from <20% to ~75% as a percentage of the amount of cerium removed from the anode. It is not possible to separate the yield of the consolidation step with the yield from the cathode reduction, as the mass of product on the cathode cannot be accurately determined due to the inclusion of salt. In the case of the fifth consolidation run, using the product of Experiment 5, it is believed that the low recovery was due to an inadequate flow of argon gas, as demonstrated by oxidation to the steel hardware. Unlike other experiments, the salt was not a clean white but was pale grey throughout, which may be another indication of cerium oxidation.

When more product metal is present, larger pieces are formed, and the recovery yield is better, suggesting that this process will be increasingly successful as larger scale experiments are performed.

D. CONCLUSION

A cell design has been produced which has been used to electrorefine cerium-gallium alloys as an analogue for impure actinides. The current efficiency is consistently high, typically close to 100%, and in several experiments all of the cerium has been oxidised from the feed. Using a steel paddle-ended cathode, the product can be removed from the salt as a hard metallic deposit incorporating entrained salt. These deposits can be recovered as solid metal pieces through a consolidation process under molten salt.

Further work is planned to study this technique on actinide materials.

References

1. J. L. Willit, W. E. Miller and J. E. Battles, *Journal of Nuclear Materials*, 195, p229 (1992)

2. B. Blumenthal and M. B. Brodsky, *Plutonium 1960*, p171, Cleaver-Hume, London (1960)

3. W. E. Miller, Z. Tomczuk, *US Patent 6,187,163* (1998)

4. R. Campbell-Kelly, *EUCHEM 2008 Conference*, Copenhagen (2008)

5. R. Campbell-Kelly, D. C. Castiglione, R. F. Watson, *IUPAC Conference,* Glasgow (2009)

6. V. V. Smolenskii et al, *Radiokhimya*, 41, *5*, p427 (1998)

Synthesis of uranium and thorium dioxides by Complex Sol-Gel Processes (CSGP)

A. Deptula[1], *M. Brykala[1], W. Lada[1], T. Olczak[1], D. Wawszczak[1], G. Modolo[2], H. Daniels[2], A.G. Chmielewski[1]

[1]*Institute of Nuclear Chemistry and Technology (INCT),*
16 Dorodna Str.,
03-195 Warsaw, Poland,
*(*Corresponding author: m.brykala@ichtj.waw.pl)*

[2]*Forschungszentrum Jülich,*
Institute of Energy Research,
Safety Research and Reactor Technology,
52425 Jülich, Germany

Abstract *– In the Institute of Nuclear Chemistry and Technology (INCT), a new method of synthesis of uranium and thorium dioxides by original variant of sol-gel method - Complex Sol-Gel Process (CSGP), has been elaborated. The main modification step is the formation of nitrate-ascorbate sols from components alkalized by aqueous ammonia. Those sols were gelled into:*

- *irregularly agglomerates by evaporation of water*
- *medium sized microspheres (diameter <150) by IChTJ variant of sol-gel processes by water extraction from drops of emulsion sols in 2-ethylhexanol-1 by this solvent*

Uranium dioxide was obtained by a reduction of gels with hydrogen at temperatures >700°C, while thorium dioxide by a simple calcination in the air atmosphere.

A. INTRODUCTION

In nuclear technology sol–gel processes [1] were proposed and used for:

- production of homogeneous irregularly shaped powders of U, Th, Pu oxides or carbides of thorium and uranium and their mixtures for pellet fabrication.
- production of nuclear fuel for High Temperature Gas Cooled Reactors (HTGR) in the form of microspheres of oxides or carbides of uranium and thorium and their mixtures.
- production of microspheres of ceramic nuclear fuels for the low energy vibrocompaction into the fuel rod for other reactors with ceramic fuel and also as a feed material for fabrication of pellets.

All sol-gel processes involve three essential steps:
I. Preparation of sol or special feed solutions “broth” from real aqueous solutions (generally nitrates of elements);
II. Gelation to the non-fluid matter, aggregates or microspheres. This step is considered the most important one, and normally the gelation techniques used, give the name to the process in which it is involved. Generally for nuclear systems 3 processes are used:

- Gelation by water extraction using 2–ethylhexanol–1 containing the surfactant SPAN–80 (ORNL processes) for microspheres or evaporation to other powders. For uranium dioxide production the main disadvantage is that U(VI), means uranyl ion, does not form stable concentrated sols and the application of a complex reduction step of UO_2^{2+} in nitrate solution is necessary.
- Gelation to microspheres, by anion extraction (Italian CNEN process),
- Gelation to microspheres, by anion neutralization:
  a) External chemical gelation uses either gaseous or dissolved ammonia for the external gelation of sol or broth droplets. As external gelation requires the mass transfer of chemicals (usually NH_3 or NH_4^+) across the phase boundary as in the water

extraction method, this method is not recommended for spheres of diameters larger then 600 μm. (SNAM, Italy).

b) Internal chemical gelation uses ammonia donor–usually hexamethylene tetramine and urea - which are added to the broth prior to gelation. The generation of ammonia is triggered off by an increase in temperature. Since the mass transfer is not necessary, this process is very suitable for the preparation of large spheres. (NUKEM, West Germany; KEMA, Netherlands).

III. In the thermal treatment step the gel is being converted to the final material. The processes in this step differ according to the type of the final product and its physical form (e.g. fine powders, spheres etc.). For uranium reduction a reducing atmosphere is necessary.

INCT has large experience in the development of sol–gel techniques since 1970. The original variant [2] of fabrication of the medium sized solid and hollow spherical (<100μm) particles [3] of ceramic materials (e.g. UO_2 and ThO_2) was elaborated here (5 Polish Patents). The process consists of the following steps: (1) preparation of concentrated metal-hydroxide sols by extraction of anions using Primene JMT; (2) formation of sol emulsion in 2–ethylhexanol–1 containing the surfactant SPAN–80; (3) gelation of drops by extraction of water with partially dehydrated EH; (4) non-destructive thermal treatment.

The goal of this work was to synthesize U–Th oxides by the Complex Sol–Gel Process (CSGP). The relevant proprietary procedure (INCT) has been patented [4] and successfully applied for the synthesis of a new generation of advanced ceramics as e.g. high temperature superconductors, hydroxyapatite, Li spinels and layered oxides as cathodes for Li–batteries, TiO_2 and titanates e.g. Li_2TiO_3 as breeding blanket for Fusion Reactor.

This process essentially consists of the following steps:

1. Preparation of starting metal-salt solution;
2. Formation of a complex sol solution by addition of a very strong complexing agent as ascorbic acid (ASC) – it is the salient feature of this process. The obtained sols have to have a high degree of amorphicity joined with homogeneous distribution of the components;
3. Partial hydrolysis by addition of ammonia-solution;
4. Gelation by evaporation of water up to the desired viscosity accompanied by partial evolution of volatile components. Obtaining of strong bonds in the network of the gels retarding premature crystallization of individual components is a big advantage of this step;
5. Drying and final thermal treatment of gels, which is carried out based on a thermal analysis (TG, DTA). Adequate parameters are very important for non-destructive calcination. However, the decomposition of aggregates containing organic compounds and nitrate ion, requires attention, due to a possibility of violent reactions and sometimes selfignition (as we observed for some systems).

The presented variant of the sol–gel process, for discussed application, is characterized by some interesting features such as: high stability of complex sols, a high degree of amorphicity joined with a homogeneous distribution of the components. We expected that uranium-ascorbate sols can be prepared directly from compounds containing of U(VI). However, the most interesting feature for this nuclear subject can be a good sinterability of powders, which we observed in other systems. Application of CSGP gives us a possibility to prepare the final product in different shapes, like irregular agglomerates or small spherical particles (with diameters below 100 μm).

According to our best knowledge CSGP has been never applied for preparation of UO_2 and ThO_2, as well as for other An oxides. It is important to recognize that the sols and gels are not in thermodynamic equilibrium, and their properties depend critically on the preparation conditions. Consequently, the effects of changes in the conditions were difficult to predict and studies were conducted for development of the best parameters requested for these complexes.

B. EXPERIMENTAL, RESULTS AND DISCUSSION

Reagents

The following reagents were used: uranium trioxide (The British Drug Mouse LTD, >97%), uranyl nitrate (Chemapol Praha), thorium nitrate (BDH Chemicals Ltd, >99%), thorium dioxide (BDH Chemicals Ltd, 99%), 2-ethylhexanol-1 (Acros Organics, 99%), SPAN-80 (Fluka) and ascorbic acid pharmaceutical grade (Takeda Europe GmBH). All other reagents used were of p.a. grade.

Analysis

Gels and products were characterized by the following methods: Thermogravimetric analysis (TG) and differential thermal analysis (DTA) with a Hungarian MON Derivatograph, Scanning Electron Microscope (SEM) observation with a Zeiss DSM 942 and Jeol JSM64-90LV.

B1. Synthesis of uranium dioxide by CSGP

Initially, starting sols with a concentration of 1M were prepared by CSGP from uranium trioxide and freshly prepared ammonium poliuranates (commercial name ADU). Obtained ascorbate-uranyl sols are deep brown in color and stable for several days. Pre-neutralization up to pH~4-5 by ammonium hydroxide (25%) was examined.

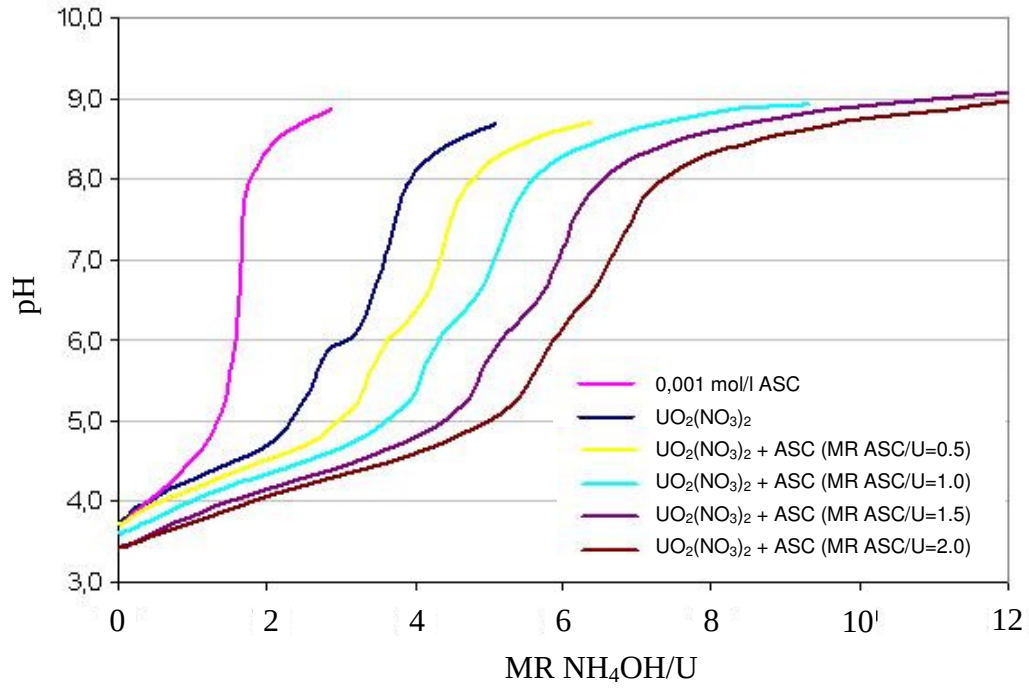

Figure 1: Potentiometric titration of 0.001 M $UO_2(NO_3)_2$ with ammonia (0.1 M). Note. Violet line show titration of titration of 0,001 mol/l ASC with ammonia.

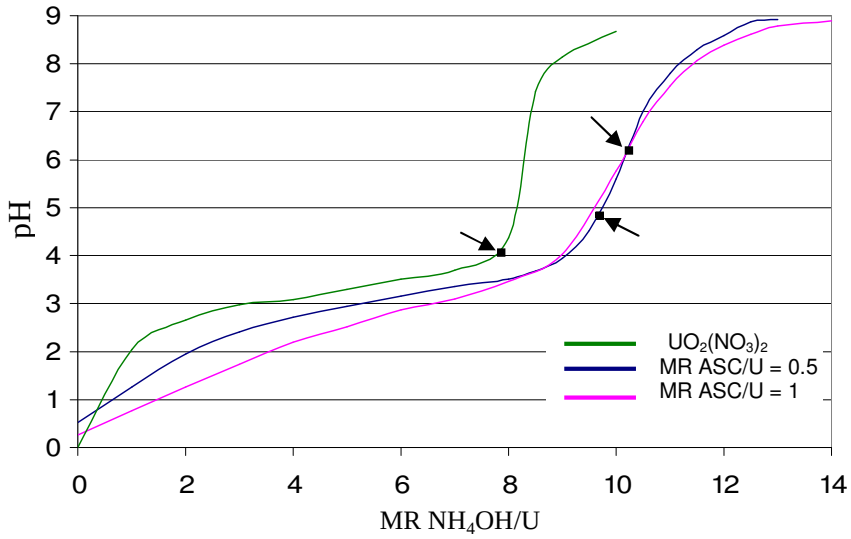

Figure 2: Potentiometric titration of concentrated sols 1 M $UO_2(NO_3)_2$ with ASC (different MR ASC/U) by ammonia (25%) (→ - precipitation points).

We have also investigated the possibility of obtaining ascorbate-based sols directly from uranyl nitrate using alkalization by aqueous ammonia. Results of potentiometric titration of various ascorbate-uranyl sols (0.001 M), obtained from uranyl nitrate, with ammonium hydroxide (0.1 M) are shown in Fig.1. In the sample without ascorbic acid, we can observe a small plateau in the pH region ~6 (MR NH_4OH/U=3) connected with polymerization of uranyl ion to polinunclear ions followed by definite increase of pH (inflection point approx. MR=3,5) representing formation of ammonium poliuranates in the solution. Those effects are considerably masked with an increase of ASC concentration, which confirms strong complexing ability of this reagent. Evidently, a value of inflection points is proportionally higher with increase of MR ASC/U. While using a very low concentration of uranyl ion, precipitation has been never observed, even at pH higher than 9. However, those sols cannot be practically gelated into microspheres. Results of the potentiometric titrations of concentrated reagents (fig.2) are completely different than presented in fig.1 which also applies for 0.1M uranyl nitrate solution [5]. It seems to be very interesting to continue fundamental studies of concentrated solutions useful in applications of sol-gel processes.

Consequently we prepared sols from concentrated uranyl nitrate (1M) with 1M ascorbic acid and alkalized to a certain pH value before precipitation (approx. pH ~ 6).

The ascorbate-uranyl sols were gelled into the following shapes:

- irregular grains - by evaporation of water from sols and drying.
- spherical particles - prepared from sols in the following procedure (see flow chart in fig.3), based on the formation of an emulsion of sols in 2-ethylhexanol-1 containing surfactant SPAN-80. Sols were introduced slowly by a needle (with a diameter 0,33 mm) under the level of vigorous mixed sols. The gelation of the emulsion droplets was carried out by water extraction. The gelled particles, generally after 30 minutes, were then separated, washed with acetone and dried. The obtained microspheres had diameters with a range mainly between 5-120 µm (fig.4).

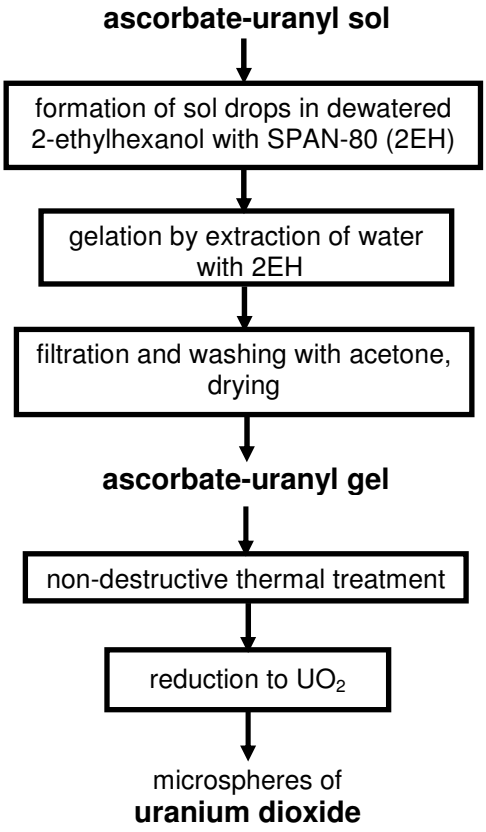

Figure 3: Flow chart of preparation of uranium dioxide in the form of microspheres (< 100 µm) by CSGP.

Next step of CSGP is thermal treatment. The gels were annealed accordingly to temperatures indicated by results of thermal analysis (TG, DTA) see fig 5. First weight loss of all obtained gels in temperatures 100-350°C is connected to evaporation of molecular water and hydroxide groups. For gels prepared from uranyl nitrate it is also connected to decomposition of the U-ASC-NO_3-NH_4OH complex with strong exothermic effect sometimes with explosion. The next weight loss with broad

exothermic effect 350-550°C, is connected with combustion of ASC and products of its decomposition. This step is generally similar also to both shape of gels derived from UO_3 and ADU as well. Only the final weight stabilization (mainly U_3O_8, fig.6) is slightly shifted (500 → 600°C) for the latter one. Reduction of U(VI) to U(IV) was not observed because reoxidation was not noted before formation of triuranium octoxide (U_3O_8).

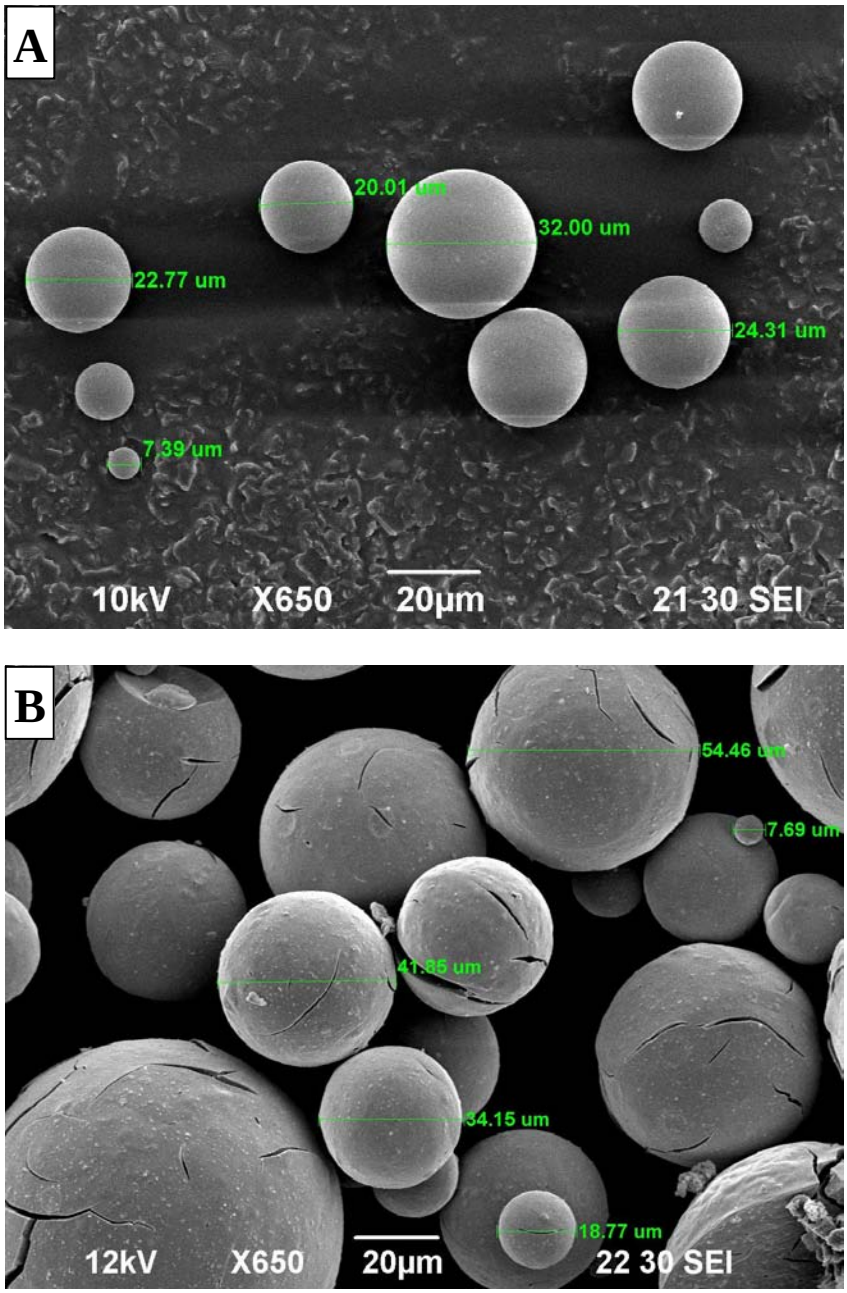

Figure 4: SEM of spherical particles of ascorbate-uranyl gel (A) and the same particles after the fast thermal treatment (B).

This thermal analysis of gels produced from uranyl shows that thermal decomposition is a complex process and it requests special procedures to avoid strong exhotermic reactions. Final reduction of material to uranium dioxide requires also special demands. The obtained triuranium octoxide was then reduced to mixture with traces of uranium dioxide (fig.7) in mixture of 5% hydrogen and 95% nitrogen atmosphere at the temperature of 900°C. For complete reduction a reducing in pure hydrogen is necessary.

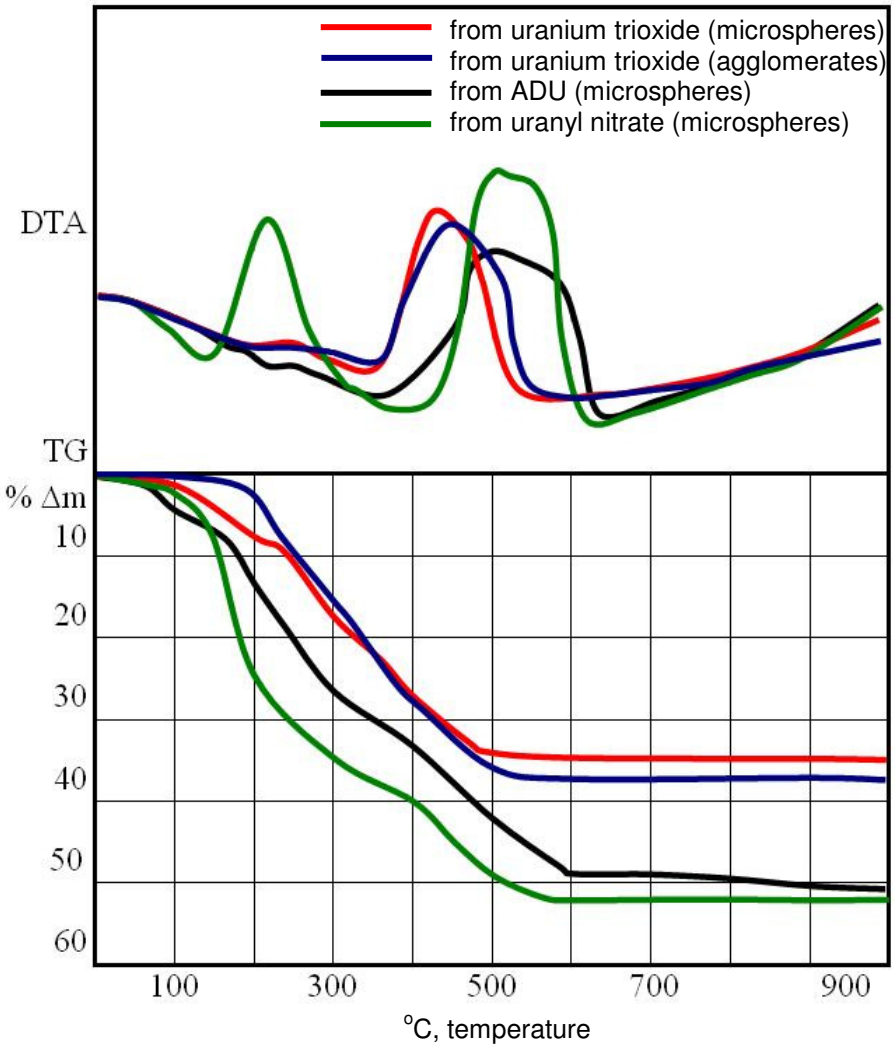

Figure 5: Thermal analysis (TG, DTA) of ascorbate-uranyl gels.

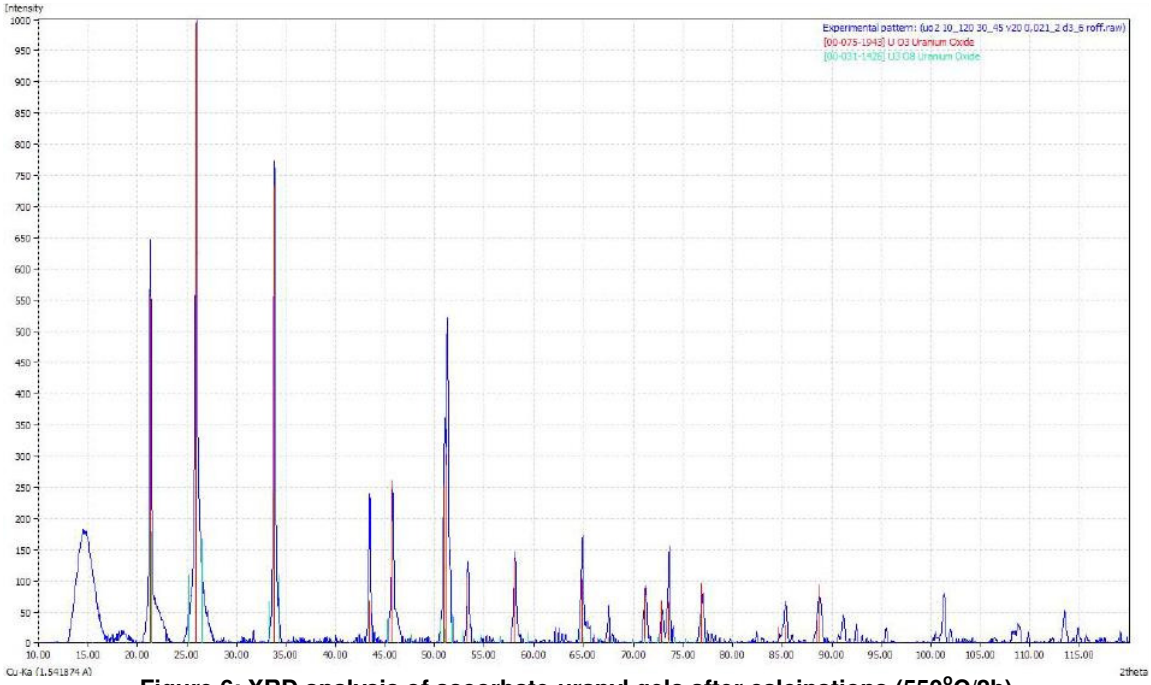

Figure 6: XRD analysis of ascorbate-uranyl gels after calcinations (550°C/2h)

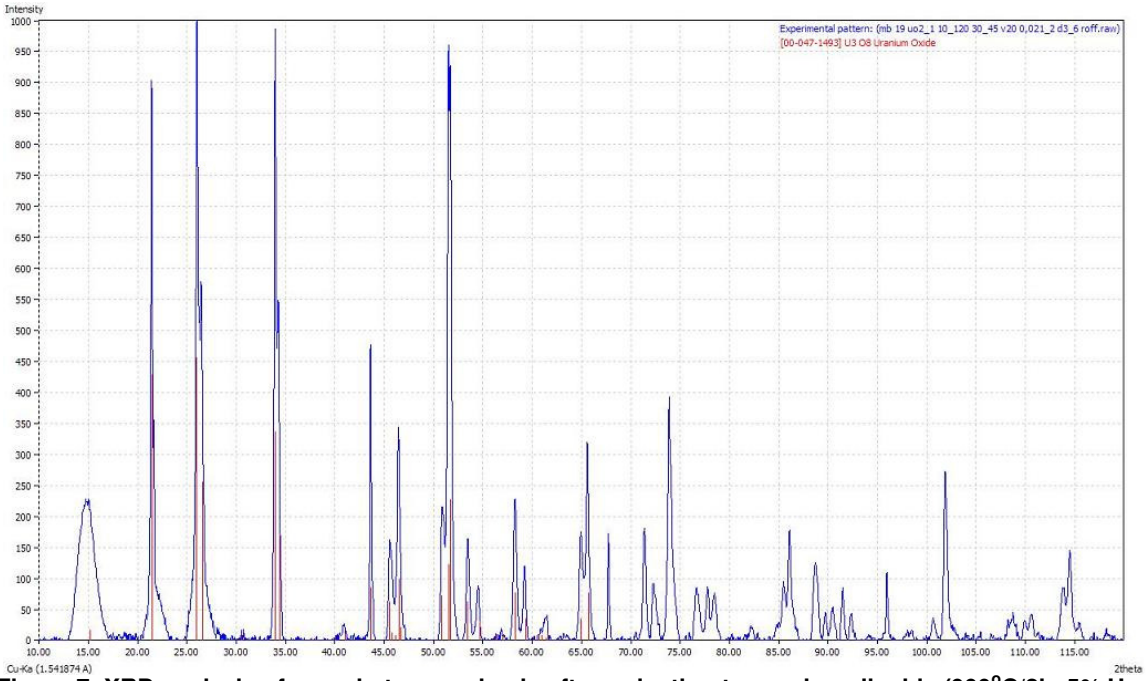

Figure 7: XRD analysis of ascorbate-uranyl gels after reduction to uranium dioxide (900°C/2h, 5% H_2 + 95% N_2)

B.2. Synthesis thorium dioxide by CSGP

The procedure of preparation thorium dioxide by CSGP is generally similar to the one of uranium dioxide preparation. Because of insolubility of commercial ThO_2 in ASC solution we decided to prepare sols from thorium nitrate and thorium hydroxide.

Preparation of thorium hydroxide was carried out by two precipitation techniques:

I) addition of ammonia (25%) to thorium nitrate solutions (0,5 M),

II) addition of a thorium nitrate solution (0,5M) to ammonia (25 %).

Temperature was 25°C and final pH≈11. The precipitate was washed repeatedly by decantation with water and then filtered through a sintered glass (G-4 Jena) plate. It was noted that the precipitation technique II, leads to formation of a precipitate which is more easily filtered than if technique I is used.

Precipitated $Th(OH)_4$ was dissolved treated with 1M ASC solutions (MR ASC/Th=2) at boiling under reflux. Solubility (11.8 mg Th/ml) was slightly higher than of commercial thorium dioxide (7.6 mg Th/ml) but definitely lower than this of uranium trioxide.

Obtained thoria-ascorbate sols have too low concentration of thorium for preparation of spherical powders by water extraction technique. Because during processing we observed formation of very fine milky like suspension (1M Th), we made same successful experiments with this. Thoria-ascorbate sols were also prepared from 1M $Th(NO_3)_4$ (MR ASC/Th=2) like uranyl gels. Irregular grains of ascorbate thorium gels were prepared by evaporation of water from sols.

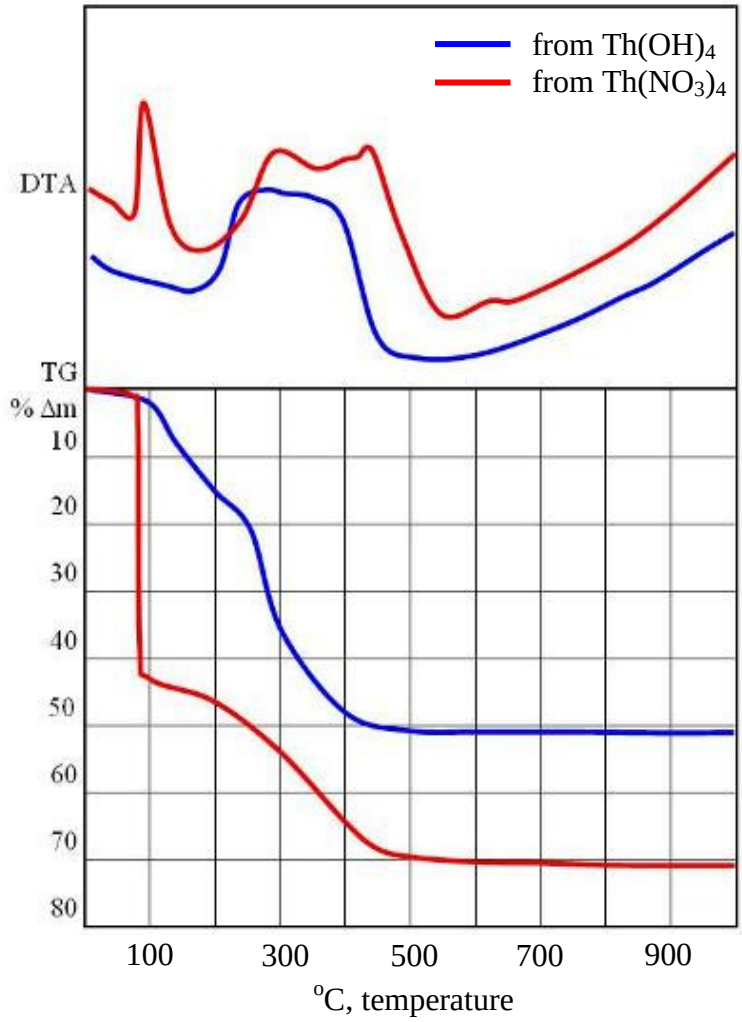

Figure 8: Thermal analysis (TG, DTA) of ascorbate-thorium sols prepared from different substrates.

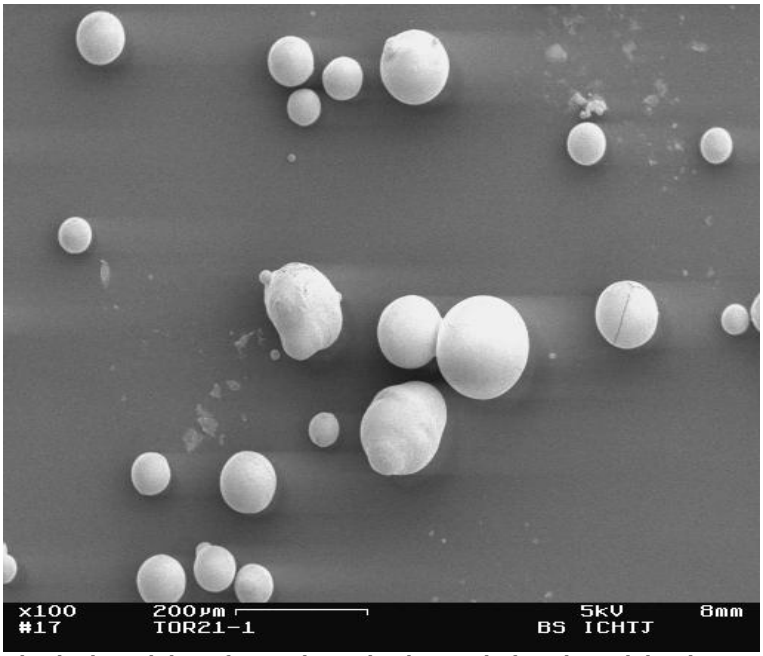

Figure 9: SEM of spherical particles of ascorbate-thorium gel after the calcination to thorium dioxide at 900°C.

In case of preparation of microspheres, we observed that emulsion of thoria-ascorbate sols in 2EH is readily formed, but gelation time was definitely longer than for of uranyl sols even at 70°C. Microspheres have generally diameter below 150 μm (fig.9). It has been observed that acetone cannot be used for washing because of a very high solubility of gels. Consequently, for washing we used carbon tetrachloride or cosmetic petroleum. The next very serious problem appears during thermal treatment of this gel (Fig.8; red line). We observed a violent exothermic reaction of ascorbic acid with nitrates at 70°C. Similar phenomenon connected with selfignition we have observed in other works during synthesis of compounds when started from nitrates and ASC [6,7].

C. CONCLUSION

1. The Complex Sol-Gel Process can be successfully applied for the preparation of homogeneous sols using complexation with ascorbic acid of various uranyl (uranium trioxide, ammonium poliuranates, uranyl nitrate) (Polish Patent Pending) [8] and thorium (hydroxide and nitrate) compounds.
2. The sols were gelled into:
    - irregular agglomerates by evaporation of water;
    - medium sized microspheres (diameter <150) IChTJ variant of sol-gel processes by water extraction from drops of emulsion sols in 2-ethylhexanol-1 by this solvent. It is necessary to underlain that for studied system, reduction of uranyl ion to U(IV) can be avoided.
3. Non destructive thermal treatment of gels to oxides in air atmosphere (U_3O_8; ThO_2) was elaborated on the basis of their thermal analysis. Special procedures were necessary for nitrate gels due to violent exothermic reactions.
4. Uranium dioxide has to be obtained from gels by reduction with hydrogen.

Aknowledgements

The work has been carried out within the collaborative Project ACSEPT (Actinide Recycling by Separation and Transmutation), contract No FP7-CP-2007-211267.

References

[1] A. DEPTULA, C. Majani, *Sol-Gel Processes And Their Applications*. ENEA Report No. RT/TIB/86/25 (1986) ENEA, Roma

[2] A. DEPTULA, A. G. Chmielewski, T. E. Wood; Sol-Gel Ceramic Beads And Bubbles - A Historical Perspective, Modern Fabrication And Cost Analysis, *Proceedings of the 9th CIMTEC, Florence, vol. D: Getting into the 2000's*. 1998, pp. 771-790

[3] A. DEPTULA, M. Brykala, W. Lada, T. Olczak, B. Sartowska, A. G. Chmielewski, Preparation of Spherical Particles of Li_2TiO_3 (with diameters below 100 μm) by Sol-Gel Process, *Fusion Engineering and Design,* 84, (2009) 681-684

[4] A. DEPTULA, W. Lada, T. Olczak, M. T. Lanagan, S. E. Dorris, K. C. Goretta, R. B. Poeppel, Method for Preparing of High Temperature Superconductors, Polish Patent, Nr 172618, 2 June 1997.

[5] A. DEPTULA, A Study of Composition of Ammonium Uranates, *Nukleonika,* 7 (1962) 265-275

[6] A. DEPTULA, T. Olczak, W. Lada, B. Sartowska, F. Croce, L. Giorgi, A. Di Bartolomeo, A. Brignocchi; Thermal Conversion of Gels Prepared by Complex Sol-Gel Process (CSGP) from the Li^+-Me^{2+}-CH_3COO^- Ascorbic Acid (ASC)-NH_4^+-OH^--H_2O Systems to $LiMn_2O_4$ and $LiNi_{1-x}Co_xO_2$ Spinels of Electrochemical Quality, *J of Sol-Gel Science and Technology*, 26, (2003) 201-206

[7] M. T. BOROWIEC, A. Deptula, W. Lojkowski, S. Gierlotka, V. P. Dyakonov, W. Lada, T. Olczak, D. Wawszczak, P. Aleshkevych, W. Domuchowski, T. Zayarnyuk, M. Barański,

M. Czech, H. Szymczak, Growth and Properties of Ytterbium Doped $KY(WO_4)_2$ Nanocomposites, *Solid State Phenomena,* 128, (2007) 25-30

[8] A. DEPTULA, M. Brykala, W. Lada, D. Wawszczak, T. Olczak, A.G. Chmielewski, „Method for Preparing of Uranium Dioxide in the Form of Spherical and Irregular Grains", Polish Patent Pending, No. P-389385, 27 October 2009.

Synthesis and structural characterisation of mixed An(IV)-An(III) actinide oxalates used as precursors for dedicated fuel or target

Christelle TAMAIN[1], Stéphane GRANDJEAN[1], Bénédicte ARAB CHAPELET[1], Francis ABRAHAM[2]

[1]CEA, Nuclear Energy Division, Marcoule, RadioChemistry & Process Department, Separation Process Chemistry Service, Actinides Chemistry and Conversion Laboratory, F-30207 Bagnols sur Cèze, France, e-mail: christelle.tamain@cea.fr
[2]UCCS, Solid Chemistry Unit, UMR CNRS 8181, ENSCL-USTL, BP 90108, 59652 Villeneuve d'Ascq Cedex, France
Tel: +33 4 66 33 92 26, Fax: +33 4 66 79 65 67, e-mail: christelle.tamain@cea.fr

Abstract – Oxalic co-conversion process plays an important role by producing mixed-actinide compounds used as starting materials as they are particularly suitable precursors of actinide oxide solid solutions. In these oxalate compounds, a mixed crystallographic site which accommodates both elements in spite of their different oxidation states has been established. The charge compensation is ensured by monovalent cations present in the acidic solution. This communication reviews the various mixed-actinide oxalates obtained by crystallization from acidic solution. First, crystallographic structures determined by X-ray diffraction from single crystals are described. Then completing data obtained by powder X-ray diffraction are presented on various systems. The different supramolecular arrangements underline the complexity of An(IV)-An(III)/Ln(III) oxalate system and the need to pursue studies on single crystals.

A. INTRODUCTION

Oxalic acid is a well-known reagent to recover actinides from nuclear wastes thanks to the very low solubility of An(IV) and An(III)/Ln(III) oxalate compounds in acidic solution. Therefore oxalic co-precipitation is one way particularly convenient for actinides co-conversion into oxalate compounds, suitable precursors of actinide oxide solid solutions (generation III/IV).
While thermodynamic parameters have been reported for a large number of actinide oxalates, structural analyses have been often limited to powder X-ray diffraction [1]. Few compounds have been studied crystallographically to determine their structure. Nowadays there is a regain of interest concerning crystallographic studies in order to establish structural databases useful to characterize powder compounds. Because of their academic importance and manipulation ease, a number of oxalates of chemically analogous lanthanide elements are known that can guide our understanding of trivalent actinide oxalates solid state chemistry. Despite these investigations, it seems difficult to fully understand the chemistry of their sometimes not so analogous actinide compounds. Moreover, even if more and more studies are dedicated to uranium or thorium oxalate structures few structural characterizations by single crystal X-ray diffraction of transuranic oxalates have been carried out yet. $Np(C_2O_4)_2.6H_2O$ is the only described structure belonging to the series $An(C_2O_4)_2.6H_2O$ [2]. Plutonium(III) oxalate $Pu_2(C_2O_4)_3.10H_2O$ isomorphic with $[Ln(H_2O)_3]_2(C_2O_4)_3.4H_2O$ [3] has just been synthesised as single crystals and studied by Runde *et al*. [4]. With monovalent cation two different An(IV)-containing structures were reported: $H_2Np_2(C_2O_4)_2.nH_2O$ [5] and $KPu(C_2O_4)_2(OH).2H_2O$ [4]. Only one structure with molecular cations $\{C(NH_2)_3\}_4[An(C_2O_4)_4.2H_2O]$ was completely described for Pu(IV) and Np(IV) [6]. Unique mixed An(IV)-An(III)/Ln(III) oxalates were discovered, synthesized and described recently.
The present work is intended as a preliminary review of the different structural mentions and observations on mixed oxalate systems either from single crystal analyses or powder compounds studies. The first step of this work aims at building the first structural database essential for powder materials identification. This part of the studies was carried out on surrogates U(IV)-Ln(III) system for practical reasons. Single crystals of M^{I}-U^{IV}-Ln^{III} systems were grown enabling to isolate and describe several new structural families such as $M_{1-x}[Ln^{III}{}_{1-x}An^{IV}{}_x(C_2O_4)_2 \cdot H_2O]$ and $M_{2+x}An^{IV}{}_{2-x}Ln^{III}{}_x(C_2O_4)_5 \cdot nH_2O$ (with M = Na^+, NH_4^+, $N_2H_5^+$) [7, 8, 9]. Then supplementary data were

obtained from An(IV)-An(III) precipitates (An = U(IV), Pu(IV), Np(IV), Pu(III), Am(III)) completing usefully the description of these novel coordination polymers [10, 11].

B. EXPERIMENTAL SECTION

Actinide(IV) or actinide(III)/lanthanide(III) solutions are prepared using specific procedures either from purified monometallic solutions or by dissolving monometallic oxides or hydroxides. Hydrazinium nitrate is used as an anti-nitrous agent to stabilize the lowest oxidation states.

B.1. Crystal growth

There are two main crystal growth methods adapted to oxalate systems: hydrothermal syntheses and methods based on the slow diffusion of the reagents through a gel. The first method is quite efficient but single crystals are formed in very specific physical chemical conditions, inherent in these crystal growth methods, far different form those used in co-precipitation process [12]. Therefore it is often quite impossible to reproduce from co-precipitated powders the structures obtained thanks to these syntheses. Arab-Chapelet *et al* obtained mixed oxalate single-crystals by slow diffusion of the metallic cations through silica gels impregnated with oxalic acid [7, 8, 9]. Two types of gels were tested from tetraethoxysilane (TEOS) and sodium metasilicate. To get rid of sodium cation and allow its substitution by another single-charged cation such as ammonium or hydrazinium cations, ionic exchange has been performed between the gel and a nitric solution of oxalic acid and ammonium or hydrazinium nitrate. Mixed U(IV)-Ln(III) oxalate single crystals were successfully formed by this last method.

B.2. Co-precipitation powder synthesis

The oxalate co-precipitates were prepared by mixing a solution of An(IV) and An(III)/Ln(III) and a concentrated $H_2C_2O_2$ solution in a nitric medium according to Grandjean *et al.* and Arab-Chapelet *et al.* [10, 11, 13]. The resulting crystallized powders were filtered off and dried at room temperature. For these An(IV)-An(III)/Ln(III) mixtures, different molar ratios were studied in order to investigate the influence of the actinide(IV) and actinide(III) nature and of the An(III)/An(IV) molar ratio on the co-precipitate structure.

C. RESULTS

C.1. Structural analysis from single crystal

Single crystal data acquisition led to elucidate unprecedented mixed structures that belong to three different series named triclinic, hexagonal and tetragonal. These three families are characterized by an unexpected mixed U(IV)-Ln(III) crystallographic site: both metallic cations are located on the same site leading to the formation of solid solutions. The charge balance is ensured by the adjustment of the single-charged ions within the structure. These partial occupation of the same site can occur because the ionic radii of U(IV) and An(III) or Ln(III) are closed [14] and because both ions can exhibit the same coordination sphere.

The crystals of the tetragonal family, with formula $M_{1-x}[Ln^{III}_{1-x}An^{IV}_{x}(C_2O_4)_2 \cdot H_2O] \cdot nH_2O$, were solved in space group P4/n. The structure is built from polyhedra of metallic atoms (actinide or lanthanide) connected by bis-bidentate oxalate groups to form a two-dimensional framework based on four-membered rings. The metallic cations are nine-fold coordinated with eight oxygen atoms from four bidentate oxalate ions and one oxygen atom from a water molecule. The polyhedra can thus be described as mono-capped square antiprims with water oxygen at the longest distance. In this structure, starting from $M[Ln^{III}(C_2O_4)_2 \cdot H_2O] \cdot nH_2O$, the lanthanide is partially substituted by the uranium(IV) in the same crystallographic site, the surplus of charge being compensated by the removal of monovalent ions Ln(III) + $M^+ \rightarrow$ An(IV). The substitution on the metallic site does not

involve significant deformation of the structure. The monovalent cations and occluded water molecules are disordered on the same crystallographic site located in the interlayer space.

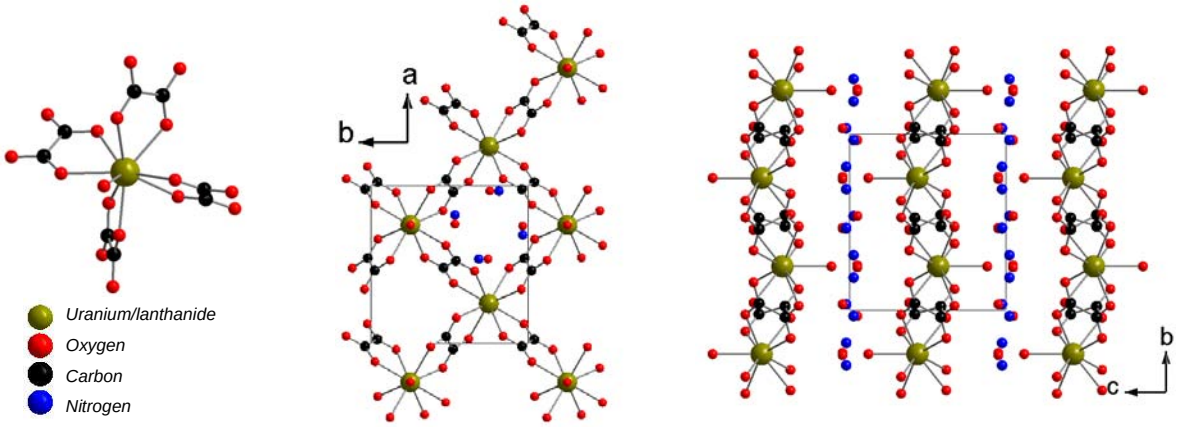

Figure 1: Building units of $M_{1-x}[Ln^{III}_{1-x}An^{IV}_{x}(C_2O_4)_2 \cdot H_2O] \cdot nH_2O$ tetragonal family (left) and projections of the crystal structure showing the stacking of the layers (right) and the four-membered rings which compose each layers (middle).

The triclinic family presents the same formula $M_{1-x}[Ln^{III}_{1-x}An^{IV}_{x}(C_2O_4)_2 \cdot H_2O] \cdot nH_2O$ as the tetragonal family besides significant crystallographic differences. Those triclinic compounds are described in space group P-1. They exhibit a three-dimensional anionic arrangement of metallic-cation-centered polyhedra linked through bis-bidentate oxalate groups displaying tunnels with elliptic cross-sections in three directions. The coordination sphere of the metallic cations is built from nine oxygen atoms from four oxalate ligands and one oxygen from a water molecule. The polyhedron can be described as a tri-capped trigonal prism. As for the tetragonal family, the presence of uranium in the structure is the consequence of the actinide to lanthanide substitution Ln(III) + $M^+ \rightarrow$ An(IV). The charge compensation is ensured by the modification of the single-charge cation rate in the cavities. The monovalent cations and non-bonded water molecules are located in the largest elliptic tunnels running along the a-axis.

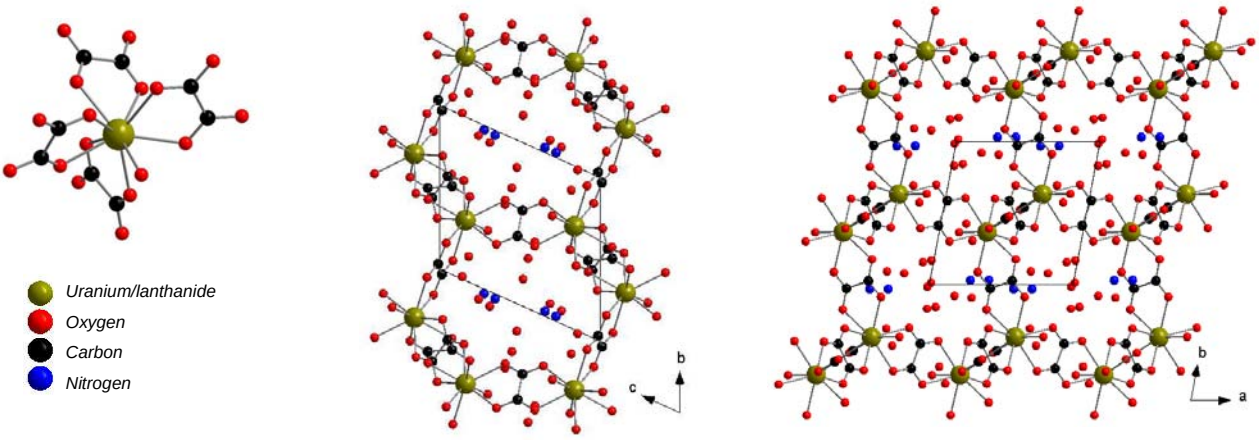

Figure 2: Building units of the $M_{1-x}[Ln^{III}_{1-x}An^{IV}_{x}(C_2O_4)_2 \cdot H_2O] \cdot nH_2O$ triclinic family (left) and projections of the crystal structure showing the three-dimensional arrangement (middle and right).

Finally, $M_{2+x}An^{IV}_{2-x}Ln^{III}_{x}(C_2O_4)_5 \cdot nH_2O$ is the characteristic formula of the hexagonal family. The crystal structure was solved in space group $P6_3/mmc$. These compounds present a three-dimensional framework of metallic and oxalate ions. The metallic-cation-centered polyhedra are linked through bis-bidentate oxalate groups forming a honeycomb-like structure. The metallic cations are ten-fold coordinated by oxygen atoms from five bis-bidentate oxalate groups. The polyhedron can thus be described as a bi-capped square antiprism. Although the overall structure has a three-dimensional network, it is interesting to first consider layers in the (001) plane. Along this plane, the polyhedra are

arranged in order to form six-membered rings. The layers are further linked by two additional bridging oxalate groups in the third direction, c-axis, creating the three-dimensional honeycomb-like metal-oxalate arrangement, the monovalent cations and free water molecules being located in the large tunnels running along the c-axis. The flexibility of the oxalate ligands allows the substitution of uranium by lanthanides from $MU^{IV}_2(C_2O_4)_5{\cdot}nH_2O$. The charge compensation is ensured by additional single-charged cations. This family does not only gather compounds crystallizing in the hexagonal symmetry. Indeed in some compounds, torsions or rotations of the bridging oxalate ligands connecting the layers lead to a decrease of the network symmetry. For example, with M = Na, distortions of the hexagonal unit cell lead to an orthorhombic or a monoclinic symmetry depending the nature of the lanthanide. This family is therefore called pseudo-hexagonal.

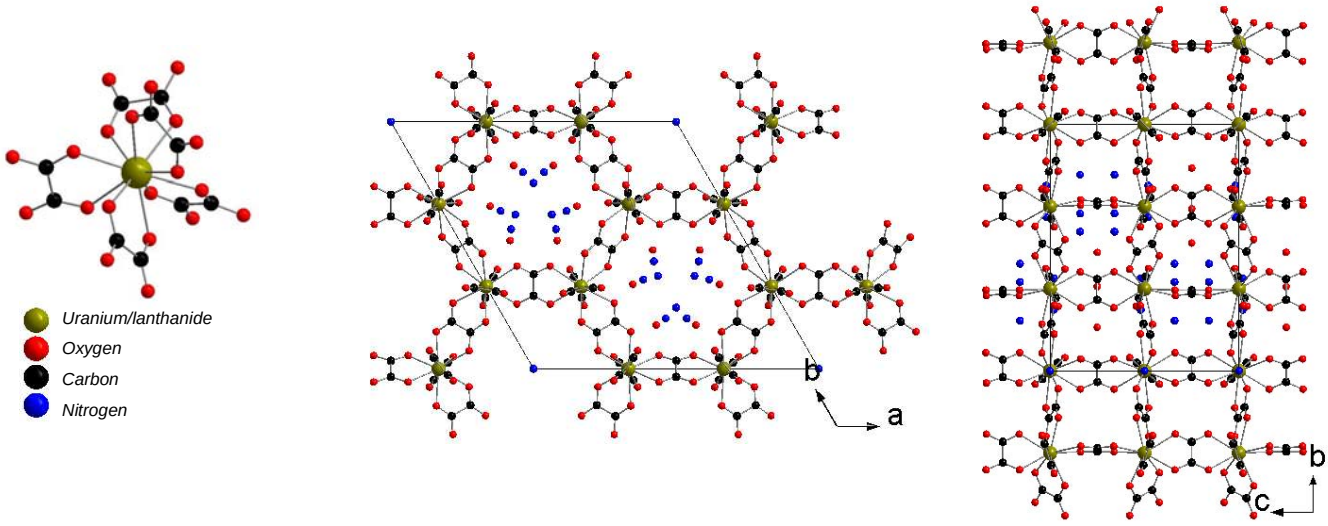

Figure 3: Building units of the $M_{2+x}An^{IV}_{2-x}Ln^{III}_x(C_2O_4)_5{\cdot}nH_2O$ pseudo-hexagonal family (left) and projections of the crystal structure showing the hexagonal rings (middle) and the three-dimensional arrangement (right).

The present results allow to initiate a phase diagram of mixed An(IV)-Ln(III) oxalate compounds. Besides chemical parameters, it seems that the ratio An(IV)/(Ln(III)+An(IV)) influences the structure of the compound. Therefore a first diagram sketch can be established including the different families described earlier.

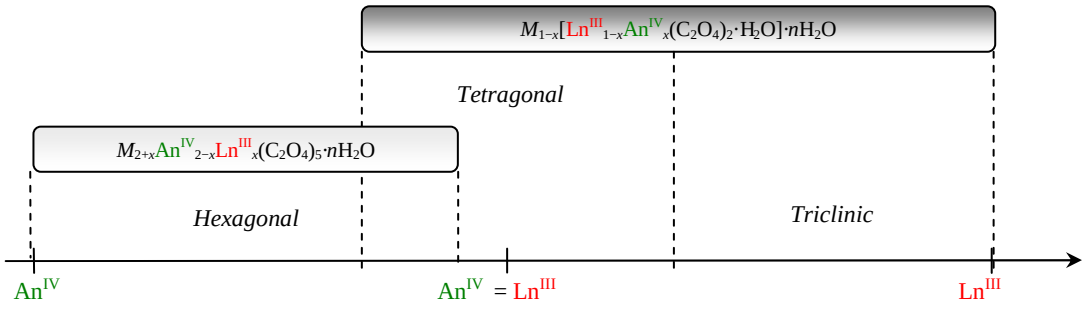

Figure 4: Phase diagram sketch for U(IV)-Ln(III) system

Owing to the importance of An(IV)-An(III) compounds in the nuclear fields, the preparations of powder samples in various synthesis conditions have been carried out to define the role of each experimental parameter and to determine the solid solution domains. The knowledge of structures likely to be formed by co-precipitation process is thus enriched thanks to these systematically synthesized powder compounds.

C.2. Extension on powder compounds

The first studies on polymetallic systems were carried out on mixed uranium(IV)-lanthanide(III) oxalate powder compounds [10]. Lanthanides are used as surrogate of actinides(III). Infra-red and solid UV-visible spectroscopies (non-presented here) confirm the molecular structure of the solid and the monovalent cation presence, and the oxidation state IV of the uranium, respectively.
The description of the solid solution domains involves an investigation of the solid compound structure while varying the Ln(III)/(An(IV)+Ln(III)) ratio. For neodymium substitution rates between 0 and 0.5, the precipitate is single-phased, characterized by a hexagonal structure isomorphic to $(NH_4)U_2(C_2O_4)_5.0.7H_2O$ and belonging to the hexagonal family previously described.

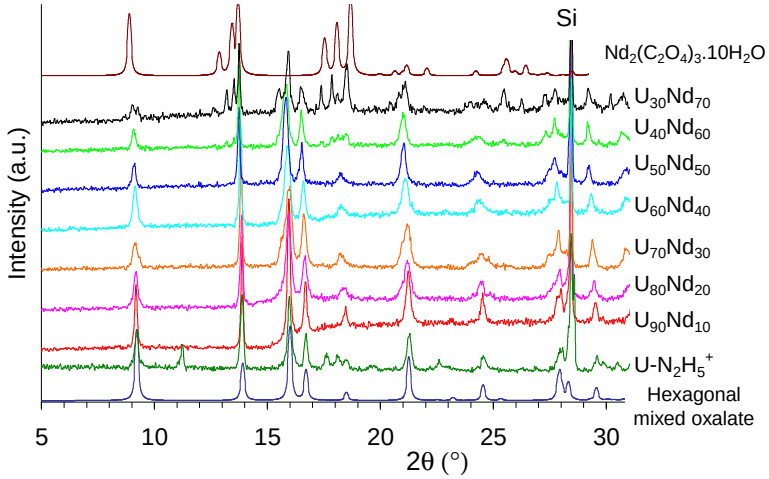

Figure 5: XRD patterns of U(IV)-Nd(III) oxalate co-precipitates

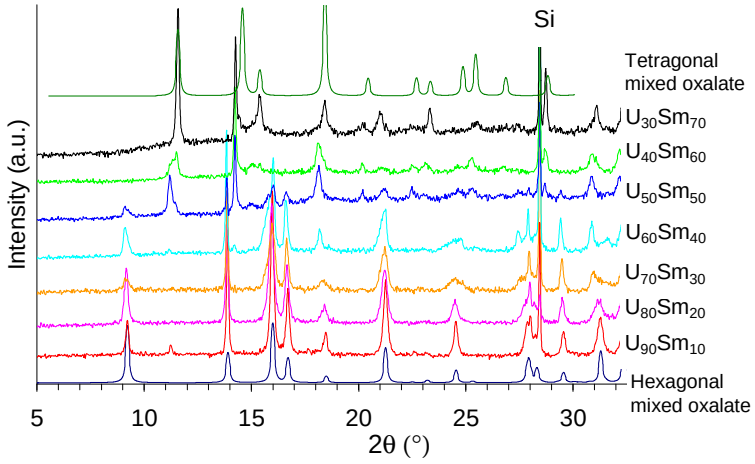

Figure 6: XRD patterns of U(IV)-Sm(III) oxalate co-precipitates

For a ratio beyond 0.5, the precipitate is no longer single-phased and is composed of a mixture of hexagonal mixed oxalate and neodymium(III) oxalate $Nd_2(C_2O_4)_3.10H_2O$ [3]. The linear variation of the unit cell parameters with the substitution rate confirms the existence of a hexagonal solid solution with the general formula $M_{2+x}An^{IV}_{2-x}Nd^{III}_x(C_2O_4)_5{\cdot}nH_2O$. The Vegard's law is thus defined within a large composition range ($0 \leq Nd/(U+Nd) \leq 0.5$).

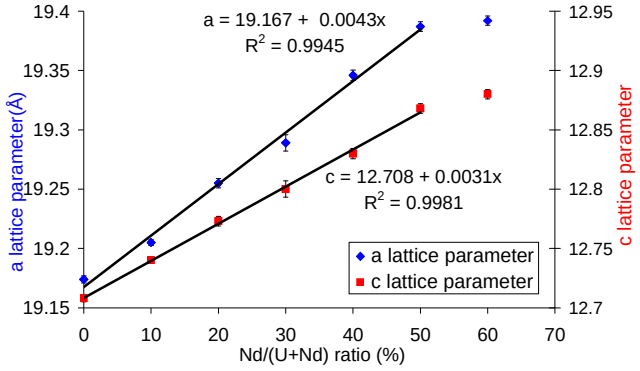

Figure 7: Determination of Vegard's law for U(IV)-Nd(III) hexagonal solid solutions confirming the large solid solution domain

The effect of the lanthanide nature was also studied. The same experiments were carried out on uranium(IV)-samarium(III) system. Concerning these last precipitates the identification is more complex. For a Sm/(Sm+U) mole ratio below 0.1, the solid is a mixture of the uranium(IV) oxalate $U(C_2O_4)_2.6H_2O$ and a compound that pertain to the hexagonal series. The precipitate is single-phased only for short ranges of composition from 0.1 to 0.3 and 0.5 to 0.7 substitution rates. In these ranges, the precipitates are respectively hexagonal and tetragonal oxalates. For $0.3 < Sm/(U+Sm) \leq 0.5$, the powders are characterized by a mixture of hexagonal and tetragonal mixed structures. Finally, beyond 0.7 the solid corresponds to a mixture of samarium(III) oxalate and tetragonal mixed oxalate.
Compared to those obtained previously with neodymium, these results highlight the influence of the trivalent cation nature on the structure of the precipitates and on the solid solution domains. Surprisingly enough, the evolution is not in agreement with the ionic radii of the Ln(III) ion. Indeed, the stability range of the hexagonal solid solution is broader for the U(IV)-Nd(III) system than the U(IV)-Sm(III) one, whereas the Sm(III) ionic radii is more similar to the U(IV) one than the Nd(III) [14].

Studies were thereafter widened to polyactinides An(IV)-An(III) compounds (An(IV) = Th, U, Np, Pu; An(III) = Pu, Am) [10, 11].. Infra-red and solid UV-visible spectroscopies (non-presented here) confirm the nature of the solid and the monovalent cations presence, and the oxidation state IV of the uranium, respectively. The An(IV)-An(III) co-precipitates formed by oxalic co-precipitation were characterized from powder diffraction patterns by analogy with uranium(IV)-lanthanide(III) oxalates described in the previous part.

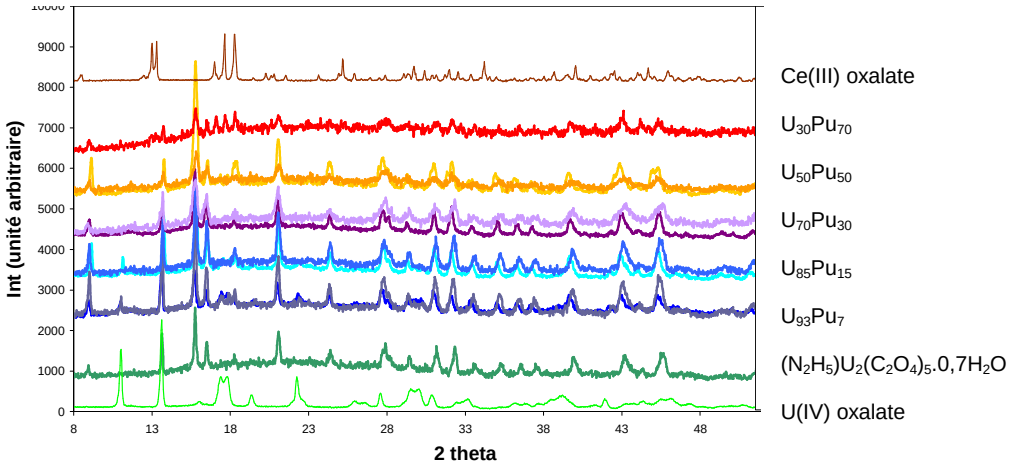

Figure 8: XRD patterns of U(IV)-Pu(III) oxalate co-precipitates for different Pu(III)/(U(IV)+Pu(III))ratio

In order to determine the solid solution domain, an identification of the compound structure for U(IV)-Pu(III) system while varying the Pu(III)/(U(IV)+Pu(III)) ratio was realized. As for the U(IV)-Nd(III) system, the precipitate is a hexagonal single-phased compound (solid solution) with the generic formula $M_{2+x}U^{IV}_{2-x}Pu^{III}_{x}(C_2O_4)_5{\cdot}nH_2O$ for substitution rate of 0-0.5. For higher substitution rate, the powders are a mixture of Pu(III) oxalate and the hexagonal solid solution. Because of the low crystallinity of the samples it was not possible to refine the cell parameters. The solid solution existence is thus evaluate only thanks to the XRD patterns and the knowledge of the U(IV)-Nd(III) system without the Vegard's law determination.

The influence of actinide nature was also studied. For a particular An(IV)/(Pu(III)+An(IV)) mole ratio, the (An(IV), Pu(III)) pair variations were analysed. Considering a Pu(III)/(An(IV)+An(III)) mole ratio close to 0.5, the precipitate structure is observed to evolved along the actinide family. Two series were identified by varying the actinide(IV) nature, $M_{2+x}An^{IV}_{2-x}An^{III}_{x}(C_2O_4)_5{\cdot}nH_2O$, and $M_{1-x}[An^{III}_{1-x}An^{IV}_{x}(C_2O_4)_2{\cdot}H_2O]{\cdot}nH_2O$, with hexagonal or tetragonal symmetry respectively. The precipitate belongs to the hexagonal serie for Th(IV) or U(IV) and to the tetragonal one for Np(IV) or Pu(IV).

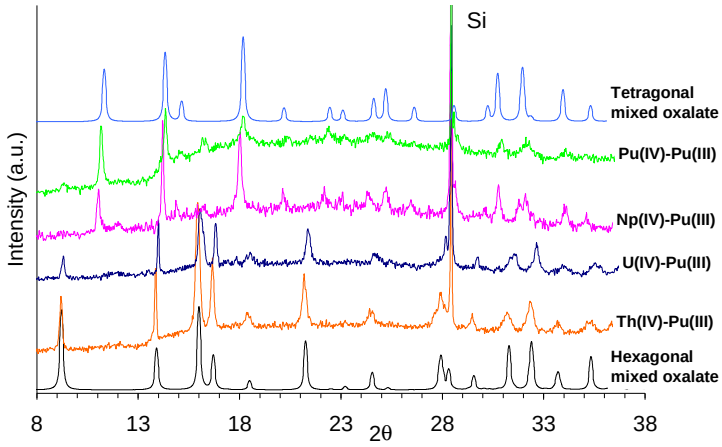

Figure 9: XRD patterns of An(IV)-Pu(III) oxalate co-precipitates

D. DISCUSSION

First studies on various An(IV)-An(III) mixtures confirm the influence, already evidenced with lanthanides, of the metal nature on the system behaviour. The various supramolecular arrangements described earlier underline the complexity of An(IV)-An(III) oxalate systems and the need to pursue studies on single crystals in order to first, improve the understanding of known structures and particularly the relationship between the tetragonal and the hexagonal families, and then, establish a new structural database more adapted to minor actinides. Indeed, the structure is influenced by the synthesis process, the metallic cation nature and the chemical conditions (nature of single charged cation, pH, process …). Even if powder compounds are by now characterized only by hexagonal or tetragonal symmetries, other structural families are likely to be formed with minor actinide, new chemical processes and parameters considering that nothing has been yet set concerning the chemical processes of generation(IV) cycles.

Synthesis routes to grow high quality single-crystals of transuranium oxalates are extremely rare. The very few syntheses of mixed oxalate single crystals presented earlier are unfortunately not useful for the minor actinide handling or under glove box conditions. It is thus necessary to set up new efficient crystal growth methods adaptable to specific manipulation conditions and allowing the synthesis of mixed $An_1(IV)/An_2(III)$ oxalate single-crystals. The considered ways are based on kinetic concepts: the idea is to delay the contact between the actinides and the oxalate ions thanks to physical constrain or chemical consideration, using dedicated precursors.
Several methods based on chemical concepts consist in using precursors of either metallic cation or oxalate ligand which slowly decompose themselves into the compound of interest according to well-

known reactions: metallic cation oxide or diethyl oxalate are thus considered. Their decomposition kinetics can be adjusted by the reaction parameters.
The last considered crystal growth method is based on a physical concept. The idea is to slow down the diffusion of both reagents adding barriers between them. The considered obstacles are membranes. The principle of this last method is the same as the gel growth methods developed by Arab-Chapelet *et al.* but without the difficulty due to the recovering of crystals, their main limitation.

E. CONCLUSION

The flexibility of the actinide coordination sphere and the oxalate versatility suggest a large number of structures likely to be formed. The single-crystal studies carried out on U(IV)-Ln(III) systems led to the description of three series of general formulas $M_{2+x}An^{IV}_{2-x}An^{III}_{x}(C_2O_4)_5 \cdot nH_2O$ (hexagonal) and $M_{1-x}[An^{III}_{1-x}An^{IV}_{x}(C_2O_4)_2 \cdot H_2O] \cdot nH_2O$ (tetragonal and triclinic). The knowledge of a part of the phase diagrams allows the characterization of An(IV)-Ln(III)/An(III) co-precipitates. The powder studies highlight the structure evolution along the lanthanide and actinide series and give a preliminary evaluation of the different solid solution domains. All these results suggest the need to pursue studies on single crystals directly on minor actinide-plutonium system (instead of surrogates) and the necessity to develop new methods of single crystal growth.

Acknowledgements

A part of this research was financially supported by AREVA NC, France. We thank Jean Luc Emin, AREVA NC, France, for encouraging this work.

References

1. W. Hummel, G.Anderegg, L. Rao, Chemical thermodynamics volume 5, OECD, Elsevier, New York (2005)

2. M.S. Grigor'ev, I.A. Charushnikova, N.N. Krot, A.I. Yanovskii, Yu.T. Struchkov, "Crystal Structure of Neptunium(IV) Oxalate Hexahydrate $Np(C_2O_4)_2.6H_2O$", Radiochemistry, 39, 5, 419-422 (1997)

3. W. Ollendorff, F. Weigel, "The crystal structure of some lanthanides oxalate decahydrates, $Ln_2(C_2O_4)_3.10H_2O$, with Ln = La, Ce, Pr, and Nd", Inorganic and Nuclear Chemistry Letters, 5, 263-269 (1969)

4. W. Runde, L.F. Brodnax, A. Bean, B.L. Scott, "Directed Synthesis of Crystalline Plutonium(III) and (IV) Oxalates: Accessing Redox-Controlled Separations in Acidic Solutions", Inorganic Chemistry, 4,13, 5967-5972 (2009)

5. I.A. Charushnikova, N.N. Krot, S.B. Katser, "Electronic Absorption Spectra and Structure of Some Neptunium(IV) Oxalates", Radiochemistry, 40, 6, 538-543 (1998)

6. G. B. Andreev, Ph. Moisy, N.A. Budantseva, A.M. Fedoseev, "Synthesis, Crystal Structure and Some properties of new Oxalates of Tetravalent Pu, Np, U and Th, $\{C(NH_2)_3\}_4[An(C_2O_4)_4].2H_2O$ and , $\{Co(NH_3)_6\}_2[An(C_2O_4)_5].4H_2O$", Pu Futures Meeting (2008)

7. B. Chapelet-Arab, G. Nowogrocki, F. Abraham, S. Grandjean, "U(IV)/Ln(III) unexpected mixed site in polymetallic oxalato complexes. Part I. Substitution of Ln(III) for U(IV) from the new oxalate $(NH_4)U_2(C_2O_4)_5.0.7H_2O$", Journal of Solid State Chemistry, 178, 3046-3054 (2005)

8. B. Chapelet-Arab, G. Nowogrocki, F. Abraham, S. Grandjean, "U(IV)/Ln(III) unexpected mixed site in polymetallic oxalato complexes: Part II. Substitution of U(IV) for Ln(III) in the new oxalates $(N_2H_5)Ln(C_2O_4)_2.nH_2O$", Journal of Solid State Chemistry, 178, 3055-3065 (2005)

9. B. Chapelet-Arab, L. Duvieubourg, G. Nowogrocki, F. Abraham, S. Grandjean, , "U(IV)/Ln(III) mixed site in polymetallic oxalato complexes: Part III. Structure of $Na[Yb(C_2O_4)_2(H_2O)].3H_2O$ and the derived quadratic series $(NH_4^+)_{1-x}[Ln_{1-x}U_x(C_2O_4)_2(H_2O)].(3+x)H_2O$, Ln = Y, Pr-Sm, Gd, Tb", Journal of Solid State Chemistry, 179, 4029-4036 (2006)

10. B. Arab-Chapelet, S. Grandjean, G. Nowogrocki, F. Abraham, "Synthesis of new mixed actinides oxalates as precursors of actinides oxide solid solutions", Journal of Alloys and Compounds, 444-445, 387-390 (2007)

11. B. Arab-Chapelet, S. Grandjean, G. Nowogrocki, F. Abraham, "Synthesis and characterization of mixed An(IV)An(III) oxalates (An(IV) = Th, Np, U or Pu and An(III) = Pu or Am)", Journal of Nuclear Materials, 373, 259-268 (2008)

12. J. Gopalakrishnan, "Chime Douce Approaches to the Synthesis of Metastable Oxide Materials", Chemistry of Materials, 7, 7, 1265-1275 (1995)

13. S. Grandjean, A. Bérès, J. Rousselle, C. Maillard, "Procédé de coprécipitation d'actinides a des états d'oxydation distincts et procédé de préparation de composés mixtes d'actinides", Brevet FR/ 04 51058 (2004)

14. R.D. Shannon, "Revised Effective Ionic Radii and Systematic Studies of Interatomic Distances in Halides and Chalcogenides", Acta Crystallographica, A32, 751-767 (1976)

Synthesis of Uranium-based Microspheres for Transmutation of Minor Actinides

Henrik Daniels, Stefan Neumeier, Giuseppe Modolo
Institut für Energieforschung, Sicherheitsforschung und Reaktortechnik (IEF-6),
Forschungszentrum Jülich GmbH, 52425 Jülich, Germany
Tel: +49(0)2461616282, Fax: +49(0)2461612450
e-mail: h.daniels@fz-juelich.de

Abstract *– Utilisation of the internal gelation process is a promising perspective for the fabrication of advanced nuclear fuels containing minor actinides (MA). The formulation of appropriate precursor solutions for this process is an important step towards a working process as the chemistry of uranium-MA systems is quite complex. In this work, actinide surrogates were utilised for basic research on their influence on the system. The ceramics obtained through thermal treatment of the gels were characterised to optimise the calcination and sintering process.*

A. INTRODUCTION

An alternative to the direct disposal of long-lived radionuclides is their separation from the original waste in connection with subsequent transmutation. One promising concept after the partitioning step is embedding the minor actinides (MA: Am, Cm, Cf) in uranium-based nuclear fuel by an internal gelation process. This will allow the MAs to be destroyed by fast-neutron reactions in the upcoming generation-IV reactors.
The method for the internal gelation of uranium was developed by the KEMA laboratory in the 1960s and is based on the decomposition of hexa-methylene-tetra-amine (HMTA), after its protonation, to ammonia in heat. This causes a drastic pH increase, resulting in hydrolysis and condensation reactions. The reactions taking place are illustrated in equations (1) to (4):

HMTA protonation:	$[(CH_2)_6N_4] + H^+$	$\leftrightarrow$	$[(CH_2)_6N_4H]^+$	(1)
HMTA decomposition:	$[(CH_2)_6N_4H]^+ + 6\ H_2O + 3\ H^+$	$\rightarrow$	$4\ NH_4^+ + 6\ CH_2O$	(2)
Uranyl hydrolysis:	$UO_2^{2+} + 2\ H_2O$	$\leftrightarrow$	$UO_2(OH)_2 + 2\ H^+$	(3)
Uranyl condensation:	$UO_2(OH)_2 + H_2O$	$\rightarrow$	$UO_3 \cdot 2H_2O\downarrow$	(4)

Several studies have been carried out on the whole subject and a common element for the fabrication of U(VI) gels is the need for a so-called acid-deficient uranyl-nitrate solution (ADUN) as precursor solution. This allows the use of a reduced quantity of HMTA due to the lower initial acidity. Moreover, a substoichiometric amount of nitrate improves the solubility of uranium and therefore allows higher concentrations. Understanding the influence of this step is crucial for the development of a working process. [1, 2, 3]
As the MAs, unlike uranium, are present in a trivalent oxidation state in the precursor solution, special attention has to be paid to their gelation behaviour, as well as to their distribution and structural influence in the gel. Therefore, in this work, Nd^{3+} was used as an MA surrogate to investigate the influence of such cations on the system. This is reasonable as the chemical properties of trivalent actinides and their corresponding lanthanides are very similar.
During the thermal treatment, phase transitions of the uranium matrix occur. After calcination at about 800 °C, uranium is present in the form of U_3O_8 which has a layered orthorhombic crystal structure [4]. Introducing quantitative amounts of trivalent actinides can have a certain impact on this structure's integrity. Investigations are necessary related to phase segregation and the general integrity of the obtained products.

B. PREPARATION OF ACID-DEFICIENT URANYL-NITRATE

There are different ways of preparing ADUN. Amongst these are: dissolution of U_3O_8 in an understoichiometric amount of HNO_3, chemical removal of nitrate by a reducing agent like formic acid, and the extraction of HNO_3 from a uranyl-nitrate solution by amines. [5]
After a series of preliminary tests, we decided to focus on extractive denitration with Primene JM-T (denoted in the following as Primene, a primary amine, M=269 g/mol, Figure 2) and this process was further investigated. Therefore, experiments concerning the appropriate molar ratio of Primene versus nitrate were undertaken: varying amounts of Primene were contacted with a uranyl-nitrate solution of which afterwards the corresponding pH and the ratio [Nitrate] / [Uranium] was determined. As seen in Figure 1, and as expected, with increasing amounts of Primene, the resulting nitrate-uranium ratio decreases after extraction in the aqueous solution while the pH increases.

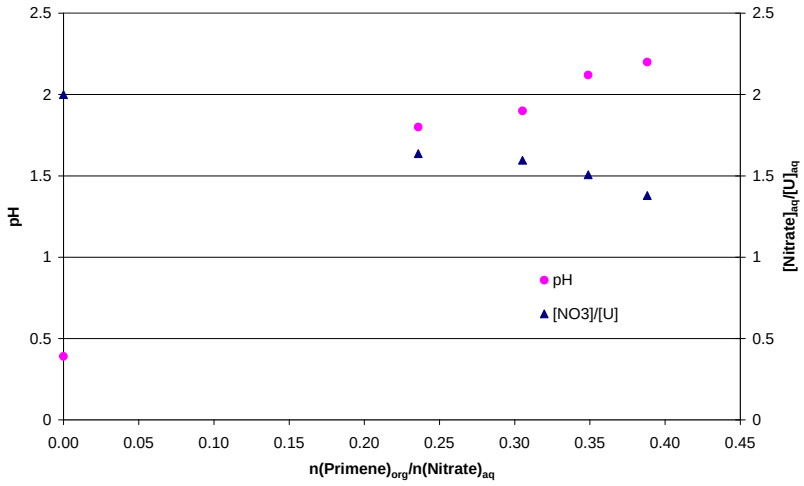

Figure 1: n(Primene) / n(Nitrate) ratio for extraction from a uranyl-nitrate solution in relation to resulting pH and [Nitrate] / [Uranium] ratio of the aqueous phase

Taking the average of 0.7 moles nitrate extracted per mole Primene into account, a 1:1 extraction mechanism as shown in Figure 2 can be assumed. This leads to a simple method for estimating the required amount of Primene by assuming a linear coherence between the amount of Primene used and the amount of nitrate extracted.

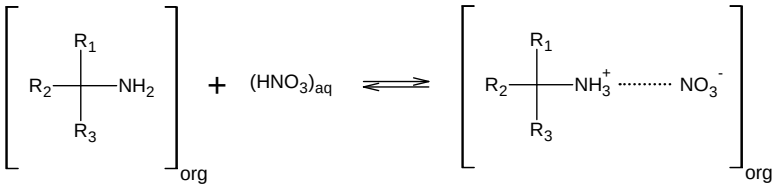

Figure 2: Nitrate extraction with Primene

It was found that with a pure 2.1-molar uranyl-nitrate solution, a denitration ratio of about 30 % can be achieved without forming precipitates. On the contrary, a typical internal-gelation stock solution (containing uranium, actinide surrogates and urea) starts to form precipitates at a ratio of more than 25 %. Therefore, the corresponding ratio of the denitrated stock solutions should be targeted to a value of not more than 20 %.

C. FABRICATION OF URANIUM-NEODYMIUM MICROSPHERES

An adapted internal gelation process as illustrated in Figure 3 was used to create uranium / neodymium microspheres [6]. A stock solution consisting of uranyl-nitrate, Nd-nitrate, urea and HMTA was created and dropped into hot silicone oil in which the gelation took place. As the spheres travelled from top to bottom in the gelation column, an increase in opacity was observed.
The obtained spheres were washed in petrol ether and ammonia solution and the metal losses in the washing solutions were measured via ICP-MS to evaluate the integrity of the gels. As all metal-concentrations in the washing solutions were in the range of 10^{-7} M to 10^{-6} M, this indicates not only complete gelation but already a certain leaching resistance.
Afterwards, the microspheres were dried at room temperature before the thermal treatment took place. Drying at room temperature led predominantly to shrinkage of the microspheres without visible crack formation. Nevertheless, the usage of too less HMTA resulted in defects after drying, when no denitrated stock solution was used (Figure 4).
Calcination was carried out at 800 °C and SEM analysis was used as an initial indicator for the quality of the obtained product.

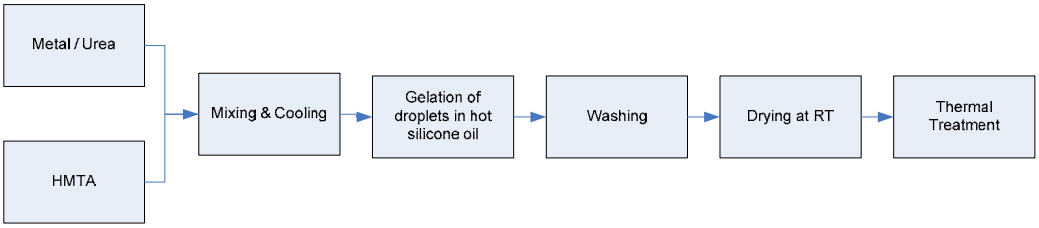

Figure 3: Flow sheet for internal gelation process

After calcination, the SEM analysis showed that the spheres generally remained intact without visible phase segregation, but crack formation was present in dependence on the initial precursor solution formulation. An amount of 2.5 moles HMTA per mole metal caused cracks, while a decrease to 2.2 moles HMTA per mole metal led to an integer surface (Figure 5).

[HMTA]/[Me] = 2.2 , no ED[1] | [HMTA]/[Me] = 1.9, no ED | [HMTA]/[Me] = 1.9, ED

Figure 4: Photos of obtained U/Nd microspheres dried at RT (not true to scale): 90% uranium & 10% neodymium

[1] Extractive denitration with Primene

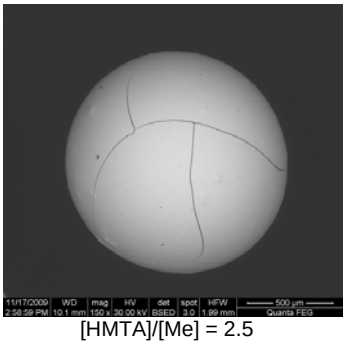

[HMTA]/[Me] = 2.5

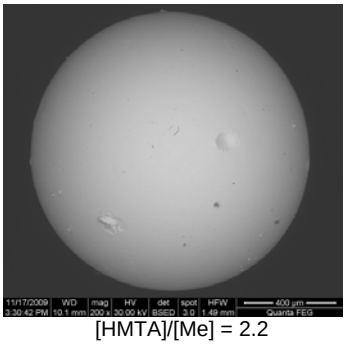

[HMTA]/[Me] = 2.2

**Figure 5: SEM pictures of calcinated U/Nd microspheres:
90% uranium & 10% neodymium; 800 °C**

D. CONCLUSION

This work demonstrates the general feasibility of an internal gelation process for creating uranium / neodymium microspheres with optional usage of acid-deficient uranyl-nitrate.
A method for extractive denitration with Primene of highly concentrated uranium solutions was evaluated. The experimental outcome led to a procedure allowing direct denitration of internal gelation stock solutions by extraction.
Fabrication of microspheres via an adapted internal gelation process with subsequent calcination of the gels was successfully carried out. Microspheres with an integer, crack-free surface were obtained when proper formulation and treatment of the stock solutions were applied.

Acknowledgements

Financial support for this research was provided by the European Commission (project ACSEPT – No. 211267).

References

1. J. L. Collins, M. H. Lloyd and R. L. Fellows, "The Basic Chemistry Involved in the Internal-Gelation Method of Precipitating Uranium as Determined by pH Measurements," *Radiochim. Acta*, 42, 121-134 (1987).

2. R. D. Hunt and J. L. Collins, "Uranium kernel formation via internal gelation," *Radiochim. Acta*, 92, 909-915 (2004).

3. V. N. Vaidya, S. K. Mukerjee, J. K. Joshi, R. V. Kamat and D. D. Sood, "A study of chemical parameters of the internal gelation based sol-gel process for uranium dioxide," *J. Nucl. Mater.*, 148, 324 - 331 (1987).

4. G. C. Allen and N. R. Holmes, "A mechanism for the UO2 to a-U308 phase transformation," *J Nucl Mater.*, 223, 231-237 (1995).

5. A. Deptula and C. Majani Sol-Gel Processes and their Applications; ENEA; 1986.

6. R. Förthmann, A. Naoumidis, H. Nickel and W. Burck Investigations on the Preparation of UO2 Microspheres by Internal Gelation of a UO2 Sol and from a Uranium(VI) Solution; Forschungszentrum Jülich GmbH; 1970.

Salts purification and redox potential measurement for the molten LiF-ThF_4-UF_4 mixture

V. Afonichkin, A. Bovet, V. Shishkin
Institute of High-Temperature Electrochemistry
22, S.Kovalevskaya st.,Yekaterinburg, 620219,Russia
Tel: 7-343-362-30-66, Fax: 7-343-374-59-92, e-mail: afonichkin@ihte.uran.ru

Abstract *– The "dry" techniques of producing and clearing of some metals fluorides, their mixtures and cakes of a given composition obtained without usage gaseous HF for experiments under the Project ISTC #3749 are developed. The products of synthesizing and purification of oxygen-containing compounds, are studied by methods X-ray diffraction analysis, gravimetry or IR spectrometry. The experimental studies confirmed that solid NH_4HF_2 can be efficiently used instead of an unsafe and corrosive HF gas for removal of oxygen-containing impurities from metal fluorides and for conversion of uranium and thorium dioxides to anhydrous tetrafluorides. These processes do not require expensive equipment and special measures of safety.*
The electrochemical behavior of UF_4 solutions in a melt 77LiF-23ThF_4 (mole%) was studied by cyclic voltammetry. Formal analysis of the obtained dependencies showed that in our experimental conditions the recharge U(IV) to U(III) is qualitatively consistent with voltammetric criteria and can be classified as reversible. However, the results of mathematical processing of voltammograms show that the basic calculated characteristics of this reaction differ from the theoretical values corresponding one-electron process controlled by the diffusion rate. This indicates quasi-reversibility of the studied reaction.

A. INTRODUCTION

To prepare the molten salt mixtures, which are to be study is scheduled in Project #3749, use fluorides of metals with a minimum content of water and impurity oxides and/or oxyfluorides. They can lead to hard-to-control changes in the chemical composition, the physico-chemical properties of the test melt, and the active surface of the electrodes and the samples, with an ultimate adverse effect on experimental results.

Most methods developed and tested at ORNL for the removal of oxide compounds from fluoride salts are based on high-temperature treatment with gas mixtures containing the toxic and corrosive hydrogen fluoride (HF). But the work with the HF gas at high temperatures requires considerable expenditures for special equipment, monitoring systems, and personnel safety. When preparing small batches of salts it is not economically justified. Therefore making and testing of laboratory "dry" techniques of producing and clearing of some metals fluorides, their mixtures and cakes of a given composition obtained without usage gaseous HF is indispensable.

Use of molten fluorides as reactor coolants & fuels is the one of the most perspective ways in the nuclear power development [1]. In this connection, special significance is attached to on-line control of the chemical composition and the redox condition of the circulating molten fluorides mixtures. A solution of these problems is a necessary condition for a safe and long MSR operation, which is largely limited by the compatibility of the container material and the molten salt fluorides mixture [2].

It was found already at early stages of MSR program at ORNL that treatment of molten fluorides by electronegative reducing metals, e.g., beryllium or zirconium depending on the solvent composition, considerably decreases the oxidizing capacity of the melts [3]. As a result, resistance of structural materials to uniform corrosion and tellurium intercrystalline corrosion can be improved. However, in MSR, when electropositive fission and corrosion products are accumulated in the fuel salt, the effect of a such fuel reducing treatment should last sufficiently long. To decrease the corrosivity of the melt, it is necessary to provide a redox buffer, which will have a considerable capacity so as to reduce oxidation impurities and maintain the melt redox potential in the required range for a long time.

The UF_4 / UF_3 buffer couple was developed at ORNL within MSBR program. The UF_4 / UF_3 couple was produced by reduction of molten salt mixture fuelled by UF_4 with beryllium or zirconium until the required ratio [U(IV)]/[U(III)] was obtained. When the active component (UF_3) of the buffer couple was spent for reduction of corrosive impurities, a metal rod was immersed into the melt again and was held there until the UF_3 concentration returned to its initial value.

The [U(IV)]/[U(III)] ratio for molten salt mixtures containing this redox buffer couple was measured most accurately and reliably by a voltammetric analysis. Parallel spectrophotometric tests of the melt samples, which required more complicated and expensive equipment, confirmed this conclusion [4].

The voltammetric method, developed at ORNL for measuring the [U(IV)]/[U(III)] ratio in the MSR fuel salt, is based on determination of the difference between the redox potential of the melt, E_{EQ}, and the voltammetric equivalent of the standard redox potential E^0 of the U(IV)/U(III) couple at [U(IV)] >> [U(III)]. In conditions of linear voltammetry, at a stationary electrode and a reversible charge exchange of the melt-soluble oxidized and reduced forms of uranium, E^0 is approximately equal to the half-wave potential $E_{1/2}$ and corresponds to the potential in the voltammogram, at which the current accounts for 85.2% of the peak current.

A necessary condition for the use of this method is the reversibility of the process of cathode reduction of the ions U (IV) to U(III). To determine the applicability of this method for control of redox potential in the molten salt mixture 77LiF-23ThF4 (mole%) with additions of UF_4 the kinetics of electroreduction of U (IV) on platinum, molybdenum and tungsten electrodes was studied.

B. PREPARATION OF SALT MIXTURES FOR EXPERIMENTS

On preparation stage of experiments with molten salts the researches were conducted on making and testing of laboratory "dry" techniques of producing and clearing of some metals fluorides, their mixtures and cakes of a given composition obtained without usage gaseous HF. Instead of it the low-melting ammonium hydrofluoride NH_4HF_2 ($T_m \approx 125\ ^0C$) was selected. The positive experience of usage of this compound for conversion of metals, their oxides and some salts in fluorides is described in the reviews, *e.g.* [5, 6]. The basis of the techniques for conversion of uranium and thorium oxides (UO_2 and ThO_2) to anhydrous tetrafluorides (UF_4 and ThF_4) with the use of NH_4HF_2 formed the results of the study Wani et al [7]. When heating such mixtures proceeds successive reactions of synthesis and decomposition. The total chemical reaction can be described by equation:

$$MeO_2 + 4NH_4HF_2 \rightarrow MeF_4 + 4NH_4F \uparrow + 2H_2O \uparrow \qquad (1)$$

(Me = Th or U, $T_{max} = 350\text{-}400^0C$)

The following processes realized in laboratory scales:

- production of anhydrous thorium tetrafluoride from crystallohydrate;
- production of anhydrous lithium fluoride;
- conversion of thorium dioxide to tetrafluoride;
- conversion of uranium dioxide to tetrafluoride.

Obtained anhydrous salts utilised for:

- production of the Li_3ThF_7 compound;
- production of the 73LiF-27UF_4 (mole %) salt cake;
- production of the 78LiF-22[UF_4+ThF_4] (mole %) salt cake;
- production of the LiF-UF_3 salt cake.

A zone melting and filtration of melts through the nickel filter have used in some cases for additive clearing salt cakes from impurity. The detailed description of these processes and outcomes of the X-ray diffraction analysis of the obtained fluorides, their mixtures and salt cakes of a different composition will be submitted in the first annual report on the Project ISTC #3749.

The main advantages of these methods of producing and clearing of fluorides from the oxygen-containing impurities and the conversion of oxides into fluorides are their simplicity, low cost and relative safety. Heating of reaction mixtures with NH_4HF_2 done gradually to a temperature not exceeding the 400^0C in loose closed crucible of glassy carbon in the air. With proper realization of processes intensive gassing, splashing and spraying the reaction mixtures does not occur. The disadvantage is the difficulty in obtaining isothermal throughout the volume of the reaction mixtures. Local overheating of the contents of the crucible can lead to side chemical reactions

involving oxygen. Thus in ThF_4, obtained from ThO_2, can appear an admixture $ThOF_2$ as a pyrolysis product , and UF_4 begins to oxidize up to UO_2F_2.

Because of the lack of simple and rapid methods for determining oxygen in the samples of the salts there remains the problem of monitoring the depth of their clearing of oxygen-containing impurities. An X-ray diffraction analysis does not provide a quantitative determination of their residual concentration in the final products of synthesis and processing.

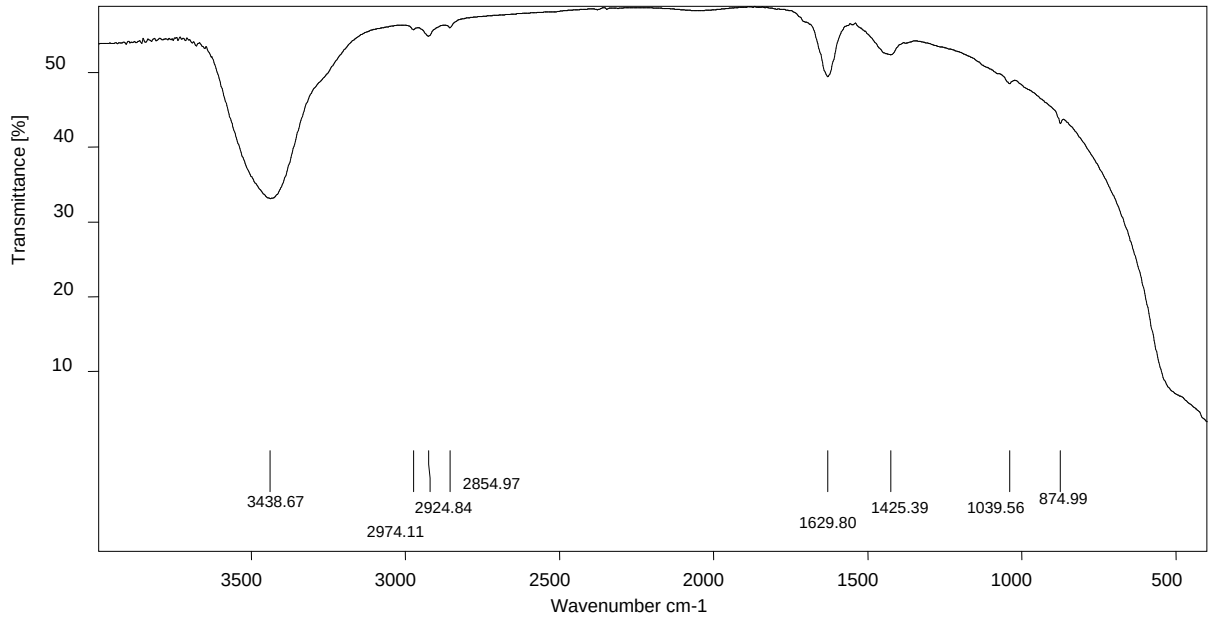

Figure 1: IR spectrum of the pellet No. 1

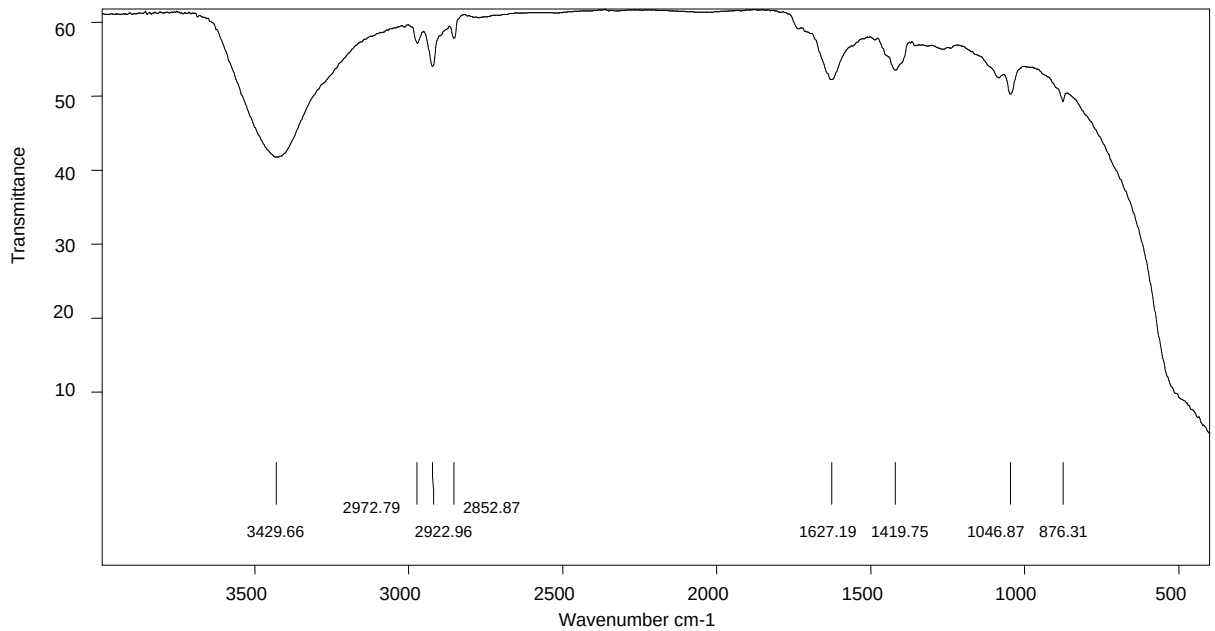

Figure 2: IR spectrum of the pellet No. 2

Therefore IR spectrometry was utilised for analysis of samples. As an example, see Figures 1, 2. They shows the IR spectra of Li_3ThF_7 salt cakes, obtained by melting purified LiF and ThF_4 in an argon atmosphere, and measured on a Tensor 27 spectrometer (Bruker) in the range of wave

numbers from 4000 to 400 cm^{-1}. Small crystals of KBr (650 mg) were mixed with a Li_3ThF_7 powder (9 mg), the mixture was ground to a fine powder on a special device, and pellets were compacted of the powder in a vacuum. Two transparent pellets of Li_3ThF_7 powders from different batches were made for the study. The pellet No. 1 contained Li_3ThF_7 after its zone refining, and the pellet No. 2 had Li_3ThF_7 taken from the bulk of the cake produced by the last melting so that the samples were free of the black inclusions insoluble in the melt.
The registered peaks at 3429.66 and 3438.67 cm^{-1}, 1627.1 and 1629.80 cm^{-1}, and 1419.75 and 1425.39 cm^{-1} are commonly related to molecules of water, which is present in a particular form (crystallohydrate, dissolved, and adsorbed) in Li_3ThF_7 samples. The method is highly sensitive to water, and the observed picture suggests an insignificant concentration of moisture in the samples. The peaks at 1046.87, 1039.56 cm^{-1} and 876.31, 874.99 cm^{-1} probably are related to low-symmetry compounds of oxygen and thorium (ThO_2 or $ThOF_2$). They are much larger in the spectrum of the second sample. A strong peak, which is related to a thorium compound of a higher symmetry (Li_3ThF_7), is registered at ~800 cm^{-1} and lower. Unfortunately, the spectrometer does not allow measuring spectra in the range of wave numbers smaller than 400 cm^{-1} so as to obtain a full spectral characteristic of the sample. This range can be covered by measuring Raman spectra. However, even these data are sufficient to conclude that the concentration of ThO_2 or $ThOF_2$ in the samples under study is extremely low.

To obtain quantitative information about the content of impurities in the tablets the calibration relations are required, built on the IR spectra of samples with a given content of each impurity. This complex and difficult task is the subject of special study.

C. VERIFICATION OF ELECTROANALYTICAL TECHNIQUE FOR REDOX POTENTIAL EVALUATION IN SALT MELTS

In order to control correctly [U(IV]/[U(III)] ratio in molten LiF-ThF_4 salt mixtures by the voltammetry, it is necessary to prove that electrochemical reaction (see Equation 2) is a reversible process governed by a simple diffusion-controlled charge transfer. Therefore the measured voltammograms should not be distorted due to side electrode processes, which hamper an exact determination of the peak current and the polarographic half-wave potential of the reaction under study. Measurement errors can increase considerably in the presence of Cr(II) ions [8], which appear in the melt corrosion products and are reduced on the working electrode in the same range of potentials as the one used for measuring the current peak of the reaction (see Equation 2). The interfering effect is also due to films on the melt surface, which can come in contact with the working electrode and alter its surface, passivation of the electrode, etc. The measurement accuracy can also be impaired by variations of the melt surface at the semisubmerged working electrode and uncontrolled fluctuations of the temperature [9].

The cyclic voltammogram of the 77LiF-23ThF_4 melt (mole %), which was measured on a tungsten working electrode at 600°C and a potential sweep rate of 0.1 V/s, as demonstrated Delpech et al [10], did not exhibit any electrode processes preceding reduction of Th^{4+} ions. It could be expected therefore that uranium ions will be reduced in two successive stages,

$$U^{4+} + e^- \rightarrow U^{3+}, \quad (2)$$

$$U^{3+} + 3e^- \rightarrow U^0, \quad (3)$$

prior to deposition of thorium in the 77LiF-23ThF_4 melt (mole %) with an UF_4 addition, which was studied by us, like in other fluoride mixtures [11-13]. An experiment showed however that an addition of UF_4 to the melt-solvent was followed by side chemical reactions, leading to the formation of an electroconductive film on the surface of the working electrode and the "electrode-electrolyte-atmosphere" triple interface above the melt. As a result, immediately after the cathodic potential sweep begins, anomalously high currents are measured, see Figure 3, impeding the registration of voltammograms. The origin of these reactions is unclear, but this phenomenon probably is not different from the phenomena described in [9] and other ORNL reports.

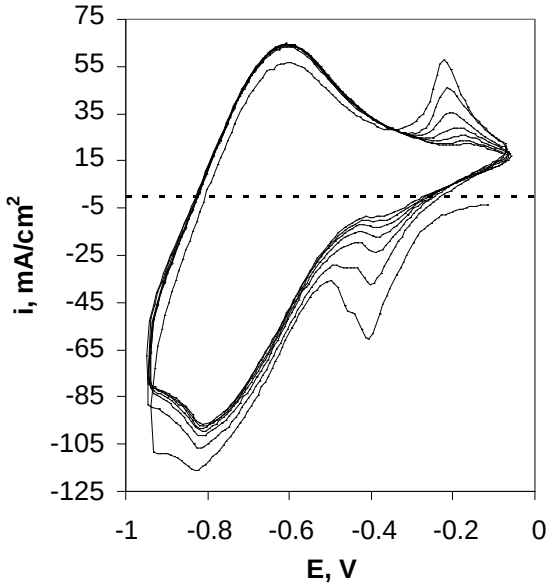

Figure 3: Variation of the shape of a cyclic voltammogram in eight cycles of continuous polarization. Solvent 77LiF-23ThF_4 (mole %) with addition of 0.34 mole % UF_4 prior to removal of impurities. T = 1023 K. v = 0.9 V/s. Pt as the reference electrode (RE); Mo as the working electrode (WR).

To remove added UF_4 and impurity electropositive ions from the melt, a rod of metallic thorium with the surface area of ≈ 4.5 cm^2 was introduced into the melt and was held there at T = 750°C for 3 hours. Then the melt was frozen and was used in the next experiment. A cyclic voltammogram of the thorium-treated melt is shown in Figure 4. It is seen that any processes related to reduction of electropositive impurity ions are absent in the initial section of the cathodic voltammogram. It was concluded from this observation that impurities should be carefully removed from the melts before analyzing the reversibility of the reaction (see Equation 2) and UF_4 should be partially reduced to UF_3 for recording of quality voltammograms for salt mixtures with UF_4 additions.

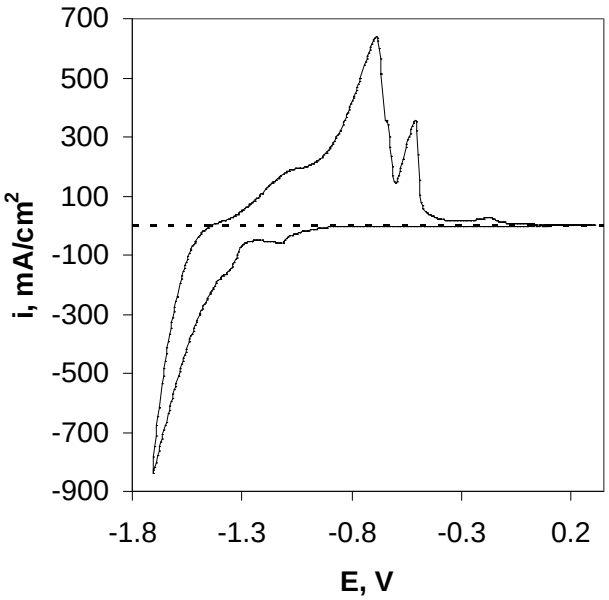

Figure 4: Cyclic voltammogram of the solvent 77LiF - 23ThF_4 (mole %) with addition of 1.6 mole % UF_4 after treatment with metallic thorium. W as WE; Pt as RE; T =1023 K; v = 0.9 V/s.

When the melts with an addition of UF_4 are treated with thorium, an uncontrolled cementation of uranium on Th takes place, and, hence, the concentration of uranium fluorides dissolved in the melt decreases. Therefore, it would be preferable to reduce the melt with metallic uranium, but this process

is hard to control, too. Moreover, the surface of a uranium rod quickly becomes inactive in impurity-containing melts, and the rod should be replaced at regular intervals.

To increase the rate, at which impurities are removed from the melt, and add U^{3+} ions to the melt, weights of a ready cake, which was synthesized by reducing the 77LiF-23UF_4 eutectic (mole %) with metallic uranium at 800°C, were charged to the salt mixture through the airlock. Given the mass of uranium dissolved during reduction of the 77LiF-23UF_4 eutectic and knowing the weight of the cake charged to the test melt, it is possible to calculate the quantity of the reducing agent added to the melt. As an example Figure 5 presents a set of cyclic voltammograms, which were measured in one and the same melt at different sweep rates, with all other things being equal.

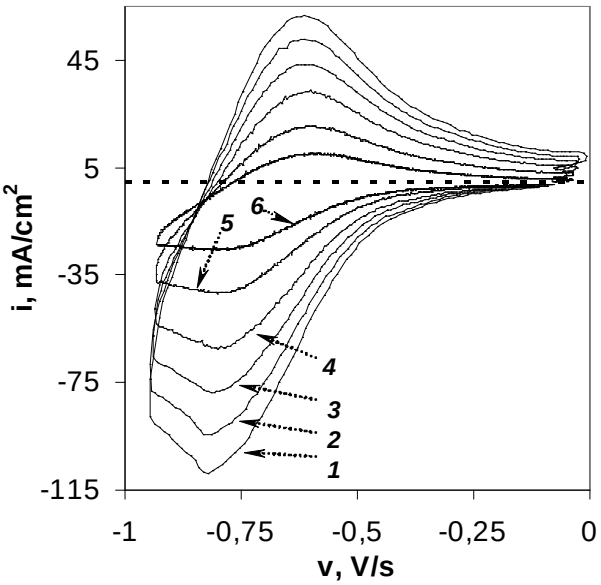

Figure 5: Effect of the potential sweep rate on the shape of voltammograms. Solvent 77LiF-23ThF_4 (mole %) with an addition of 0.339 mole %UF_4. T = 1023 K. Pt as RE; Mo as WE; v = (1) 1.0, (2) 0.8, (3) 0.6, (4) 0.4, (5) 0.2, (6) 0.08 V/s.

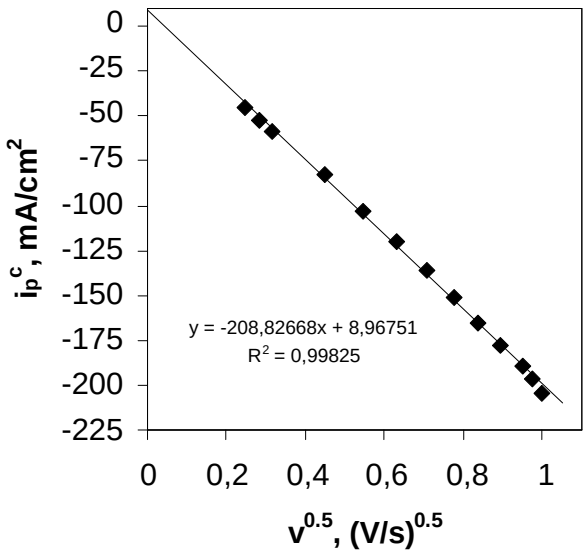

Figure 6: Effect of the potential sweep rate on the density of the cathodic peak current. Solvent: 77LiF-23ThF_4 (mole %) with an addition of 0.656 mole % UF_4. T = 1023 K. Pt as RE. Mo as WE.

The influence of the concentration of UF_4 in the melt and the rate of potential sweep on the value of the cathodic peak current and its potential was investigated and analyzed using standard voltammetric criteria of reversibility [14]. Formal analysis of the dependencies presented in Figures 5-7 showed that in our experimental conditions the electrode reaction (see Equation 2) is qualitatively consistent with these criteria and can be classified as reversible. However, the results of mathematical processing of the cathode and the cyclic voltammograms show that the basic calculated characteristics of this reaction (the number of electrons involved in the reaction, the potential difference of cathodic current peak and half-peak, as well as cathodic and anodic current peaks) differ substantially from the theoretical values corresponding one-electron process controlled by the diffusion rate. These facts can be explained by the slow chemical reactions preceding or following an act of recharging U(IV) ions, for example, reaction formation or dissociation of fluoride complexes of uranium, the adsorption of the depolarizer or a product of recharging, and so on. In this case, using equation (2) to determine [U(IV)]/[U(III)] in the studied fluoride melt can lead to significant errors.

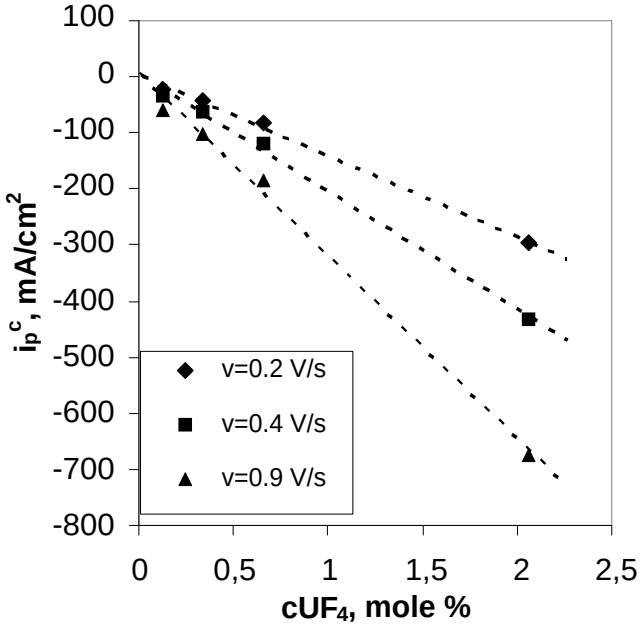

Figure 7: Dependence of the density of the cathodic peak current on the UF_4 concentration in the 77LiF-23ThF_4 (mole %) melt. T = 1023 K. Pt as RE, Mo as WE.

D. CONCLUSION

The experimental studies confirmed that solid NH_4HF_2 can be efficiently used instead of an unsafe and corrosive HF gas for removal of oxygen-containing impurities from metal fluorides and for conversion of uranium and thorium dioxides to anhydrous tetrafluorides. These processes do not require expensive equipment and special measures of safety.

An X-ray diffraction analysis does not provide a quantitative determination of the residual concentration of oxygen-containing impurities in the final products of synthesis and processing. Special methods and instruments are required for this purpose.

The laboratory studies have revealed that well reproducible and analyzable cathodic and cyclic voltammograms are measured only in partially reduced LiF-ThF_4-UF_4 melts with UF_3 additions, which are freed from electropositive impurity ions.

Linearity of the dependences i_p^c vs. [UF_4] and i_p^c vs. $v^{1/2}$, as well as the independence of the E_p^c of v in the experiment qualitatively consistent with the voltammetric criteria of reversibility of the investigated electrode process (see Equation 2). However, its main quantitative characteristics (the number of electrons involved in the reaction, the potential difference of cathodic current peak and half-peak, as well as cathodic and anodic current peaks) differ substantially from the theoretical values corresponding to the one-electron process of recharging with a diffusion control. This indicates quasi-reversibility reaction (2).

Platinum, tungsten or molybdenum can be used as the material of the reference and working electrodes. If the electrodes are made of different materials, the thermal emf affects the results of potentiometric and voltammetric measurements.

Aknowledgements

The generous financial support of this work by the ISTC # 3749 Project is gratefully acknowledged.

References

1. A Technology Roadmap for Generation IV Nuclear Energy Systems. GIF-002-00. December 2002. – 91 p.

2. P. N. Haubenreich, J. R. Engel. Experience with the Molten-Salt Reactor Experiment. *Nucl. Appl. & Technol*. 8 *2* 118 (1970).

3. J. H. Shaffer. Preparation and Handling of Salt Mixtures for the Molten Salt Reactor Experiment. MSR Project, Prog. Rep. ORNL-4616 (1971), p. 11.

4. H. W. Jenkins, D. L. Manning, G. Mamantov, J. P. Joung. EMF, Voltammetric, and Spectrophotometric Measurements on the U(IV)/U(III) Couple in Molten LiF-BeF_2-ZrF_4. MSR Project, Prog. Rep. ORNL-4396 (1969), p. 201.

5. Ammonium Fluorides. Yu.A. Buslaev, N.K. Sokovikova (Ed.). In: Results of Science and Engineering. Ser. Neorgan. Khimiya, v. 15, Moscow, 1988, 154 p. (in Russian).

6. E.G. Rakov and E. I. Mel'nichenko. The Properties and Reactions of Ammonium Fluorides. *Russian Chemical Reviews*, 53 *9* 851 (1984).

7. R. N. Wani, S. J. Patwe, U. R. K. Rao and K. S. Venkateswarlu. Fluorination of oxides of uranium and thorium by ammonium hydrogen fluoride. *J. Fluor. Chem.*, 44 *2* 177 (1989).

8. J. M. Dale, Theoretical Considerations of the Voltammetric In-Line Determination of U(III). MSR Project, Prog. Rep. ORNL-4782 (1972), p. 80.

9. J. M. Dale, A. S. Meyer, In-Line Chemical Analysis of Molten Fluoride Salt Streams. MSR Project, Prog. Rep. ORNL-4728 (1972), p. 69.

10. S. Delpech, G. Picard, Etudes physico-chimiques de fluorures fondus a base de ThF_4. www.gedeon.prd.fr/ATELIERS/11_12_decembre_2006/exposes/Thorium_Delpech.pdf

11. C. Hamel, P. Chamelot, A. Laplace, E. Walle, O. Dugne, P. Taxil, “Reduction process of uranium(IV) and uranium(III) in molten fluorides”. *Electrochim. Acta*, 52 *12* 3995 (2007).

12. P. Soucek, F. Lisy, R. Tulackova, J. Uhlir, R. Mraz, “Development of Electrochemical Separation Methods in Molten LiF-NaF-KF for the Molten Salt Reactor Fuel Cycle” *J. Nucl. Sci. and Technol.* 42 *12* 1017 (2005).

13. M. Straka, M. Korenko, F. Lisy, Electrochemistry of uranium in LiF–BeF_2 melt, J. Radioanal. Nucl. Chem 284 *1* 245 (2010).

14. A.M. Bond. *Polarographic Methods in Analytical Chemistry*, p. 136-137, Khimiya, Moscow 1983 (in Russian).

Neutronic and Fuel Cycle Consideration: From Single Stream to Two- fluid Th-U Molten Salt System

O. S. Feynberg, V. V. Ignatiev,
RRC - Kuchatov Institute, 123182,
Kurchatov sq.1, Moscow, RF
Tel:+7-499-196-79-41, Fax: +7-499-196-86-79, e-mail: Feinberg@nsi.kiae.ru

Abstract *–Main part of molten salt reactor (MSR) programs in US, Russia and Europe supported on-site reprocessing development and study of various reactor arrangements that had potential to breed new fuel. In this paper unification of homogeneous MOlten Salt Actinide Recycler & Transmuter (MOSART) system with Th containing molten salt blanket is considered. The two-fluid hybrid MOSART is non-moderated system, with a LiF-(NaF)-BeF_2-$TRUF_3$-(UF_4) fuel salt and a LiF-ThF_4-(BeF_2) blanket salt circulated through two separate flow channels. The starting fuel can be TRU of different composition from PWR spent fuel (UOX, MOX and minor actinide bearing fuels), and "'fresh" TRU is added as needed to compensate for burn-up and build up of fission poisons. Fuel and blanket salts would be processed in a nearby cell to remove fission products and to recover the bred product. The processing rate would correspond to removal of uranium from the blanket on a 15-day cycle and rare earth fission products from the core on a 300 day cycle. All portions of the systems in contact with the fluoride salts would be fabricated of Ni base HN80MTY alloy. Neutronic and fuel cycle calculations were done recently ISTC#3749 project to obtain estimates of critical masses, concentrations of actinides fluorides at BOL and EOL and breeding ratio vs. core / blanket configurations. Plant flowsheet was developed sufficiently during the study to give an indication of feasibility for two main scenarios when all ^{233}U available from blanket is returned to (1) vendor or to (2) MOSART core, but no optimization studies were made.*

A. BACKGROUND

In order to provide sustainable nuclear power development recent years have demonstrated a growing interest in the circulating-fuel systems based on molten salt fluorides [1]. These systems are adaptable to variety of embodiments because of advantages of high temperatures at low pressures, the wide range of solubility of actinides compounds in these salts, optical transparency and radiation damage resistance of these fluorides. Compared with solid-fuelled reactors, fluid fuel molten salt systems provide: lower fissile inventories, no limit on fuel burn up, continuous fission-product removal, no expense on fabricating of new fuel elements, adding makeup fuel as needed, which precludes the need for providing excess reactivity, etc. These systems present a promising flexible option in response to the goals and criteria assigned to future nuclear systems: fuel cycle sustainability, safety, environmental impact, proliferation resistance, diversity of applications and economics.

Nuclear energy systems employing liquid salt fluorides have been investigated by Oak Ridge National Laboratory (ORNL, USA) in the 60's and 70's [2-4]. The favourable experience gained from the 8 MWt MSRE test reactor operated from 1965 to 1969 led to the design of a 1000 MWe molten salt breeder reactor (MSBR) with a core graphite moderator, thermal spectrum and thorium-uranium fuel cycle. 1000MWe MSBR designs of two main configurations were developed at ORNL: (1) single stream [3] and (2) two-fluid [4].

From the point of view of fuel cycle characteristics two-fluid fuel circuit configuration where fertile and fissile materials are dissolved in separate streams, has some advantages in comparison with single stream systems where fissile and fertile are components of one molten salt mixture. Blanket in such kind of systems contains only fertile elements, core may contain one (fissile) or two (fissile and fertile in heterogeneous option) salt streams divided by the construction materials with low absorption cross-sections. Two-fluid system will have maximal meaning of breeding ratio in the blanket and minimal fuel loading in the central core part. Beside these the system can have attractive meanings of temperature reactivity coefficients – fuel moves out of the core due heating and at the same time amount of thorium in blanket is constant. Only construction difficulties connected with heterogeneous structure of such kind breeder limited its development.

In both configurations (two and one-fluid), salt(s) served as fuel and blanket fluid(s) at temperatures ≤ 700^{o}C. The technical feasibility of such systems, which key parameters are resulted in Table 1 (first two columns), now does not raise the doubts.

Optimum fuel salt for MSBR [4] represents a binary mixture of LiF and BeF_2, very poorly absorbing neutrons (lithium is enriched to 99.995 % on ^{7}Li) in which fluorides of fissile and/ or fertile materials UF_4 / ThF_4 are dissolved. For LiF-BeF_2 melt solubility of UF_4 and ThF_4 is more than 20 mole % at melting temperature of about 500 °C; vapour pressure at temperature 700°C is less than 10 Pa.

MSBR [4] possesses good characteristics, but demands continuous removal of soluble fission products (removal time for lanthanides is about 30 days). Creation of such intensive system for fission products clean up in MSBR (first of all, for single stream one) is a challenge, in particular, remain difficulties on actinide losses to waste and selection of constructional materials for the fuel clean up unit. Note, that for two fluid system based on molten LiF-BeF_2 salt mixture in comparison with single fluid one based on LiF-BeF2-ThF_4 it is possible, to manage lanthanides removal much more effectively [4].

In Russia, the molten salt program was started in the second half of 1970th [5]. These studies were also directed on the improvement of the MSBR type concepts. Within recent ISTC#1606 project main focus was placed on experimental and theoretical evaluation of single stream MOlten Salt Actinide Recycler & Transmuter (MOSART) system [6,7]. It was shown that optimum spectrum for MOSART is intermediate/fast spectrum of homogeneous core without graphite moderator. Promising configuration for 2400 MWt MOSART is the homogeneous cylindrical core (3.6 m high and 3.4 m in diameter) with 0.2 m graphite reflector filled by 100 % of molten 15LiF-58NaF-27BeF_2 or 73LiF-27BeF_2 salt mixture. It is feasible to design critical homogeneous core fuelled only by transuranium elements (TRU) trifluorides from UOX and MOX PWR spent fuel while equilibrium concentration for trifluorides of actinides (about 1 mole% for the rare earth removal cycle 300 epdf) is truly below solubility limit at minimal fuel salt temperature in primary circuit 600^{o}C (see Table 1). The effective flux of such system is near 1x10^{15} n/cm^{2} /s [7]. Due to possibility of operation without additional neutron sources, MOSART loaded only by TRU from spent nuclear fuel has maximum capacity, high enough transmutation efficiency and can be loaded by the fuel of wide range of compositions. The fraction required of MOSART units in nuclear power system is about 25%.

Table 1: The basic characteristics of molten salt systems under consideration

	MSBR [3,4]		MSFR [10]		MOSART [6,13]	
Type	breeder		breeder		burner / converter	
Neutron spectrum	thermal		fast		fast	
Number of fluid streams	2	1	2	2	1	2
Thermal capacity, MW	2250	2250	3000	3000	2400	2400
Fuel salt temperature, ^{o}C	566/704	566/704	600/750	700/850	600 / 720	600 / 720
Fuel salt composition, in mole %	68LiF 31BeF_2 0.2UF_4	72LiF 16BeF_2 12ThF_4 0.2UF_4	77.5LiF 20ThF_4 2.5UF_4	78LiF 16ThF_4 6.5$TRUF_3$	72LiF 27BeF_2 1$TRUF_3$	72LiF 27BeF_2 1$TRUF_3$
Blanket salt composition, in mole %	71LiF 2BeF_2 27ThF_4	no	78LiF 22ThF_4	78LiF 22ThF_4	no	75LiF 5BeF_2 20ThF_4
Fuel cycle	U -Th	U -Th	U- Th	TRU-Th-U	without U,Th	TRU-Th-U
Fission product removal time, epdf	30-50	10-30	418	418	300	300

Recent molten salt Th-U breeder developments in Europe (CNRS, France) [8-10] also addresses advanced large power unit without graphite in the core and fast neutron spectrum (MSFR). In MSFR, prior ORNL concept has been revisited by removing graphite and BeF_2. The neutron spectrum is fast and the reprocessing rate strongly reduced down to 40 litres per day to get a positive breeding gain. The reactor is started with ^{233}U or with Pu and minor actinides (MA) mixture from PWR spent fuel (see Table 1). For MSFR [10] as solvent system for fuel and blanket circuits it is offered to consider molten 78LiF-22ThF_4 ($T_{melting}$ =565^{o}C). Note that this solvent has essentially higher melting temperature and solubility for actinide trifluorides, in comparison with well established 72LiF-16BeF_2-12ThF_4 melt ($T_{melting}$ =504 ^{o}C). MSFR exhibit large negative temperature and void reactivity coefficients, a unique safety characteristic not found in solid-fuel fast reactors. ^{233}U production rate in MSFR is about 100 kg/yr. Compared to MSBR basic difficulty of MSFR is that it requires essentially higher starting loadings of fissile materials (5060 kg of UF_4 or 11200 kg of $TRUF_3$) and fuel concentrations for criticality [8,9] (see Table 1). In MFSR starting loading [10] concentration of UF_4 ($TRUF_3$) in fuel salt will make, accordingly, 2.5 (6.5) mole %. Because of limits on solubility of

$TRUF_3$ molten 78LiF-16ThF_4-6.5$TRUF_3$ mixture can be realized only at the minimum temperature in fuel circuit >700^{0}C [11,12]. In this case the maximum core temperature of fuel salt makes 850^{0}C [10]. That will demand development of a new constructional material for MSFR fuel circuit since developed for MSBR and MOSART Ni-Mo alloys of Hastelloy N type are certified only for temperatures <750^{0}C. As advanced high performance material for MSFR design recently has been proposed new Ni-W-Cr alloy [9].
At the same time MSFR with 77.5LiF-20ThF_4-2.5UF_4 starting loading can be realized at the maximum temperature in a fuel circuit < 750^{0}C on the basis of already available Ni-Mo alloys [5,6]. There is only one question where to get ^{233}U for starting loading.
Unification of MOSART system with Th containing molten salt blanket [13] can provide (1) its core operation with minor actinide bearing fuels basing on additional ^{233}U support or (2) effective production of ^{233}U required for starting uranium loading of MSFR. In first case, when the core is processed unburned actinides are returned to the core along with any ^{233}U available from the blanket. In second case uranium processed from blanket is removed for MSFR loading, but in both cases thorium – bearing salt is returned to the blanket.
From the point of view of structure such symbiosis MFSR + hybrid MOSART can have advantage, since allows to use in a greater degree already available technology at temperatures to 700 – 750^{0}C. Symbiosis MFSR + hybrid MOSART reflect main advantage of MSRs which concern fuel cycle flexibility. MSR can work with wide range of fuel loadings without design changing and thus can be included in different scenario of nuclear power development. Beside this it can be realized on the base of existing technologies within technological margins.
This paper mainly focused on the calculation of critical masses, concentrations of actinide fluorides at BOL and EOL and breeding ratios vs. core / blanket configurations and processing rates for hybrid MOSART system when all ^{233}U available from blanket is returned to MSFR vendor.

B. SYSTEM DESCRIPTION

The two-fluid hybrid MOSART is non-moderated system, with a LiF-(NaF)-BeF_2-$TRUF_3$-(UF_4) fuel salt circulating through the homogeneous core and a LiF-ThF_4-(BeF_2) blanket salt. All portions of the systems in contact with the fluoride salts would be fabricated of Ni base HN80MTY alloy. Fig. 1 shows the core / blanket configurations that were used to evaluate its neutronics and fuel cycle feasibility. As can be seen two basic configurations where core with blanket fill right circular cylinder were considered: two-region with simple cylinder core (A) and three–region with ring core (B). In two-region configuration cores from 2 m up to 3.6 m in diameter and from 2m up to 3.6m height are considered (variants V1-V6). In three-region configuration cores from 1.1 to 0.9 m width with 3.2 m height (V7-V9) are investigated. In main cases width for external blanket is 0.6m. The fuel circuit in its external part would be very similar to that of reference MOSART design with 18 m^3 (V1-V3) and 10-11m^3 (V4-V9) salt volume out of the core. Radial, bottom, and top graphite reflectors of 0.2 m width are attached to the reactor vessel.
Fuel salt is based on 17LiF-58NaF-25BeF_2 mixture (mole%) with a melting point of 479°C or on 73LiF-27BeF_2 mixture with a melting point of about 580°C. The specific salts were chosen, in part, because of their high solubility (up to 3 mole % at 600°C) for actinide and lanthanide trifluorides – a requirement for only TRU burning. In our investigations we assumed that solubility limit must not exceed 2.5 mole % taking into account calculation and experimental uncertainties [6,7]. The lithium is enriched to 99.99% ^{7}Li. The blanket salt is LiF-ThF_4 eutectic or ternary 75LiF-5BeF_2-20ThF_4 mixture. The melting point of the blanket salt is 565°C or lower.
At nominal conditions, the fuel and blanket salts enter the reactor vessel at 620°C and transport 2400MWt to the secondary salt in the primary heat exchanger, four in parallel for the core and two in parallel for the blanket. Heat is transferred from the fuel and blanket salts to the power conversion system using a secondary NaF-$NaBF_4$ salt with a composition of 8–92 mole %.
On Fig. 2 fertile and fissile flowsheet for hybrid MOSART is presented for two main scenarios when all ^{233}U available from blanket is returned to (1) MSFR vendor or to (2) MOSART core. Starting fuel is plutonium and minor actinides from UOX PWR spent fuel after 1 year cooling (some other more hard types are possible). TRU are added to compensate for burn up and build up of fission product poisons. When the core fuel is processed, the unburned TRUs and uranium are returned to the core.
Fuel salt is sparged by He for removal of tritium, xenon, and krypton. Fuel and blanket salts would be processed in a nearby cell to remove fission products and to recover the bred product. The processing rate would correspond to removal of uranium from the blanket on a 15-day cycle and rare earth fission products from the core on a 300 day cycle
More rapid processing would reduce parasitic neutron losses but it would also increase the losses of actinides to the waste stream. The uranium removal from fuel salt can be managed by volatility process. Next fuel salt clean up steps of Li,Be/F system are based on the method of reductive extraction in liquid bismuth. Reductive extraction of actinides from molten Li,Na,Be/F salt into liquid bismuth with their subsequent re-extraction into purified salt flow is the most acceptable method of actinide recycling. In order to purify molten Li,Na,Be/F salt from lanthanides, it will

be necessary to use distillation and cocrystallization processes. Application of lanthanides cocrystallization with cerium trifluoride can sufficiently decrease salt solvent amount, which is to be processed by high-temperature distillation.
The blanket is also processed by volatility process; the uranium is removed but thorium bearing salt is returned to the blanket. In our calculations main stream of ^{233}U removed from blanket is transferred for MSFR starting loading.

C. CALCULATION RESULTS

MCNP-4B+ORIGEN2.1 was chosen as the tool for calculation investigations on all stages of optimization studies. This calculation tool was adapted to the MSR within 1606 ISTC project [7] and here was only added by the option which gives the opportunity to calculate the thorium containing multizone configurations.
The main calculation results for two-fluid hybrid MOSAR system are collected in table 2 and given on fig.3-4.
As can be seen in two-zone system filled with 15LiF-58NaF-27BeF_2 (height 3.6 m, diameter 3.4 m) the equilibrium concentration of TRU is not higher than 1 mol.% (var. V1-V3). For variants based on reference MOSART core, blanket size and material don't effect on the critical fuel loading. As it can be seen in the table 2 the production of ^{233}U can be increased up to 115 kg/year by rising of blanket width up to optimal 50-60 cm. The increasing of ThF_4 fraction in the blanket salt (higher than 16-20%) has no significant influence on the ^{233}U production rate.
In the variant with the decreased size (diameter 2.4m, var.V4) the equlibrium concentrations of actinides trifluorides increase from 1 to 2 mole% due to more hard spectrum in the core. ^{233}U production rate in the blanket becomes higher up to 180 kg/yr. Further decreasing of the core diameter up to 2m (V5) elevates the equillibrium consentrations of the actinides trifluorides up to 2.5 mole%. ^{233}U production rate in this variant is near 200kg/yr.
For two-zone system use of 73LiF-27BeF_2 (V6) solvent system instead of 15LiF-58NaF-27BeF_2 (V4) in the core permits to reduce TRU loading down to 50% , but this leads to some decreasing of ^{233}U production rate in fertile salt from 180 to 150 kg/yr.
Transition to ring core geometry (V7) gives the opportunity to raise ^{233}U production rate in fertile salt up to 254 kg/yr, but equilibrium concentration of actinide trifluorides reaches 2.5 mole %. The initial and equilibrium loadings of TRUs in the fuel salt move up respectively.
Replacement of molten 15LiF-58NaF-27BeF_2 mixture (V7) on 73LiF-27BeF_2(V8) salt in the ring core leads to simultaneous relief of equilibrium concentrations of actinides trifluorides in the central zone (from 2.5 down to 1.4 mole %) and ^{233}U production rate in the blanket (from 254 kg/yr to 241kg/yr).
For the cost of additional fuel salt specific power increase it is possible to improve ^{233}U production rate in the blanket of three-zone configuration based on ring core up to 286kg/yr (V9). Thus the variants with ring core geometry afford broad capabilities to increase the rates of new fuel production.
As mentioned above there are two main scenarios for new fuel utilization: when all ^{233}U available from blanket is returned to (1) MSFR vendor or to (2) MOSART core.
Within first scenario for accumulation of initial ^{233}U loading for MSFR (5200 kg) it will be required about 18-20 yrs of hybrid MOSART operation.
As for the second scenario the return of all ^{233}U produced to the fuel circuit on a 15-day cycle permits to reduce equilibrium concentration of $TRUF_3$ (after 8-10 years) in fuel salt from 2.1 down to 0.45 mol.% (for ring core V9). The ^{233}U production rate in this case will be 300 kg/yr and this scenario gives the chance for utilization of minor actinide bearing fuels within solubility limit for actinides trifluorides. The optimisation of these possibilities will be given in near future.

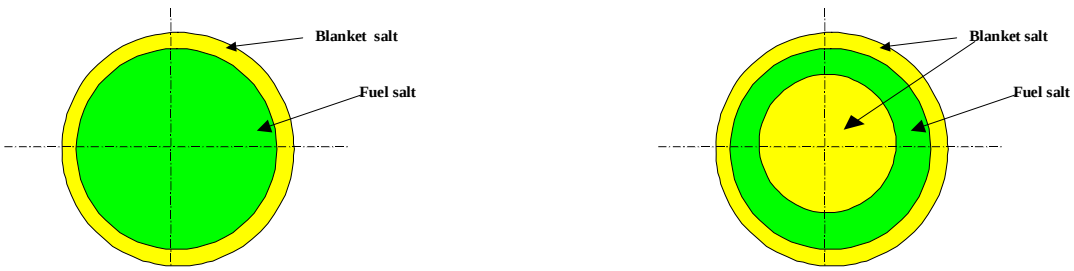

Figure 1: Cylindrical and ring core / blanket configurations

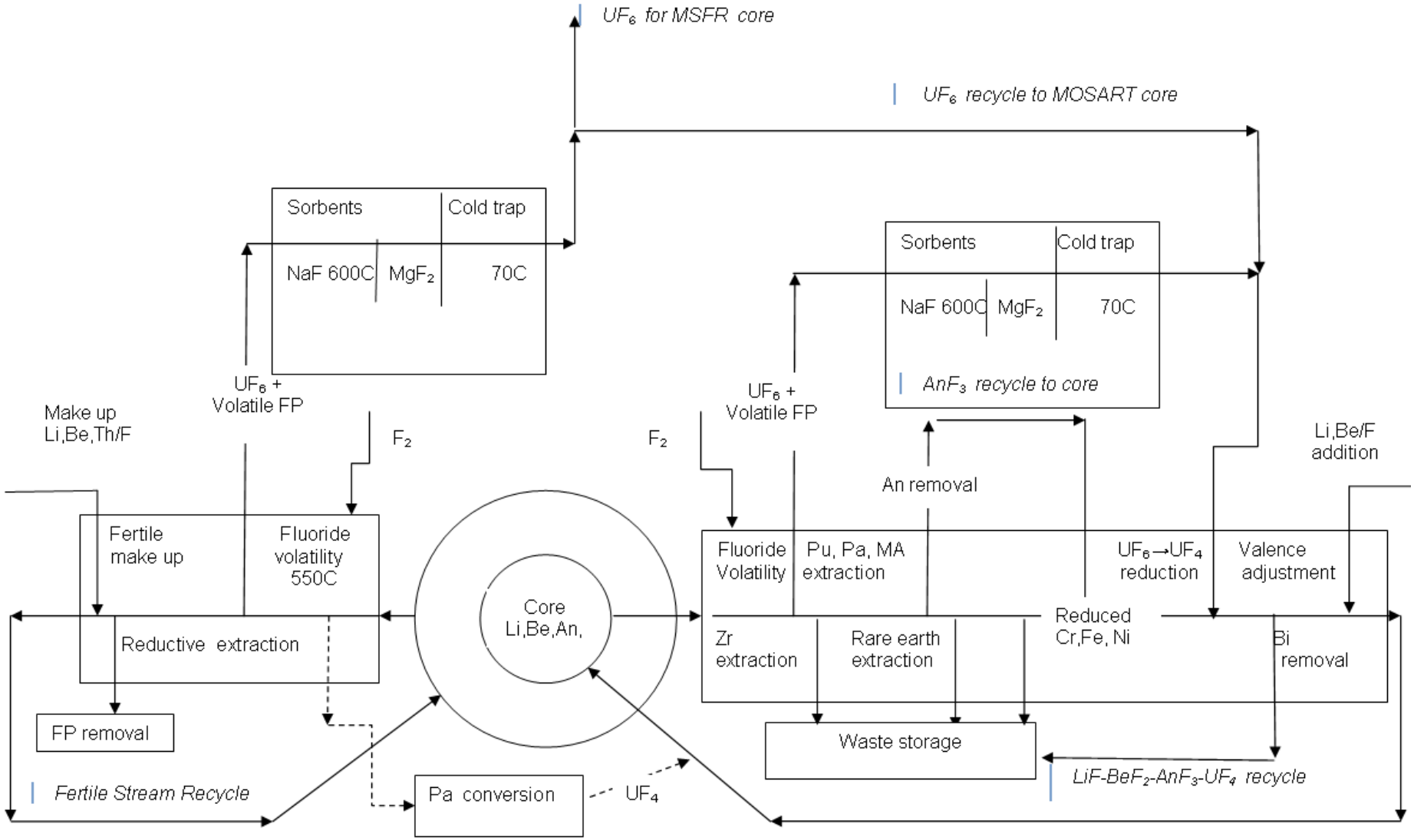

Figure 2: Fertile and fissile hybrid MOSART flowsheet

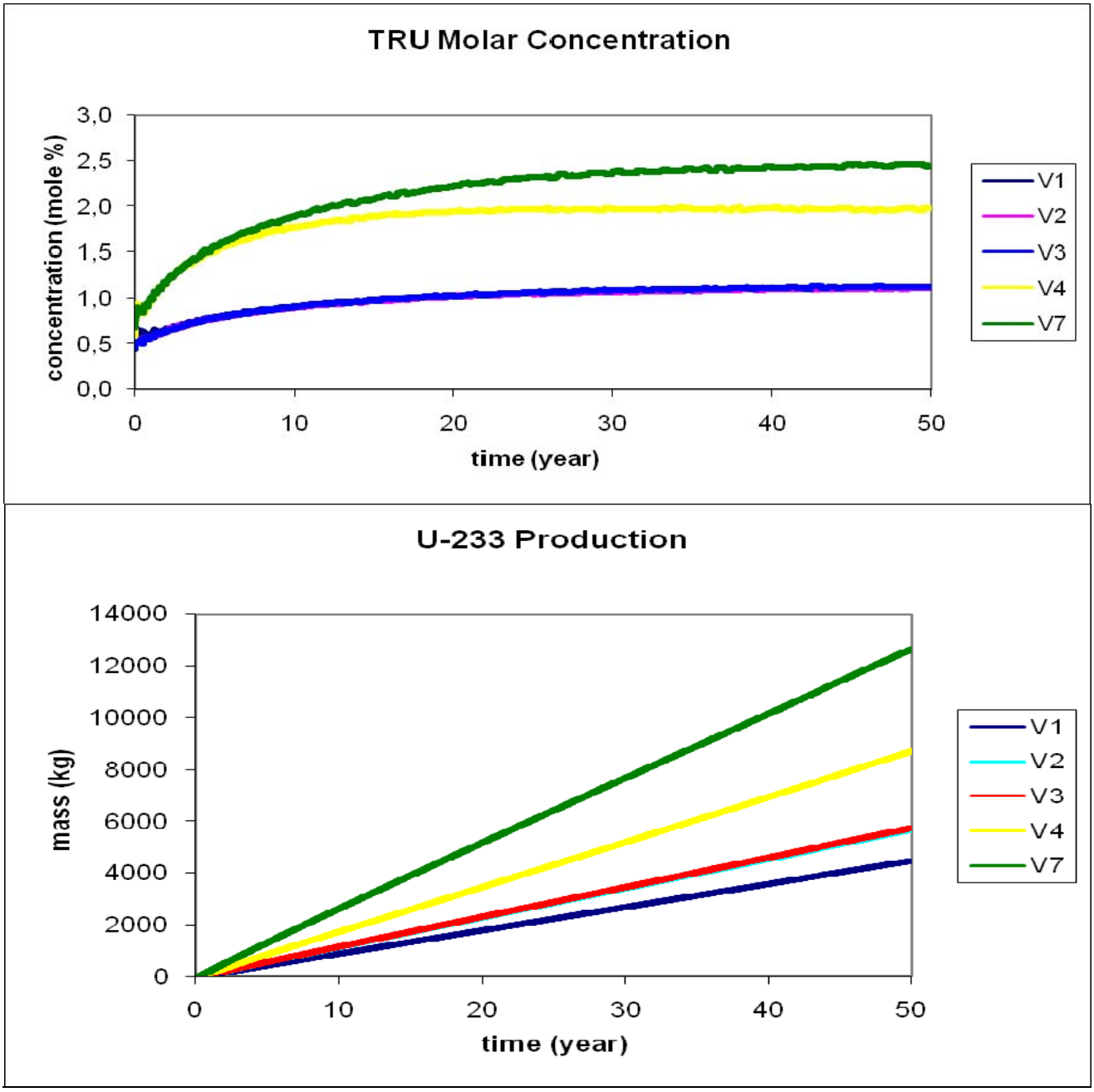

Figure 3: Critical concentrations of TRUs in Li,Na,Be/F (a) salt and rates of ^{233}U production in the blanket (b) vs. time for the cores with different configurations: V1,V2,V3 - cores of reference MOSART size, V4 – core of reduced size, V7- ring core.

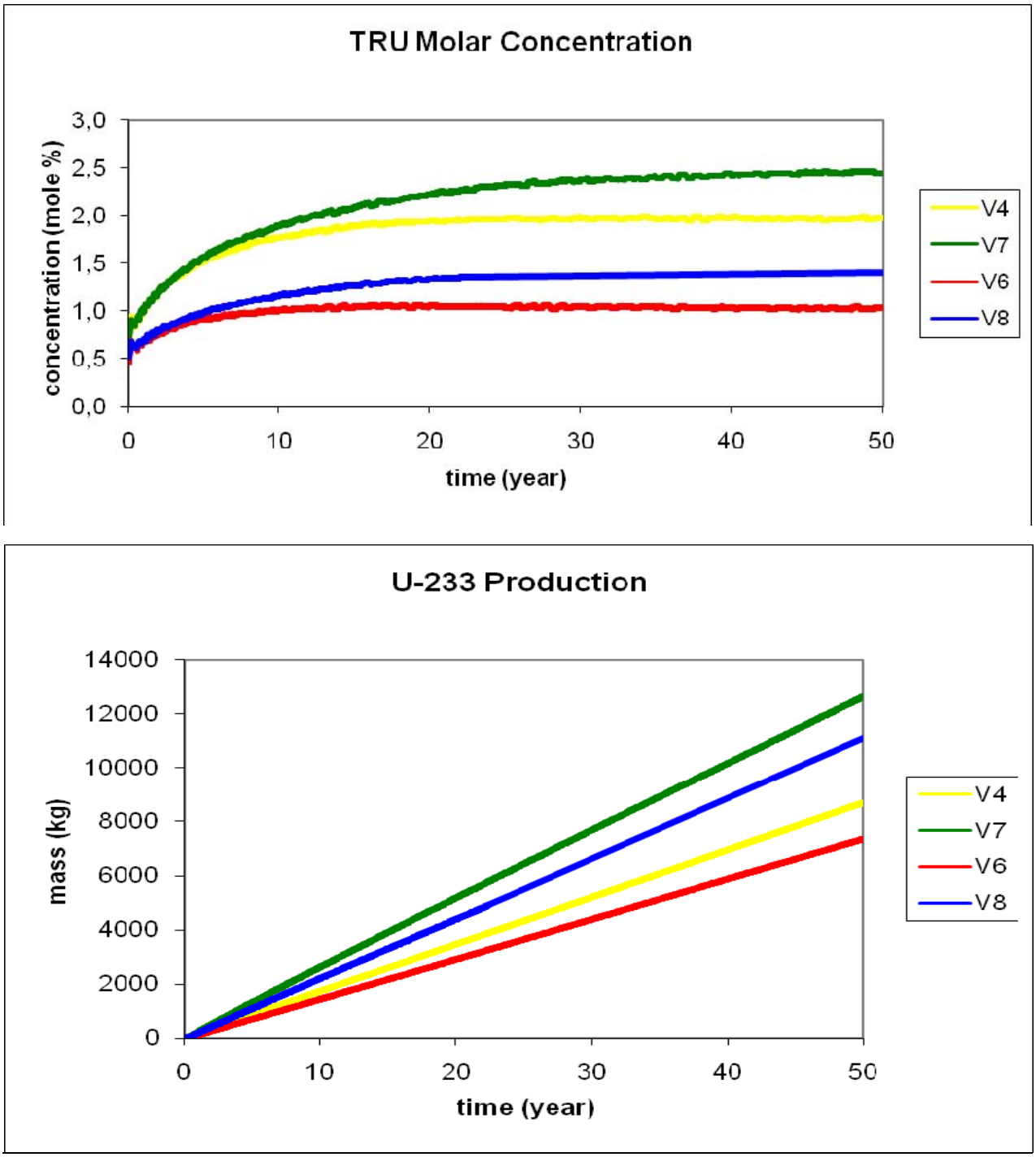

Figure 4: Critical concentrations of TRUs (a) in fuel salt and rates of ^{233}U production in the blanket (b) vs. time for the cores with different salt solvent : V4,V6 –cylindrical zones with fuel salt based on Li,Na,Be/F and 73LiF-27BeF_2 correspondingly; V7,V8 – ring cores with fuel salt based on Li,Na,Be/F and 73LiF-27BeF_2 correspondingly;

Table 2: Characteristics of two-fluid hybrid MOSART systems

Variant	V1	V 2	V 3	V4	V5	V6	V 7	V 8	V 9
Radius / height of the core, m	1.7/3.6	1.7/3.6	1.7/3.6	1.2/2.4	1.0/2.0	1.2/2.4	0.5/1.6/3.2	0.5/1.6/3.2	0.7/1.6/3.2
Width (radius) of the blanket, m	0.2	0.6					0.6 (0.5/0.7 radius of the blanket centre)		
Fuel salt, mole %	17LiF-58NaF-25BeF_2					73LiF-27BeF_2	17LiF-58NaF-25BeF_2	73LiF-27BeF_2	
Blanket salt, mole%	75LiF-5BeF_2-20ThF_4		67LiF-5BeF_2-28ThF_4	75LiF-5BeF_2-20ThF_4					
Fuel salt volume, м^3	56.2			20	17	20	32.2		32.2
Fuel salt specific power, W/cm^3	73.6			221	382	221	103.4		115.4
TRU concentration at EOL, mol.%	1.1			2.1	2.56	1.1	2.5	1.4	2.1
TRU loading at BOL, t	3.02	3.17		1.41	1.32	1.55	2.57	2.73	2.88
TRU loading at EOL, t	7.70	7.71	7.76	4.88	4.91	3.53	9.44	6.80	9.91
^{233}U production,kg/yr	90	113	115	180	200	150	254	241	286

CONCLUSION

- A study was made to examine the conceptual feasibility of hybrid two-fluid MOSART system. New fast-spectrum design options and salt compositions with high enough solubility for actinide trifluorides are being examined because of new goals. Experimental data base created within the ISTC#1606 and #3749 projects was used for development of hybrid MOSART technology as applied to consumption of transuranic elements and ^{233}U production while extracting their energy.
- The two-fluid hybrid MOSART is non-moderated system, with a LiF-(NaF)-BeF_2-$TRUF_3$-(UF_4) fuel salt and a LiF-ThF_4-(BeF_2) blanket salt circulated through two separate flow circuits. The starting fuel can be TRU of different composition from PWR spent fuel (UOX, MOX and minor actinide bearing fuels), and "'fresh" TRU is added as needed to compensate for burn-up and build up of fission poisons. There are two main scenarios for new fuel utilization: when all ^{233}U available from blanket is returned to (1) MSFR vendor or to (2) MOSART core.
- In both scenarios variants with ring geometry with molten 73LiF-27BeF_2 cores afford better capabilities for the lower critical inventories, higher rates of new fuel production and choice of fuel salt specific power compared to LiF-NaF-BeF_2 cores.
- From the point of view of system structure symbiosis MFSR + hybrid MOSART can have advantage, since allows us to use in a greater degree already available technology at temperatures to 700 – 750^{0}C. For accumulation of necessary loading for MSFR (5200 kg) 18-20 years of hybrid MOSART system operation is needed. Symbiosis MFSR + hybrid MOSART reflect main advantage of MSRs which concern fuel cycle flexibility.
- As for scenario 2 not only TRU's from UOX and MOX PWR spent fuel can be used to feed the hybrid MOSART core but also minor actinide bearing fuels. These possibilities will be discussed in details in later works.

References

1. Forsberg CW et al. (2007) Liquid salt applications and molten salt reactors. *Revue Generale Nucleaire*, 4: 63-71
2. Haubenreich PN and Engel JR (1970) Experience with the molten-salt reactor experiment. *Nuclear Applications and Technology* 8 (2): 107-140
3. Bettis ES et al. (1970) The design and performance feature of a single fluid molten salt reactor. *Nuclear Applications and Technology* 8 (2): 190
4. Robertson RC et al. (1970) Two-fluid molten-salt breeder reactor design study*, Report ORNL 4528,* Oak Ridge, USA, 80p
5. Novikov VM Ignatiev VV Fedulov VI and Cherednikov VN (1990) *Molten Salt Reactors: Perspectives and Problems.* Moscow, USSR: Energoatomizdat
6. Ignatiev V et al. (2005) Characteristics of molten salt actinide recycler and transmuter system. In: *Proceedings of International Conference on Emerging Nuclear Energy Systems. Brussels, Belgium, 21-26 August:* paper ICQ064
7. ISTC # 1606 project final report (2007), International scientific and technical centre, Moscow, July
8. Renault C et al. (2009) European molten salt reactor. In: *Proceedings of Seventh European Commission Conference on Euroatom Research and Training in Reactor Systems. Prague, Czech Republic, 22 - 24 June*
9. Delpech S et al. (2009) Reactor physics and reprocessing scheme for innovative molten salt reactor system. *Journal of Fluorine Chemistry* 130 (1): 11-17
10. Merle-Lucotte E et al. (2009) Optimizing the Burning Efficiency and the Deployment Capacities of the Molten Salt Fast Reactor, In: *Proceedings of Global 2009. Paris, France, 6-11 September: 1865-1872*
11. Fredricksen JA, Gilpatrick LO, Barton CJ. (1969) Solubility of cerium trifluoride in molten mixtures of LiF, BeF_2 and ThF_4, *Report ORNL-TM-2335,* Oak Ridge, USA, 23p
12. Vaidya VN et al. (1973) Molten salt chemistry. Part IV, Solubility behavior of PuF3 in fluoride salts of interest in molten salt reactor technology, *Report BARC-676, Bombay, India*
13. Ignatiev V, Feynberg O (2009) MOlten Salt Actinide Recycler & Transmuter System: Fuel Cycle and Safety Related Issues, In*: Proceedings of ICENES 2009, Ericeira, Portugal, 29 June -02 July*

Electrochemical Reduction of solid UO_2 in Molten Fluoride Salts

Mathieu Gibilaro[1,2], Laurent Cassayre[1], Laurent Massot[1], Pierre Chamelot[1], Rikard Malmbeck[2], Olivier Dugne[3], Patrick Allegri[3]

[1] *Laboratoire de Génie Chimique UMR 5503, Département Procédés Electrochimiques, Université de Toulouse, 31062 Toulouse Cedex, France*

[2] *Institute for Transuranium Element, P.O. Box 2340, 76125 Karlsruhe, Germany*

[3] *CEA Marcoule- DEN/DTEC/SGCS, Laboratoire de Métallographie et d'Analyse Chimique, BP17171, 30207 Bagnols Sur Ceze Cedex*

Corresponding Author: cassayre@chimie.ups-tlse.fr Tel: +33 561557468 Fax: +33 561556139

Abstract – *The direct electrochemical reduction of UO_2 solid pellets was carried out in LiF-CaF_2 (+ 2wt % Li_2O) at 850°C. An inert gold anode was used instead of the usual reactive sacrificial carbon anode. In this case, reduction of oxide ions yields O_2 gas evolution on the anode. Electrochemical characterisations of UO_2 pellets have been performed by linear sweep voltammetry at 10 mV/s and reduction waves associated to its direct reduction have been observed at a potential 150mV more positive in comparison with the solvent reduction. Then, galvanostatic electrolyses runs have been realised and products were characterised by SEM-EDX, EPMA/WDS and XRD. In one of the runs, uranium oxide was partially reduced and three phases were observed: non reduced UO_2 in the centre, pure metallic uranium on the external layer and an intermediate phase representing the initial stage of reduction taking place at the grain boundaries. In another run, the UO_2 sample was fully reduced. Due to oxygen removal, the U matrix had a typical coral-like structure which is characteristic of the pattern observed after the electroreduction of solid oxides.*

A. INTRODUCTION

Advanced nuclear fuel cycles are under development worldwide in order to minimise the amount of high radiotoxic waste generated by operation of the nuclear power plants. The new technologies have to be economically competitive, environmentally safe and resistant to proliferation. Within most of the developed future fuel cycles, recycling of actinides (Cm, Pu, Am, Np) from spent nuclear fuel is required due to their significant impact on its radiotoxicity. Pyrochemical methods represent one of the promising options to fulfil this task. In the pyrometallurgical process being developed in the Institute for Transuranium elements [1], all actinides are group-selectively recovered in a form of actinide-aluminium (An-Al) alloys by an electrorefining process in molten LiCl-KCl using solid aluminium cathodes. The remaining actinides from the used melts are recovered by an exhaustive electrolysis; also as An-Al alloys. The back extraction of actinides from the alloys is provided by a three-step chlorination route: The salt remaining on the electrode is distilled, the pure alloys are chlorinated by chlorine gas or HCl and the formed $AlCl_3$ is sublimated yielding pure actinide chlorides.

However, oxide fuels are not suited for the electrorefining process, since these metallic oxides are mostly insoluble in molten salts. Therefore, a preliminary step is required to convert oxides into metal which can be afterwards easily dissolved in molten salts by anodic dissolution.

The lithium reduction process has been developed for the pyrochemical recycling of oxide fuels using lithium metal as a reductant to convert actinide oxides into metal. Usami *et al.* [2] successfully applied this technique to AmO_2 in LiCl at 650°C for Li_2O concentration lower than 5.1 wt%: more than 99.9% of Am has been recovered into solid Am phase. This technology was also employed for UO_2 and PuO_2 with 3% of Am at 650°C [3] leaving particles of UO_2 totally reduced. For Pu sample, small

amounts of Pu and Am were detected in the salts. Moreover, AmO_2 reduction was only efficient for low Li_2O concentration (<1.8wt %). Thus an additional step is needed to control and decrease Li_2O concentration as it accumulates in the salt during the process.

To avoid these problems, a more efficient process has been elaborated: the direct electrochemical reduction. This pyroprocess has been developed by Chen et al. [4], who first demonstrated the direct electroreduction of TiO_2 into Ti at 950°C in molten $CaCl_2$. This innovative method is called the FFC Cambridge process (Fray-Farthing-Chen). The overall reaction is the electroreduction of a solid oxide MO_2 into metal M at the cathode (Eq. 1) and the evolution of CO and CO_2 at the anode (Eq. 2-3); the oxide ions released from the cathode are transported through the support electrolyte and oxidised at a carbon anode:

$$MO_2 + 4e^- = M + 2O^{2-}(salt) \qquad (1)$$

$$O^{2-}(salt) + C(s) = CO(g) + 2e^- \qquad (2)$$

$$2O^{2-}(salt) + C(s) = CO_2(g) + 4e^- \qquad (3)$$

As O^{2-} ions produced at the cathode are simultaneously consumed at the anode, the oxide ions concentration remains constant in the molten salt, preventing accumulation during the experiment. Moreover, the troublesome handling of Li metal is also avoided.

On top of multiple applications to the preparation of various metals (Ti [5], Nb [6], Si [7]…), the FFC process is also studied in the framework of nuclear spent fuel reprocessing. The electroreduction of UO_2 and MOX (UO_2-PuO_2) have been studied in LiCl or $CaCl_2$ [8-10].

During the metallic oxide reduction in $CaCl_2$ at 850°C, the uranium metal cohered due to the high operating temperature and formed a dense layer on the sample surface. This prevents the external diffusion of oxygen ions to the salt, and stops the reduction process of UO_2. In LiCl baths at lower temperature (650°C), no dense metallic skin was observed on the surface and both UO_2 and MOX samples were reduced in their centre.

One of the major troubles with the FFC process is the use of a reactive carbon anode where CO_2 gas is released. The final product often contains carbides, due to the reduction of carbonates CO_3^{2-}, formed by the reaction of the CO_2(g) with O^{2-} dissolved in the salt [11].

In this work, a different category of electrolyte was tested, i.e. the molten fluorides, with the advantage of using an inert gold anode on which oxygen ions are oxidised into O_2 [12]:

$$2O^{2-} = O_2(g) + 4e^- \qquad (4)$$

This anodic reaction, which is difficult to control in chloride salts due to the close potentials of Cl_2 and O_2 evolution, should avoid the carbides formation at the cathode.

The first part of the work was focused on the electrochemical characterisation of the UO_2 samples in fluoride salts by linear sweep voltammetry. Galvanostatic electrolyses have been performed on small amounts of oxides (~200-300 mg) and the reaction products have been characterised by SEM-EDX, EPMA/WDS and XRD.

B. EXPERIMENTAL

The cell used consisted of a vitreous carbon crucible placed in a cylindrical vessel made of refractory steel. The inner part of the walls was protected against fluoride vapors by a graphite liner. Experiments were performed under an inert argon (U grade) atmosphere. More details can be found in a previous paper [13].

The electrolyte (200g) consisted of the eutectic LiF-CaF_2 (SDS 99.99%) dehydrated by heating under a vacuum (3.10^{-2} bar) from room temperature up to the melting point for 72 h. Lithium oxide (Li_2O) powder (Cerac 99.5%) was used to provide oxide ions into the bath.

UO_2 was used in the form of sintered pellets (95%). The oxide pellets, attached with a molybdenum mesh and connected to the current lead by a molybdenum wire, were used as working electrodes. The auxiliary electrode was a gold wire with a large surface area (S=3.6cm²) and all potentials were referred to a platinum wire (0.5mm diameter), acting as a quasi-reference electrode $Pt/PtO_x/O^{2-}$ [14]. Although this electrode is sensitive to oxide concentration in the bath, its potential remains stable for high oxide concentration (>1wt %).

The electrochemical experiments were performed with an Autolab PGSTAT 30 potentiostat/galvanostat. After resin embedding and polishing, the cathode bulk was examined with a Scanning Electron Microscope (ZEISS Supra55) equipped with an EDX probe (Oxford SDD X-Max), X-Ray Diffraction (Bruker D8) and Electron Probe Micro Analysis combined with Wavelength Dispersive Spectrometer (CAMECA SX 100).

C. RESULTS AND DISCUSSION

C.1. Solvent selection

In order to perform the direct reduction of the uranium oxide, the solvent selection is primordial: the uranium formation has to occur at a potential more positive than that of the alkaline deposition. The Gibbs energy of the reaction ($\Delta_r G°$) between the metallic oxide UO_2 and the alkaline metal (Ca, Na or Li), according to Eq. (5), provides a good indication on the reduction potential of the oxide:

$$UO_2 + Alkaline(=Ca, Li, Na) = U + Alkaline\ oxide \qquad (5)$$

If $\Delta_r G°$ is negative, the reduction of the oxide occurs at a potential more positive than the solvent alkaline deposition and the direct reduction is then achievable from a thermodynamical point of view. Calculations have been performed with the data compiled in the HSC Chemistry 5.11 software [15]. According to these thermochemical considerations, the direct electroreduction of UO_2 has been investigated in the eutectic LiF-CaF_2 at 850°C. Oxide ions were introduced in the bath using Li_2O additions at a concentration of 2wt %, which is lower than its solubility limit in LiF-CaF_2 [16].

C.2. Influence of oxide ions

Cathode reactions

Figure 1 presents linear sweep voltammetries at 10mV/s on a Mo wire and on a mesh performed in LiF-CaF_2 with and without oxide ions.

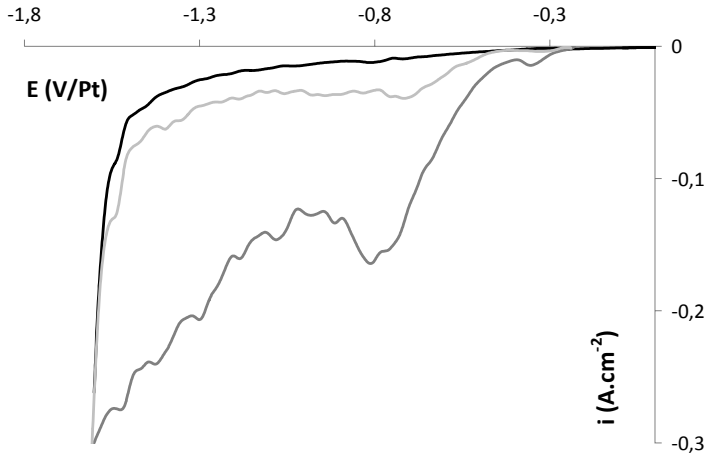

Figure 1: Linear sweep voltammetries on Mo in LiF- CaF_2 at 10mV/s; black: without oxide, light grey: with oxides on Mo wire, dark grey: with oxides on Mo mesh.

In the linear voltammograms plotted in the pure fluoride salt on Mo without Li_2O addition, no reduction current is observed between 0 and -1.5V/Pt, and the metallic lithium deposition occurs at -1.6V/Pt. With Li_2O presence in the solvent, a new cathodic current is observed on Mo electrode at around -0.8V/Pt and is proportional to its immersed surface: the recorded current increases with an increase of Mo surface. We can assume that an oxide layer is spontaneously formed when Mo and oxide ions are both present in the molten salt. According to the Mo-O phase diagram [17], only MoO_2 exists at 850°C. To remove it, linear sweep voltammetries in the reductive sense are performed until the complete disappearance of the cathodic current most probably corresponding to Eq. (6):

$$MoO_2 + 4e^- = Mo + 2O^{2-} \quad (6)$$

Anode reactions

The expected anodic reactions on a gold electrode in fluoride media in the presence of oxide ions are either the anodic dissolution of gold or the oxygen gas formation. To avoid the consumption of the Au electrode, the Li_2O quantity in the melt has to be controlled. Linear sweep voltammetries plotted on Au at 10mV/s for two different concentrations of oxide ions are presented in Figure 2.

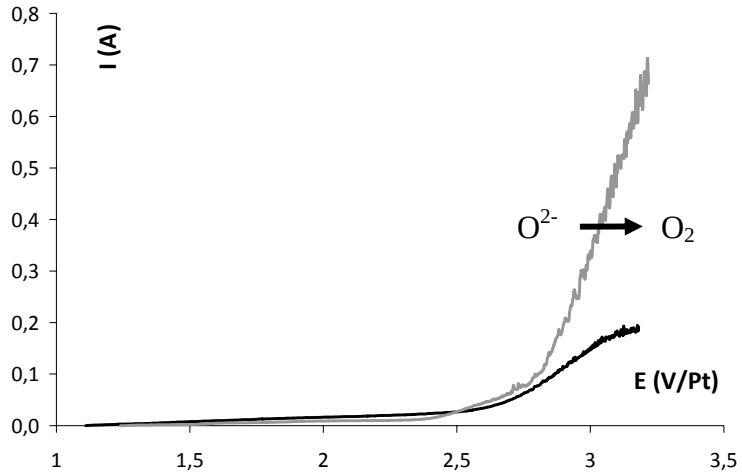

Figure 2: Linear sweep voltammetries on Au electrode in LiF-CaF_2 at 10mV/s at 850°C; the black curve is plotted for 0.5wt % Li_2O and the grey curve for 2wt % Li_2O.

At low concentration (0.5wt % Li_2O), a diffusion plateau of O^{2-} ions is observed at around 2.8V/Pt with an intensity of 150mA and for a potential higher than 3V, the Au electrode is oxidised. An increase of oxide ions concentration (2wt % Li_2O) avoids the anodic dissolution of Au. Thus, from those results, attention was paid to work in LiF-CaF_2 with 2wt % Li_2O.

C.3. Electrochemical reduction of uranium oxide pellets

Electrochemical characterisation by linear sweep voltammetry

Figure 3 shows the linear voltammetries obtained at 10mV/s on UO_2 sample, previously cleaned from the molybdenum oxide layer.

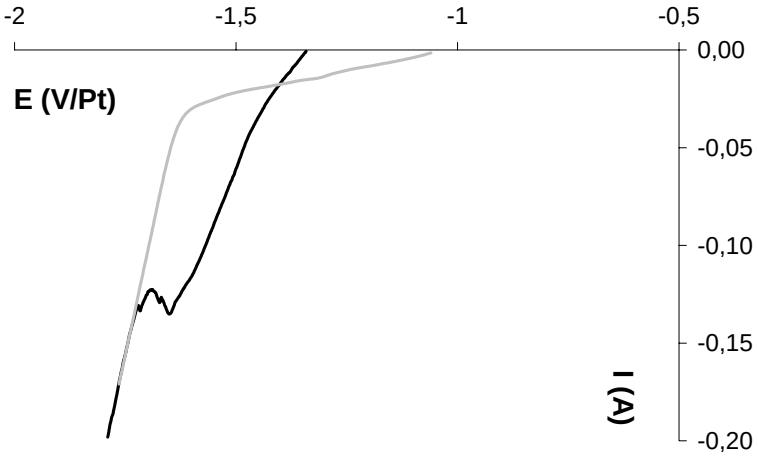

Figure 3: Linear voltammetries in LiF-CaF_2-Li_2O (2wt %) at 10mV/s and 850°C; the black curve is plotted on UO_2 sample after removal of the Mo oxide and the grey curve is the solvent reduction.

An additional reduction current peak is clearly observed before the solvent deposition at around -1.45V/Pt and is attributed to the direct electrochemical reduction of UO_2 in fluoride salts, confirming the previous thermodynamic analysis. It can be noticed that the oxide layer after its removal did not perturb the electrochemical signal.

Galvanostatic electrolysis of uranium oxide

Direct electrochemical reduction runs have been conducted in galvanostatic mode as the potentiostatic mode was not found to be adapted to this. Indeed, during the electrolyses, the oxides were gradually reduced into metal, leading to a noticeable modification of their electronic conductivity and thus of the ohmic drop in the circuit.
Five reduction tests were carried out in LiF-CaF_2 containing 2wt % Li_2O at 850°C; the applied cathodic current was increased between each test. The results concerning the two most interesting runs are presented in this section. The first noticeable UO_2 reduction experiment was performed at -150mA during 8000s, corresponding to 200% of the coulombs theoretically calculated from the oxide pellet weight. The cross section is observed by SEM and is presented in Figure 4.

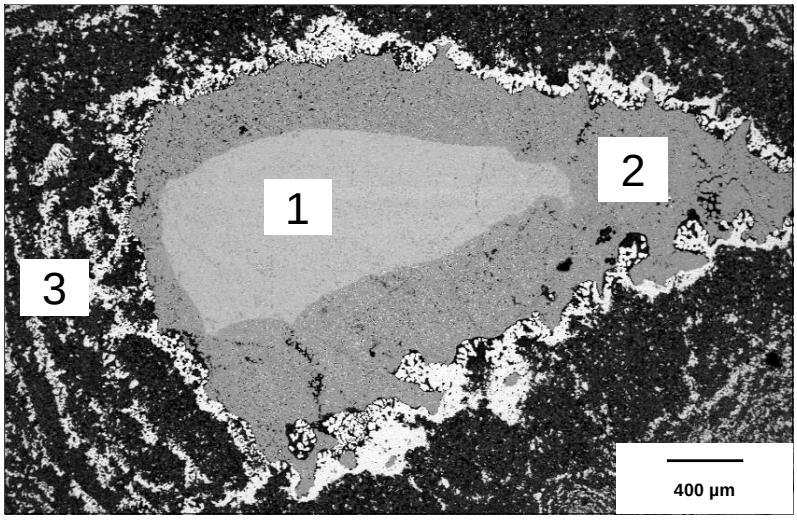

Figure 4: SEM observation of UO_2 pellet cross section after electrolysis (test 1) at 850°C in LiF-CaF_2-Li_2O (2wt %).

Three different zones are present. The internal zone (1) corresponds to the remaining part of UO_2, meaning that the sample was not fully reduced. A focus of zones 2 and 3 is shown in Figure 5.

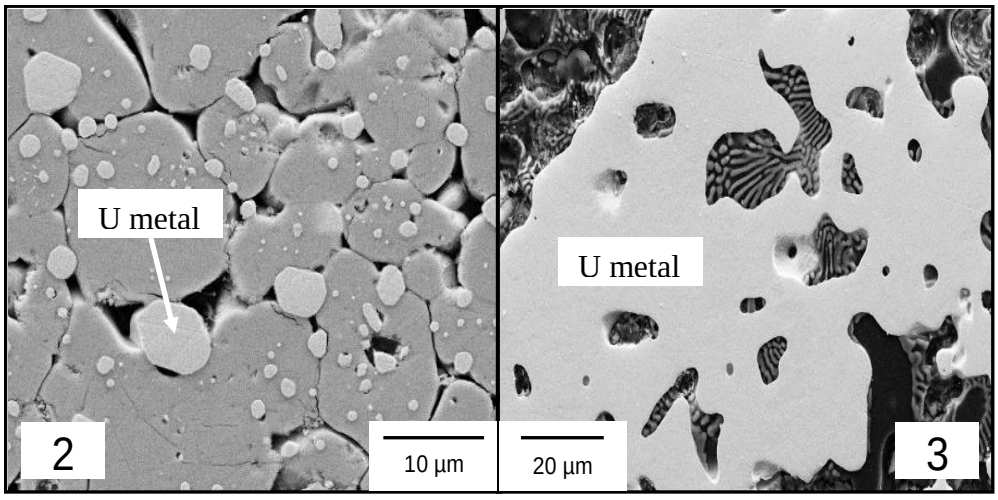

Figure 5: Focus on zones 2 and 3 observed by SEM of UO_2 pellet after electrolysis (test 1) at 850°C in LiF-CaF_2-Li_2O (2wt %).

Compared with the initial material, the intermediate zone (2) surface was cracked. At the grain boundaries, fluoride salts are detected by EDX-SEM; shiny particles are also observed and were analysed with EPMA-WDS: they are composed of uranium metal. Thus, the initial stage of reduction is observed at the grain boundary in this partially reduced region with uranium metallic grains. Kurata *et al.* [8] have already observed this phenomenon: the grain boundary is reduced prior to the bulk due to a better diffusion rate along itself.
The external layer of the pellet (3) is composed of uranium metal (EDX analysis) and has a typical coral-like structure due to oxygen removal. These observations showed that the direct reduction took place progressively in the pellet starting from the outside.
So, the metallic oxide gets reduced first at the grain boundaries into U metal. As metal is being produced, it extends the point of contact to further oxide grains, which can be successively reduced. This test demonstrated that metallic uranium was obtained with uranium oxide as starting material.

Another run realised with a higher current (I=-0,3A during 7200s) allowed to prove that the full reduction of UO_2 was achievable in fluoride salts. The polished cross section is presented in Figure 6.

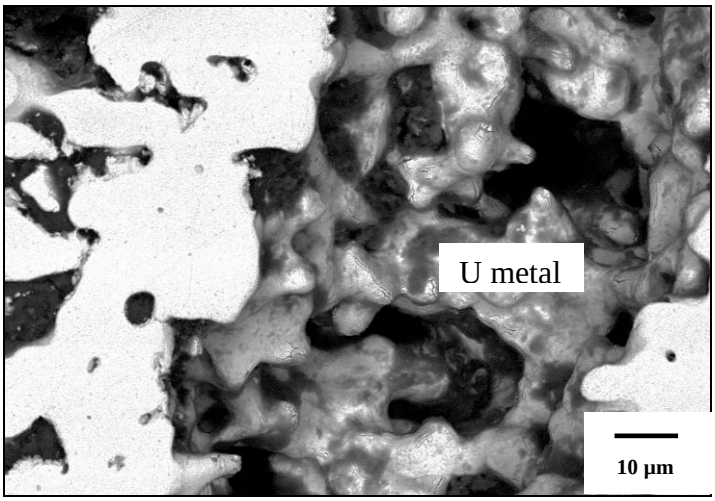

Figure 6: SEM observation of UO_2 pellet cross section after electrolysis (test 2) at 850°C in LiF-CaF_2-Li_2O (2wt %).

On the left part of the picture, the product after electrolysis has a very porous surface, specific of the direct electrochemical reduction, suggesting that the pellet was completely reduced. On the right part, we can see the 3D structure due to salts dissolution: uranium metal forms a continuous network where gaps are formed by oxygen removal and uranium rearrangement.

XRD analysis revealed the presence of the following phases: uranium metal, uranium dioxide, uranium oxide hydrate, lithium fluoride, calcium fluoride and calcium oxide. Lithium and calcium compounds come from the solvent and uranium oxide was most probably formed by the spontaneous oxidation of uranium metal due to air exposure [18]. It can be noticed that no carbides or mixed U-Ca-Li-F compounds were detected in the sample.

However, the experimental charge is seven times higher than the required theoretical one. The electrode potential versus time during the galvanostatic electrolysis is plotted in Figure 7.

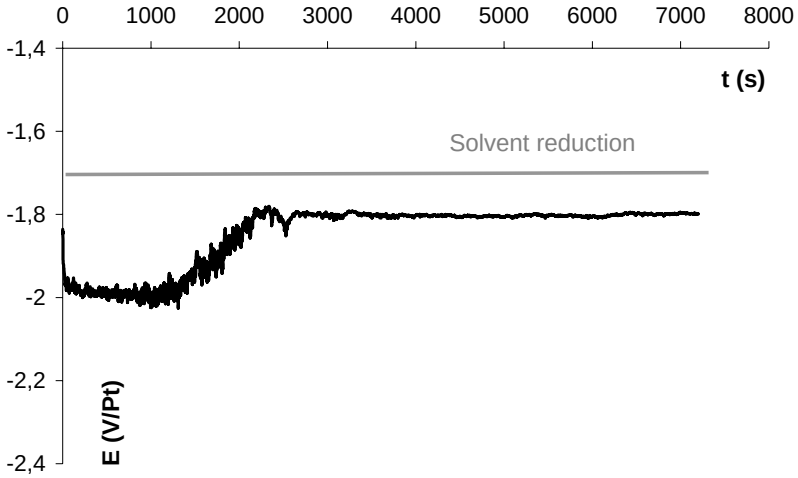

Figure 7: UO_2 pellet potential during galvanostatic electrolysis versus time at 850°C in LiF-CaF_2-Li_2O: I=-0,3A and t=7200s.

Comparing the solvent reduction potential and the electrode potential during the electrochemical reduction, it appears that Li metal was formed during the entire process. Combined to the direct electrochemical reduction, the indirect reduction of UO_2 by metallic Li took place:

$$UO_2 + 4Li = U + 2Li_2O \qquad (7)$$

A significant amount of the intensity is then used for Li deposition and yields to a very low current efficiency. To avoid the solvent reduction, the current should be stepwise decreased during the experiment when the potential reaches the Li^+/Li reduction potential.

D. CONCLUSIONS

For the first time, fluoride salts have been tested in this work instead of the usual chloride molten salts ($CaCl_2$ and LiCl) in order to evaluate their potentialities as electrolytes for the direct electrochemical reduction of UO_2. An inert oxygen-evolving gold electrode was used as an anode, instead of the commonly used carbon anode which produces CO_2 and leads to the formation of carbides in the reduced cathodic product. A complete conversion into metal was achieved at 850°C without formation of a dense metallic layer and XRD analysis did not reveal the presence of any carbide phase. Moreover, partially reduced sample indicates the presence of metallic uranium at the grain boundary, showing that the reduction process took place progressively in the pellet starting from the outside. These important results call for more investigations on the use of fluoride mixtures as electrolytes for the direct reduction process.

Acknowledgements

This work was supported by the European ACSEPT (FP7-CP-2007-211 267) program.

References

1. P. SOUCEK, R. Malmbeck, E. Mendes, C. Nourry, J.P. Glatz “Recovery of Actinides from Spent Nuclear Fuel by Pyrochemical Reprocessing”, *Proceedings of Global 2009,* Paris, France (2009)
2. T. USAMI, T. Kato, M. Kurata, T. Inoue, H.E. Sims, S.A. Beetham, J.A. Jenkins, “Lithium reduction of americium dioxide to generate americium metal”, *Journal of Nuclear Materials*, 304, 50-55 (2002)
3. T. USAMI, M. Kurata, T. Inoue, H.E. Sims, S.A. Beetham, J.A. Jenkins, “Pyrochemical reduction of uranium dioxide and plutonium dioxide by lithium metal”, *Journal of Nuclear Materials*, 300, 15–26 (2002)

4. G. Z. CHEN, D.J. Fray, T.W. Farthing, “Direct electrochemical reduction of titanium dioxide to titanium in molten calcium chloride”, *Nature*, 407, 361-364 (2000)
5. C. SCHWANDT, D.J. Fray, “Determination of the kinetic pathway in the electrochemical reduction of titanium dioxide in molten calcium chloride”, *Electrochimica Acta*, 51, 66–76 (2005)
6. T. H. OKABE, I. Park, K.T. Jacob, Y. Waseda, “Production of niobium powder by electronically mediated reaction (EMR) using calcium as a reductant”, *Journal of Alloys and Compounds*, 288, *1-2*, 200-210 (1999)
7. K. YASUDA., T. Nohira, R. Hagiwara, Y.H. Ogata, “Direct electrolytic reduction of solid SiO_2 in molten $CaCl_2$ for the production of solar grade silicon”, *Electrochimica Acta*, 53, 106–110 (2007)
8. M. KURATA, T. Inoue, J. Serp, M. Ougier, J.P. Glatz, “Electro-chemical reduction of MOX in LiCl. *Journal of Nuclear Materials*”, 328, 97-102 (2004)
9. M. IZUKA, Y. Sakamura, T. Inoue, “Electrochemical reduction of (U-40, Pu-5, Np)O_2 in molten LiCl electrolyte”, *Journal of Nuclear Materials*, 359, 102-113 (2006)
10. M. IZUKA, T. Inoue, M. Ougier, J.P. Glatz, “Electrochemical reduction of (U, Pu)O_2 in molten LiCl and $CaCl_2$ electrolytes”, *Journal of Nuclear Science and Technology*, 44, *5*, 801-813 (2007)
11. Y. SAKAMURA, M. Kurata, T. Inoue, “Electrochemical reduction of UO_2 in molten $CaCl_2$ or LiCl”, *Journal of the Electrochemical Society*, 153, *3*, D31-D39 (2006)
12. L. MASSOT, L. Cassayre, P. Chamelot, P. Taxil, “On the use of electrochemical techniques to monitor free oxide content in molten fluoride media”, *Journal of Electroanalytical Chemistry*, 606, *17*, 17-23 (2007)
13. P. CHAMELOT, P. Taxil, B. Lafage, “Voltammetric studies of tantalum electrodeposition baths”, *Electrochimica Acta*, 39, 2571-2575 (1994)
14. A. D. GRAVES, D. Inman, “Adsorption and the differential capacitance of the electrical double layer at platinum/halide metal interfaces”, *Nature*, 208, 481-482 (1965)
15. HSC Chemistry 5.11, *Chemical reaction and equilibrium software with extensive thermochemical database*, Outokumpu, (2002)
16. R. G. REDDY, S.G. Kumar, “Solubility and thermodynamic properties of Li_2O in LiF-CaF_2 melts”, *Metallurgical and Materials Transitions B,* 24B, 1031-1035 (1993)
17. L.L.Y. CHANG, B. Phillips, “Phase relations in refractory metal- oxygen systems”, Journal *of the American Ceramic Society*, 53, 527-533 (1969)
18. O. BONINO, O. Dugne, C. Merlet, E. Gat, P. Holliger, M. Lahaye, “Study of surface modification of uranium and UFe_2 by various surface analysis techniques”, *Journal of Nuclear Materials*, 294, 305-314 (2001)

Conditioning of Minor Actinides in Monazite-type Ceramics

C. Babelot, S. Neumeier, A. Bukaemskiy, G. Modolo, H. Schlenz, D. Bosbach
Institut für Energieforschung, Sicherheitsforschung und Reaktortechnik (IEF-6),
Forschungszentrum Jülich GmbH, 52425 Jülich, Germany
Tel: +49 2461 61 2752, Fax: +49 2461 61 2450, e-mail: c.babelot@fz-juelich.de

Abstract *– Monazite-type ceramics are promising candidates for the conditioning of minor actinides. Monazite ($LaPO_4$) was prepared by hydrothermal synthesis and its hydrated form ($LaPO_4 \cdot 0.5H_2O$) was synthesised by co-precipitation. The first characterisation results, structural and morphological combined with thermal behaviour and physical properties, are presented.*

A. INTRODUCTION

Plutonium and the minor actinides (MA) neptunium, americium and curium are mainly responsible for the long-term radiotoxicity of the high active waste (HAW) generated during nuclear power operation. If these long-lived radionuclides are removed from the HAW by partitioning and converted by neutron fission (transmutation) into shorter-lived or stable elements, the remaining waste loses most of its long-term radiotoxicity. Thus, partitioning and transmutation (P&T) are considered as attractive options for reducing the burden on geological disposals. As an alternative, these separated MAs can also be conditioned (P&C strategy) in specifically adapted ceramics to ensure their safe final disposal over long periods of time.

At the moment, spent fuel elements are foreseen either for direct disposal in deep repositories, while the highly reactive liquid waste produced during reprocessing must be conditioned industrially using a vitrification process before final disposal. Although the widely used borosilicate glasses meet most of the specifications for a mixture of radionuclides comprising up to 40 elements, ceramic matrices appear to be even more suitable in terms of the solubility of certain radionuclides (e.g. separated americium) and resistance to leaching and radiation. The development of new materials based on tailor-made highly specific ceramics with extremely stable behaviour would make it possible to improve the final storage of long-lived high-level radiotoxic waste.
Because of the increasing need for the immobilization of large quantities of HLW, there is, however, a strong motivation to reconsider many of the alternative types of wasteform and to identify new candidate materials, such as alternative glass compositions, glass-ceramic materials, and ceramics.
These materials should be able to condition specific fission products or minor actinides after their partitioning. The research on crystalline ceramic waste forms as hosts for selected actinides (Am, Cm, Np and Pu) and mobile fission products (I, Cs), is done on different components: synroc, perovskite, zirconolite, zircon, zirconates, pyrochlore and monazite, among others ceramics [1; 2].

Owing to their good properties, e.g. irradiation resistance and chemical durability, monazite-type ceramics have been chosen in this study as promising host matrices for the conditioning of tri- and tetravalent actinides [3].
$REPO_4$ ceramics are named after their natural mineral analogue: monazite for *RE* = La to Gd (monoclinic structure) and xenotime for *RE* = Tb to Lu and Y (tetragonal structure).
To avoid radioactive dust formation, synthesis routes like conventional solid state reaction are not advisable. Thus wet chemical routes such as hydrothermal synthesis and precipitation were chosen within our recent research. Structural and morphological results applying XRD and SEM are presented here combined with thermal behaviour and physical properties.

B. MONAZITE AND RHABDOPHANE

Wet-chemical methods were applied in this work for the preparation of $LaPO_4$ and $LaPO_4 \cdot 0.5H_2O$. Monazite samples were prepared by hydrothermal synthesis. This fabrication process partly followed that described by Meyssamy [4]. Rhabdophane ($LaPO_4 \cdot 0.5H_2O$) powders were synthesised by

precipitation from lanthanum–citrate chelate solution (La–Cit) and phosphoric acid. This process was partially adapted from the route described by Boakye et al. [5].

After the synthesis, the thermal behaviour of the dried powders was investigated from room temperature up to 1000°C by thermogravimetry (TG) coupled with differential scanning calorimetry analysis (DSC) in air atmosphere with a heating rate of 10 K/min. Figure 1 shows the comparison of the TG-DSC measurements for monazite ($LaPO_4$) and rhabdophane ($LaPO_4{\cdot}0.5H_2O$, at pH=5 after washing). The mass loss of the monazite sample is about 4% while the one of the rhabdophane is about 10% after a thermal treatment up to 1000°C. This difference is partly caused by the residual crystal water contained in the rhabdophane structure.
For both powders a broad endothermic peak is observed between 100 and 200°C, which can be explained by the elimination of adsorbed gas and residual water. For the rhabdophane powder, an additional endothermic peak at ~270°C is observed which is linked to the elimination of the 0.5 mol of the crystal water.
The broad exothermic peak between 600 and 800°C belongs to the phase transformation from hexagonal to monoclinic (from rhabdophane to monazite) structure. Naturally, this peak does not appear on the monazite plot (magenta plot).

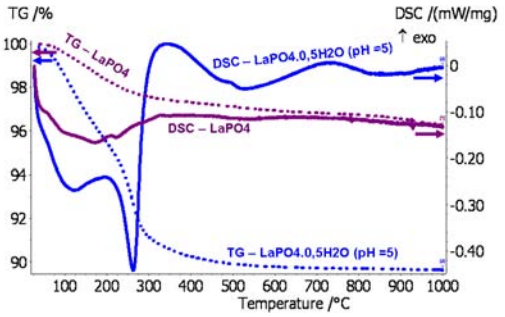

Figure 1 : TG-DSC measurements of monazite and rhabdophane (washed until pH=5) powders.

Figure 2 shows the X-ray diffraction patterns of the dried monazite (left) and rhabdophane (right) powders. The XRD result of the monazite ($LaPO_4$) sample confirms that the phase is pure. After calcination of the rhabdophane powder at 1000°C, XRD results show the similitude of the monazite (light blue) and the calcined rhabdophane (dark blue). The hexagonal to monoclinic phase transformation occurs. The FWHM (full width at half maximum) decreased for the 1000°C-calcined rhabdophane due to beginning of the material recrystallization. The diffractogram of rhabdophane powder also confirms the purity of this phase just after the precipitation.

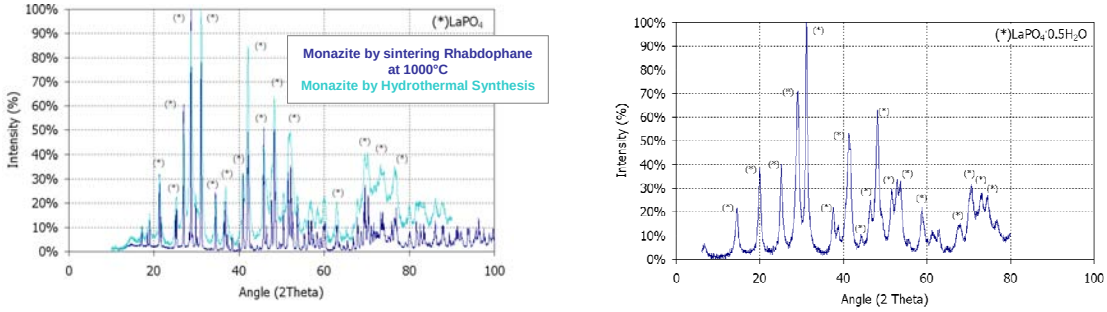

Figure 2: XRD patterns of monazite obtained after hydrothermal synthesis and by calcination of rhabdophane (left). XRD of rhabdophane for comparison (right).

The morphology of the powder was studied with scanning electron microscopy (SEM) as shown in Figure 3. The rhabdophane particles were round and their diameter sizes is between 0.1 and 2 µm.

The rhabdophane particles consolidate together during a heating process at 1000°C. This is the beginning of the sintering process. The comparison between the left and the right photo in Figure 3 shows significantly the beginning of the densification.

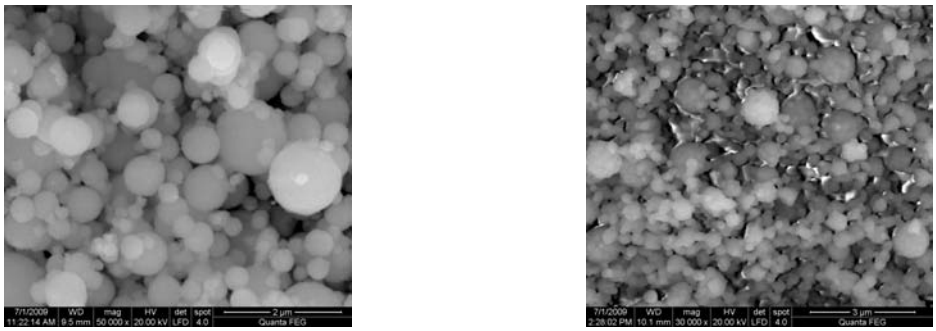

Figure 3: SEM images of $LaPO_4 \cdot 0.5H_2O$ sample (left) and of calcined (1000°C) $LaPO_4 \cdot 0.5H_2O$ sample (right).

The investigated powders were compacted by cold uniaxial pressing, applying pressures between 130 and 510 MPa. The pellets were made by powder synthesised by hydrothermal synthesis. The relative green density and the relative sintered density both depend on the applied pressure (see
Figure 4). The results of the relative green density in relation to the logarithm of the pressure show that the values form a linear function. This is typical behaviour for ceramic materials [6]. After the sintering at 1400°C, the relative sintered density of the pellets was determined by Archimedes method, i.e. by hydrostatic weighing in water (see Figure right). The value of the pressure related to the maximal density - optimal pressure - is between 250 and 400 MPa. The sintered density at this optimal pressure is above 98% of theoretical density.

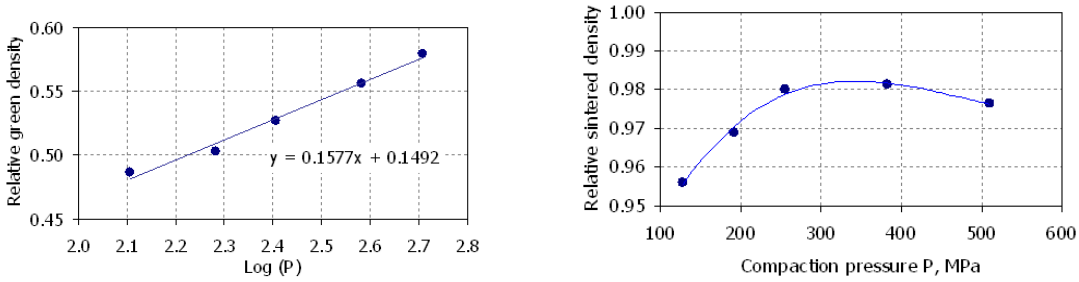

Figure 4: Compressibility curve for monazite powders (left) and relative sintered density of monazite pellets, as a function of compaction pressure (right).

C. CONCLUSION AND OUTLOOK

Monazite-type ceramics, as a promising candidate for the conditioning of minor actinides, were studied in this work. Monazite ($LaPO_4$) and Rhabdophane ($LaPO_4 \cdot 0.5H_2O$) powders were prepared by wet hydrothermal synthesis and by co-precipitation. The thermal analysis and XRD show that the monazite powders are already crystalline after synthesis and subsequent drying, whereas the Rhabdophane crystallizes at temperatures over 800°C to the monoclinic monazite structure. On the base of the synthesised monazite powder, pellets with a 98% of the theoretical density were prepared by cold pressing and sintering.
In order to simulate actinide integration into the lattice structure of the monazite-type matrix, lanthanide-doped monazite/xenotime matrices, $La_{(1-x)}Ln_xPO_4$ (Ln = Nd, Eu, Gd or Er, x = 0.10 to 1.00) have been synthesised, but have yet to be characterised. The full characterisation of the ceramic compounds is in progress and it is foreseen to study also the behaviour of immobilized actinides, such as americium and curium.
Primary focus of this work is the study of the thermodynamic properties of the solid matrices. Additionally the corrosion behaviour of synthetic ceramics will be investigated in detail on an atomic basis. To this end, the ceramics will be subjected to leach tests under conditions of relevance for final

repositories. The second essential parameter describing the stability of the host phases is the resistance to radiolysis. Radiation damage to the monazite type ceramics will be induced either by direct doping with radioactive nuclides or by means of ion bombardment.

Aknowledgements

This work is supported by the Ministerium für Innovation, Wissenschaft, Forschung und Technologie des Landes (MIWFT) Nordrhein-Westfalen; AZ: 323-005-0911-0129.

References

1. G. R. Lumpkin, "Ceramic waste forms for actinides," *Elements,* 2 *6* 365-72 (2006).

2. P. Trocellier, "Chemical durability of high level nuclear waste forms," *Annales De Chimie-Science Des Materiaux,* 26 *2* 113-30 (2001).

3. E. H. Oelkers and J. M. Montel, "Phosphates and nuclear waste storage," *Elements,* 4 *2* 113-16 (2008).

4. H. Meyssamy, K. Riwotzki, A. Kornowski, S. Naused, and M. Haase, "Wet-chemical synthesis of doped colloidal nanomaterials: Particles and fibers of $LaPO_4$: Eu, $LaPO_4$: Ce, and $LaPO_4$: Ce,Tb," *Advanced Materials,* 11 *10* 840 (1999).

5. E. E. Boakye, P. Mogilevsky, and R. S. Hay, "Synthesis of nanosized spherical rhabdophane particles," *Journal of the American Ceramic Society,* 88 *10* 2740-46 (2005).

6. A. A. Bukaemskiy, D. Barrier, and G. Modolo, "Compressibility and sinterability of CeO_2-8YSZ powders synthesized by a wet chemical method," *Journal of the European Ceramic Society,* 29 *10* 1947-54 (2009).

Actinide Sciences at ITN – Basic Studies in Chemistry with Potential Interest for Partitioning, Fuel Fabrication and More

M. Almeida[2], J.B. Branco[1], J.M. Carretas[1], A. Cruz[1], M. Dias[2], A.C. Ferreira[1], T.A. Gasche[1], A.P. Gonçalves[2], M.S. Henriques[2], J.P. Leal[1], E. B. Lopes[2], G. Lopes[1], C. Lourenço[1], J. Marçalo[1], L. Maria[1], B. Monteiro[1], E. Mora[1], I. Paiva[3], C.C.L. Pereira[1], L.C. J. Pereira[2], I.C. Santos[2], Y. Verbovytskyy[2], J. C. Waerenborgh[2]

Instituto Tecnológico e Nuclear ([1] Inorganic and Organometallic Chemistry, Chemical and Radiopharmaceutical Sciences Unit; [2] Solid State, Chemical and Radiopharmaceutical Sciences Unit; [3] Radioprotection and Radioactive Waste, Radiological Protection and Safety Unit)
2686-953 Sacavém, Portugal
Tel: +351-21-9946170, Fax: +351-21-99946185, e-mail: jmarcalo@itn.pt

Abstract *– The current activities in the area of actinide chemistry at ITN, comprising basic research studies in inorganic and organometallic chemistry, catalysis, gas-phase ion chemistry, thermochemistry, and solid state chemistry, are briefly described.*

A. INTRODUCTION

At ITN there is an established experience in actinide chemistry, comprising basic research studies in inorganic and organometallic chemistry, catalysis, gas-phase ion chemistry, thermochemistry, and solid state chemistry. Here we present several recent examples of the current activities in this area.

B. INORGANIC AND ORGANOMETALLIC CHEMISTRY

Investigation of new coordination environments for the actinides (Th and U), lanthanides and Y, based on O- and/or N-donor ligands, with interest in organic synthesis, luminescence applications and lanthanide/actinide separations [1,2].

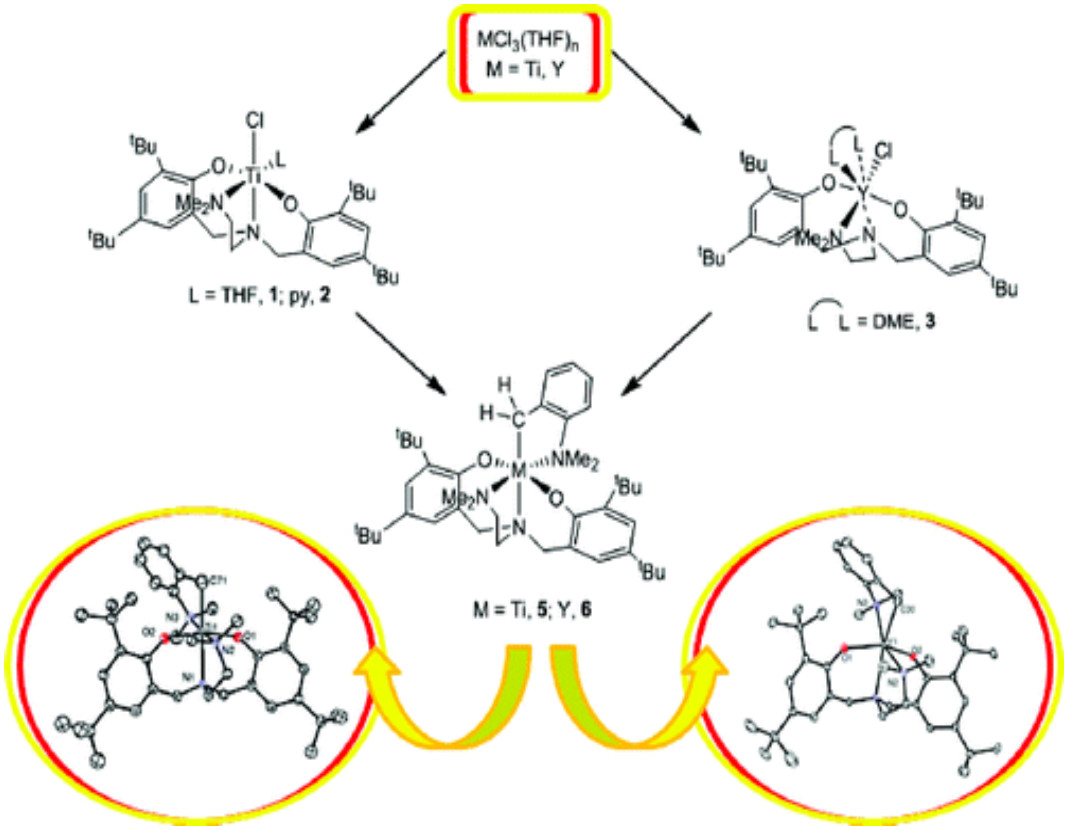

Figure 1: Synthesis and molecular structures of Ti and Y diamine bis(phenolate) complexes [1]

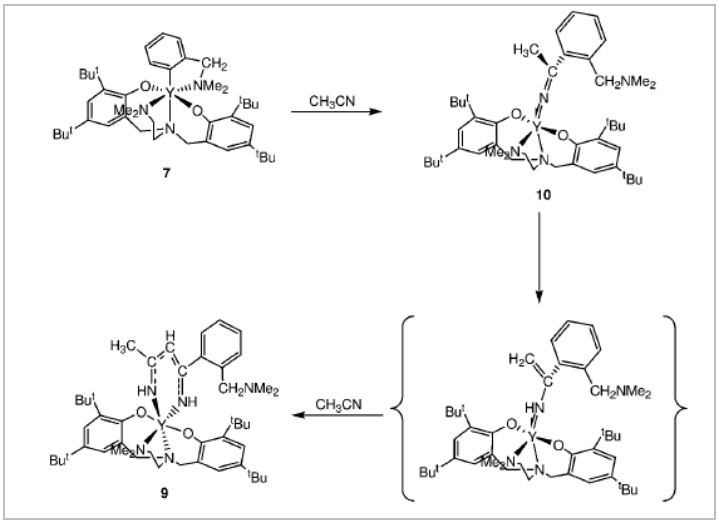

Figure 2: Reaction a Y complex with CH_3CN to yield a ketimide ligand; further reaction with CH_3CN involves a second nitrile insertion [1]

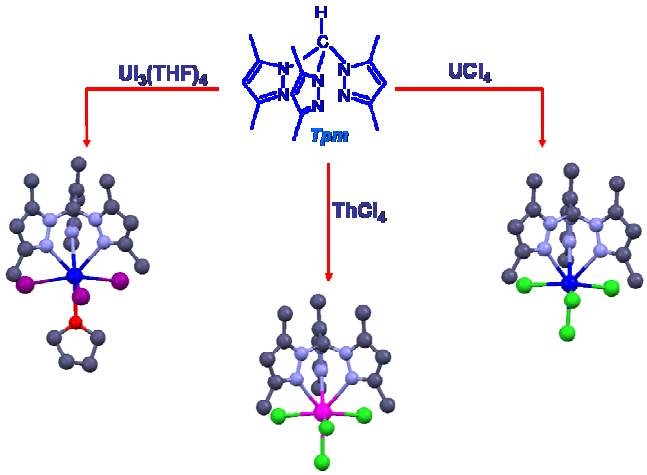

Figure 3: Synthesis and molecular structures of Th and U tris(3,5-dimethyl-pyrazolyl)methane-halide complexes [2]

C. CATALYSIS

Study of f-element (Th, U and the lanthanides) containing intermetallic compounds and nanostructured materials as catalysts or catalytic precursors for reactions of environmental interest, like the decomposition of volatile organic compounds and the use of methane and carbon dioxide as C1 feedstocks [3,4].

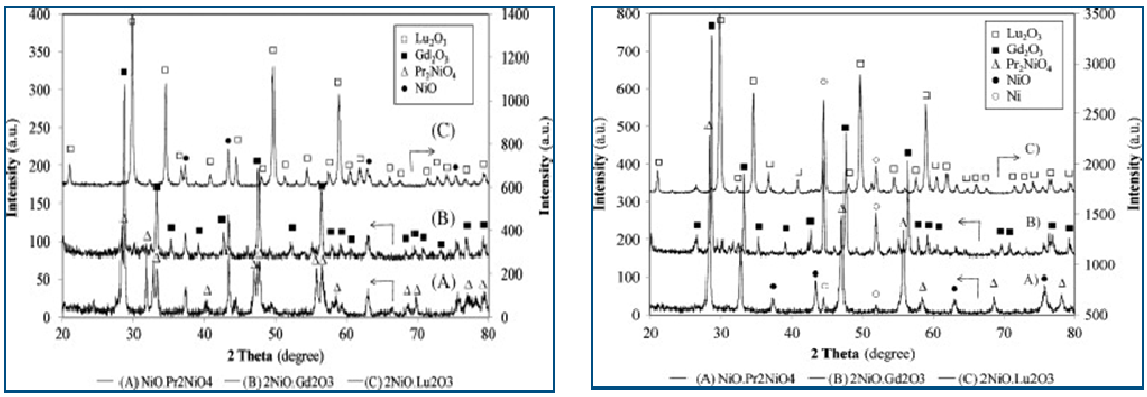

Figure 4: Bimetallic Ni-lanthanide oxides as catalysts in the partial oxidation of methane - XRD patterns before and after reaction [3]

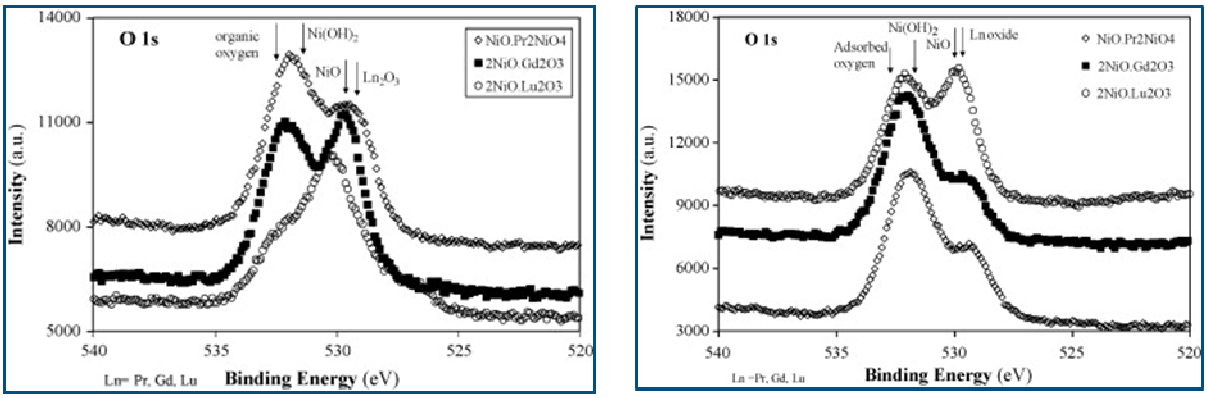

Figure 5: Bimetallic Ni-lanthanide oxides as catalysts in the partial oxidation of methane - XPS O 1s region before and after reaction [3]

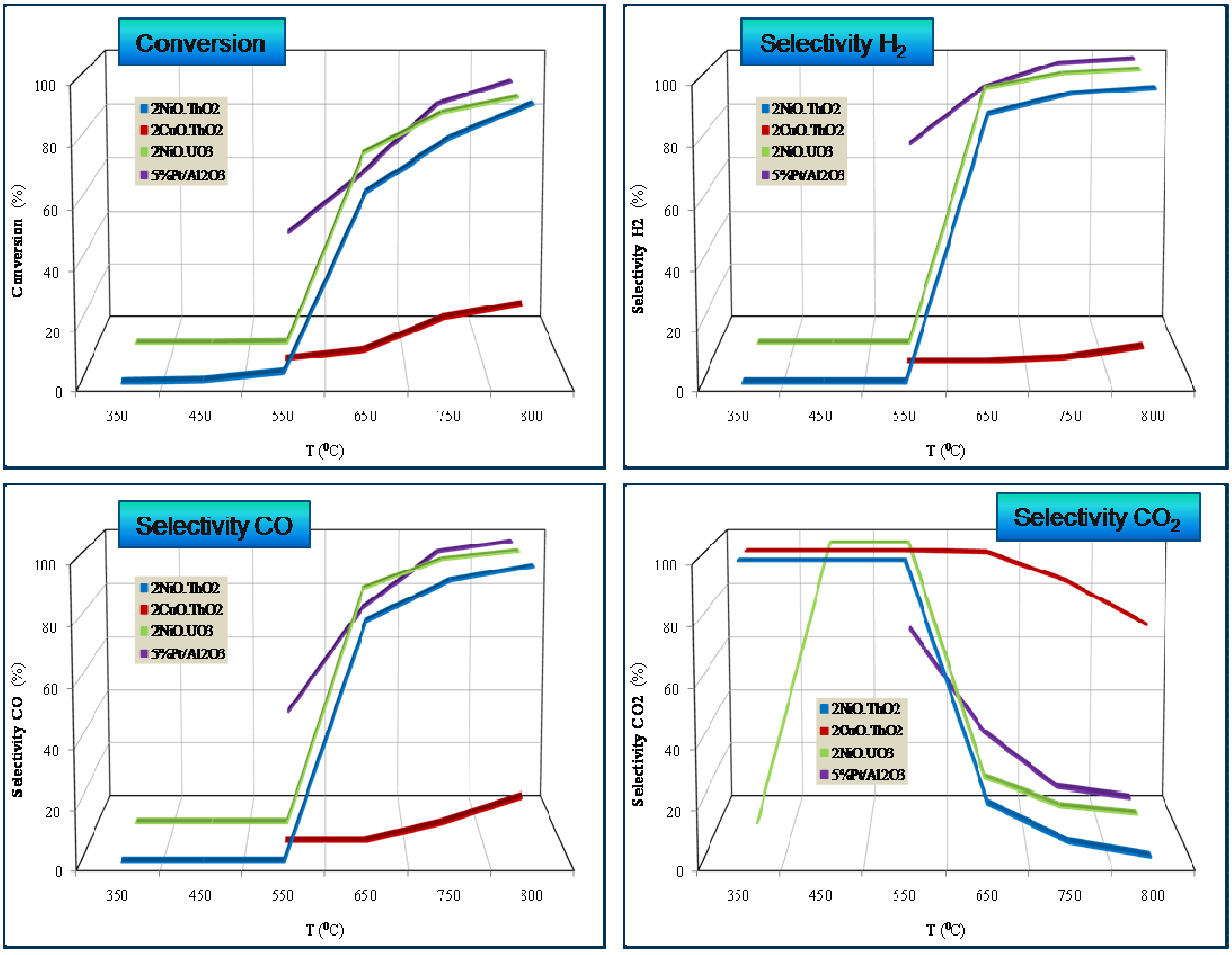

Figure 6: Partial oxidation of methane over bimetallic copper- and nickel-actinide oxides (Th, U) [4]

D. GAS-PHASE ION CHEMISTRY

Determination of key physicochemical properties of actinide (from Th to Cm) and lanthanide species based on gas-phase ion chemistry studies, using advanced mass spectrometric techniques [5-7].

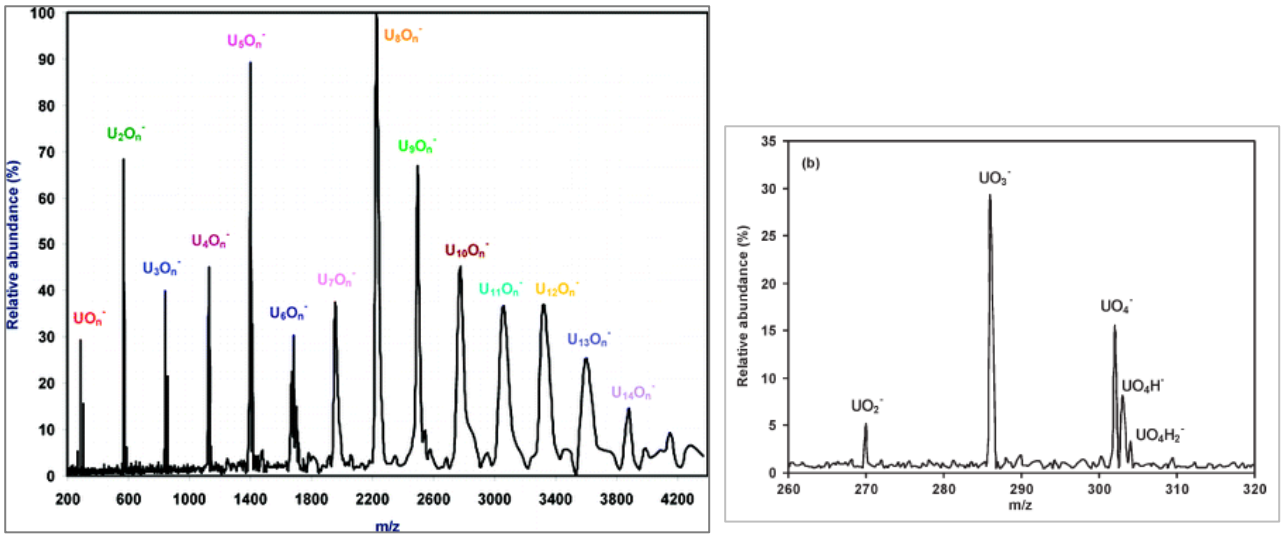

Figure 7: LDI(-) mass spectrum of a powdered anhydrous UO_3 sample [5]

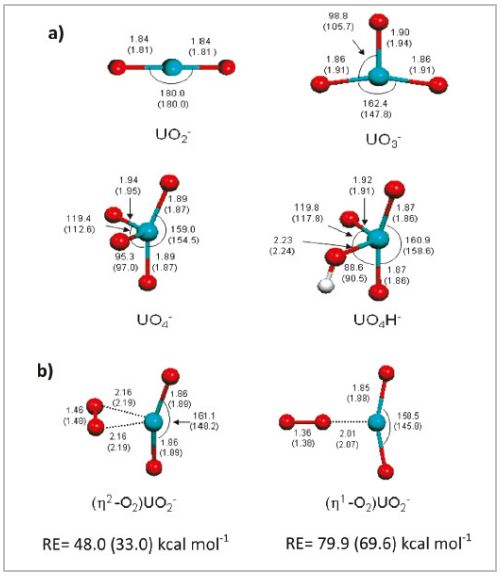

Figure 8: (a) UO_2^-, UO_3^-, UO_4^-, and UO_4H^- at PW91/ZORA (B3LYP/SDD) level of theory; (b) high-energy isomers of UO_4^- [6]

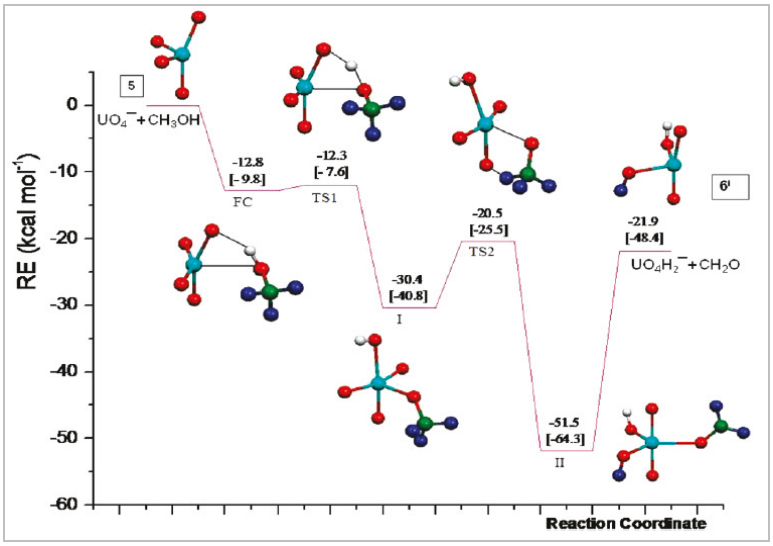

Figure 9: PEP for the reaction UO_4^- + CD_3OH (doublet spin state) at PW91/ZORA [B3LYP/SDD] level of theory [6]

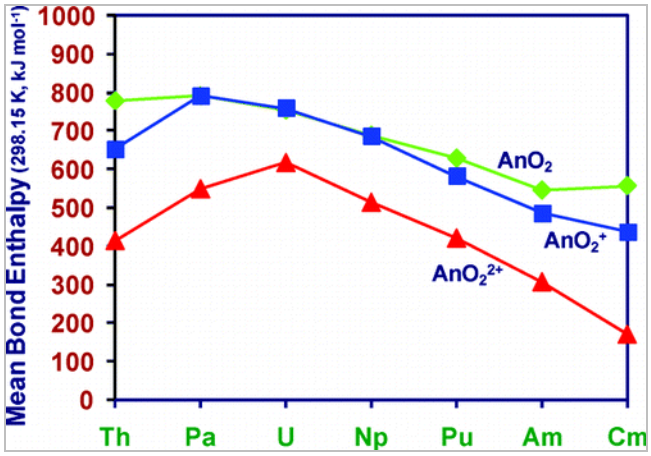

Figure 10: Actinide oxide energetics - mean bond enthalpies of neutral and cationic actinide dioxides [7]

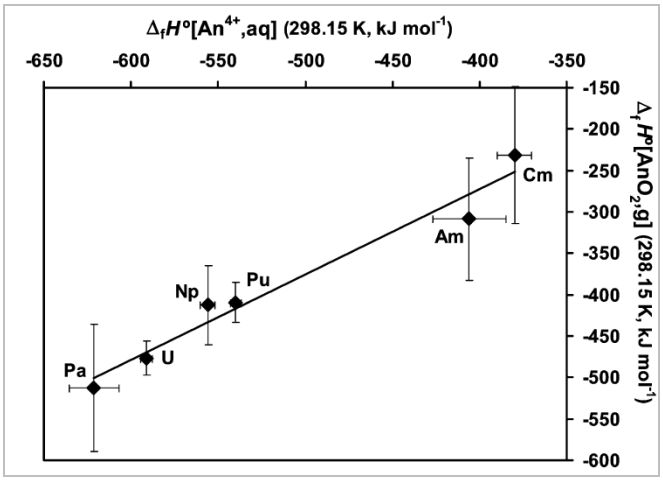

Figure 11: Actinide oxide energetics - experimental $\Delta_f H°[AnO_2,g]$ as a function of $\Delta_f H°[An^{4+},aq]$ [7]

E. THERMOCHEMISTRY

Examination of the energetics of f-element (Th, U and the lanthanides) compounds in solution and solid state, using calorimetry and thermal analysis techniques [8,9].

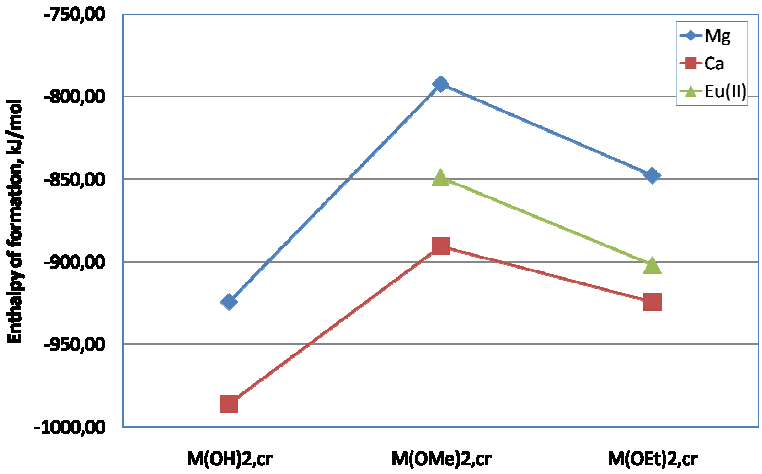

Figure 12: Enthalpies of formation of M(II) hydroxides and alkoxides [8,9]

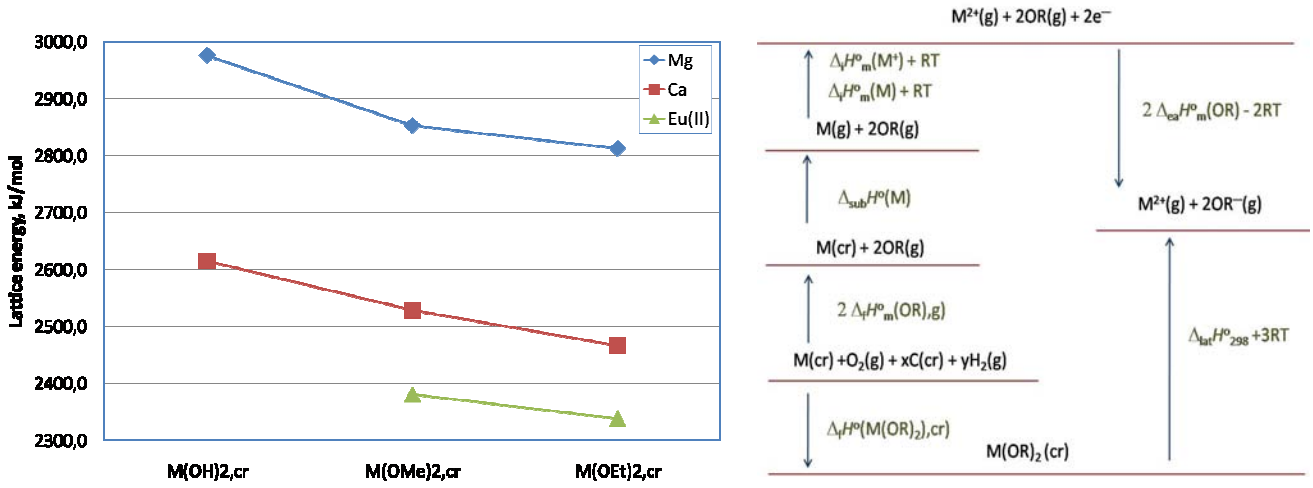

Figure 13: Lattice energies of the M(II) alkoxides and hydroxides and Born-Haber cycle used in the calculations [8,9]

F. SOLID STATE CHEMISTRY

Study of ternary phase diagrams, binary and ternary intermetallics, borides, carbides and nitrides containing f-elements (Th, U and the lanthanides), obtained by high temperature or electrochemical synthesis; investigation of the phase relations and study of the solid state, electrical, thermal and magnetic properties of the compounds [10-13].

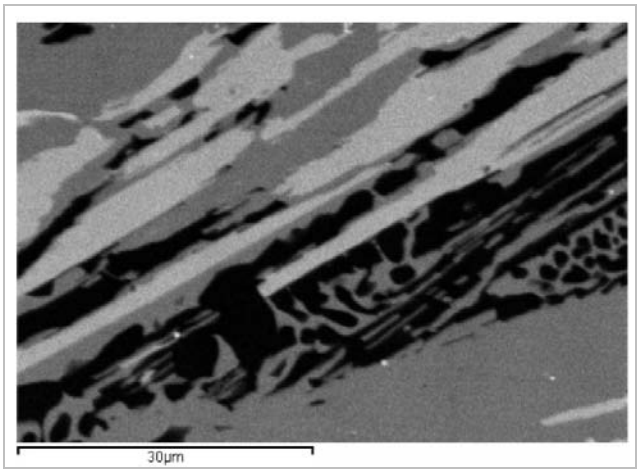

Figure 14: EDS-SEM image of a UFe_5Si_3 sample - UFe_2Si_2 (gray), UFe_5Si_3 (dark gray), Fe_3Si (black) [10]

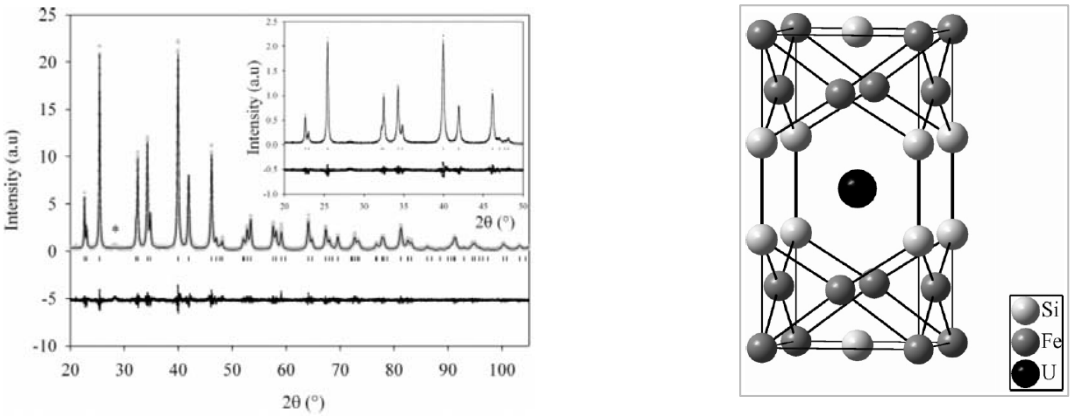

Figure 15: Powder diffraction patterns and crystal structure of UFe_5Si_3 [10]

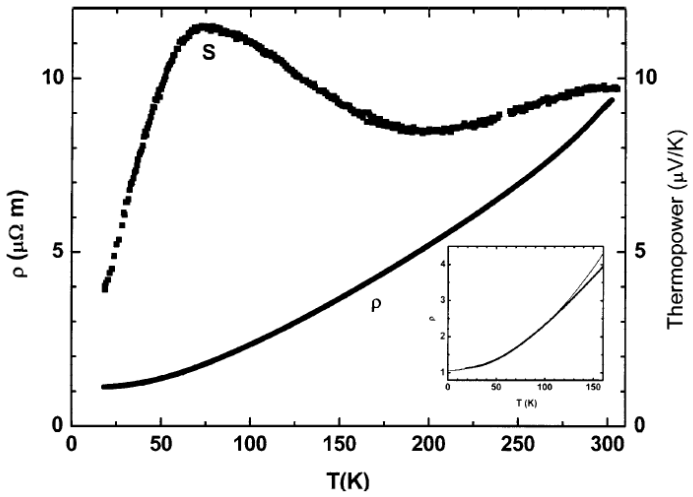

Figure 16: Temperature dependencies of the electrical resistivity and thermoelectric power of UFe_5Si_3 [10]

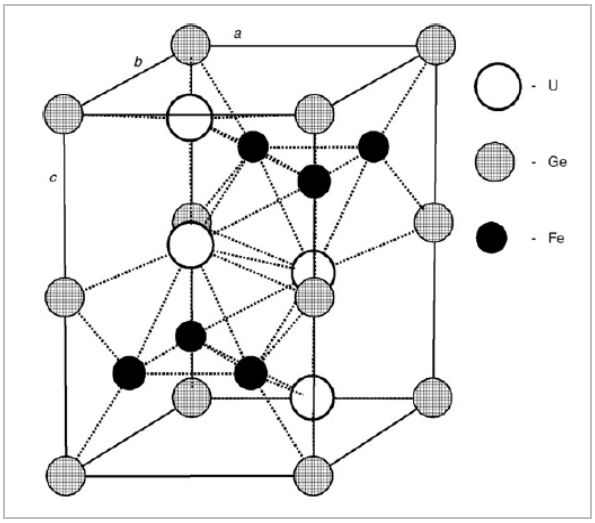

Figure 17: U_2Fe_3Ge unit cell [11]

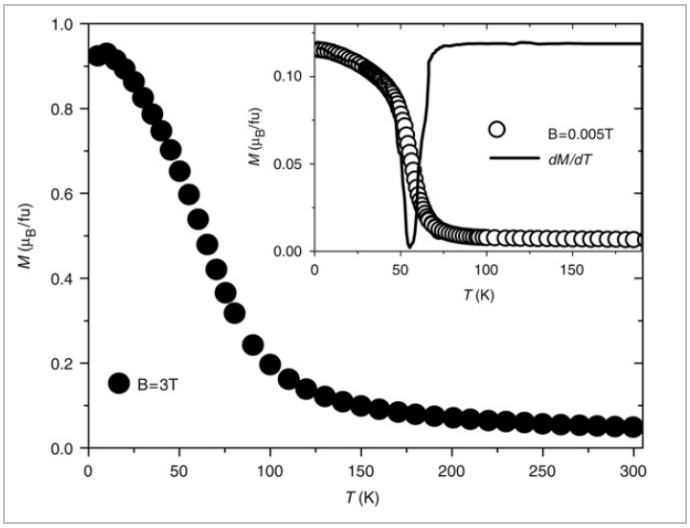

Figure 18: Temperature dependence of the magnetization of U_2Fe_3Ge [11]

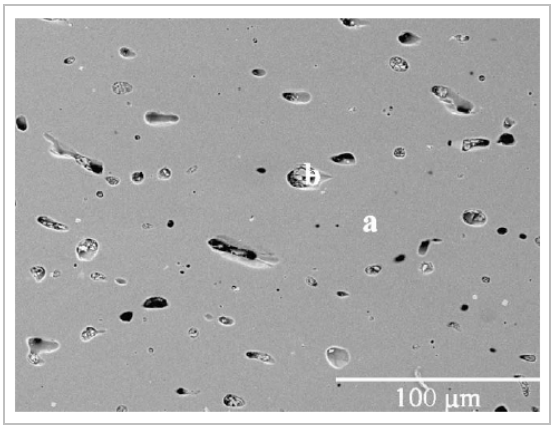

Figure 19: SEM micrograph of a UFe_5Ga_7 sample - (a) UFe_7Ga_5 (b) eutectic phase [12]

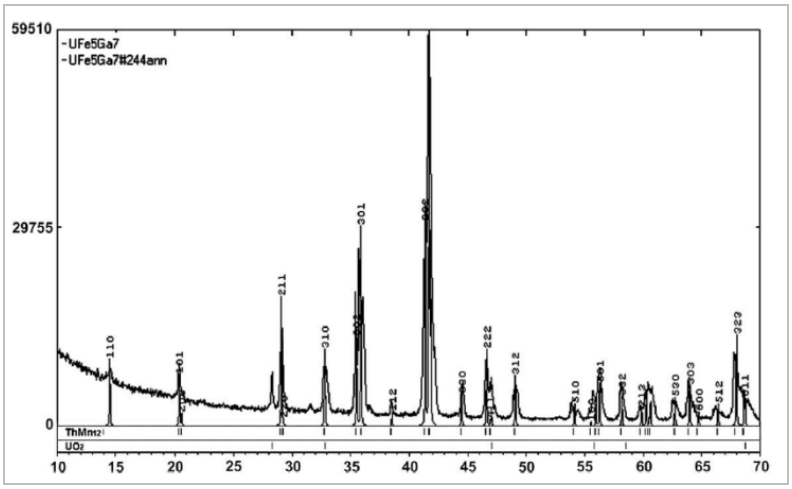

Figure 20: Powder diffraction patterns of UFe_7Ga_5 [12]

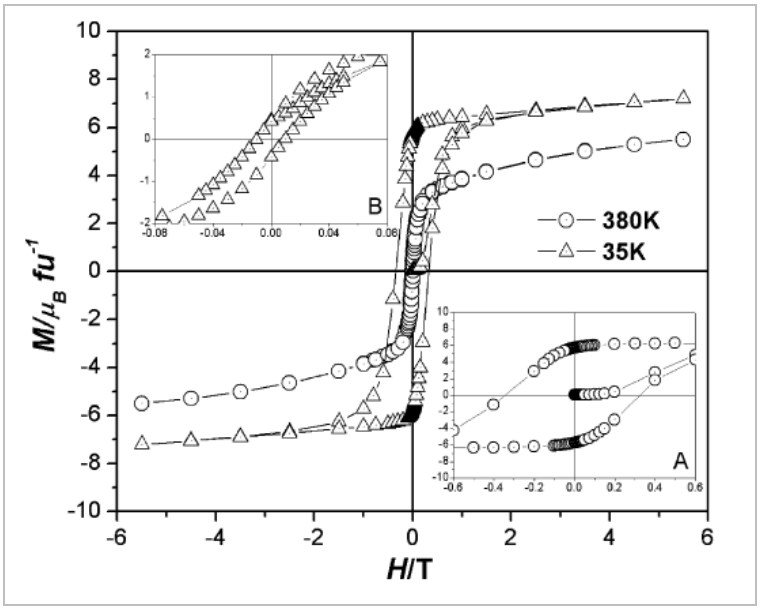

Figure 21: Field dependence of the magnetization and hysteresis loops for UFe_7Ga_5 [12]

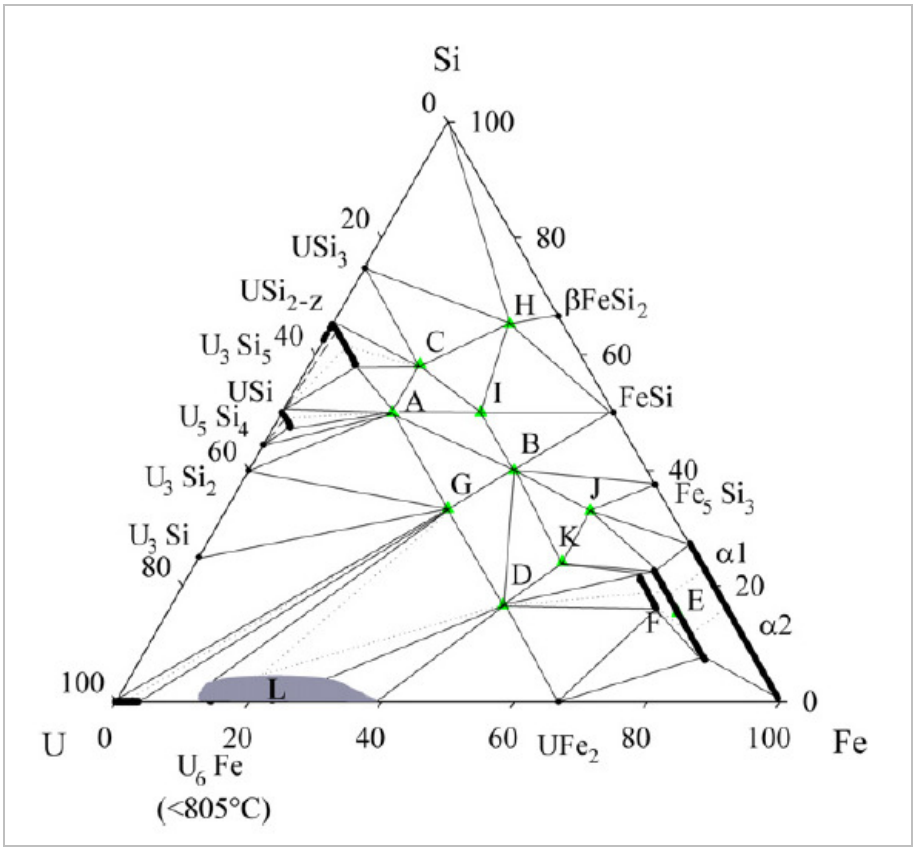

Figure 22: Ternary phase diagrams - isothermal section at 900 ºC of the U-Fe-Si system [13]

G. CONCLUSION

Actinide (and lanthanide) chemistry studies at ITN will be pursued connecting basic research with potential applications in nuclear and non-nuclear areas.

Aknowledgements

The authors are grateful to the external co-workers whose names appear in the references. The work was financially supported by Fundação para a Ciência e a Tecnologia through projects and research grants.

References

1. S. BARROSO, J. Cui, J. M. Carretas, A. Cruz, I. C. Santos, M. T. Duarte, J. P. Telo, N. Marques, A. M. Martins, “Diamine bis(phenolate) M(III) (Y, Ti) complexes: synthesis, structures, and reactivity”, *Organometallics*, 28, 3449 (2009).

2. J. CUI, J. M. Carretas, A. Cruz, L. Maria, I. C. Santos and J. Marçalo, “New starting compounds for U(III), U(IV) and Th(IV) coordination chemistry: synthesis and structures of tris(pyrazolylmethane)-halide complexes”, manuscript in preparation.

3. A. C. FERREIRA, A. M. Ferraria, A. M. Botelho do Rego, A. P. Gonçalves, M. R. Correia, T. A. Gasche and J. B. Branco, “ Partial oxidation of methane over bimetallic nickel–lanthanide oxides”, *J. Alloys Comp.*, 489, 316 (2010).

4. A. C. FERREIRA, A. P. Gonçalves, T. A. Gasche, A. M. Ferraria, A. M. Botelho do Rego, M. R. Correia, A. M. Bola and J. B. Branco, “Partial oxidation of methane over bimetallic copper- and nickel-actinide oxides (Th, U)”, *J. Alloys Comp.*, 497, 249 (2010).

5. J. MARÇALO, M. Santos, A. Pires de Matos and J. K. Gibson, “Molecular uranates: laser synthesis of uranium oxide anions in the gas phase”, *Inorg. Chem.*, 48, 5055 (2009).

6. M. C. MICHELINI, J. Marçalo, N. Russo and J. K. Gibson, “Gas-phase reactions of uranate ions, UO_2^-, UO_3^-, UO_4^-, and UO_4H^-, with methanol: a convergence of experiment and theory”, *Inorg. Chem.*, 49, 3836 (2010).

7. J. MARÇALO and J. K. Gibson, “Gas-phase energetics of actinide oxides: an assessment of neutral and cationic monoxides and dioxides from thorium to curium”, J. Phys. Chem. A, 113, 12599 (2009).

8. C. HIPÓLITO and J. P. Leal, “Standard molar enthalpies of formation of Eu(II) alkoxides”, manuscript in preparation.

9. T. BARREIRA and J. P. Leal, “Standard molar enthalpies of formation of Mg and Ca alkoxides”, *Eur. J. Inorg. Chem.*, 987 (2000).

10. D. BERTHEBAUD, A. P. Gonçalves, O. Tougait, M. Potel, E. B. Lopes and H. Noël, “Novel intermetallic compound UFe_5Si_3: a new room-temperature magnet with an original atomic arrangement”, *Chem. Mater.*, 19, 3441 (2007).

11. M. S. HENRIQUES, O. Tougait, H. Noël , L. C. J. Pereira, J. C. Waerenborgh and A. P. Gonçalves, “Evidence of uranium magnetic ordering on U_2Fe_3Ge”, *Solid State Commun.*, 148, 159 (2008).

12. M. S. HENRIQUES, P. Mora, M. M. Cruz , H. Noël, O. Tougait, V. H. Tran and A. P. Gonçalves, “Crystal structure and magnetic properties of UFe_5Ga_7”, *J. Nucl. Mater.*, 389, 160 (2009).

13. D. BERTHEBAUD, O. Tougait, A. P. Gonçalves and H. Noël, “Phase relations and stabilities at 900 ºC in the U-Fe-Si ternary system”, *Intermetallics*, 16, 373 (2008).

Theoretical Modelling of Europium(III) and Americium(III) Complexes with BTBP Ligands -

W.P. Oziminski and J. Narbut

Abstract *– Tetra-N-dendate derivatives of bis([1,2,4]-triazin-3-yl)-2,2'-biyridine (BTBP) selectively extract tervalent actinides over lanthanides from nitric acid solutions. A hypothesis was tested that the selectivity is due to a greater contributions into the metal-ligand bonding from the 5f orbitals than from the 4f ones. Molecular modelling of Eu(III) and Am(III) complexes with BTBP ligands was carried out, and the electron population of the bonding MOs in the complexes was examined. The cationic complexes of the stoichiometries 1:1 and 1:2, as well as the neutral [M(BTBP)(NO3)3] species, were modelled. The calculations were done by using Gaussian 03 package. Becke three-parameter hybrid functional B3LYP was used. Stuttgart-Dresden SDD small-core ECP pseudo-relativistic basis set was employed for metal atoms and standard all-electron Pople 6-31G(d) double valence basis set – for other atoms. Frequency calculations proved that the obtained stationary points had been the true minima on the potential energy surface. Thermodynamic functions of the complex formation were calculated, related to the hydrated metal ions. The Atoms in Molecules (AIM) and Natural Bond Orbitals (NBO) theories were used to analyse the differences in the metal-ligand bonding. The effect of addition of four ethyl chains to the BTBP molecule on the bonding energies was also analysed after full optimization of geometry of the complexes. The results indicate larger covalent metal-ligand interactions in the case of the Am(III) than Eu(III) complexes. The electron density at bond critical points (AIM), and bond orders (NBO) indicate stronger bonding of Am than Eu to BTBP. Charge transfer from the ligands to the Am(III) ion is also larger. The analysis of canonical symmetry-adapted orbitals (HOMO, HOMO–1 and other) and of semi-localized Natural Localized Molecular Orbitals (NLMOs) supports these observations. Larger contribution to bonding from 5f orbitals of Am than from 4f orbitals of Eu has been evidenced. The contribution from other valence subshells (7s/6s and 6d/5d) has also been discussed.*

Irradiation effects on neptunium oxidation states

A. Deptula1, M. Milkowska1,W. Lada1, T. Olczak1, F.Zaza2, A.G.Chmielewski1
1 Institute of Nuclear Chemistry and Technology (INCT), 03-195 Warsaw, Poland 2 Italian National Agency for New Technologies, Energy and Environment (ENEA), CR Casaccia, Rome, Italy

Abstract *– Our patented complex sol-gel process has been used for synthesis of silica glasses designed to contain high-level nuclear wastes. Cs, Sr, Co, and Nd (generically denoted Me) were used, the last as surrogate of actinides. Gels in the form of powders and monoliths were prepared by hydrolysis and polycondensation of tetraethoxide/Me nitrate solutions, which contained ascorbic acid as catalyst. Thermal treatment studies were conducted for the powders. Transformation to final products was studied by thermogravimetric analysis, infrared spectroscopy, and X-ray diffraction. Preliminary testing of Me leaching was completed.*

Vitrification of nuclear wastes by a complex sol-gel process

A. Deptula[1], M. Milkowska[1],W. Lada[1], T. Olczak[1], F.Zaza[2], A.G.Chmielewski[1]

[1] *Institute of Nuclear Chemistry and Technology (INCT),*
16 Dorodna Str, 03-195 Warsaw, Poland
a.deptula@ichtj.waw.pl
[2] *Italian National Agency for New Technologies, Energy and Environment (ENEA), CR Casaccia, Rome, Italy*

Abstract *– Our patented complex sol-gel process has been used for synthesis of silica glasses designed to contain high-level nuclear wastes. Cs, Sr, Co, and Nd (generically denoted Me) were used, the last as surrogate of actinides. Gels in the form of powders and monoliths were prepared by hydrolysis and polycondensation of tetraethoxide/Me nitrate solutions, which contained ascorbic acid as catalyst. Thermal treatment studies were conducted for the powders. Transformation to final products was studied by thermogravimetric analysis, infrared spectroscopy, and X-ray diffraction. Preliminary testing of Me leaching was completed.*